



# Impact of Freeze-Thaw on Liquefaction Potential and Dynamic Properties of Mabel Creek Silt



**Prepared By:**  
Yu Zhang

**December 2009**

**Prepared For:**

**Alaska University Transportation Center  
Duckering Building Room 245  
P.O. Box 755900  
Fairbanks, AK 99775-5900**

**Permafrost Technology Foundation  
1216 Range View Road  
North Pole, AK 99705**

**INE/AUTC # 12.13**

**REPORT DOCUMENTATION PAGE**

Form approved OMB No.

Public reporting for this collection of information is estimated to average 1 hour per response, including the time for reviewing instructions, searching existing data sources, gathering and maintaining the data needed, and completing and reviewing the collection of information. Send comments regarding this burden estimate or any other aspect of this collection of information, including suggestion for reducing this burden to Washington Headquarters Services, Directorate for Information Operations and Reports, 1215 Jefferson Davis Highway, Suite 1204, Arlington, VA 22202-4302, and to the Office of Management and Budget, Paperwork Reduction Project (0704-1833), Washington, DC 20503

1. AGENCY USE ONLY (LEAVE BLANK)

2. REPORT DATE

3. REPORT TYPE AND DATES COVERED

February 2009

Final Report (8/2007-9/2009)

4. TITLE AND SUBTITLE

Impact of Freeze- Thaw on Liquefaction Potential and Dynamic Properties of Mabel Creek Silt

5. FUNDING NUMBERS

AUTC#107041  
DTRT06-G-0011

6. AUTHOR(S)

Yu Zhang

7. PERFORMING ORGANIZATION NAME(S) AND ADDRESS(ES)

Alaska University Transportation Center  
P.O. Box 755900  
Fairbanks, AK 99775-5900

8. PERFORMING ORGANIZATION REPORT NUMBER

INE/AUTC 12.13

9. SPONSORING/MONITORING AGENCY NAME(S) AND ADDRESS(ES)

Permafrost Technology Foundation  
1216 Range View Road  
North Pole, AK 99705

10. SPONSORING/MONITORING AGENCY REPORT NUMBER

11. SUPPLEMENTARY NOTES

12a. DISTRIBUTION / AVAILABILITY STATEMENT

No restrictions

12b. DISTRIBUTION CODE

13. ABSTRACT (Maximum 200 words)

This study examines the influence of temperature rise and freeze-thaw cycles on the soil liquefaction potential. More specifically, dynamic properties and post-cyclic-loading settlement of fine-grained soils are evaluated in this study. The results can be used to predict seismic response of partially frozen, frozen, or thawed fine-grained soils in seismic subarctic regions. In other words, the influence of seasonal climate change on the seismic response of Mabel Creek silt is reported in this study. Systematic laboratory tests were conducted for the purpose of addressing the influence of temperature and cycles of freeze-thaw on liquefaction of Mabel Creek silt.

14- KEYWORDS: Liquefaction (Stpk), Freeze thaw durability (Rktg), Temperature (Rktm), Freeze thaw tests (Gbjdnf),

15. NUMBER OF PAGES  
215

16. PRICE CODE

N/A

17. SECURITY CLASSIFICATION OF REPORT

Unclassified

18. SECURITY CLASSIFICATION OF THIS PAGE

Unclassified

19. SECURITY CLASSIFICATION OF ABSTRACT

Unclassified

20. LIMITATION OF ABSTRACT

N/A

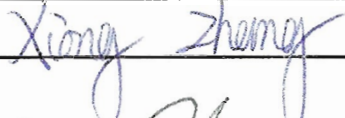
IMPACT OF FREEZE-THAW ON LIQUEFACTION POTENTIAL AND  
DYNAMIC PROPERTIES OF MABEL CREEK SILT

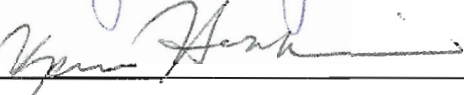
By  
Yu Zhang

RECOMMENDED:

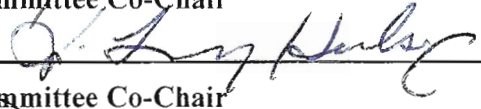
  
\_\_\_\_\_

  
\_\_\_\_\_

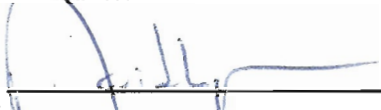
  
\_\_\_\_\_

  
\_\_\_\_\_

Committee Co-Chair

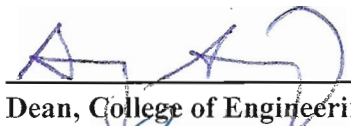
  
\_\_\_\_\_

Committee Co-Chair

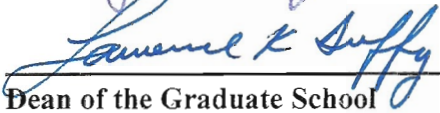
  
\_\_\_\_\_

Chair, Department of Civil and Environmental  
Engineering

APPROVED:

  
\_\_\_\_\_

Dean, College of Engineering and Mines

  
\_\_\_\_\_

Dean of the Graduate School

  
\_\_\_\_\_

Date

**IMPACT OF FREEZE-THAW ON LIQUEFACTION POTENTIAL AND  
DYNAMIC PROPERTIES OF MABEL CREEK SILT**

**A  
DISSERTATION**

**Presented to the Faculty  
of the University of Alaska Fairbanks**

**in Partial Fulfillment of the Requirements  
for the Degree of**

**DOCTOR OF PHILOSOPHY**

**By**

**Yu Zhang, B.S., M.S.**

**Fairbanks, Alaska**

**December 2009**

## Abstract

In the early winter of 2002 (November), the Alaska Denali earthquake ( $M_w=7.9$ ) caused significant damage in partially frozen fine-grained soil and extensive liquefaction was observed in glacial fine-grained saturated soil surface deposits near Tok, Alaska. It illustrated that there was a need to evaluate the seismic response and liquefaction potential of fine-grain soil in cold regions; however, until now most of the research on the liquefaction phenomenon and seismic response were mainly about soil in non-cold regions. The seismic response and liquefaction potential of soils in cold regions, especially those of fine-grained nature, has not been studied thoroughly and therefore is not well-understood.

This document presents a laboratory study on liquefaction potential and cyclic response of fine-grained soil in cold regions. As the main features of the soil in the ground of cold regions, temperature change at below freezing temperatures or near-freezing temperatures, and the seasonal climate change were evaluated on liquefaction potential, dynamic properties, and post-cyclic-loading settlement of fine-grained soils. Increasing temperatures from near freezing to the completely thawed temperature (i.e., 24 °C, 5 °C, 1 °C, and 0.5 °C) were used to thaw the frozen Mabel Creek silt to simulate temperature change on it, or the Mabel Creek silt experienced several freezing and thawing alternating processes (i.e., 1, 2, and 4 freeze-thaw cycles) to simulate seasonal climate change. Triaxial strain-controlled cyclic tests were conducted to evaluate liquefaction potential, dynamic properties, and post-cyclic-loading settlement.

Based on this limited laboratory effort, results show that in most cases, temperature rise and freeze-thaw cycles can impact: a) liquefaction potential, b) dynamic properties and c) post-cyclic-loading settlement of fine-grained soils. However, there

was one case exception and this is described in the following sentence. When a fine-grained soil was conditioned in a partially frozen state, the possibility and threat of liquefaction significantly increased.

## Table of Contents

	Page
<b>Signature Page</b> .....	<b>i</b>
<b>Title Page</b> .....	<b>ii</b>
<b>Abstract</b> .....	<b>iii</b>
<b>Table of Contents</b> .....	<b>v</b>
<b>List of Tables</b> .....	<b>viii</b>
<b>List of Figures</b> .....	<b>ix</b>
<b>List of Appendices</b> .....	<b>xvii</b>
<b>Acknowledgements</b> .....	<b>xviii</b>
<b>Technical Summary</b> .....	<b>xix</b>
<b>1 Introduction</b> .....	<b>1</b>
1.1 Problem statement .....	1
1.2 Outline of dissertation.....	2
<b>2 Review of Previous Studies</b> .....	<b>5</b>
2.1 Impact of ground temperature and freeze-thaw process on physical and mechanical properties of soil .....	5
2.2 Liquefaction in partially frozen or frozen soil .....	6
2.3 Dynamic properties of fine-grained soil .....	8
2.4 Post-cyclic-loading-induced settlement.....	10
2.4.1 Influence factors on post-cyclic-loading-induced settlement .....	11
2.4.2 Prediction of post-cyclic-loading-induced settlement .....	12
<b>3 Experimental Program</b> .....	<b>15</b>
3.1 Material tested .....	15
3.2 Cyclic triaxial tests .....	24
3.2.1 University of Alaska Fairbanks (UAF) cyclic triaxial apparatus.....	25
3.2.2 Specimen preparation, saturation, and consolidation .....	28
3.2.3 Specimen thermal conditioning .....	32
3.2.3.1 Thermal conditioning at 24 °C, 5 °C, 1 °C, 0.5 °C, and -0.2 °C .....	32
3.2.3.2 Thermal conditioning through freeze-thaw cycles .....	32
3.2.3.3 Thermal conditioning at 0.5 °C, and -0.2 °C though three different paths .....	35
3.2.4 Cyclic triaxial strain-controlled test.....	36
3.2.5 Dissipation of excess pore pressure and post testing measurements .....	37

3.3	Data reduction.....	38
<b>4</b>	<b>Impact of Temperature and Freeze-Thaw Cycles on Excess Pore Pressure Generation in Mabel Creek Silt.....</b>	<b>42</b>
4.1	Introduction.....	42
4.2	Excess pore water pressure generation at various temperatures.....	42
4.3	Impact of temperature on excess pore water pressure generation .....	51
4.4	Comparison of results with previous research efforts .....	54
4.5	Pore water pressure generation at freeze-thaw cycles .....	56
4.6	Impact of freeze-thaw cycles on pore water pressure generation of Mabel Creek silt.....	58
4.7	Discussion of pore water pressure generation at freeze-thaw cycles .....	64
4.8	Prediction of pore water pressure generation of Mabel Creek silt .....	66
4.9	Impact of thermal condition paths on pore pressure generation of Mabel Creek silt.....	72
4.10	Summary.....	75
<b>5</b>	<b>Dynamic Properties of Mabel Creek Silt.....</b>	<b>78</b>
5.1	Introduction.....	78
5.2	Dynamic properties of unfrozen Mabel Creek silt .....	79
5.3	Dynamic properties of Mabel Creek silt conditioned at 24 °C, 5 °C, 1 °C, 0.5 °C, and -0.2 °C .....	80
5.4	Temperature effect on dynamic properties .....	98
5.4.1	Temperature effect on shear modulus .....	98
5.4.2	Temperature effect on damping ratio .....	105
5.5	Discussion of dynamic properties at various temperatures .....	111
5.6	Dynamic properties of Mabel Creek silt conditioned by the freeze-thaw cycles .....	115
5.7	The effect of freeze-thaw cycle on dynamic properties.....	122
5.7.1	Effect of freeze-thaw cycles on shear modulus .....	122
5.7.2	Freeze-thaw cycle effects on damping ratio .....	128
5.8	Discussion of dynamic properties at various freeze-thaw cycles .....	133
5.9	Thermal conditioning path effect on dynamic properties.....	137
5.10	Degradation of dynamic shear modulus in undrained cyclic tests .....	143
5.11	Summary.....	148
<b>6</b>	<b>Post-cyclic-loading Settlement.....</b>	<b>152</b>
6.1	Post-cyclic-loading settlement for unfrozen Mabel Creek silt .....	153
6.2	Post-cyclic-loading settlement of Mabel Creek silt conditioned at 0.5 °C, 1 °C, 5 °C, and 24 °C.....	155
6.3	Post-cyclic-loading settlement of Mabel Creek silt conditioned by the freeze-thaw cycles .....	157
6.4	Soil types effect on post-cyclic-loading settlement of unfrozen state .....	158



6.5	Temperature rise effect on post-cyclic-loading settlement for frozen or partially frozen Mabel Creek silt .....	160
6.6	Freeze-thaw-cycles effect on post-cyclic-loading settlement of frozen or partially frozen Mabel Creek silt .....	161
6.7	Determination of post-cyclic-loading volumetric strain as a function of cyclic shear strain on Mabel Creek silt .....	163
6.8	Summary .....	167
<b>7</b>	<b>Discussion .....</b>	<b>169</b>
7.1	Temperature effect on liquefaction potential, dynamic properties, and cyclic-loading-induced settlement .....	169
7.2	Effect of freeze-thaw cycles on liquefaction potential, dynamic properties, and cyclic-loading-induced settlement .....	171
<b>8</b>	<b>Conclusion .....</b>	<b>173</b>
	<b>References .....</b>	<b>176</b>

## List of Tables

		Page
Table 2.1	Effect of various factors on maximum shear modulus ( $G_{\max}$ ), modulus reduction ( $G/G_{\max}$ ), and damping ratio (D) of normally consolidated and moderately overconsolidated clays (after Dobry and Vucetic 1987) .....	9
Table 2.2	Effect of various factors on shear modulus (G) and damping ratio (D) of frozen soil (combine data from Stevens 1975; Andersland and Anderson 1978; Vinson 1978; Czajkowski and Vinson 1980; Vinson et al. 1983; Fukuda and Huang 1991).....	10
Table 3.1	Soil index properties of Mabel Creek silt .....	21
Table 3.2	Setup and the sensors used in triaxial system .....	27
Table 3.3	Cyclic strain-controlled tests on unfrozen Mabel Creek silt specimens .....	29
Table 3.4	Cyclic strain-controlled tests on Mabel Creek silt specimens conditioned to a target temperature.....	30
Table 3.5	Cyclic strain-controlled tests on Mabel Creek silt specimens subjected to freeze-thaw cycles .....	31
Table 3.6	Cyclic strain-controlled tests on Mabel Creek silt specimens subjected to freeze-thaw cycles .....	31
Table 4.1	PEC for GMP model on Mabel Creek silt and corresponding $R^2$ .....	68
Table 5.1	Degradation parameter of shear modulus on Mabel Creek silt.....	144
Table B.1	Earthquake magnitude, equivalent cycles, and duration (Seed et al. 1976).....	188

## List of Figures

		Page
Figure 2.1	Chart for determination of post-liquefaction volumetric strain as a function of factor of safety (after Ishihara 1996).....	14
Figure 3.1	Sampling location at milepost 76.2 on the Tok Cutoff Highway in Alaska .....	16
Figure 3.2	Liquefaction-induced lateral spreading in Tok Cutoff Highway embankment (abutment of Slana River Bridge embankment, which is 1 km away from Mabel Creek Bridge) .....	16
Figure 3.3	Test log in bore holes (after MACTEC Engineering and Consulting 2004).....	20
Figure 3.4	SPT value in tested bore holes (after MACTEC Engineering and Consulting 2004) .....	20
Figure 3.5	Grain size distribution of Mabel Creek silt .....	22
Figure 3.6	Optimum moisture content curve for Mabel Creek silt.....	24
Figure 3.7	(a) schematic drawing of test apparatus (b) installation of thermistors in cylindrical triaxial soil specimen .....	26
Figure 3.8	Modified triaxial test system .....	27
Figure 3.9	Typical thermistor records and vertical displacements during specimen conditioning at 24 °C, 5 °C, 1 °C, 0.5 °C, and -0.2 °C.....	34
Figure 3.10	Typical thermistor records and vertical displacements from specimens subjected to freeze-thaw cycles .....	34
Figure 3.11	Typical thermistor records and vertical displacements during specimens conditioning at 0.5 °C and -0.2 °C through different paths .....	36
Figure 3.12	Typical result from a cyclic strain-controlled test on Mabel Creek silt specimen conditioned at 0.5°C with $\sigma'_3=100$ kPa, $\gamma=0.3\%$ and post-consolidation void ratio of 1.046 .....	37
Figure 3.13	Typical pore water pressure generation under cyclic loading in Mabel Creek silt subjected to 2 freeze-thaw cycles (a) $\gamma=0.1\%$ , $\sigma'_3=101$ kPa, and $e=1.045$ (b) $\gamma=0.8\%$ , $\sigma'_3=101$ kPa, and $e=1.044$ .....	40
Figure 3.14	Hysteretic stress–strain relationship for cyclic loading (after Vinson 1978).....	41
Figure 4.1	Excess pore pressure ratio ( $r_u$ ) versus $N$ in unfrozen Mabel Creek silt.....	43
Figure 4.2	Excess pore pressure ratio ( $r_u$ ) versus cyclic shear strain in unfrozen Mabel Creek silt.....	44
Figure 4.3	Excess pore pressure ratio ( $r_u$ ) versus $N$ in Mabel Creek silt conditioned at 24 °C .....	45
Figure 4.4	Excess pore pressure ratio versus cyclic shear strain in Mabel Creek silt conditioned at 24 °C.....	46
Figure 4.5	Excess pore pressure ratio ( $r_u$ ) versus $N$ in Mabel Creek silt conditioned	

	at 5 °C .....	46
Figure 4.6	Excess pore pressure ratio ( $r_u$ ) versus cyclic shear strain on Mabel Creek silt conditioned at 5 °C .....	47
Figure 4.7	Excess pore pressure ratio ( $r_u$ ) versus N on Mabel Creek silt conditioned at 1 °C.....	48
Figure 4.8	Excess pore pressure ratio versus cyclic shear strain on Mabel Creek silt conditioned at 1 °C.....	48
Figure 4.9	Excess pore pressure ratio ( $r_u$ ) versus N on Mabel Creek silt conditioned at 0.5 °C.....	49
Figure 4.10	Excess pore pressure ratio versus cyclic shear strain on Mabel Creek silt conditioned at 0.5 °C.....	49
Figure 4.11	Excess pore pressure ratio ( $r_u$ ) versus N on Mabel Creek silt conditioned at -0.2 °C .....	50
Figure 4.12	Temperature rise effect on pore water pressure generation of frozen or partially frozen Mabel Creek silt at $\gamma=0.1\%$ .....	52
Figure 4.13	Temperature rise effect on pore water pressure generation of frozen or partially frozen Mabel Creek silt at $\gamma=0.3\%$ .....	52
Figure 4.14	Excess pore water pressure ratio versus temperature at $\gamma=0.1\%$ .....	53
Figure 4.15	Excess pore water pressure ratio versus temperature at $\gamma=0.3\%$ .....	53
Figure 4.16	Pore water pressure generation curves of Mabel Creek silt conditioned at different temperature and $N=10$ .....	54
Figure 4.17	Comparison of pore pressure generation among Mabel Creek silt conditioned at various temperatures, clean sand and sand with fines.....	55
Figure 4.18	The bound of pore pressure generation in Mabel Creek silt conditioned at various temperatures .....	55
Figure 4.19	Excess pore pressure ratio ( $r_u$ ) versus N on Mabel Creek silt conditioned after 2 freeze-thaw cycles .....	56
Figure 4.20	Excess pore pressure ratio versus cyclic shear strain on Mabel Creek silt conditioned after 2 freeze-thaw cycles.....	57
Figure 4.21	Excess pore pressure ratio ( $r_u$ ) versus N on Mabel Creek silt conditioned after 4 freeze-thaw cycles .....	58
Figure 4.22	Excess pore pressure versus cyclic shear strain on Mabel Creek silt conditioned after 4 freeze-thaw cycles .....	58
Figure 4.23	Comparison of the pore water pressure generation in Mabel Creek silt conditioned at different freeze-thaw cycles at $\gamma=0.1\%$ .....	60
Figure 4.24	Comparison of the pore water pressure generation in Mabel Creek silt conditioned at different freeze-thaw cycles at $\gamma=0.3\%$ .....	60
Figure 4.25	Comparison of the pore water pressure generation on Mabel Creek silt conditioned at different freeze-thaw cycles at $\gamma=0.8\%$ .....	61
Figure 4.26	Excess pore water pressure versus the number of freeze-thaw cycles on Mabel Creek silt conditioned at $\gamma=0.1\%$ .....	62
Figure 4.27	Excess pore water pressure versus the number of freeze-thaw cycles on	

	Mabel Creek silt conditioned at $\gamma=0.3\%$ .....	62
Figure 4.28	Excess pore water pressure versus the number of freeze-thaw cycles on Mabel Creek silt conditioned at $\gamma=0.8\%$ .....	63
Figure 4.29	Pore water pressure generation curves of Mabel Creek silt conditioned at different number of freeze-thaw cycles at $N=10$ .....	64
Figure 4.30	Comparison of pore pressure generation among Mabel Creek silt conditioned at various freeze-thaw cycles, clean sand and sand with fines .....	65
Figure 4.31	Bound of pore pressure generation in Mabel Creek silt conditioned at various freeze-thaw cycles.....	65
Figure 4.32	The comparison of predicted $r_u$ from GMP model and measured $r_u$ on unfrozen Mabel Creek silt .....	68
Figure 4.33	The comparison of predicted $r_u$ from GMP model and measured $r_u$ on Mabel Creek silt conditioned at $24\text{ }^\circ\text{C}$ or experiencing 1 freeze-thaw cycle.....	69
Figure 4.34	The comparison of predicted $r_u$ from GMP model and measured $r_u$ on Mabel Creek silt conditioned at $5\text{ }^\circ\text{C}$ .....	69
Figure 4.35	The comparison of predicted $r_u$ from GMP model and measured $r_u$ on Mabel Creek silt conditioned at $1\text{ }^\circ\text{C}$ .....	70
Figure 4.36	The comparison of predicted $r_u$ from GMP model and measured $r_u$ on Mabel Creek silt conditioned at $0.5\text{ }^\circ\text{C}$ .....	70
Figure 4.37	The comparison of predicted $r_u$ from GMP model and measured $r_u$ on Mabel Creek silt experiencing 2 freeze-thaw cycles .....	71
Figure 4.38	The comparison of predicted $r_u$ from GMP model and measured $r_u$ on Mabel Creek silt experiencing 4 freeze-thaw cycles .....	71
Figure 4.39	PEC versus the conditioning temperature on Mabel Creek silt .....	72
Figure 4.40	PEC versus the number of freeze-thaw cycles on Mabel Creek silt.....	72
Figure 4.41	Effect of thermal conditioning paths on pore water pressure history of Mabel Creek silt at target temperature of $0.5^\circ\text{C}$ and $\gamma=0.3\%$ .....	73
Figure 4.42	Effect of thermal conditioning paths on pore water pressure generation curve of Mabel Creek silt at target temperature of $0.5\text{ }^\circ\text{C}$ .....	74
Figure 4.43	Effect of thermal conditioning paths on pore water pressure history of Mabel Creek silt at target temperature of $-0.2^\circ\text{C}$ and $\gamma=0.1\%$ .....	74
Figure 4.44	Effect of thermal conditioning paths on pore water pressure generation curve of Mabel Creek silt at target temperature of $-0.2\text{ }^\circ\text{C}$ .....	75
Figure 5.1	Shear modulus ( $G$ ) on unfrozen Mabel Creek silt: (a) $G$ vs $N$ ; (b) $G$ vs $r_u$ ; (c) $G$ vs $\gamma$ .....	82
Figure 5.2	Damping ratio ( $D$ ) on unfrozen Mabel Creek silt: (a) $D$ vs $N$ ; (b) $D$ vs $r_u$ ; (c) $D$ vs $\gamma$ .....	83
Figure 5.3	Shear modulus ( $G$ ) on Mabel Creek silt conditioned at $24\text{ }^\circ\text{C}$ : (a) $G$ vs $N$ ; (b) $G$ vs $r_u$ ; (c) $G$ vs $\gamma$ .....	84
Figure 5.4	Damping ratio ( $D$ ) on Mabel Creek silt conditioned at $24\text{ }^\circ\text{C}$ : (a) $D$ vs $N$ ;	

	(b) D vs $r_u$ ; (c) D vs $\gamma$ .....	86
Figure 5.5	Shear modulus (G) on Mabel Creek silt conditioned at 5 °C: (a) G vs N; (b) G vs $r_u$ ; (c) G vs $\gamma$ .....	87
Figure 5.6	Damping ratio (D) on Mabel Creek silt conditioned at 5 °C: (a) D vs N; (b) D vs $r_u$ ; (c) D vs $\gamma$ .....	90
Figure 5.7	Shear modulus (G) on Mabel Creek silt conditioned at 1 °C: (a) G vs N; (b) G vs $r_u$ ; (c) G vs $\gamma$ .....	91
Figure 5.8	Damping ratio (D) on Mabel Creek silt conditioned at 1 °C: (a) D vs N; (b) D vs $r_u$ ; (c) D vs $\gamma$ .....	92
Figure 5.9	Shear modulus (G) on Mabel Creek silt conditioned at 0.5 °C: (a) G vs N; (b) G vs $r_u$ ; (c) G vs $\gamma$ .....	93
Figure 5.10	Damping ratio (D) on Mabel Creek silt conditioned at 0.5 °C: (a) D vs N; (b) D vs $r_u$ ; (c) D vs $\gamma$ .....	94
Figure 5.11	Shear modulus (G) on Mabel Creek silt conditioned at -0.2 °C: (a) G vs N; (b) G vs $r_u$ ; (c) G vs $\gamma$ .....	96
Figure 5.12	Damping ratio (D) on Mabel Creek silt conditioned at -0.2 °C: (a) D vs N; (b) D vs $r_u$ ; (c) D vs $\gamma$ .....	97
Figure 5.13	Temperature rise effect on shear modulus of Mabel Creek silt .....	99
Figure 5.14	Shear modulus versus cyclic shear strain on Mabel Creek silt conditioned at the different temperatures for N=10.....	100
Figure 5.15	The normalized modulus reduction ( $G/G_{max}$ ) versus $\gamma$ in specimens conditioned at various temperatures .....	101
Figure 5.16	Shear modulus (G) versus $r_u$ on Mabel Creek silt conditioned at the various temperatures .....	103
Figure 5.17	Shear modulus versus the conditioned temperature on Mabel Creek silt for $\gamma=0.005\%$ .....	104
Figure 5.18	Shear modulus versus the conditioned temperature on Mabel Creek silt for $\gamma=0.1\%$ .....	104
Figure 5.19	Shear modulus versus the conditioned temperature on Mabel Creek silt for $\gamma=0.3\%$ .....	105
Figure 5.20	Temperature rise effect on damping ratio of Mabel Creek silt .....	107
Figure 5.21	Damping ratio versus cyclic shear strain on Mabel Creek silt conditioned at the different temperatures for N=10.....	108
Figure 5.22	Damp ratio (D) versus $r_u$ on Mabel Creek silt conditioned at the different temperatures .....	109
Figure 5.23	Damping ratio versus the conditioned temperature on Mabel Creek silt for $\gamma=0.005\%$ .....	110
Figure 5.24	Damping ratio versus the conditioned temperature on Mabel Creek silt for $\gamma=0.1\%$ .....	110
Figure 5.25	Damping ratio versus the conditioned temperature on Mabel Creek silt for $\gamma=0.3\%$ .....	111
Figure 5.26	Comparison of damping ratio between Mabel Creek silt conditioned at	

	various temperatures and frozen Alaska silt .....	113
Figure 5.27	Comparison of shear modulus between Mabel Creek silt conditioned at various temperatures and frozen Alaska silt .....	113
Figure 5.28	Comparison of damping ratio between Mabel Creek silt conditioned at various temperatures and fine-grained soil (from Vucetic and Dobry 1991).....	114
Figure 5.29	Comparison of normalized shear modulus reduction between Mabel Creek silt conditioned at various temperatures and fine-grained soil (from Vucetic and Dobry 1991).....	114
Figure 5.30	Shear modulus (G) on Mabel Creek silt conditioned at 2 freeze-thaw cycles:(a) G vs N; (b) G vs $r_u$ ; (c) G vs $\gamma$ .....	118
Figure 5.31	Damping ratio (D) on Mabel Creek silt conditioned at 2 freeze-thaw cycles:(a) D vs N; (b) D vs $r_u$ ; (c) D vs $\gamma$ .....	119
Figure 5.32	Shear modulus (G) on Mabel Creek silt conditioned at 4 freeze-thaw cycles:(a) G vs N; (b) G vs $r_u$ ; (c) G vs $\gamma$ .....	120
Figure 5.33	Damping ratio (D) on Mabel Creek silt conditioned at 4 freeze-thaw cycles:(a) D vs N; (b) D vs $r_u$ ; (c) D vs $\gamma$ .....	121
Figure 5.34	Effect of freeze-thaw cycles on shear modulus of Mabel Creek silt .....	123
Figure 5.35	Shear modulus versus cyclic shear strain on Mabel Creek silt that experienced the different freeze-thaw cycles for N=10 .....	124
Figure 5.36	The modulus reduction ( $G/G_{max}$ ) versus $\gamma$ in specimens conditioned at various freeze-thaw cycles.....	125
Figure 5.37	Shear modulus (G) versus $r_u$ on Mabel Creek silt experiencing the different freeze-thaw cycles .....	126
Figure 5.38	Shear modulus versus number of freeze-thaw cycles on Mabel Creek silt for $\gamma=0.005\%$ .....	127
Figure 5.39	Shear modulus versus number of freeze-thaw cycles on Mabel Creek silt for $\gamma=0.1\%$ .....	127
Figure 5.40	Shear modulus versus number of freeze-thaw cycles on Mabel Creek silt for $\gamma=0.3\%$ .....	128
Figure 5.41	Shear modulus versus number of freeze-thaw cycles on Mabel Creek silt for $\gamma=0.8\%$ .....	128
Figure 5.42	Effect of freeze-thaw cycles on damping ratio of Mabel Creek silt .....	130
Figure 5.43	Damping ratio versus cyclic shear strain on Mabel Creek silt experiencing the different freeze-thaw cycles for N=10.....	131
Figure 5.44	Damping ratio (D) versus $r_u$ on Mabel Creek silt experiencing the different freeze-thaw cycles.....	132
Figure 5.45	Damping ratio versus number of freeze-thaw cycles on Mabel Creek silt for $\gamma=0.005\%$ .....	134
Figure 5.46	Damping ratio versus number of freeze-thaw cycles on Mabel Creek silt for $\gamma=0.1\%$ .....	134
Figure 5.47	Damping ratio versus number of freeze-thaw cycles on Mabel Creek	

	silt for $\gamma=0.3\%$ .....	135
Figure 5.48	Damping ratio versus number of freeze-thaw cycles on Mabel Creek silt for $\gamma=0.8\%$ .....	135
Figure 5.49	Comparison of damping ratio between Mabel Creek silt conditioned at various freeze-thaw cycles and fine-grained soil (from Vucetic and Dobry 1991).....	136
Figure 5.50	Comparison of normalized shear modulus reduction between Mabel Creek silt conditioned at various freeze-thaw cycles and fine-grained soil (from Vucetic and Dobry 1991) .....	136
Figure 5.51	Effect of thermal conditioning paths on G of Mabel Creek silt at the target temperature of $0.5\text{ }^{\circ}\text{C}$ .....	139
Figure 5.52	Effect of thermal conditioning paths on D of Mabel Creek silt at the target temperature of $0.5\text{ }^{\circ}\text{C}$ .....	140
Figure 5.53	Effect of thermal conditioning paths on G of Mabel Creek silt at the target temperature of $-0.2\text{ }^{\circ}\text{C}$ .....	141
Figure 5.54	Effect of thermal conditioning paths on D of Mabel Creek silt at the target temperature of $-0.2\text{ }^{\circ}\text{C}$ .....	142
Figure 5.55	The degradation curves of unfrozen Mabel Creek silt and Mabel Creek silt conditioned at $0.5^{\circ}\text{C}$ , $1^{\circ}\text{C}$ , $5^{\circ}\text{C}$ , and $24^{\circ}\text{C}$ at $\gamma=0.1\%$ .....	145
Figure 5.56	The degradation curves of unfrozen Mabel Creek silt and Mabel Creek silt conditioned at $0.5^{\circ}\text{C}$ , $1^{\circ}\text{C}$ , $5^{\circ}\text{C}$ , and $24^{\circ}\text{C}$ at $\gamma=0.3\%$ .....	145
Figure 5.57	Degradation parameter (t) versus $\gamma$ on unfrozen Mabel Creek silt and Mabel Creek silt conditioned at $0.5\text{ }^{\circ}\text{C}$ , $1\text{ }^{\circ}\text{C}$ , $5\text{ }^{\circ}\text{C}$ , and $24\text{ }^{\circ}\text{C}$ .....	146
Figure 5.58	The degradation curves of Mabel Creek silt experiencing freeze-thaw cycles at $\gamma=0.1\%$ .....	147
Figure 5.59	The degradation curves of Mabel Creek silt experiencing freeze-thaw cycles at $\gamma=0.3\%$ .....	147
Figure 5.60	The degradation curves of Mabel Creek silt experiencing freeze-thaw cycles at $\gamma=0.8\%$ .....	148
Figure 5.61	Degradation parameter (t) versus $\gamma$ on Mabel Creek silt experiencing freeze-thaw cycles .....	149
Figure 6.1	Reconsolidated volume strain versus excess pore water pressure ratio on unfrozen Mabel Creek silt.....	154
Figure 6.2	Reconsolidated volume strain versus the max shear strain on unfrozen Mabel Creek silt.....	155
Figure 6.3	Reconsolidated volume strain versus excess pore water pressure ratio on Mabel Creek silt conditioned at $1\text{ }^{\circ}\text{C}$ , $5\text{ }^{\circ}\text{C}$ , and $24\text{ }^{\circ}\text{C}$ .....	156
Figure 6.4	Reconsolidated volume strain versus excess pore water pressure ratio on Mabel Creek silt conditioned at $0.5\text{ }^{\circ}\text{C}$ .....	156
Figure 6.5	Reconsolidated volume strain versus excess pore water pressure ratio on Mabel Creek silt conditioned after 2 freeze-thaw cycles.....	157
Figure 6.6	Reconsolidated volume strain versus excess pore water pressure ratio	



	on Mabel Creek silt conditioned after 4 freeze-thaw cycles .....	158
Figure 6.7	Comparison of reconsolidated volumetric strains between sand, silty sand, and Mabel Creek silt.....	159
Figure 6.8	Comparison of the characteristics of post-liquefaction volumetric strains between sand and Mabel Creek silt.....	160
Figure 6.9	Temperature rise effect on reconsolidated volumetric strain of Mabel Creek silt due to dissipation of pore water pressure .....	162
Figure 6.10	The freeze-thaw cycles effect on reconsolidated volumetric strain of Mabel Creek silt due to dissipation of pore water pressure .....	162
Figure 6.11	Chart for determination of the post-cyclic-loading volumetric strain as a function of cyclic shear strain on unfrozen Mabel Creek silt .....	164
Figure 6.12	Chart for determination of the post-cyclic-loading volumetric strain as a function of cyclic shear strain on unfrozen Mabel Creek silt conditioned at 0.5 °C.....	164
Figure 6.13	Chart for determination of the post-cyclic-loading volumetric strain as a function of cyclic shear strain on unfrozen Mabel Creek silt conditioned at 1 °C.....	165
Figure 6.14	Chart for determination of the post-cyclic-loading volumetric strain as a function of cyclic shear strain on unfrozen Mabel Creek silt conditioned at 5 °C.....	165
Figure 6.15	Chart for determination of the post-cyclic-loading volumetric strain as a function of cyclic shear strain on unfrozen Mabel Creek silt after 1 freeze-thaw cycle .....	166
Figure 6.16	Chart for determination of the post-cyclic-loading volumetric strain as a function of cyclic shear strain on unfrozen Mabel Creek silt after 2 freeze-thaw cycles .....	166
Figure 6.17	Chart for determination of the post-cyclic-loading volumetric strain as a function of cyclic shear strain on unfrozen Mabel Creek silt after 1 freeze-thaw cycles .....	167
Figure 7.1	Unfrozen water content versus conditioned temperature in Mabel Creek silt .....	170
Figure 7.2	Volumetric strain change during freezing and thawing process versus temperature .....	171
Figure 7.3	Volumetric strain change versus the number of freeze-thaw cycles on Mabel Creek silt.....	172
Figure B.1	Soil profile.....	184
Figure B.2	Temperature profile .....	185
Figure B.3	Reduction factor with depth below level or gently sloping ground surfaces. (After Seed and Idriss 1971).....	186
Figure B.4	Modulus reduction curves for fine-grained soils of different plasticity. (After Vucetic and Dobry 1991) .....	188
Figure B.5	Excess pore pressure ratios versus cyclic shear strain on unfrozen	

	Mabel Creek silt (in this study).....	189
Figure B.6	Excess pore pressure ratios versus cyclic shear strain on Mabel Creek silt experiencing 1 freeze-thaw cycle (in this study) .....	189
Figure B.7	Chart for determination of the post-cyclic-loading volumetric strain as a function of cyclic shear strain on unfrozen Mabel Creek silt (in this study) .....	190
Figure B.8	Chart for determination of the post-cyclic-loading volumetric strain as a function of cyclic shear strain on unfrozen Mabel Creek silt after 1 freeze-thaw cycle (in this study).....	190

## List of Appendices

	Page
Appendix A. Determination of Void Ratio in Saturated Soil.....	183
Appendix B. Case Analysis.....	184

## Acknowledgements

It has been more than 6 years before the eve of my Ph.D. degree defense. These 6 years were difficult and full of disappointment and countless lonely nights in the laboratory. The moment of success feels sweet yet short. Just as Dr. Hulsey told me, pursuing a Ph.D. degree was like a waveform, the peak was sweet but short and the valley was the biggest portion. Certainly, the short attainment of the peak can never be separated from the support provided by the school, faculty, friends, and family during the valley. I would like to acknowledge everyone who helped me in these 6 years. It was your help that made my accomplishment of the Ph.D. possible.

First, I would like to thank Dr. J. Leroy Hulsey. Your encouragement and support has kept me continuing and finally completing this program. I want to thank Dr. Lutfi Raad for bringing me into the door of research. I want to thank Dr. Kenan Hazirbaba for directing my research and his patience during this period. I would also like to thank my committee (Dr. Yuri Shur, Dr. Doug Goering, Dr. Joey Yang and Dr. Xiong Zhang) for your valuable time and effort.

Thanks to my wife and my family for their support, understanding and love during the difficult times.

I also thank the faculties in the Department of Civil and Environmental Engineering, fellow graduate students and friends for your help, support and friendship. They are Dr. Jenny Liu, Dr. Horacio Toniolo, Suzette Stachow, Gary Tyndall, Felicia Burud, Joel Bailey, Matt Bray, Kim Kouli, Jianfeng Xu, Peng Li, Xianwu Chen, and Sue Beck.

This research work was supported by Alaska EPSCoR NSF award #EPS-0701898, the state of Alaska, Permafrost Technology Foundation, and Alaska University transportation.

## Technical Summary

This study examines the influence of temperature rise and freeze-thaw cycles on the soil liquefaction potential. More specifically, dynamic properties and post-cyclic-loading settlement of fine-grained soils are evaluated in this study. The results can be used to predict seismic response of partially frozen, frozen, or thawed fine-grained soils in seismic subarctic regions. In other words, the influence of seasonal climate change on the seismic response of Mabel Creek silt is reported in this study. Systematic laboratory tests were conducted for the purpose of addressing the influence of temperature and cycles of freeze-thaw on liquefaction of Mabel Creek silt. The Alaska University Transportation Center (AUTC) and the Permafrost Technology Foundation (PTF) co-funded the work presented in this report.

In November 2002, silts in the Mabel Creek area liquefied causing damage to roadways, roadway embankments, and backfill at some bridge abutments. Because of the damage, Mabel Creek silt was selected for this study. This silt is a fine-grained material commonly encountered in naturally seismically active subarctic regions. The soil samples used in this study were obtained near Northway, Alaska at Mile 76.2 on the Tok Cutoff Highway. The soil belongs to USCS class: ML. Extensive liquefaction was observed in the partially frozen fine-grained soil nearby during the Denali Earthquake in November 2002.

Systematic laboratory tests were conducted for the purpose of addressing the influence of temperature and freeze-thaw cycles on liquefaction potential of the Mabel Creek silt. Increasing temperatures from near freezing to the completely thawed temperature (i.e., 0.5 °C, 1 °C, 5 °C, and 24 °C) were applied to thaw the frozen Mabel Creek silt specimens and to simulate temperature rise on it. Several freezing and thawing alternating processes were used to simulate seasonal climate change.

Triaxial strain-controlled cyclic tests were conducted to evaluate liquefaction potential and the influence of temperature on dynamic properties. After the cyclic loading tests were completed, soil samples were reconsolidated to evaluate settlement for a post-cyclic-loading state. In this study, liquefaction potential was evaluated as the pore water pressure ratio ( $r_u$ ), which is the ratio of pore water pressure to initial effective confining pressure. Dynamic properties were evaluated by damping ratio (D) and dynamic shear modulus (G). Post-cyclic loading settlement was investigated by the reconsolidated volumetric strain ( $\epsilon_v$ ), which is the ratio of the volume change due to dissipation of pore water pressure following cycle loading to the initial total volume of soil specimen.

Partially frozen (conditioned at 0.5 °C) specimens were found to liquefy more readily than unfrozen specimens. The excess pore water pressure at the end of the 10<sup>th</sup> loading cycle was referred to as  $r_{u,10}$ , which reflects the liquefaction potential. The higher the  $r_{u,10}$ , the smaller the effective confining pressure and the easier for the soil to lose strength. Ten cycles of loading with a constant shear strain amplitude of 0.3% caused an  $r_{u,10}$  of 0.488 on the unfrozen specimen, but a much higher  $r_{u,10}$  of 0.582 on partially frozen Mabel Creek silt. Freeze-thaw cycles were found to densify the Mabel Creek silt and decrease liquefaction potential. After conditioning the specimen for 1 freeze-thaw cycle, the pore water pressure at the 10<sup>th</sup> load cycle decreased  $r_{u,10}$  to 0.392; however, additional freeze-thaw cycles did not cause further change to the liquefaction potential.

Freeze-thaw cycles were also found to affect the dynamic properties of the Mabel Creek silt. Generally, the first freeze-thaw cycle was found to densify the silt, increase the shear modulus (G), and increase the damping ratio (D). Additional freeze-thaw cycles on the Mabel Creek silt had only minor effects on both liquefaction potential and the dynamic properties. For a constant shear strain with amplitude of 0.1%, the shear modulus and damping ratio on the unfrozen specimens at the end of the 10<sup>th</sup>

loading cycle ( $G_{10}$  and  $D_{10}$ ) were 11808 kPa (1713 psi) and 0.138, respectively. After a specimen was exposed to one freeze-thaw cycle, the shear modulus ( $G_{10}$ ) and damping ( $D_{10}$ ) were 13785 kPa (1999 psi) and 0.163, respectively. When specimen conditioning was changed from two (2) freeze-thaw cycles to four (4) freeze-thaw cycles, the shear modulus at the 10<sup>th</sup> load cycle ( $G_{10}$ ) decreased slightly from 13834 kPa (2006 psi) to 14834 kPa (2151 psi). Damping ( $D_{10}$ ) values at 2 and 4 freeze-thaw cycles were found to be 0.174 and 0.180; however, when a specimen was conditioned in the partially frozen state,  $G_{10}$  increased to 19539 kPa (2833 psi) and  $D_{10}$  decreased to 0.320.

Partially frozen Mabel Creek silt was found to have the lowest post-cyclic-loading settlement. The lowest post-cyclic-loading settlement occurred because of an existing ice structure. Consider an unfrozen specimen of Mabel Creek silt. After the first freeze-thaw cycle, a specimen of this Mabel Creek silt shows a decrease in post-cyclic-loading settlement as compared with an unfrozen specimen of the same silt. However, further freeze-thaw cycles do not change post-cyclic-loading settlement. If the excess pore water pressure ratio of 0.8 is dissipated after seismic loading, the potential settlement of the partially frozen specimens is represented as the reconsolidated volumetric strain ( $\epsilon_v$ ). The  $\epsilon_v$  was 0.92%, which means that the settlement was 0.92 feet for a soil layer 100 ft thick. When specimens were subjected to 1, 2, and 4 freeze-thaw cycles, and the thawed specimens were subjected to cyclic loading, the reconsolidated volumetric strain reached approximately 1.64% for each of these conditions. The unfrozen specimen subjected to cyclic loading had an  $\epsilon_v$  of 2.16%, which was higher than the  $\epsilon_v$  of Mabel Creek silt subjected to freeze-thaw cycles.

Based on this limited laboratory effort, results show that in most cases temperature rise and freeze-thaw cycles can increase liquefaction potential, shear modulus, damping ratio and post-cyclic-loading settlement of fine-grained soils; however, there

was one case to be specially noted. When a fine-grained soil was conditioned in a partially frozen state, the possibility and threat of liquefaction increased strongly. These findings are very important. As the price of land increases, the pressure to build in marginal soils increases. Therefore, these findings make an important contribution to the engineering community. They can be used for both design and investigation of seismically active sites, especially when considering the design of a newly constructed foundation site in partially frozen silt (for example, coastal regions, river valleys, and the margin of lakes) in subarctic regions.



# 1 Introduction

## 1.1 Problem statement

Since the 1964 Alaska Earthquake ( $M_w=9.2$ ), there have been numerous research efforts on the subject of liquefaction. Liquefaction typically occurs when an earthquake shakes saturated cohesionless soils. Saturation is when the voids between soil particles are completely filled with water. Earthquake loading causes the pore water pressure to increase due to undrained conditions (i.e., pore water pressure cannot dissipate quickly). Significant increase of pore water pressure can cause easy movement of the soil particles. This may finally lead to a complete loss of shear strength of the ground. This phenomenon is known as “liquefaction.” The loss of shear strength due to liquefaction can cause extensive damage, including settlement and tilting of buildings and bridge abutments, collapse of offshore structures, lateral spreading and cracking of slopes, flow failures of earth dams, cracking of pavements, and flotation of buried structures to the ground surface (Dobry et al. 1982).

Previous research efforts on the liquefaction phenomenon and cyclic resistance of soils mainly focused on grounds with moderate temperatures (e.g., Lee and Seed 1967; Seed 1968; Seed and Idriss 1971; Finn et al. 1971; Castro 1975; Youd and Idriss 2001; Bray and Sancio 2006; Boulanger and Idriss 2006). The seismic response and liquefaction potential of soils in cold regions, especially those of fine-grained nature, have not been studied thoroughly and therefore are not well understood. This study was aimed at addressing the need to investigate the liquefaction potential and dynamic characteristics of commonly encountered soil types in Alaska. In an attempt to identify a cold-region soil liquefaction response, the author embarked on an extensive experimental research program

Saturated fine-grained, non-plastic to low-plasticity soil deposits are commonly encountered in the seismically active Arctic region. Moderate to strong shaking of such deposits can lead to significant pore pressure generation and ultimately to liquefaction if the pore water is completely unfrozen. If the pore water is fully frozen, no pore pressure is generated. As the ground temperature nears the freezing point (i.e., 0°C), the state of the pore water becomes “partially frozen”. The response of the ground to earthquake loading in this case is completely different from either the fully frozen or the unfrozen case. The stiffness of the ground typically increases with decreasing temperature (Vinson 1978); however this increase in stiffness may not translate into decreasing liquefaction potential. This is because formation of ice layers within the ground can lead to a decrease in permeability. Together with earthquake loading, this may become a significant contributing factor to liquefaction of the ground at near-freezing temperature. During the November 3, 2002, Denali Earthquake, significant liquefaction damage was observed at near-freezing ground temperatures (Yashinsky and Eiding 2003).

The objectives of this study are to explore:

- The effect of ground temperature on the cyclic resistance and dynamic properties of fine-grained soils,
- The role of freeze-thaw cycles (i.e., seasonal variation of ground temperature) on liquefaction potential and cyclic behavior of fine-grained soils, and
- The cyclic-induced settlement of fine-grained soil, considering unfrozen conditions and near-freezing temperature, as well as freeze-thaw cycles.

## **1.2 Outline of dissertation**

Chapter 1 briefly introduces the characteristics of seismic events and the necessity and significance of research regarding liquefaction potential and dynamic behavior of

fine-grained soil in cold regions. Near-freezing ground temperature and seasonal freeze-thaw cycles are considered very important factors and constitute the major objectives in this study. Furthermore, organization of this dissertation is briefly described.

Chapter 2 presents the literature review of soil liquefaction potential, cyclic-loading-induced dynamic properties, and post-cyclic-loading settlement. The influence of ground temperature and freeze-thaw cycles on these parameters is reviewed.

Chapter 3 introduces the laboratory test methodology that was used in this study. A discussion is included to describe how the material used for testing was selected. Also, other subjects included are: index properties of the test material; modifications of the triaxial chamber; sample reconstitution of the test material; saturation and consolidation of test specimens, thermal conditioning of the test specimens; and the test procedure used to conduct strain-controlled cyclic tests. Raw data reduction was used to obtain the soil's liquefaction potential and dynamic properties.

Chapter 4 discusses the impact of ground temperature and freeze-thaw cycles on pore pressure generation (liquefaction potential) of fine-grained soil. The liquefaction potential of fine-grained soil is evaluated by pore pressure history and excess pore pressure generation curves among specimens conditioned at various temperatures or various freeze-thaw cycles.

Chapter 5 provides a discussion on the influence of ground temperature and freeze-thaw cycles on shear modulus and damping ratio. These dynamic properties were evaluated by comparing dynamic shear modulus and damping ratio with respect to number of loading cycles, cyclic shear strain, and excess pore pressure ratio. Moreover, degradation of dynamic shear modulus in undrained cyclic loading tests on

specimens at various temperatures or freeze-thaw cycles is analyzed. A prediction model is provided for the degradation of dynamic shear modulus at these conditions.

Chapter 6 discusses the influence of soil type (silt, silty sand and clean sand), ground temperature, and freeze-thaw cycles on post-cyclic-loading settlement of a fine-grained soil. A series of charts is produced to predict post-cyclic-loading settlement according to a given equivalent cyclic shear strain and a given number of loading cycles.

Chapter 7 presents a discussion on how the ground temperature and freeze-thaw cycles affect the soil's liquefaction potential, dynamic properties, and post-cyclic-loading settlement.

Chapter 8 summarizes findings and lists the conclusions drawn from this study.

## **2 Review of Previous Studies**

### **2.1 Impact of ground temperature and freeze-thaw process on physical and mechanical properties of soil**

Soil micro fabric, and physical and mechanical properties can be affected by soil temperature (Andersland and Anderson 1978). It has been reported that the freezing and thawing process substantially affects hydraulic conductivity of compacted silts and clays (Chamberlain and Gow 1978; Konrad 1989; Benson et al. 1995; Zimmie and La Plante 1990; Othman and Benson 1993). Chamberlain and Gow (1978) reported that the hydraulic conductivity increased with the increasing number of freeze-thaw cycles. They attributed this increase of hydraulic conductivity to the formation of ice lenses. When ice melts in frozen soil, the resulting cavities act as channels to increase the permeability of the soil. Othman and Benson (1993) showed that hydraulic conductivity could increase by one or two orders of magnitude after just one freeze-thaw cycle, but there was no further increase in hydraulic conductivity after 3 to 5 freeze-thaw cycles. Greater changes in permeability also occurred with faster rates of freezing.

Change of void ratio due to freeze-thaw processes was also reported (Konrad 1989; Viklander 1998; Qi et al. 2008). Viklander (1998) and Qi et al. (2008) reported a critical void ratio in fine-grained soil. They also showed that both both loose and dense fine-grained soil would eventually reach the critical void ratio after many freeze-thaw cycles. The variation of the pore pressure during freeze-thaw processes was recorded on saturated low-plastic clayey silt by Eigenbrod et al. (1996). They found that the pore water pressure varied cyclically during freezing. Formation of ice lenses during freezing increased pore water pressure, and this decreased the effective stress toward zero so as to speed up the formation of ice lenses. As more and more ice

lenses formed, further increase in the pore water pressure promoted suction toward the growing ice lenses adjacent to the unfrozen soil portion, and this appeared to cause the pore water pressure to decrease. Then, decreasing pore water pressure caused an increase of effective stress and thus, compressed the soil. The compression of soil inversely increased pore water pressure once more. Such cyclic variation of pore water pressure during freezing continued until steady state was reached. A sudden drop in pore water pressure was reported as a thawing began, and this was associated with a sudden drop in specific volume as ice transformed to water. As the soil continued to thaw, there was an increase in permeability and fissures, which dissipated the thawed water. This caused an increase in pore water pressure. From the above, it is clear that changes in microstructure and physical properties during freeze-thaw processes eventually can cause changes in mechanical properties.

Moreover, changes in mechanical properties are strongly affected by drainage conditions during freezing and thawing (Alkire 1981; Alkire and Morrison 1983). Alkire (1981) studied the freeze-thaw processes on a silt by conducting a series of triaxial tests for different drainage conditions during freezing and thawing. His results showed that the drained frozen and the undrained thawed condition produced the lowest post-thaw shear strength, the highest water content, and the largest strain at failure for a post-thaw state. During repeated loading tests, softer stress-strain curves and lower strength were found on undrained fine-grained soil experiencing a freeze-thaw cycle in comparison with samples not subjected to a freeze-thaw cycle (Alkire and Morrison 1983).

## **2.2 Liquefaction in partially frozen or frozen soil**

The liquefaction resistance of fine-grained soil has been extensively investigated by a number of researchers. Most previous investigations on cyclic resistance and liquefaction potential in fine-grained soils were conducted for unfrozen ground

conditions. Understanding how ground temperature or the freezing-thawing process affects liquefaction potential is difficult. It is further complicated if susceptibility to a random excitation, such as a seismic event, is to be addressed for soil at near freezing temperature (i.e., partially frozen glacial fine-grained soils).

Using field studies and numerical analysis, Finn and Yong (1978) and Finn et al. (1978) showed that sandwiched soil layers were easily liquified by seismic events when a saturated cohesionless soil layer is interstratified by a frozen surficial layer and a perennially frozen layer. This occurs because the frozen layers sealed the boundary of unfrozen saturated layers and prevented dissipation of the pore pressure that is caused by seismic events. Therefore, the liquefaction potential increased. However, the studies of Finn and Yong (1978) and Finn et al. (1978) did not consider the influence of the ground temperature, especially near-freezing temperature, on liquefaction potential.

In the past, many of the studies that were conducted to investigate the influence of the freezing and thawing processes on soil liquefaction resistance were aimed at obtaining high-quality undisturbed samples for liquefaction tests by a quick-freezing method. Goto (1993), Yoshimi et al. (1994) and Yoshimi and Goto (1996) investigated the effect of the uni-directional quick freeze-thaw cycle on liquefaction resistance of clean sand and sand with various fines ranging from 0 to 20%. They concluded that a quick uni-directional freeze-thaw cycle did not affect the liquefaction resistance of clean sand; however, the quick-freezing method disturbed clean sand with fines, and a correction factor was needed to describe liquefaction resistance. Moreover, an undrained condition during freezing was found to strongly increase disturbance of sampling, but a drained condition during freezing did not. Quick-freezing may be argued to be inconsistent with seasonal climate change (a much slower temperature change).

### 2.3 Dynamic properties of fine-grained soil

Dynamic properties of fine-grained soil are very important characteristics that reflect the soil's response under dynamic loading. Dynamic shear modulus ( $G$ ) and damping ratio ( $D$ ) are two important dynamic properties to represent the relationship between stress-strain and energy dissipation under dynamic loading. These two properties can be used to determine wave propagation and corresponding response of stress and strain in soil.

As soil is a nonlinear material, dynamic shear modulus and damping ratio in soil are determined by many factors. In unfrozen soils, it was found that factors, such as confining pressure, void ratio, geologic age, cementation, overconsolidation ratio, plasticity index, cyclic strain, strain rate, and number of loading cycles, all played roles in these two properties (Hardin and Drnevich 1972; Kokusho et al. 1982; Dobry and Vucetic 1987). Based on previous studies, the effect of the above factors was summarized by Dobry and Vucetic (1987) as shown in Table 2.1.

Usually, the effect of ground temperature on dynamic properties has been investigated in frozen soil with varying water content and temperature. In past decades, many studies have been done to investigate the dynamic properties of frozen soil by using the longitudinal-wave test, cyclic triaxial test, resonant column test, and ultrasonic test. Consensus knowledge on the dynamic properties of frozen soil has been obtained. Temperature, strain amplitude, frequency, confining pressure, and void ratio or water content—all these factors influence the dynamic stiffness and the damping properties of frozen soil (Stevens 1975; Andersland and Anderson 1978; Vinson 1978; Czajkowski and Vinson 1980; Vinson et al. 1983; Fukuda and Huang 1991). These conclusions are summarized in Table 2.2.

Decrease of temperature in frozen soil below the thaw point generally increases



dynamic stiffness and decreases damping ratio. Also, an increase in water content generally increases dynamic stiffness and decreases damping ratio at a temperature close to the thaw point. The situation is reverse when the temperature decrease is far below the thaw point (Stevens 1975; Andersland and Anderson 1978; Vinson 1978; Czajkowski and Vinson 1980; Vinson et al. 1983; Fukuda and Huang 1991). Prior to this study, the investigation of the influence of the near-freezing temperature in fine-grained soil on dynamic properties was limited.

**Table 2.1 Effect of various factors on maximum shear modulus ( $G_{\max}$ ), modulus reduction ( $G/G_{\max}$ ), and damping ratio (D) of normally consolidated and moderately overconsolidated clays (after Dobry and Vucetic 1987)**

Increasing factor	$G_{\max}$	$G/G_{\max}$	D
Confining pressure, $\sigma'_0$	Increases with $\sigma'_0$	Stays constant or increases with $\sigma'_0$	Stays constant or decreases with $\sigma'_0$
Void ratio, e	Decreases with e	Increases with e	Decreases with e
Geologic age, $t_g$	Increases with $t_g$	May increase with $t_g$	Decreases with $t_g$
Cementation, c	Increases with c	May increase with c	May decrease with c
Overconsolidation, OCR	Increases with OCR	Not affected	Not affected
Plasticity index, PI	Increases with PI if OCR>1; Stays about constant if OCR=1	Increases with PI	decreases with PI
Cyclic strain, $\gamma$	--	Decreases with $\gamma$	Increases with $\gamma$
Strain rate, $\dot{\gamma}$ (frequency of cyclic loading)	Increases with $\dot{\gamma}$	G increases with $\dot{\gamma}$ ; G/G <sub>max</sub> probably not affected if G and G <sub>max</sub> are measured at same $\dot{\gamma}$	Stays constant or may increase with $\dot{\gamma}$
Number of loading cycles, N	Decreases after N cycles of large $\gamma$ but recovers later with time	Decreases after N cycles of large $\gamma$ ( $G_{\max}$ measured before N cycles)	Not significant for moderate $\gamma$ and N

**Table 2.2 Effect of various factors on shear modulus (G) and damping ratio (D) of frozen soil (combine data from Stevens 1975; Andersland and Anderson 1978; Vinson 1978; Czajkowski and Vinson 1980; Vinson et al. 1983; Fukuda and Huang 1991)**

Increasing factor	G	D
Temperature below freezing point, T	Decreases with T	Increases with T; increasing rate of D increases with T
Cyclic strain, $\gamma$	Decreases with $\gamma$	increases with $\gamma$
Frequency, f	Increases with f; Change rates of G in low f is greater than change rates of G in high f	Decreases with f; Change rates of D in low f is greater than change rates of D in high f
Confining pressure, $\sigma'_0$	Not affected	Not affected, except that D tends to decrease with $\sigma'_0$ at T close to freezing point
Water content, WC	Increases with WC at high below-freezing temperature; Decreases with WC at low below-freezing temperature;	Decreases with WC at high below-freezing temperature; Increases with WC at low below-freezing temperature;
Plasticity index, PI	Increases with PI	decreases with PI
Cyclic strain, $\gamma$	Decreases with $\gamma$	Increases with $\gamma$
Strain rate, $\dot{\gamma}$ (frequency of cyclic loading)	G increases with $\dot{\gamma}$ ; $G/G_{\max}$ probably not affected if G and $G_{\max}$ are measured at same $\dot{\gamma}$	Stays constant or may increase with $\dot{\gamma}$
Number of loading cycles, N	Decreases after N cycles of large $\gamma$ ( $G_{\max}$ measured before N cycles)	Not significant for moderate $\gamma$ and N

## 2.4 Post-cyclic-loading-induced settlement

Soil liquefaction not only causes loss of soil strength, but also subsidence of the ground surface. After a seismic event, volume change of the soil deposit is usually found with dissipation of excess pore water pressure. This change in volume is manifested as settlement of the ground surface. Dramatic settlements are often observed after earthquakes. Volumetric strains about 1% to 10% and maximum settlements of more than 0.5m have been observed during previous earthquakes:

Niigata Earthquake 1964, Tokachi-oki Earthquake 1968 and Nihonkai-chubu Earthquake 1983 (Nagase and Ishihara 1988). Since ground subsidence always causes the greatest damage to the infrastructure and land based structures, investigation of post-cyclic-loading settlement is very important.

#### **2.4.1 Influence factors on post-cyclic-loading-induced settlement**

Lee and Albaise (1974) conducted cyclic triaxial tests on 6 different uniformly graded clean sand samples with medium grain size from 0.1mm to 3.0mm in order to investigate earthquake induced settlement. The impact of effective confining pressures (varied from 15 psi to 60 psi) and relative densities (varied from 30% to 85%) on the reconsolidated volumetric strain,  $\epsilon_v$ , which is the ratio of the discharged water volume,  $\Delta V$ , to the gross soil volume,  $V$ , was studied respectively. Static loading was also applied to check the influence of loading types. Results of the study revealed that reconsolidated volumetric strain under non-liquefaction conditions increased with an increase in effective confining pressure, an increase in grain size of the soil, a decrease of relative density, and an increase of excess pore pressure. The types of static loading and cyclic loading did not affect reconsolidated volumetric strain.

Nagase and Ishihara (1988) conducted irregular cyclic shear tests on Fuji River sand under uni-directional and multi-directional loading conditions. Specimens with relative density of 47%, 73%, and 93% were studied. The results indicated that the reconsolidated volumetric strain was uniquely dependent on the excess pore pressure under no-liquefaction conditions; however, under liquefaction conditions, maximum shear strain replaced the excess pore pressure as the controlling factor for the reconsolidated volumetric strain. The direction of irregular loading was found to have no effect on the reconsolidated volumetric strain.

Ohara and Matsuda (1988) investigated the settlement induced by undrained cyclic

strain-controlled simple shear test strain tests on Kaolin Clay. The parameters including number of loading cycles from 10 to 200, cyclic shear strain from 0.05% to 3%, and an overconsolidation ratio from 1 to 6 were investigated. These studies were done to understand the mechanism of cyclic-loading-induced settlement on clay. Ohara and Matsuda (1988) found that the clay's seismic settlement was dependent on the overconsolidation ratio and excess pore pressure. This was true, regardless of the number of cycles and cyclic shear strain. It was found that increasing overconsolidation ratio and decreasing excess pore pressure decreased cyclic-loading-induced settlement.

Chien et al. (2002) compared the influence of the fine content on the seismic settlement on Yunlin sand with 0-30% fines and relative densities from 35% to 75%. Their conclusion showed that decrease of relative density and increase of fine contents increased the liquefaction-induced settlement. However, Derakhshandia et al. (2008) conducted cyclic loading tests on Monterey sand with 0-20% fines and found that fine contents did not cause much difference on cyclic-loading-induced settlement under non-liquefaction conditions.

#### **2.4.2 Prediction of post-cyclic-loading-induced settlement**

Tokimatsu and Seed (1987) developed prediction charts for earthquake induced settlement in saturated sand under non-liquefaction and liquefaction conditions. They pointed out that in liquefaction conditions, earthquake induced settlement of saturated sand could be derived from the equivalent cyclic stress ratio and soil's SPT-N value. But for non-liquefaction conditions, earthquake induced settlement was determined by generated excess pore pressure ratio or normalized stress ratio.

Ishihara (1996) proposed a better prediction chart by coordinating the relationship between the volume change of saturated sand and maximum shear strains and the

relationship between the factor of safety and the maximum shear strains. This chart could be used to predict the post-cyclic-loading settlement directly from the factor of safety against liquefaction and SPT-N value (or relative density) regardless of non-liquefaction or liquefaction conditions, as shown in Figure 2.1.

Tsukamoto et al. (2004) provided a procedure for evaluating post-liquefaction settlement on silty sand with about 20% fines by using the irregular excitation time history simulating the 1995 Kobe Earthquake. This procedure used the relationships between factor of safety against liquefaction, relative density, and reconsolidated volumetric strain to derive the post-liquefaction settlement.

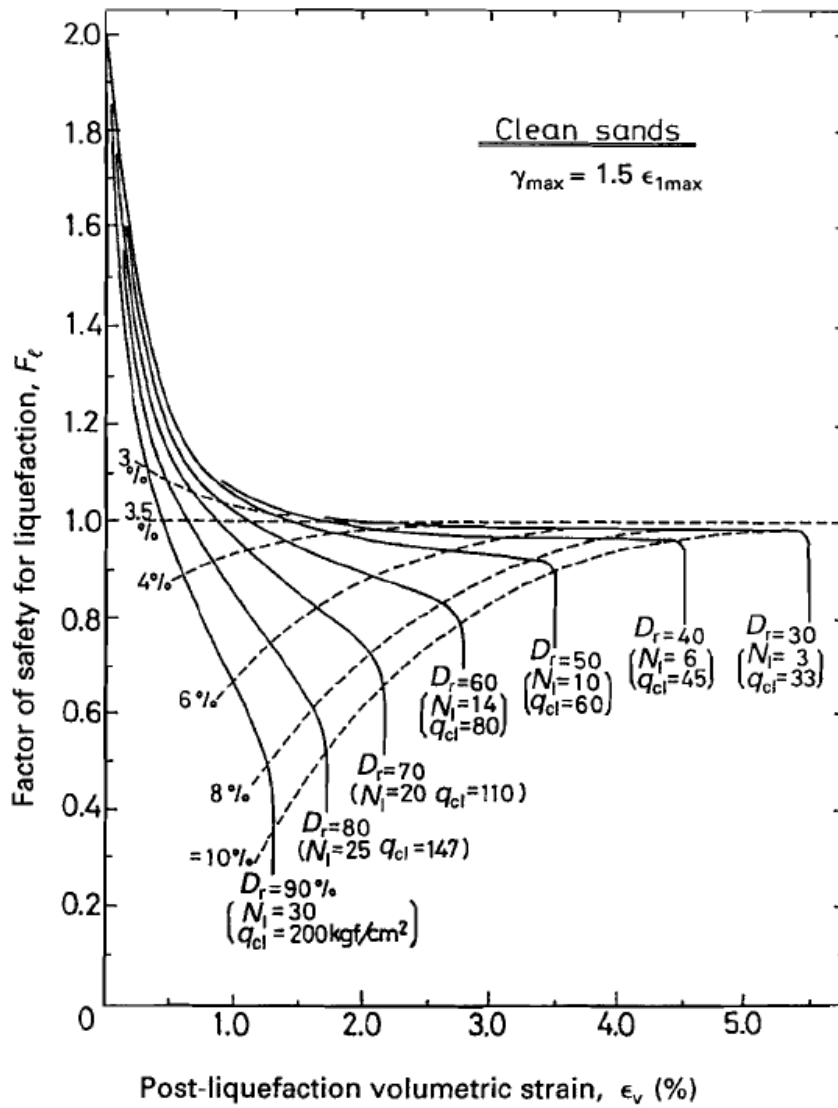


Figure 2.1 Chart for determination of post-liquefaction volumetric strain as a function of factor of safety (after Ishihara 1996)

### **3 Experimental Program**

Cyclic triaxial, undrained, stress-controlled and strain-controlled tests were conducted on a fine-grained soil to investigate liquefaction potential, dynamic properties, and cyclic-loading-induced settlement. Two series of tests were carried out. The first series of tests was performed on specimens conditioned at 24 °C, 5 °C, 1 °C, 0.5 °C, and -0.2 °C. This series focused on the impact of ground temperature, especially at near-freezing state, on excess pore pressure generation and cyclic resistance. The second series of tests was conducted on specimens subjected to various numbers of freeze-thaw cycles. This was done to investigate how freeze-thaw cycles affect: a) excess pore pressure generation and b) the dynamic characteristics. To evaluate cyclic-loading-induced settlement, the results from all of the tests performed throughout this study were used. At the end of each test, the drainage valves on the triaxial test chamber were opened and the volume change with dissipation of pore water pressure was measured.

#### **3.1 Material tested**

Soil samples were obtained from a site near Mabel Creek Bridge and Slana River Bridge on the Tok Cutoff Highway in Alaska, as shown in Figure 3.1. An excavator was used to dig down approximately 3 meters deep in the bank of Mabel Creek. Disturbed soil samples were collected for the purpose of reconstituting soil specimens in the laboratory. This soil will be referred to as Mabel Creek silt throughout this document. The reason why this specific site was selected for soil sampling is that extensive liquefaction and associated damages were observed at and around this location during the November 3, 2002, Denali Earthquake ( $M_w=7.9$ ). The maximum horizontal and vertical deformations around the Slana River bridge (see Figure 3.2), which is about 1 km south of the Mabel Creek bridge, were measured to be about 75 cm and 45 cm, respectively.

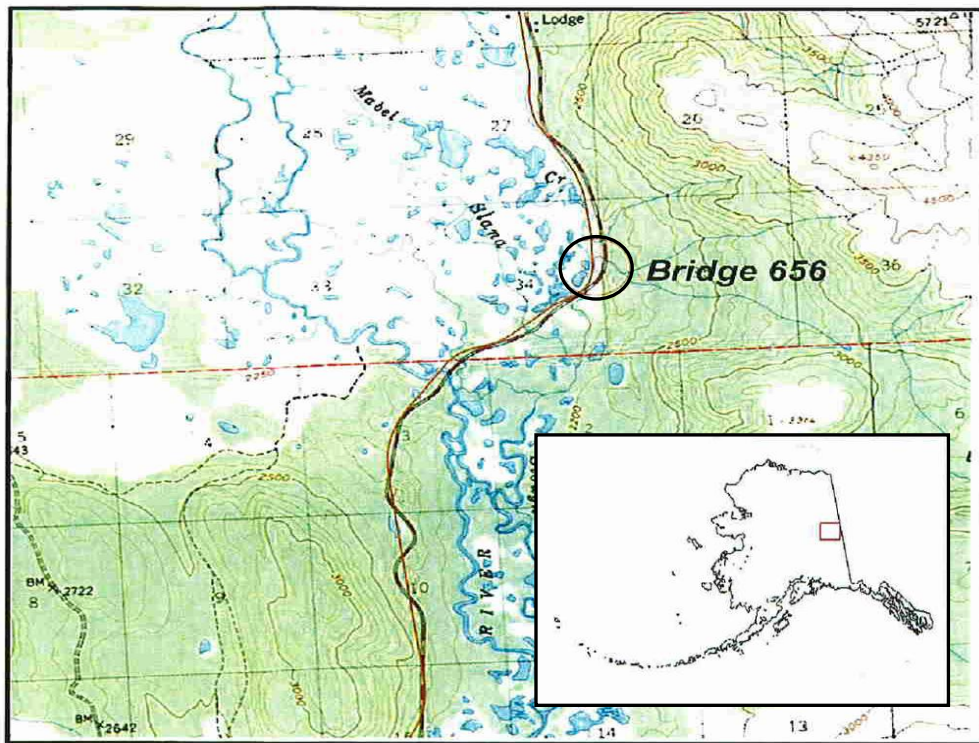


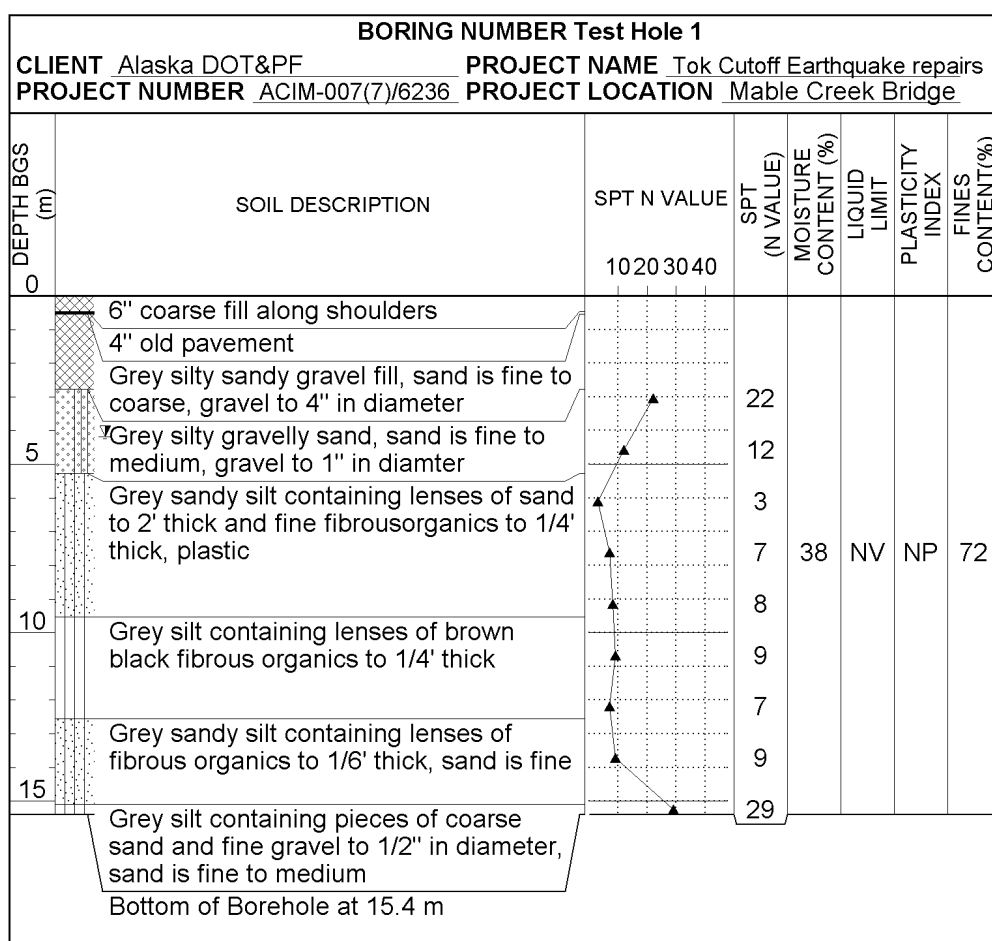
**Figure 3.1** Sampling location at milepost 76.2 on the Tok Cutoff Highway in Alaska



**Figure 3.2** Liquefaction-induced lateral spreading in Tok Cutoff Highway embankment (abutment of Slana River Bridge embankment, which is 1 km away from Mabel Creek Bridge)

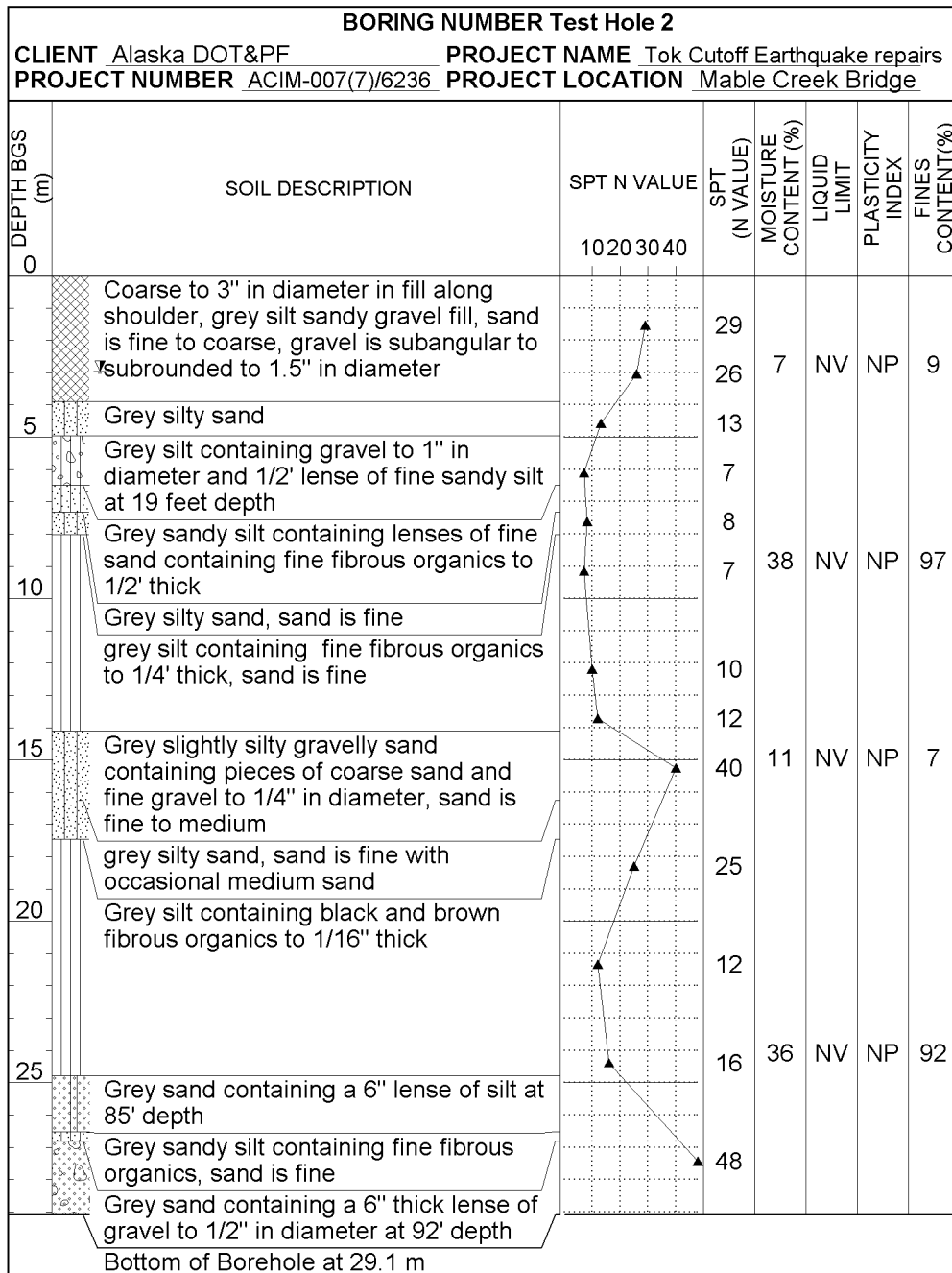


After the earthquake, Alaska Department of Transportation and Public Facilities (AK DOT&PF) initiated a repair program for the damaged transportation infrastructure around the site. Through this repair program a fairly extensive site investigation was conducted. Four boring logs from the site are presented in Figure 3.3. To better evaluate the stratigraphy, SPT results from the four boreholes are replotted together and presented in Figure 3.4. Consisting mainly of silt, the layer of concern in these profiles is located below the top layers of fill at about a 6 to 12 m depth below the ground surface. The SPT-values ( $N_{60}$ ) were relatively low, ranging from 4 to 12. Due to the relatively shallow water table, which is located at approximately 2.95-4.05 m below the ground surface, the layer of concern was fully saturated.



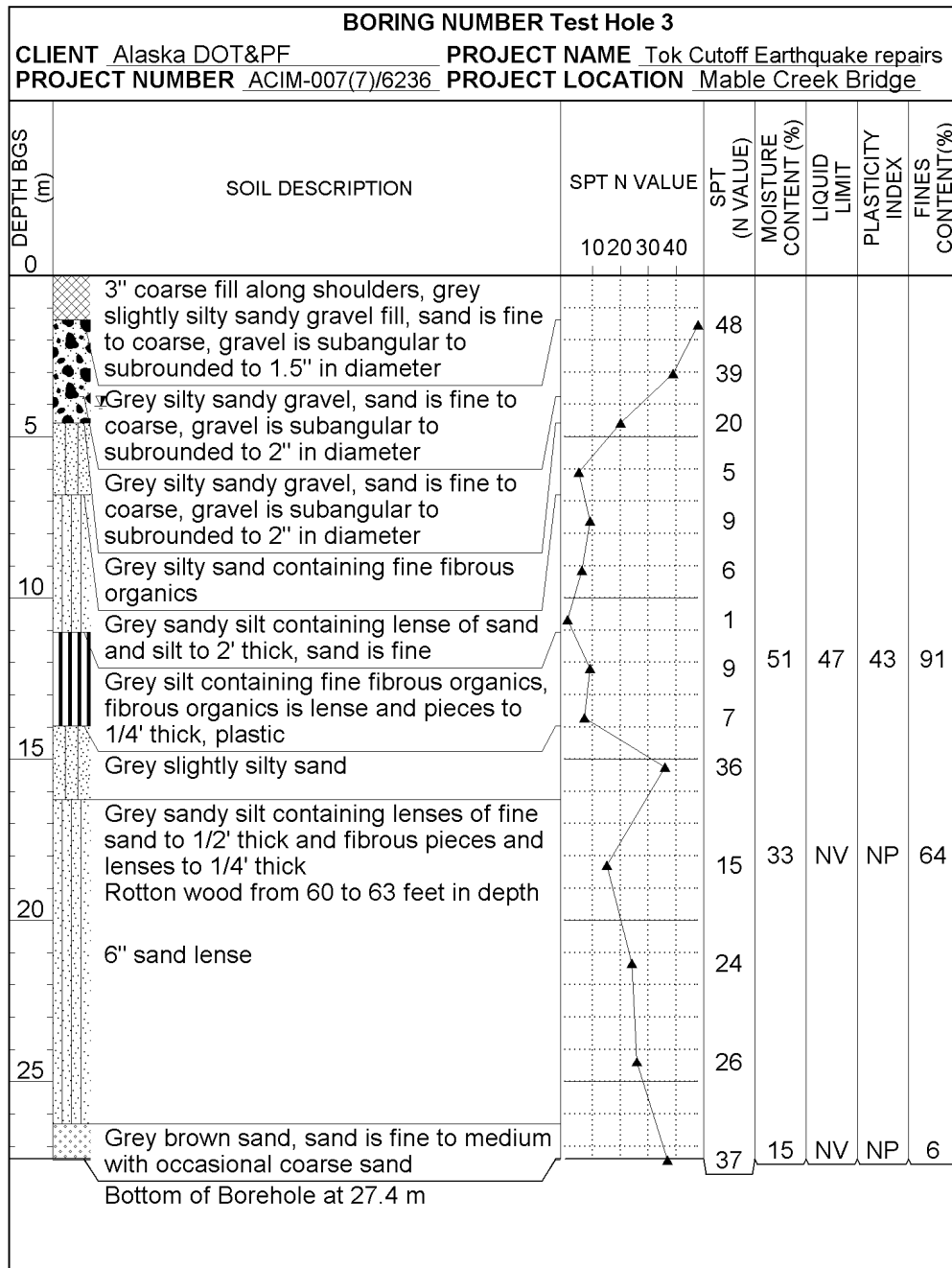
(a) Test log in Bore Hole 1

**Figure 3.3 Test log in bore holes (after MACTEC Engineering and Consulting 2004)**



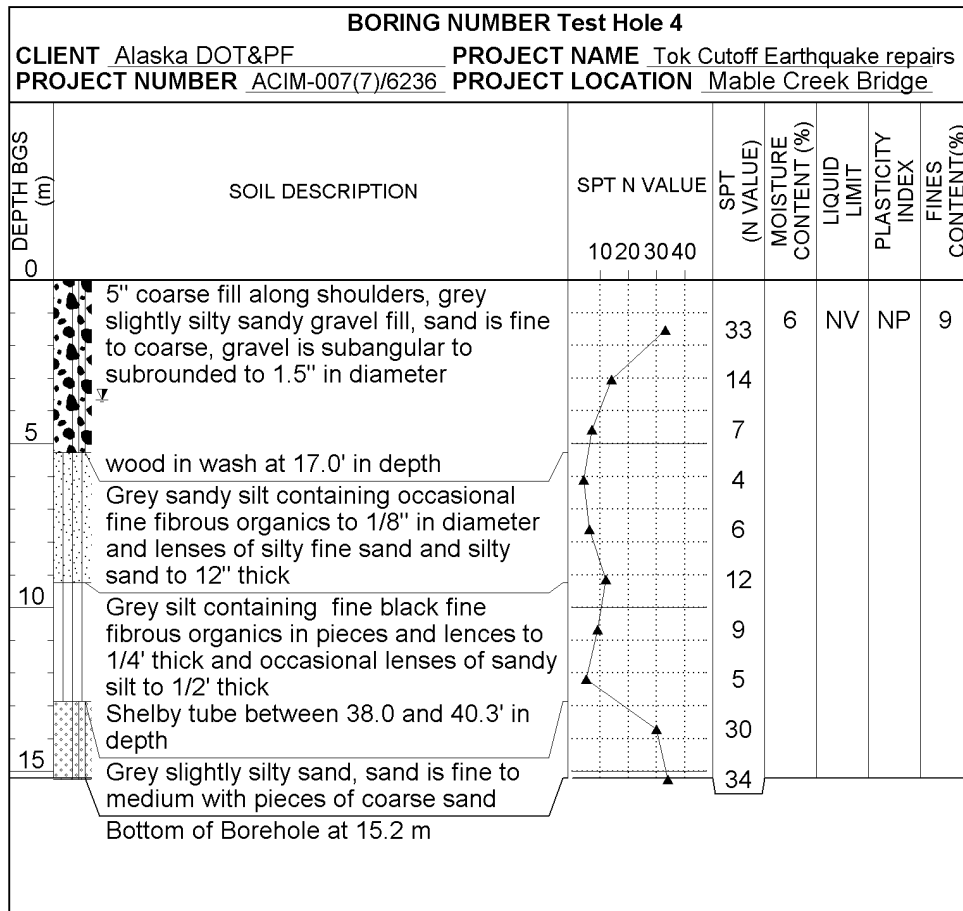
(b) Test log in Bore Hole 2

Figure 3.3 Test log in bore holes (after MACTEC Engineering and Consulting 2004)



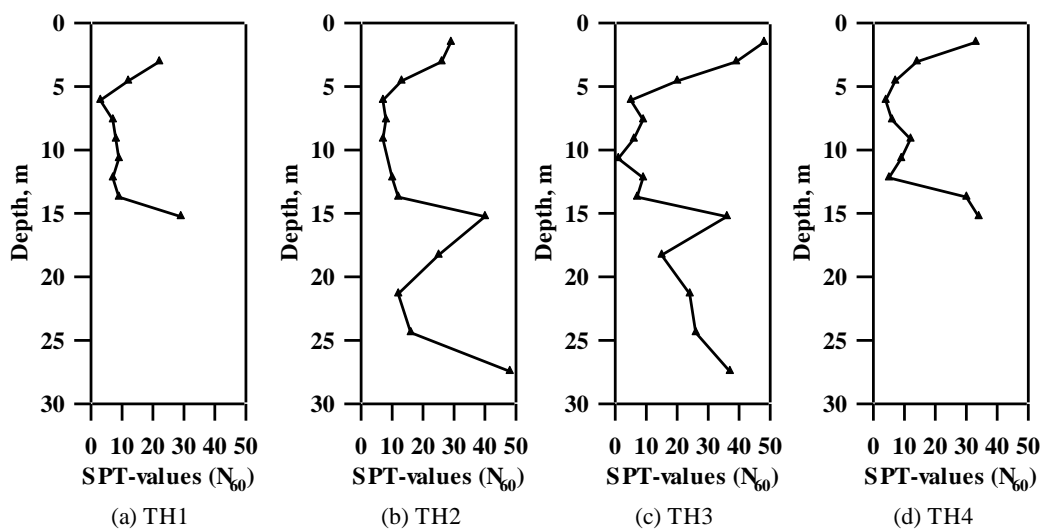
(c) Test log in Bore Hole 3

Figure 3.3 Test log in bore holes (after MACTEC Engineering and Consulting 2004)



(d) Test log in Bore Hole 4

**Figure 3.3 Test log in bore holes (after MACTEC Engineering and Consulting 2004)**



**Figure 3.4 SPT value in tested bore holes (after MACTEC Engineering and Consulting 2004)**

A series of conventional geotechnical tests were conducted to characterize Mabel Creek silt. Index properties including grain size distribution, specific gravity, Atterberg limits, optimum water content, and maximum and minimum index void ratios were determined. The results from these tests are summarized in Table 3.1.

The grain size distribution of Mabel Creek silt was determined in general accordance with ASTM D422-63, Standard Test Method for Particle Size Analysis of Soils. The Mabel Creek silt may be classified as an ML type soil as per USCS. Approximately 99% of this soil was measured to pass through No. 200 sieve (74  $\mu\text{m}$ ). The mean grain size  $D_{50}$  was found to be 0.007 mm. The coefficient of uniformity,  $C_u$ , was measured as 7.50 and the coefficient of curvature,  $C_c$ , was found to be 1.48. The grain size distribution is presented in Figure 3.5.

**Table 3.1 Soil index properties of Mabel Creek silt**

USCS Classification Symbol	ML
Specific Gravity, $G_s$	2.78
D10	0.0012 mm
D50	0.007 mm
D60	0.009 mm
Coefficient Of Uniformity, $C_u$	7.50
Coefficient Of Curvature, $C_c$	1.48
Liquid Limit (%)	34.5 %
Plastic Limit (%)	29.2 %
Plasticity Index	5.3
Optimum Water Content (ASTM D1557)	20.2 %
Maximum Dry Unit Weight(ASTM D1557)	1570 kg/m <sup>3</sup>
Max Index Density(ASTM D4253)	1270 kg/m <sup>3</sup>
Min Index Void Ratio(ASTM D4253)	1.18
Min Index Density(ASTM D4254)	600 kg/m <sup>3</sup>
Max Index Void Ratio(ASTM D4254)	3.67

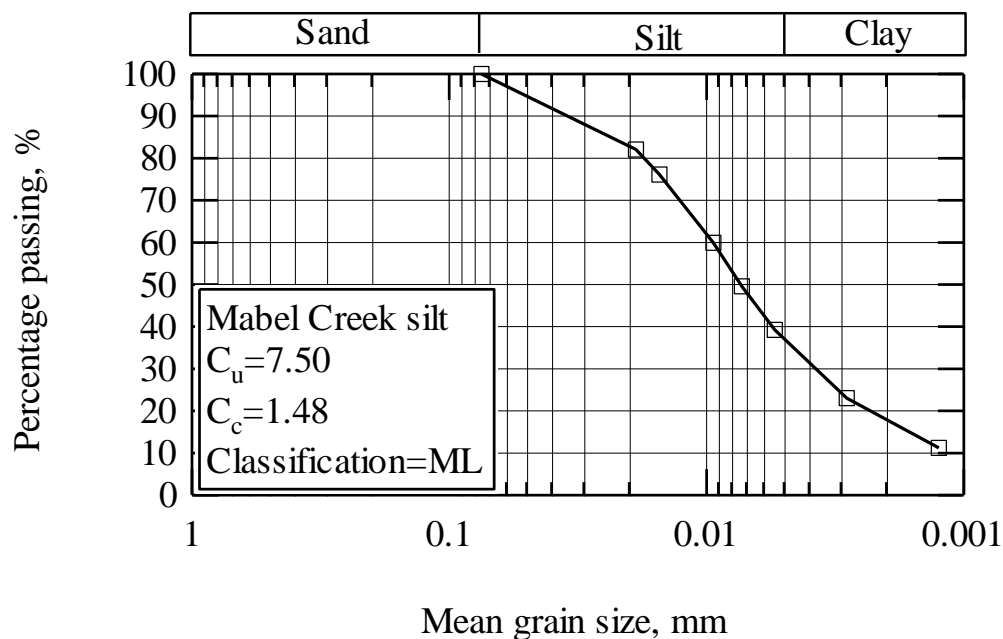


**Figure 3.5 Grain size distribution of Mabel Creek silt**

The specific gravity for each soil was determined in general accordance with ASTM D854-00, Standard Test Method for Specific Gravity of Soil. It was found to be 2.78.

The liquid and plastic limits of the Mabel Creek silt were measured in accordance with the procedures outlined in ASTM D4318-00. The plastic limit was measured as 29.2% and the liquid limit was measured as 34.5%. These measurements indicate a plasticity index of 5.3, which refers to a low plasticity type soil.

ASTM D1557-02 was applied to determine the optimum moisture content and the corresponding dry density of the Mabel Creek silt.

Dry soil samples were weighed to approximately 2kg. Water was measured to 0.1g of the target moisture content for each test. Target moisture contents of up to 20% of the dry soil weight were tested in about 5% increments. The soil and water test samples were hand mixed and stored in sealed plastic bags for a minimum of 24 hours before compaction.

The modified compaction was performed by a Soil Test Mechanical Soil Compactor (model CN-4235) in 4 inch diameter molds conforming to the requirements of ASTM D1557-02. Each test was performed in 5 lifts and 25 blows per lift using a round foot on the mechanical rammer.

After compaction, the test samples were dried, either in whole or in part, to determine the resulting moisture content. The optimum water content and the corresponding dry density were found to be 20.2% and  $1570 \text{ kg/m}^3$ , respectively, and are shown in Figure 3.6.

There is no ASTM procedure to determine the maximum index density (i.e., minimum void ratio) for silt. The ASTM D4253-00 procedure, which determines maximum index density of soils using a vibration table, is limited to soils with less than 15% fine content. Hazirbaba (2005) performed vibratory table tests and Modified Proctor compaction tests to determine the minimum void ratios of a sand with different fine contents and concluded that smaller void ratio values (i.e., denser state of soil) may be obtained from Modified Proctor test at fines content larger than 20%. Thus, the Modified Proctor procedure (ASTM D1557-02) was adopted for determining the minimum void ratio of Mabel Creek silt. Through this approach, the minimum index void ratio ( $e_{min}$ ) for Mabel Creek silt was found to be 0.77 with a corresponding maximum index density ( $\gamma_{max}$ ) of  $1570 \text{ kg/m}^3$ .

The ASTM procedure for minimum index density (ASTM D4254-00) is similarly limited to soils with less than 15% fine content. Despite this limitation, repeatable minimum index density values for Mabel Creek silt were successfully obtained from the two applicable methods, namely Method B and Method C, presented in the ASTM D4254-00 specification. The measured minimum index density values were  $600 \text{ kg/m}^3$  from Method B and  $620 \text{ kg/m}^3$  from Method C. Because the repeatability of the result from Method B was slightly better, the result from Method B was used as the

minimum index density with a corresponding maximum void ratio of 3.67.

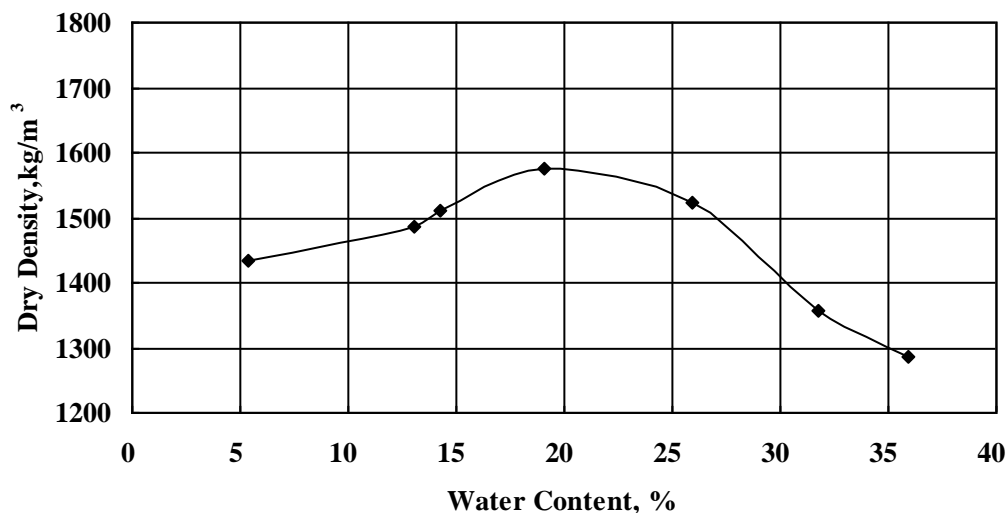


**Figure 3.6 Optimum moisture content curve for Mabel Creek silt**

### 3.2 Cyclic triaxial tests

In terms of loading conditions, the two commonly used approaches for conducting cyclic triaxial tests are: 1) stress-controlled approach, and 2) strain-controlled approach. The strain-controlled approach was adopted as the core testing procedure for this study because the main mechanism for the occurrence of liquefaction under seismic loading conditions is the generation of excess pore water pressure, and the generation of excess pore pressure is more directly related to the induced shear strains than stresses (Hazirbaba 2005). Additionally, strain-controlled tests provide more realistic pore pressure measurements than stress-controlled tests, and generation of excess pore water pressure in strain-controlled tests is less sensitive to factors such as relative density, soil fabric, and previous loading (Dobry et al. 1982). Thus, a more fundamental approach to study the seismic response and liquefaction potential of soils would be to examine the pore water pressure generation mechanism directly through strain-controlled cyclic tests.



### **3.2.1 University of Alaska Fairbanks (UAF) cyclic triaxial apparatus**

MTS type triaxial (TX) equipment was employed to carry out the cyclic loading testing program for this study. A sketch of the testing system used is shown in Figure 3.7, and a picture of the triaxial cell is presented in Figure 3.8. The testing equipment was modified to closely simulate the in-situ freezing process of soils. The top cap and bottom platen of the triaxial setup were designed to be connected to an external cooling unit, which allows for controlling the temperature of the triaxial specimen. Additionally, antifreeze coolant was used to further decrease the temperature of the soil specimen. The antifreeze coolant was gone through a helical brass coil surrounding the triaxial specimen to create a multi-dimensional freezing process. To minimize heat loss and help maintain a constant target temperature during the freezing process, the triaxial cell was insulated with a Styrofoam box. To continuously monitor and control the temperature inside the triaxial cell and around the soil specimen, six (6) separate thermistors were installed, as shown in the schematical drawing in Figure 3.7. The displacement was measured with a high precision LVDT, and the load was monitored using a load cell. Details of the sensors used are presented in Table 3.2.

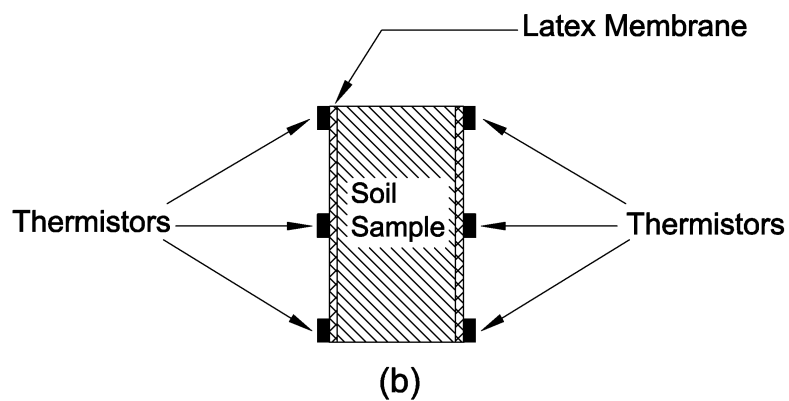
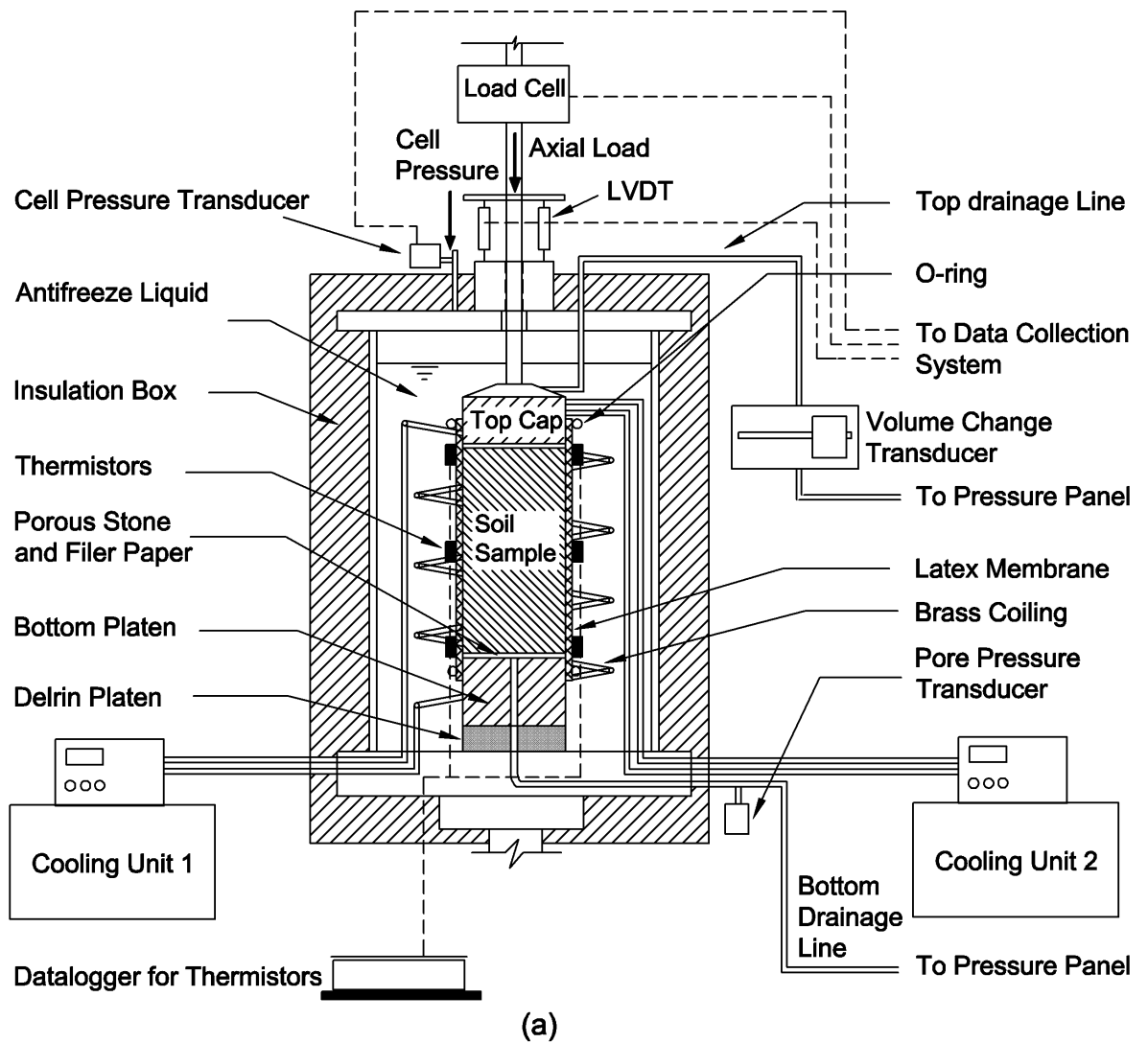
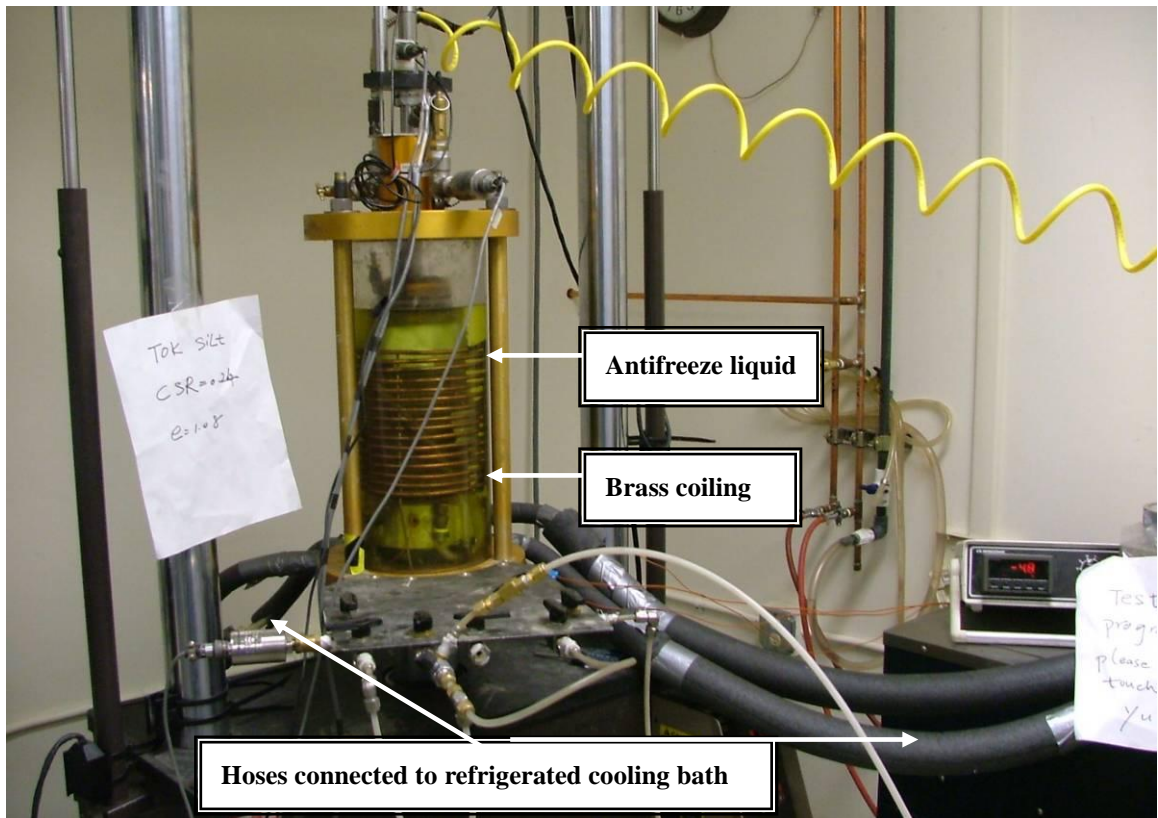


Figure 3.7 (a) schematic drawing of test apparatus (b) installation of thermistors in cylindrical triaxial soil specimen



**Figure 3.8** Modified triaxial test system

**Table 3.2** Setup and the sensors used in triaxial system

Setup or sensors	Range	Sensitivity
External cooling unit	-50 °C~40 °C	±0.02 °C
Thermistor	-80 °C~75 °C	±0.1 °C
Precision LVDT	± 0.50 mm	±0.001 mm
Load cell	± 500 lb	± 1 lb
Pore water pressure transducer	± 100 psi	±0.20 psi
Volume change transducer	80 ml	± 1 ml

### 3.2.2 Specimen preparation, saturation, and consolidation

The specimens tested were 101.6 mm in diameter and 211.0mm in height. They were reconstituted by the undercompaction method (Ladd 1978) with initial water content that produced 50 % saturation in the specimen. The moist soil was placed in layers within the mold. To compensate for densification during compaction, the bottom layers were formed to have slightly looser densities than the layers above them. Thus, approximately uniform density distribution throughout the specimen could be attained through the whole compaction process. The drilling borehole data (Figure 3.3) showed that the fully saturated Mabel Creek silt layer had a water content of about 38%. Using the measured specific gravity of 2.78 for Mabel Creek silt, the average in situ void ratio corresponding to 100 kPa effective confining pressure was found to be 1.06. Thus, all specimens were prepared at a target void ratio of 1.06. The procedure for calculating the void ratio is presented in Appendix A. The slight densification that typically occurred during saturation and consolidation was accounted for by forming the specimens at an initial void ratio of 1.08. A list of the tests performed is presented in Table 3.3, Table 3.4, Table 3.5, and Table 3.6. Here the unfrozen specimen in those tables is referred to as the specimen without any freezing or thawing conditioning.

To help expedite the saturation process, the specimen was first percolated with carbon dioxide for about 1 hour at a pressure difference (i.e., the head between top and bottom of the specimen) of approximately 10 kPa. Then, the specimen was flushed with de-aired water. The flushing of de-aired water at a relatively low pressure difference of 15 kPa was completed in about 24 hours. Full saturation of the specimen was achieved through application of backpressures of approximately 100 kPa. After a minimum acceptable B-value of 0.95 was obtained, the consolidation procedure was started. All of the specimens were isotropically consolidated to the desired effective confining stress of approximately 100 kPa. Some of the tests were conducted at a slightly higher or lower effective confining stress than 100 kPa. This was due to the

fluctuation in the air pressure source over the long duration of testing (especially for specimens conditioned at different temperatures). Nonetheless, constant effective confining stress was maintained throughout each test. Following completion of consolidation, the group of specimens prepared for the study of moderate ground conditions (i.e., unfrozen soil) were directly subjected to undrained cyclic strain-controlled triaxial tests. The testing procedures after the consolidation stage for the specimens that were conditioned to a target temperature and for those subjected to freeze-thaw-cycles are discussed in the following section.

**Table 3.3 Cyclic strain-controlled tests on unfrozen Mabel Creek silt specimens**

Test No.*	Post-consolidation void ratio (e)	Effective confining pressure, kPa ( $\sigma'_3$ )	B-value at the end of saturation (B)	Cyclic shear strain,% ( $\gamma$ )
U1	1.052	102	0.98	0.005
U2	1.052	101	0.98	0.010
U3	1.052	101	0.98	0.030
U4	1.055	101	0.96	0.050
U5	1.052	103	0.97	0.100
U6	1.056	101	0.97	0.300
U7	1.050	101	0.95	0.800

Note: U: Unfrozen silt specimen

**Table 3.4 Cyclic strain-controlled tests on Mabel Creek silt specimens conditioned to a target temperature**

Test No.*	Post-consolidation void ratio (e)	Effective confining pressure, kPa ( $\sigma'_3$ )	B-value at the end of saturation (B)	Cyclic shear strain,% ( $\gamma$ )
F2401	1.052	98	0.97	0.005
F2402	1.052	98	0.97	0.100
F2403	1.041	98	0.97	0.300
F2404	1.038	101	0.98	0.800
F501	1.056	107	0.98	0.005
F502	1.056	107	0.98	0.100
F503	1.051	100	0.98	0.300
F101	1.056	100	0.98	0.005
F102	1.056	100	0.98	0.100
F103	1.066	108	0.98	0.300
F051	1.046	102	0.96	0.005
F052	1.046	101	0.96	0.100
F053	1.052	100	0.95	0.300
FN021	1.051	106	0.98	0.030
FN022	1.051	97	0.97	0.100

Note: F240: Specimen conditioning at 24.0 °C  
 F50: Specimen conditioning at 5.0 °C  
 F10: Specimen conditioning at 1.0 °C  
 F05: Specimen conditioning at 0.5 °C  
 FN02: Specimen conditioning at -0.2 °C

**Table 3.5** Cyclic strain-controlled tests on Mabel Creek silt specimens subjected to freeze-thaw cycles

Test No.*	Post-consolidation void ratio (e)	Effective confining pressure, kPa ( $\sigma'_3$ )	B-value at the end of saturation (B)	Cyclic shear strain,% ( $\gamma$ )
FT201	1.050	103	0.97	0.010
FT202	1.045	101	0.98	0.100
FT203	1.050	102	0.97	0.300
FT204	1.044	101	0.96	0.800
FT401	1.046	101	0.98	0.005
FT402	1.043	103	0.97	0.100
FT403	1.046	101	0.98	0.300
FT404	1.039	102	0.99	0.800

Note: FT20: Specimen experienced 2 freeze-thaw cycles

FT40: Specimen experienced 4 freeze-thaw cycles

**Table 3.6** Cyclic strain-controlled tests on Mabel Creek silt specimens subjected to freeze-thaw cycles

Test No.*	Post-consolidation void ratio (e)	Effective confining pressure, kPa ( $\sigma'_3$ )	B-value at the end of saturation (B)	Cyclic shear strain,% ( $\gamma$ )
F05P21	1.051	100	0.97	0.005
F05P22	1.051	100	0.97	0.300
F05P23	1.038	101	0.98	0.800
F05P31	1.053	101	0.98	0.005
F05P32	1.053	101	0.98	0.300
F05P33	1.060	101	0.98	0.800
FN02P21	1.046	101	0.95	0.050
FN02P22	1.061	102	0.96	0.100
FN02P31	1.069	101	0.98	0.050
FN02P32	1.061	102	0.96	0.100

Note: F05P22: Specimen at 0.5 °C by Path 2

F05P23: Specimen at 0.5 °C by Path 3

FN02P22: Specimen at -0.2 °C by Path 2

FN02P23: Specimen at -0.2 °C by Path 3

### **3.2.3 Specimen thermal conditioning**

As discussed earlier, two series of tests were performed. In the first series of tests, where the impact of various ground temperatures was the subject of investigation, each soil specimen was first brought to the frozen state and then conditioned to a target temperature. For the second series of specimens, where the impact of freeze-thaw cycles on cyclic resistance and dynamic characteristics was the subject of investigation, soil specimen conditioning was achieved by a target number of freeze-thaw cycles. The details for each of these conditioning are outlined below.

#### **3.2.3.1 Thermal conditioning at 24 °C, 5 °C, 1 °C, 0.5 °C, and -0.2 °C**

After consolidation, each specimen was frozen multiaxially under drained conditions at a confining effective pressure of approximately 100 kPa. During the freezing process, chilled coolant at -25 °C was circulated through the top cap and the brass coiling around the specimen. The change in temperature around the specimen was continuously monitored using thermistors, as shown in Figure 3.9. It took about 20 to 24 hours to reach a stable condition at about -10 °C, which was selected as a target freezing temperature to ensure a fully frozen state. Once the frozen state was achieved, the specimen was conditioned back to a target temperature (e.g., 24 °C, 5 °C, 1 °C, 0.5 °C, and -0.2 °C). During thermal conditioning, the change in the height of the specimen was also monitored and recorded, as shown in Figure 3.9. Conditioning was complete when the target temperature was obtained and no further change in height was observed. An acceptable target temperature existed when the thermistor readings were stable.

#### **3.2.3.2 Thermal conditioning through freeze-thaw cycles**

The conditioning of the specimens in this series was achieved through a similar procedure to the one outlined above. The only difference was that after the



fully-frozen state was achieved at  $-10^{\circ}\text{C}$ , the thawing process was initiated by exposing the triaxial cell to room temperature. In this series of tests, the soil specimens were subjected to 1, 2, or 4 freeze-thaw cycles. Since 1 to 2 conditioning freeze-thaw cycles were found to cause only a slight change in pore water pressure generation, 3 freeze-thaw cycle conditioning was skipped. After the conditioning of 2 freeze-thaw cycles, a 4 freeze-thaw cycle conditioning was conducted for the purpose of observing the apparent difference in pore water pressure generation in specimens conditioned at additional freeze-thaw cycles. Typical thermistor records of specimens subjected to freeze-thaw cycles are presented in Figure 3.10. It should be noted that the record for 1 freeze-thaw cycle is identical to that of the specimen conditioned at  $24^{\circ}\text{C}$  in the first series of tests (Figure 3.9a).

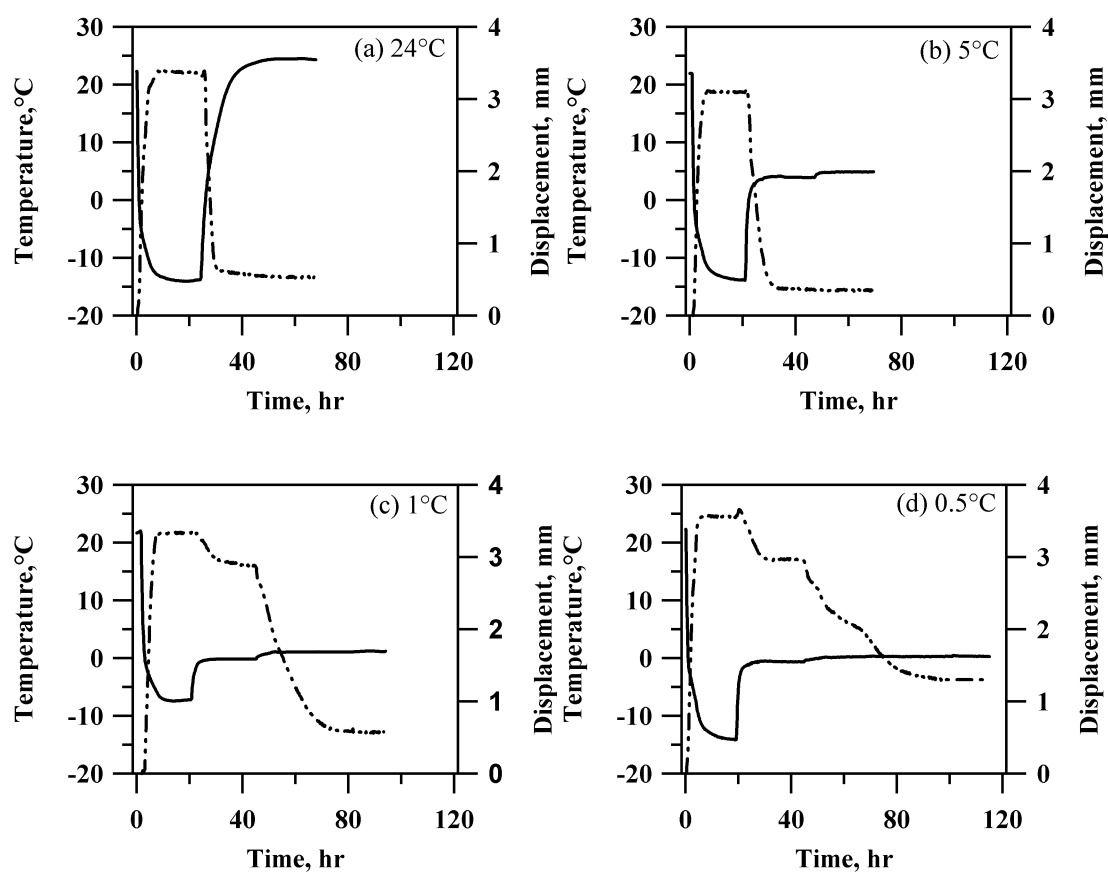


**Figure 3.9** Typical thermistor records and vertical displacements during specimen conditioning at  $24^{\circ}\text{C}$ ,  $5^{\circ}\text{C}$ ,  $1^{\circ}\text{C}$ ,  $0.5^{\circ}\text{C}$ , and  $-0.2^{\circ}\text{C}$

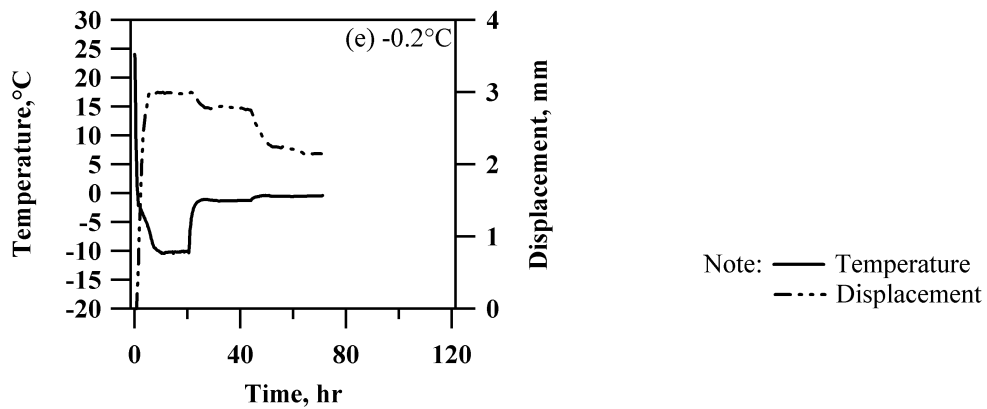


Figure 3.9 Typical thermistor records and vertical displacements during specimen conditioning at  $24^{\circ}\text{C}$ ,  $5^{\circ}\text{C}$ ,  $1^{\circ}\text{C}$ ,  $0.5^{\circ}\text{C}$ , and  $-0.2^{\circ}\text{C}$

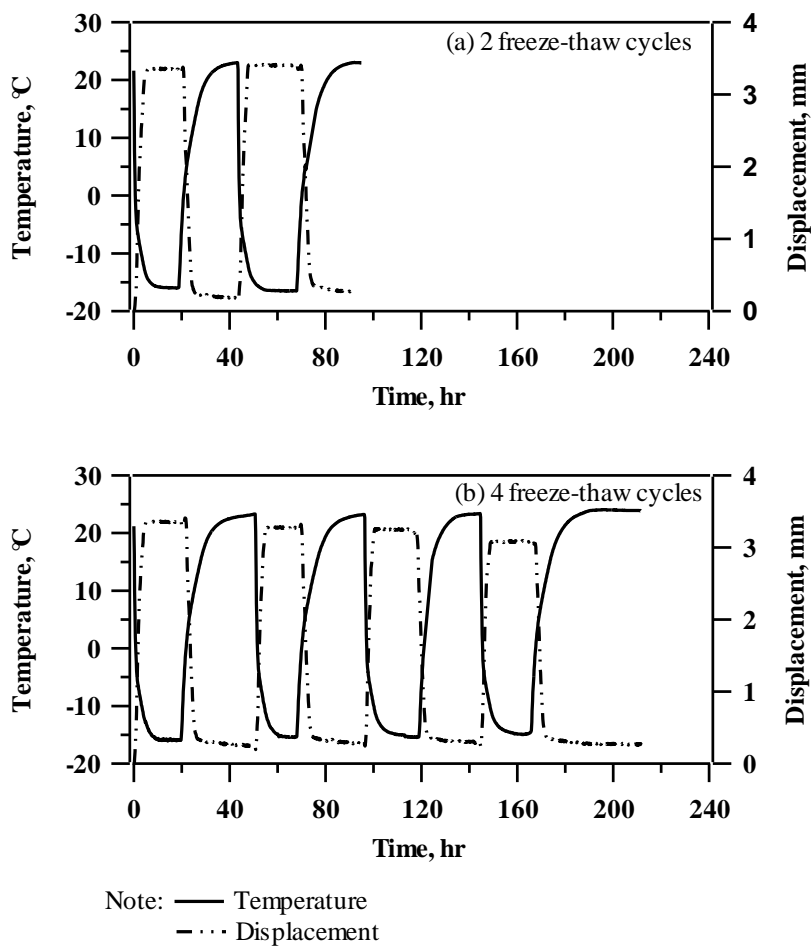


Figure 3.10 Typical thermistor records and vertical displacements from specimens subjected to freeze-thaw cycles

### 3.2.3.3 Thermal conditioning at 0.5 °C, and -0.2 °C through three different paths

To investigate if thermal conditioning paths affect dynamic response of Mabel Creek silt, the target near-freezing temperatures of 0.5 °C and -0.2 °C were reached by three different paths. All these thermal conditionings were started after consolidation. These thermal conditioning paths are displayed below:

The target temperature of -0.2 °C:

Path 1: The consolidated silt specimen → -10 °C for about 24 hrs → -1.2 °C for about 24 hrs → -0.2 °C for about 48 hrs → strain-controlled cyclic tests;

Path 2: The consolidated silt specimen → -10 °C for about 24 hrs → -0.2 °C for about 6-7 days → strain-controlled cyclic tests;

Path 3: The consolidated silt specimen → -0.2 °C for about 48 hrs → strain-controlled cyclic tests.

The target temperature of 0.5 °C:

Path 1: The consolidated silt specimen → -10 °C for about 24 hrs → -0.5 °C for about 24 hrs → 0.5 °C for about 48 hrs → strain-controlled cyclic tests;

Path 2: The consolidated silt specimen → -10 °C for about 24 hrs → 0.5 °C for about 6-7 days → strain-controlled cyclic tests;

Path 3: The consolidated silt specimen → 0.5 °C for about 48 hrs → strain-controlled cyclic tests.

Typical thermistor records from specimens at -0.2 °C and 0.5 °C through different thermal conditioning paths are presented in Figure 3.11. Thermal Conditioning Path 1 for -0.2 °C and 0.5 °C is shown in Figure 3.9d and Figure 3.9e.

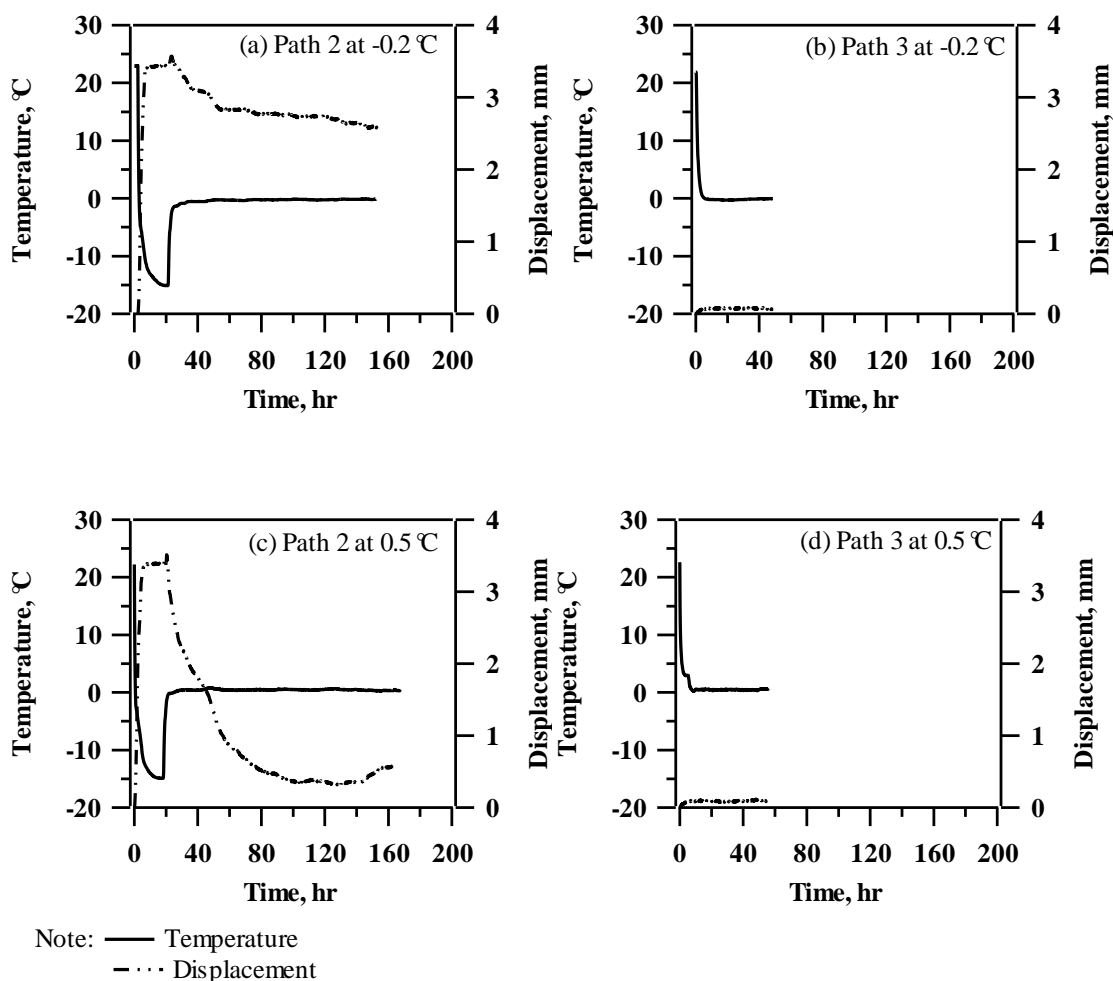


**Figure 3.11** Typical thermistor records and vertical displacements during specimens conditioning at 0.5 °C and -0.2 °C through different paths

### 3.2.4 Cyclic triaxial strain-controlled test

Following thermal conditioning, the triaxial test chamber drainage valves were closed and a cyclic loading test was started. Sinusoidal strain amplitudes were applied at 0.1 Hz frequency, and the pore pressure response was monitored. The experiment was continued for 50 loading cycles or until an excess pore pressure ratio of 0.90 or higher was obtained.

Using elasticity theory and a Poisson's ratio of 0.5 for undrained conditions (Ishihara

1996) the induced shear strains were calculated by the following equation:

$$\gamma = 1.5\varepsilon_{a,\max} \quad (3.1)$$

where:  $\gamma$  = cyclic shear strain;

$\varepsilon_{a,\max}$  = the peak axial strain.

A typical result from a strain-controlled test is shown in Figure 3.12. A specimen of Mabel Creek silt was subjected to a constant shear strain amplitude of 0.3% (Figure 3.12a). Excess pore pressure was generated with increasing loading cycles (Figure 3.12b). The sinusoidal peak shear stress decreased with increasing loading cycles (Figure 3.12c). Shear stress-shear strain curves shown in Figure 3.12d reflect that the specimen became softer and softer with increasing loading cycles.

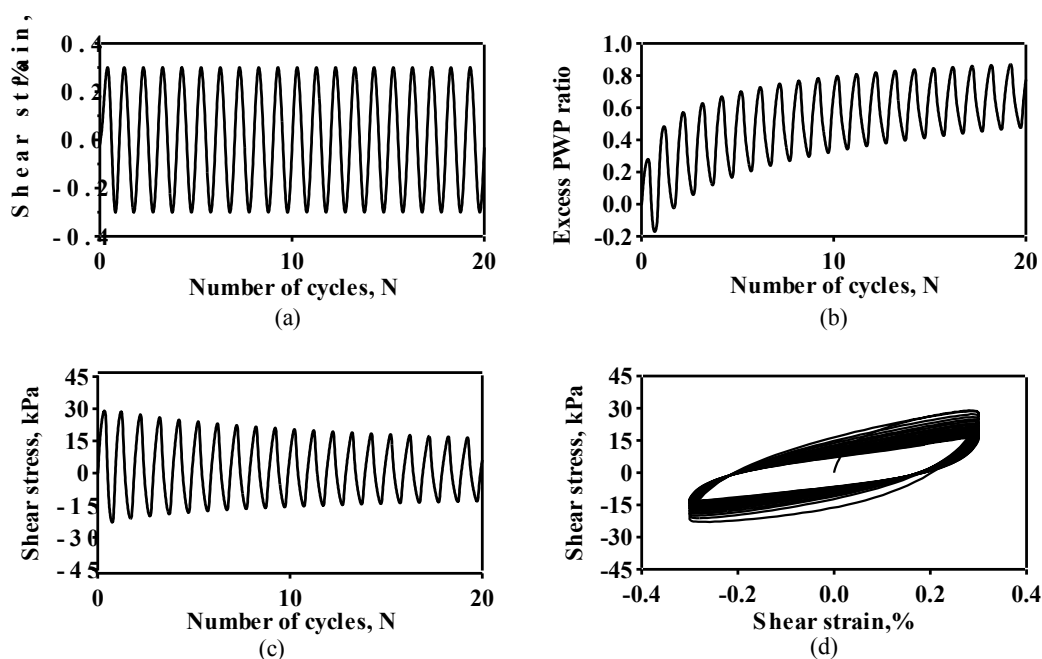


**Figure 3.12** Typical result from a cyclic strain-controlled test on Mabel Creek silt specimen conditioned at 0.5°C with  $\sigma'_3=100$  kPa,  $\gamma=0.3\%$  and post-consolidation void ratio of 1.046

### 3.2.5 Dissipation of excess pore pressure and post testing measurements

Dissipation of excess pore pressure through drainage was allowed after completion of

the test. The change in volume due to pore pressure dissipation was measured using a volume change transducer connected to the specimen. The vertical displacement was also monitored and recorded.

### 3.3 Data reduction

Processing of the experimental raw data was conducted as follows:

Excess pore water pressure generation in soils is typically defined by the excess pore water pressure ratio,  $r_u$ , which is given by the following equation:

$$r_u = \Delta u / \sigma'_3 \quad (3.2)$$

where

$\Delta u$  = excess pore pressure at the end of loading cycle, sometimes referred to as cycle end pore pressure; and

$\sigma'_3$  = the initial effective confining pressure.

Figure 3.13. shows a typical record of excess pore pressure generation versus number of loading cycles for induced shear strain levels of 0.1% (Fig. 3.12a) and 0.8% (Fig. 3.12b). Excess pore pressure generation in cyclic testing follows a pattern similar to that of loading (e.g., sinusoidal in this case). Although excess pore pressure ratio can be calculated at any time during a loading cycle, the value that is commonly used is defined by taking into account the excess pore pressure at the end of loading cycle. The dotted line in Fig. 3.12 represents such excess pore pressure values, and all of the values of excess pore pressure ratio throughout this document are evaluated based on cycle end measurements.

Experimental results were also used to compute the shear modulus and damping ratio,

which are the two commonly used dynamic properties for soils. This was done by evaluating certain characteristics of the hysteresis loops formed during cyclic testing as shown in Figure 3.14. The inclination of the loop may be used to compute the Young's Modulus (E) using Equation 3.3. The shear modulus is then calculated through Equation 3.4 assuming a typical Poisson's ratio of 0.5 for saturated undrained soils.

$$E = \sigma_{dmax} / \epsilon_{max} \quad (3.3)$$

Further,

$$\gamma = (1 + \nu) \epsilon \text{ and } G = E/2/(1 + \nu) \quad (3.4)$$

where

$\sigma_{dmax}$  = the maximum deviator stress as shown in Figure 3.14;

$\epsilon_{max}$  = the maximum axial strain as shown in Figure 3.14;

G = the shear modulus;

$\gamma$  = the shear strain; and

$\nu$  = the Poisson's ratio that may be taken as 0.5 for saturated undrained specimens.

For the damping ratio, the energy dissipated during each loading cycle and strain energy is evaluated from the hysteresis loop. The area enclosed by the loop defines the energy dissipation and the area of the triangle gives the elastic strain energy. The damping ratio is then computed using Equation 3.5.

$$D = A_{LOOP} / (4\pi A_{TRIANGLE}) \quad (3.5)$$

where

$A_{LOOP}$  = area enclosed by the hysteresis loop and the energy dissipation per cycle as shown in Figure 3.14;

$A_{TRIANGLE}$  = area of the shaded triangle and the maximum strain energy as shown in

Figure 3.14.

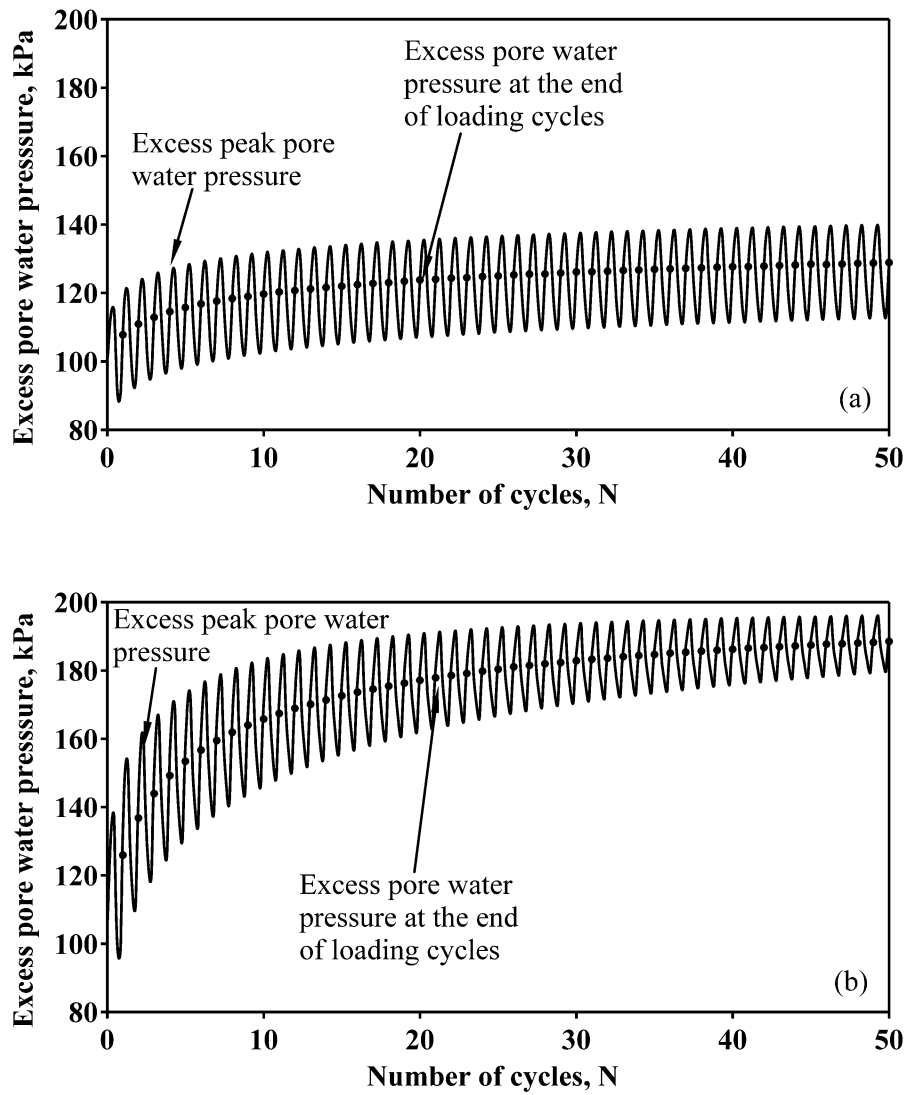


**Figure 3.13** Typical pore water pressure generation under cyclic loading in Mabel Creek silt subjected to 2 freeze-thaw cycles (a)  $\gamma=0.1\%$ ,  $\sigma'_3=101$  kPa, and  $e=1.045$  (b)  $\gamma=0.8\%$ ,  $\sigma'_3=101$  kPa, and  $e=1.044$



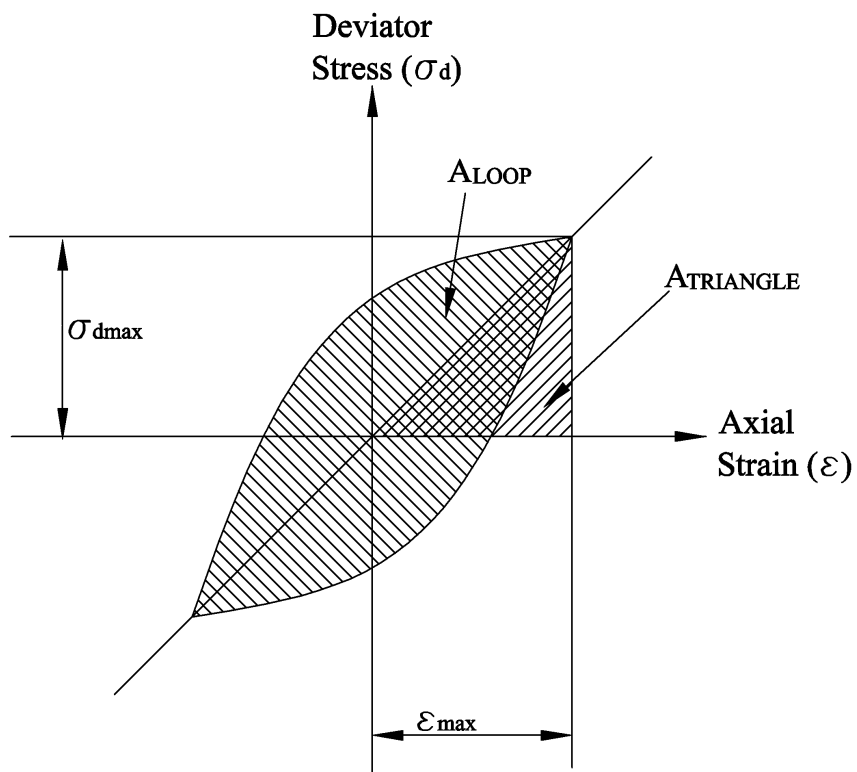


Figure 3.14 Hysteretic stress-strain relationship for cyclic loading (after Vinson 1978)

## **4 Impact of Temperature and Freeze-Thaw Cycles on Excess Pore Pressure Generation in Mabel Creek Silt**

### **4.1 Introduction**

Two groups of undrained cyclic triaxial strain-controlled tests were conducted on reconstituted Mabel Creek silt specimens. The tests in the first series were performed on specimens conditioned at the following temperatures: 24 °C, 5 °C, 1 °C, 0.5 °C, and -0.2 °C. The second series of tests were performed on specimens subjected to various freeze-thaw cycles. The unfrozen specimens refer to the specimens without any freezing or thawing treatments. The results from the unfrozen specimen were considered as a baseline in this study. Results from each of these testing series are presented and discussed in the following sections.

### **4.2 Excess pore water pressure generation at various temperatures**

Figure 4.1 shows the pore water pressure generation in unfrozen specimens for various induced shear strain levels in terms of excess pore pressure ratio,  $r_u$ , versus number of loading cycles,  $N$ , which is defined as pore pressure history (Hazirbaba 2005). This case represents a moderate (i.e., unfrozen) ground condition. The induced shear strain level ranged between 0.005% and 0.8%. Figure 4.1a summarizes the results for the small shear strain levels of 0.005%, 0.01%, and 0.03%. At the smallest induced shear strain level of 0.005%, no excess pore pressure was developed. For the cyclic shear strain of 0.01%, very little excess pore pressure was developed. Excess pore pressure ratio was found to be about 0.6% at  $N=10$ , and it remained under 2% throughout the test (i. e., 50 loading cycles). This finding is important in terms of defining the threshold shear strain level ( $\gamma_t$ ) (Dobry et al. 1982), below which no volume change under drained condition and little to no excess pore pressure under undrained condition occurs during cyclic loading. Typical values of  $\gamma_t$  are 0.01% to

0.015% for sands and 0.024% to 0.06% for cohesive soils (Hsu and Vucetic 2006). The fact that minimal excess pore pressure was developed at the 0.01% induced shear strain in an unfrozen specimen indicates a threshold shear strain level larger than 0.01%. This is in agreement with the findings of Hsu and Vucetic (2006). Thus, the threshold cyclic shear strain for unfrozen specimens should be slightly larger than 0.01%. For  $\gamma=0.05\%$ , the excess pore pressure ratio at  $N=10$  is 12%, with a maximum value of 23% obtained at  $N=50$ . At higher levels of induced cyclic shear strain, larger pore pressure values were obtained. For  $\gamma=0.8\%$ ,  $r_u$  was 25% for  $N=1$  and increased to about 93% at the end of the test ( $N=50$ ) (Figure 4.1b).

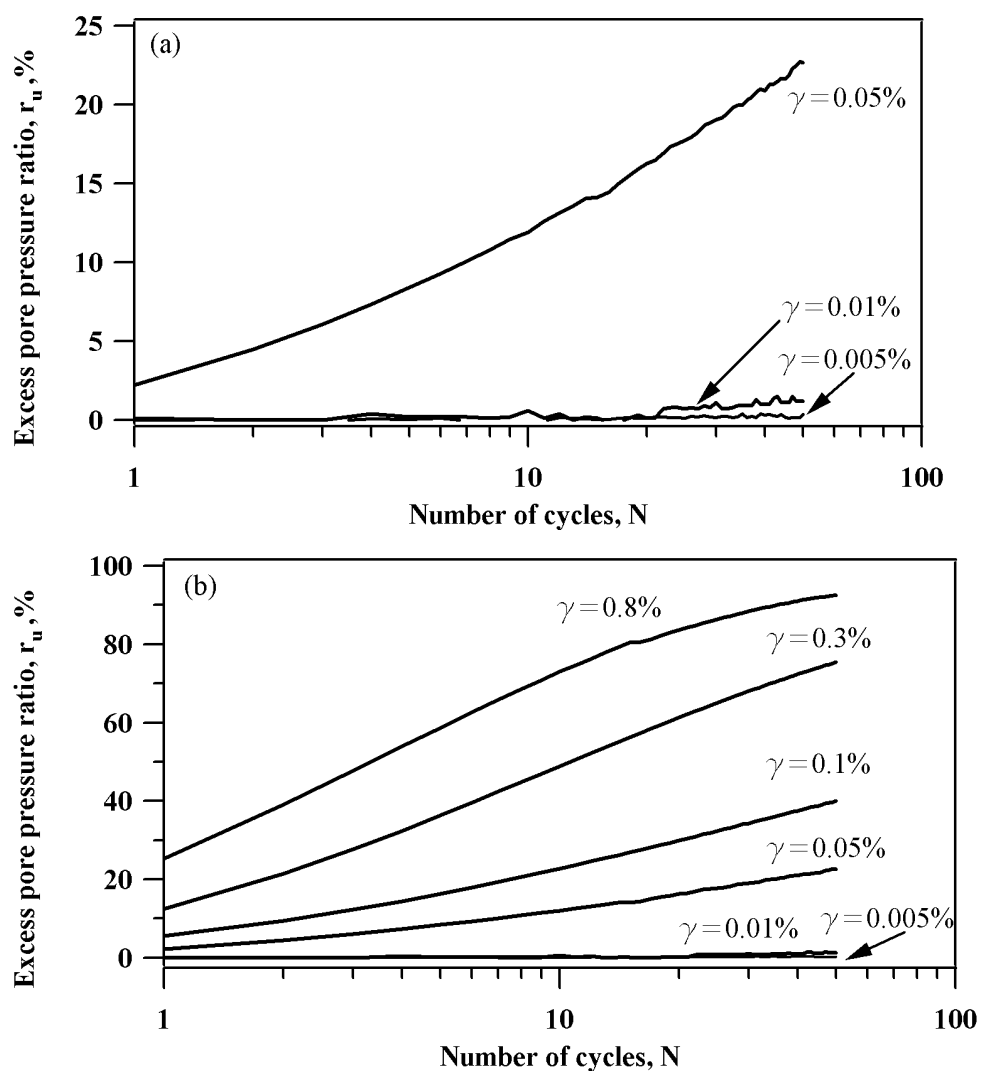


**Figure 4.1** Excess pore pressure ratio ( $r_u$ ) versus N in unfrozen Mabel Creek silt

The excess pore water pressure generation in unfrozen specimens is also presented versus induced cyclic shear strain for different number of loading cycles in Figure 4.2. The existence of the threshold shear strain level can be better seen from these curves. At and around  $\gamma=0.01\%$ , no significant pore pressure was developed for 50 loading cycles as discussed earlier. Figure 4.2 shows the strong relationship between excess pore pressure and induced cyclic shear strain.

Excess pore pressure generation measured from specimens conditioned at 24 °C (i.e., thawed back to 24 °C from fully-frozen state) is presented in Figure 4.3. The smallest induced shear strain level in this case was  $\gamma=0.005\%$ . At this strain level, no appreciable pore pressure generation was recorded. For  $\gamma=0.1\%$ , the excess pore pressure ratio increased from 2% at  $N=1$  to 15% at  $N=10$  and to 26% at  $N=50$ . The results from  $\gamma=0.005\%$  to  $\gamma=0.1\%$  indicate that the threshold shear strain for specimens conditioned at 24 °C should be somewhere between these two shear strain levels. Excess pore pressure ratio at  $\gamma=0.3\%$  was found to be about 10% at  $N=1$ , 39% at  $N=10$  and 61% at  $N=50$ . For  $\gamma=0.8\%$ ,  $r_u$  was 29% at  $N=1$ , and it increased progressively to 65% at  $N=10$  and to 87% at  $N=50$ .

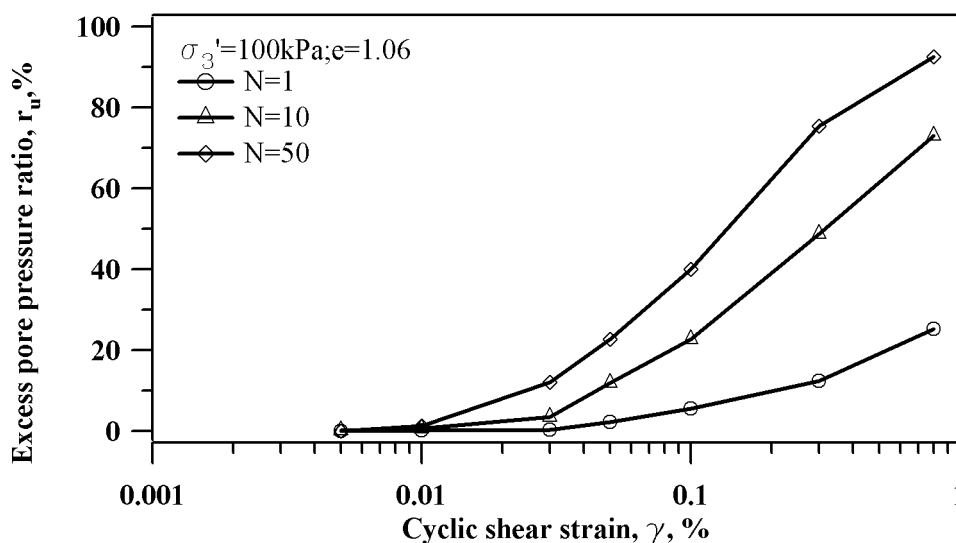


**Figure 4.2** Excess pore pressure ratio ( $r_u$ ) versus cyclic shear strain in unfrozen Mabel Creek silt

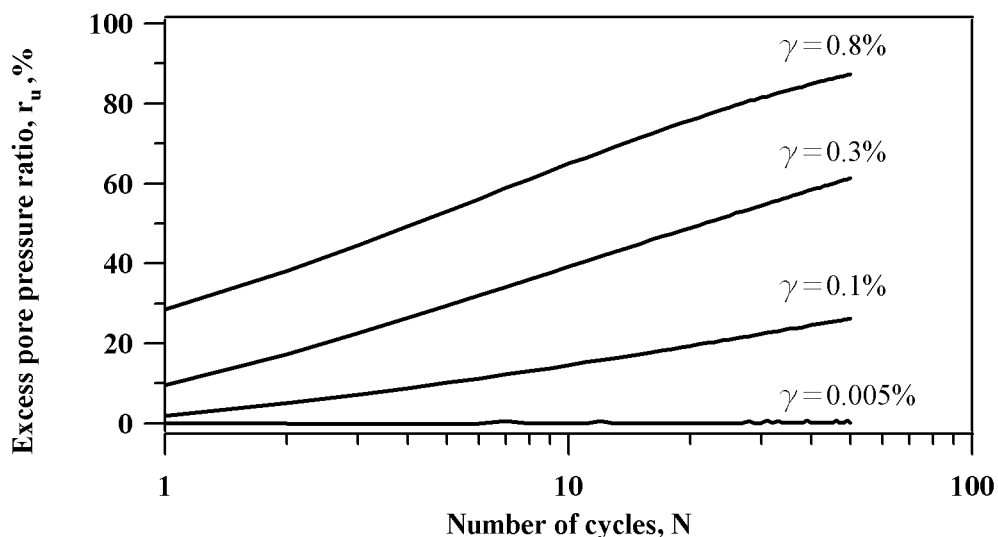


**Figure 4.3** Excess pore pressure ratio ( $r_u$ ) versus N in Mabel Creek silt conditioned at 24 °C

Figure 4.4 shows the pore pressure generation curves for the specimens conditioned at 24 °C. A trend very similar to that of the unfrozen specimens (Figure 4.2) was revealed.

Figure 4.5 displays the pore water pressure generation from specimens conditioned at 5 °C. In this case, the induced cyclic shear strain levels were 0.005%, 0.1%, and 0.3%. For the small cyclic shear strain of 0.005%,  $r_u$  remained under 1% throughout the test. For  $\gamma=0.1\%$ ,  $r_u$  increased progressively from about 1% at  $N=1$ , to 14% at  $N=10$ , and to about 26% at  $N=50$ . Excess pore pressure ratio for  $\gamma=0.3\%$  are 9% at  $N=1$ , 37% at  $N=10$ , and approximately 60% at  $N=50$ .

The pore pressure generation curve for the specimens conditioned at 5 °C is presented in Figure 4.6. As can be seen, no change in excess pore pressure ratio was seen at  $\gamma=0.005\%$ . The fact that the threshold shear strain level is larger than  $\gamma=0.005\%$  is

confirmed. As the induced cyclic shear strain level increased, so did the generation of excess pore water pressure.

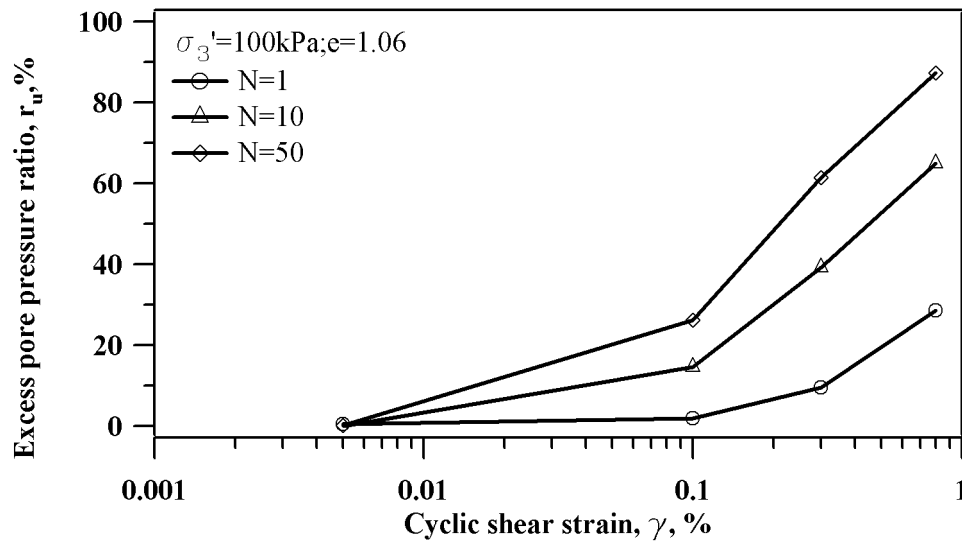


Figure 4.4 Excess pore pressure ratio versus cyclic shear strain in Mabel Creek silt conditioned at 24 °C

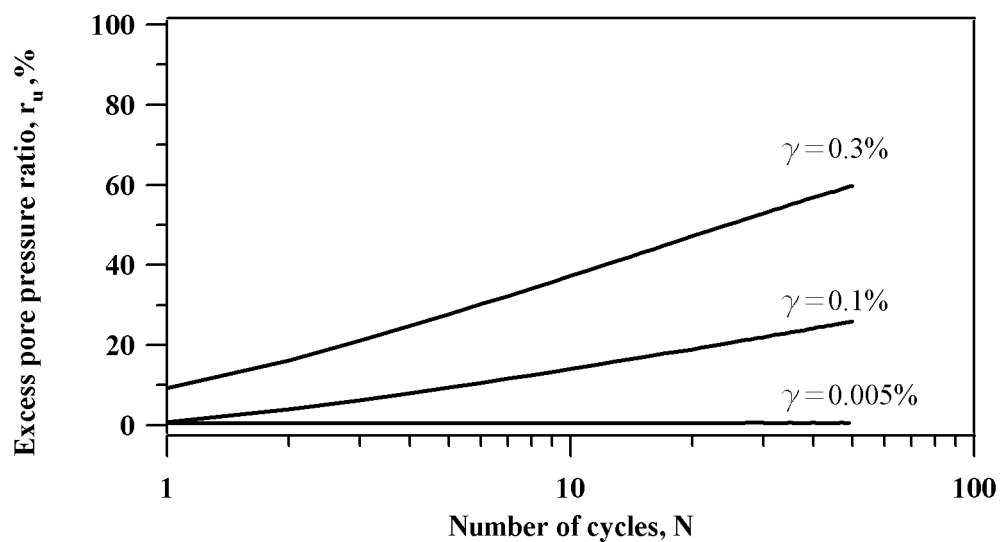
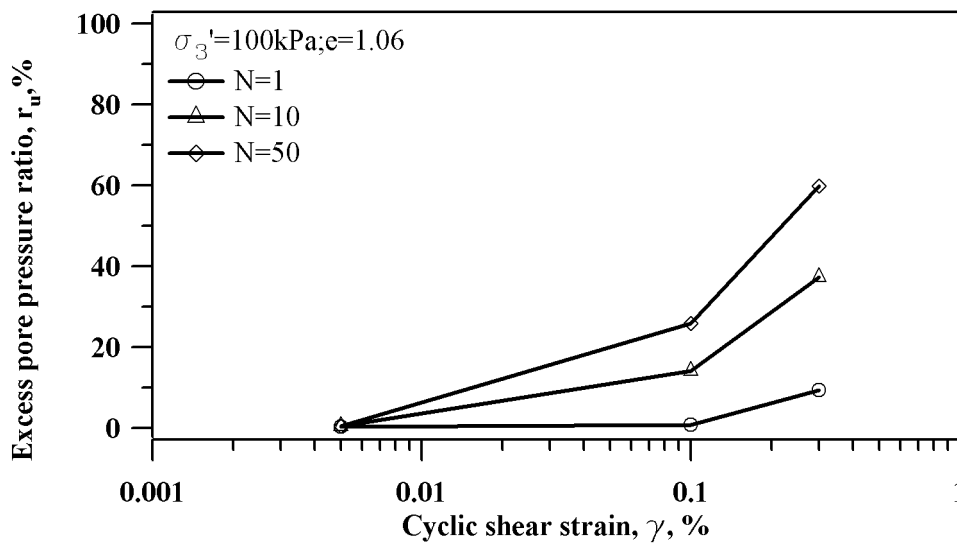


Figure 4.5 Excess pore pressure ratio ( $r_u$ ) versus  $N$  in Mabel Creek silt conditioned at 5 °C



**Figure 4.6** Excess pore pressure ratio ( $r_u$ ) versus cyclic shear strain on Mabel Creek silt conditioned at 5 °C

Figure 4.7 shows the pore water pressure history from soil specimens conditioned at 1 °C. The induced cyclic shear strain levels are 0.005%, 0.1%, and 0.3%. For  $\gamma=0.005\%$ , the maximum value of excess pore pressure ratio is 0.3% at  $N=50$ . Thus  $\gamma=0.005\%$  may be considered less than the cyclic threshold shear strain for specimens conditioned at 1°C. For  $\gamma=0.1\%$ , the excess pore water pressure ratio increased progressively from 5% at  $N=1$ , to 18% at  $N=10$ , and to 30% at  $N=50$ . Larger excess pore water pressure was obtained at  $\gamma=0.3\%$  with  $r_u$  of 5% at  $N=1$ , 30% at  $N=10$ , and 50% at  $N=50$ .

Figure 4.8 presents the pore pressure generation curve for specimens conditioned at 1 °C.

Test results of the excess pore water pressure generation from specimens conditioned at 0.5 °C are presented in Figure 4.9 and Figure 4.10. Similar to previous recordings at various temperatures, no significant  $r_u$  (<1.5%) was recorded at  $\gamma=0.005\%$ . For  $\gamma=0.1\%$ , measured  $r_u$  values were 5% at  $N=1$ , 26% at  $N=10$  and 42% at  $N=50$ . Finally,

for  $\gamma=0.3\%$ , significant excess pore pressure was developed immediately after the first cycle and accumulated throughout the test. Excess pore pressure ratio were measured as 20% at  $N=1$ , 58% at  $N=10$ , and 83% at  $N=50$ . The excess pore pressure generation curves obtained from the specimens conditioned at  $0.5\text{ }^{\circ}\text{C}$  are shown in Figure 4.10.

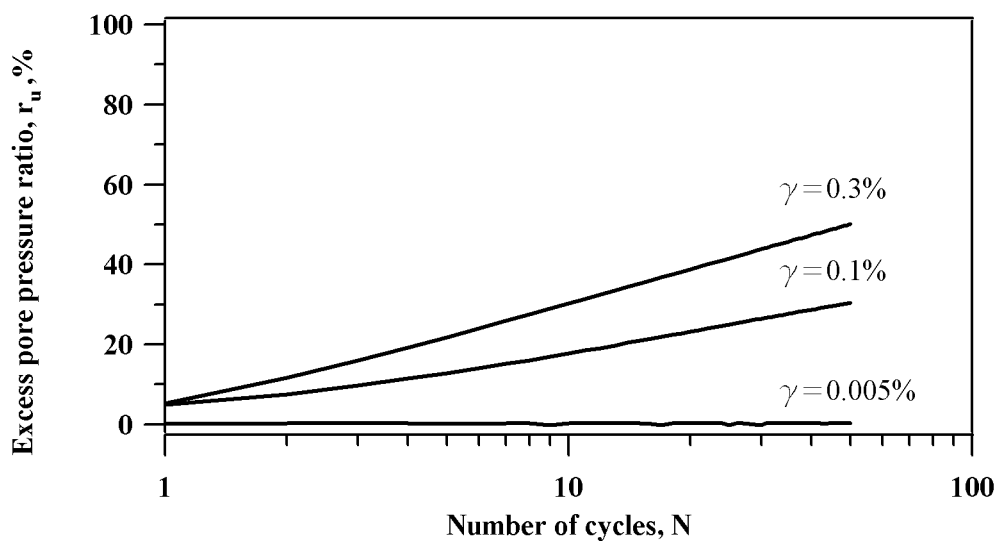


Figure 4.7 Excess pore pressure ratio ( $r_u$ ) versus N on Mabel Creek silt conditioned at  $1\text{ }^{\circ}\text{C}$

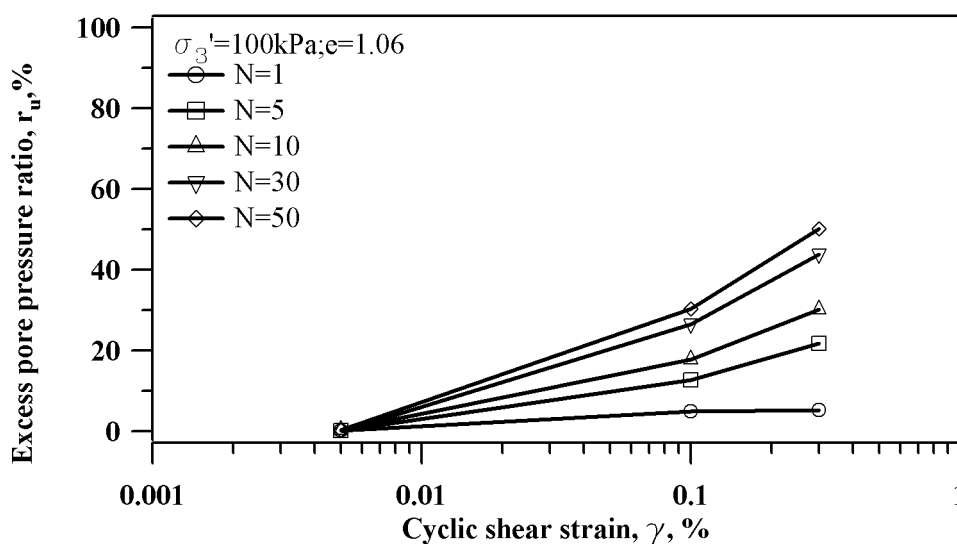
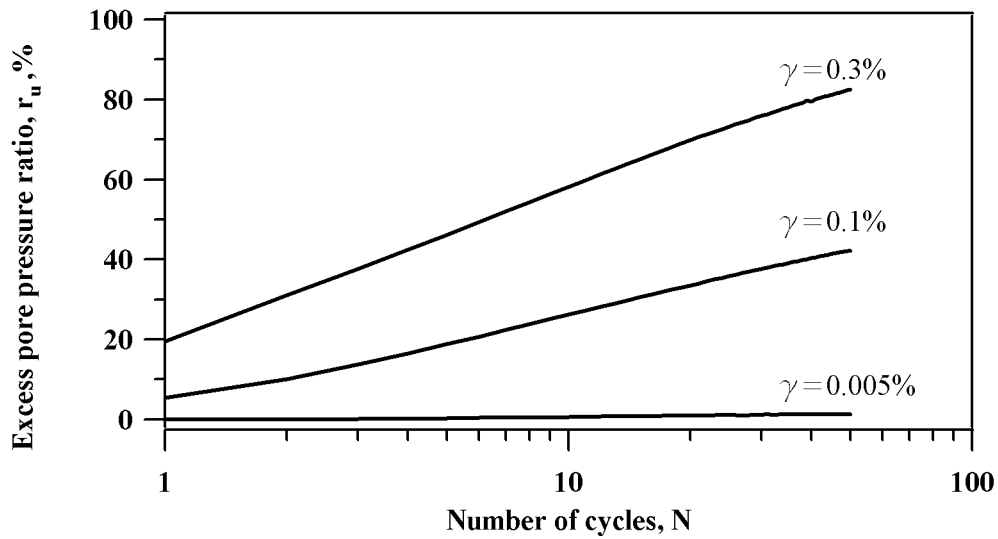
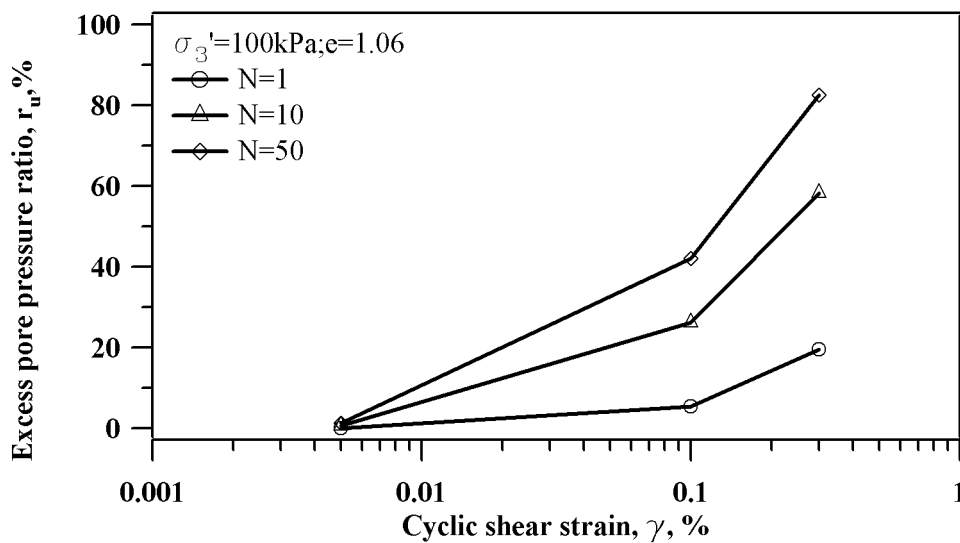


Figure 4.8 Excess pore pressure ratio versus cyclic shear strain on Mabel Creek silt conditioned at  $1\text{ }^{\circ}\text{C}$





**Figure 4.9** Excess pore pressure ratio ( $r_u$ ) versus  $N$  on Mabel Creek silt conditioned at  $0.5\text{ }^{\circ}\text{C}$



**Figure 4.10** Excess pore pressure ratio versus cyclic shear strain on Mabel Creek silt conditioned at  $0.5\text{ }^{\circ}\text{C}$

Excess pore water pressure histories from the specimens conditioned at  $-0.2\text{ }^{\circ}\text{C}$  are presented in Figure 4.11. The induced shear strain levels were 0.03% and 0.1%. The specimens in this case displayed completely different behavior from those conditioned at warmer temperatures. For  $\gamma=0.03\%$ , the excess pore water pressure increased

slightly and remained under 4% throughout the test. However, interestingly, at  $\gamma=0.1\%$  the excess pore pressure ratio showed a decreasing trend with increasing number of loading cycles, and eventually negative pore pressure was recorded as  $-7.5\%$  at  $N=50$ . It has already been established that near or below  $0^\circ\text{C}$  a portion of the pore water is still at unfrozen state (Neresova and Tsytoovich 1963) and that the interaction between unfrozen and frozen pore water contents during freezing may lead to development of negative pore pressure (Eigenbrod et al. 1996). Thus, although the test at  $\gamma=0.1\%$  on the specimen conditioned to  $-0.2^\circ\text{C}$  was executed at the equilibrium condition, development of the negative excess pore pressure with cyclic loading may be attributed to the redistribution of the unfrozen pore water within the specimen. It may be argued that at smaller induced shear strain levels, as observed in the case of  $\gamma=0.03\%$ , such redistribution of the unfrozen water does not occur and therefore the temperature equilibrium condition is sustained indicating no negative excess pore pressure development within the specimen.

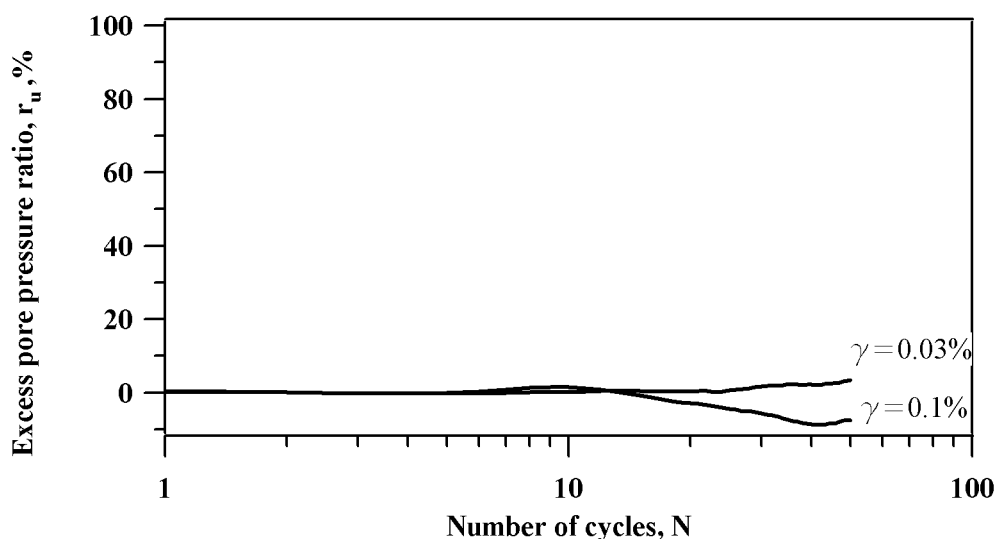


**Figure 4.11** Excess pore pressure ratio ( $r_u$ ) versus N on Mabel Creek silt conditioned at  $-0.2^\circ\text{C}$

### 4.3 Impact of temperature on excess pore water pressure generation

The impact of temperature on excess pore water pressure generation is analyzed using the results presented above. The analysis in this section focuses mainly on comparing the trends from each of the ground temperatures investigated.

Figure 4.12 displays a comparison of the results from specimens conditioned at different temperature and subjected to  $\gamma=0.1\%$ . It is interesting to note that the excess pore pressure values obtained from specimens conditioned at 5 °C and 24 °C were almost identical for all loading cycles, and that these values appear to form the lower bound of pore pressure history at  $\gamma=0.1\%$ . The largest pore pressure values, indicating the upper bound in Figure 4.12, were obtained from the specimen conditioned at 0.5 °C. The unfrozen specimen experienced less pore pressure generation than that of the specimen conditioned at 0.5 °C and more than those conditioned at 1 °C, 5 °C, and 24 °C. As discussed in the previous section, the excess pore pressure in the specimen conditioned at -0.2°C followed a different pattern with negative values even after  $N=13$ .

Figure 4.13 shows trends of excess pore pressure generation similar to those presented in Figure 4.12 for  $\gamma=0.3\%$ . The upper bound for this strain level is also from the specimen conditioned at 0.5 °C. However, the lower bound pore pressure generation history was conditioned at 1 °C.

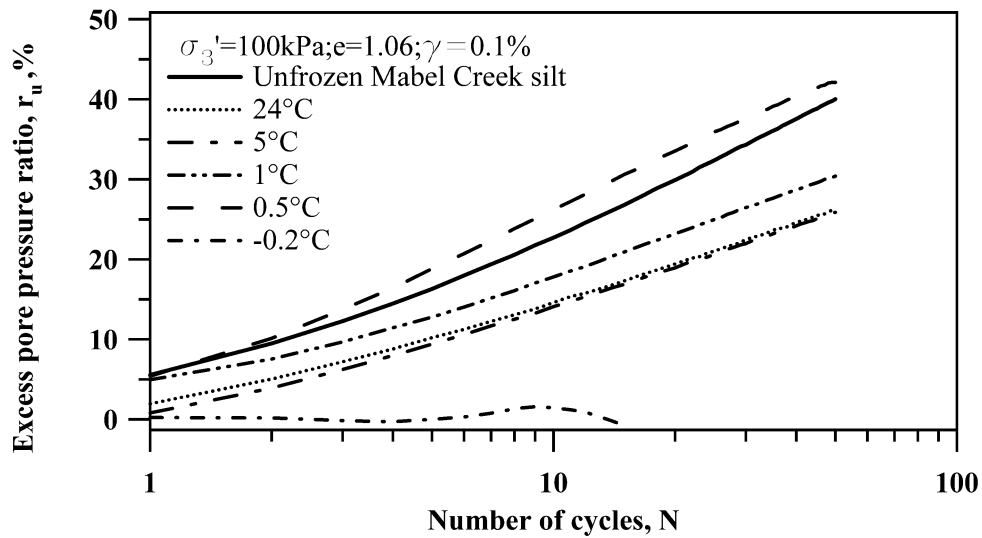


Figure 4.12 Temperature rise effect on pore water pressure generation of frozen or partially frozen Mabel Creek silt at  $\gamma=0.1\%$

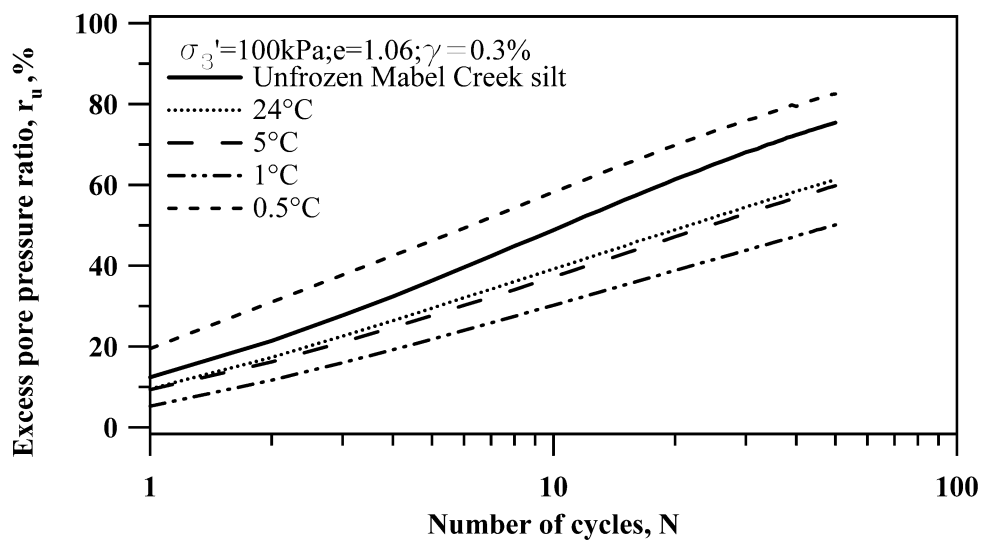


Figure 4.13 Temperature rise effect on pore water pressure generation of frozen or partially frozen Mabel Creek silt at  $\gamma=0.3\%$

The variation of excess pore pressure with temperature for  $\gamma=0.1\%$  and  $\gamma=0.3\%$  is shown in Figure 4.14 and Figure 4.15, respectively. The excess pore pressure generation appears to remain constant between  $24^{\circ}\text{C}$  and  $1^{\circ}\text{C}$ . Significant increase occurs at  $0.5^{\circ}\text{C}$ . The results also indicated that pore pressure generation in unfrozen

specimens was always larger than that of conditioned specimens with the exception of those conditioned at 0.5 °C.

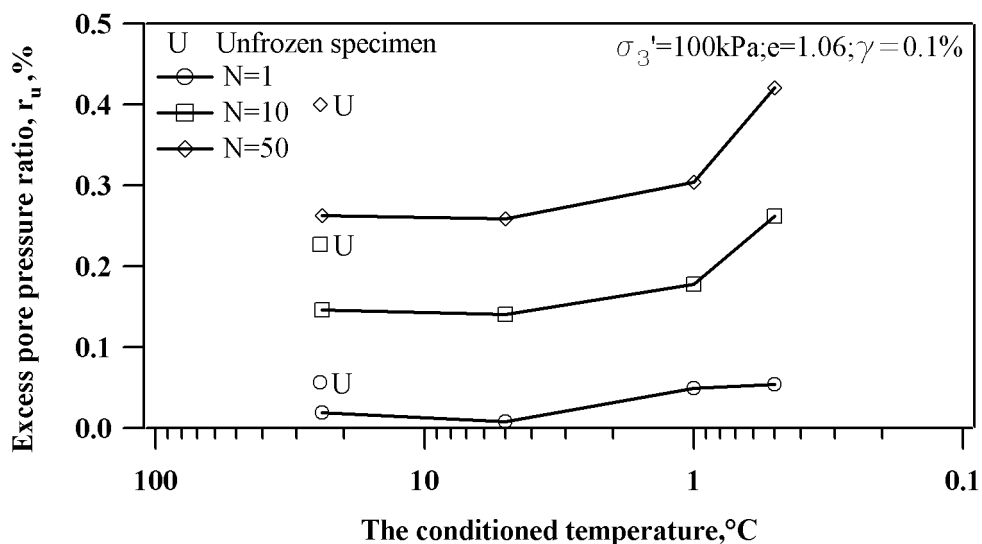


Figure 4.14 Excess pore water pressure ratio versus temperature at  $\gamma=0.1\%$

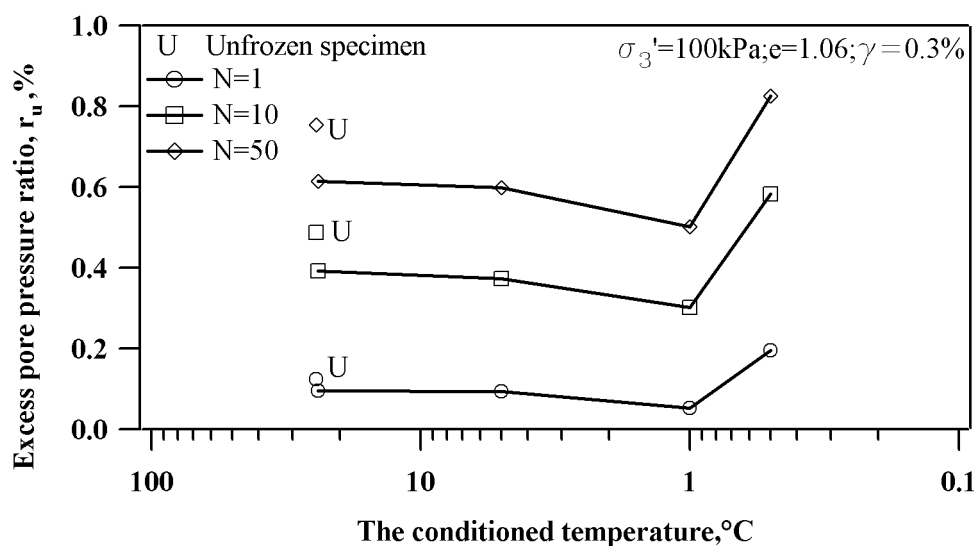
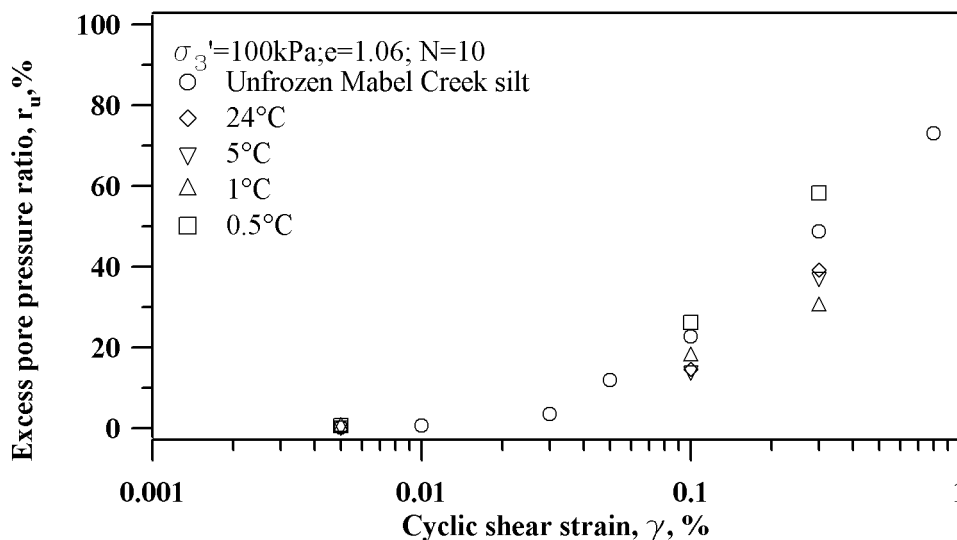


Figure 4.15 Excess pore water pressure ratio versus temperature at  $\gamma=0.3\%$

The pore water pressure generation curves from all of the specimens tested under this category are presented in Figure 4.16. As in the excess pore pressure histories, the specimens conditioned at 0.5 °C are found to form the upper bound curve.



**Figure 4.16** Pore water pressure generation curves of Mabel Creek silt conditioned at different temperature and  $N=10$

#### 4.4 Comparison of results with previous research efforts

As discussed in Chapter 2, previous efforts generally focused on moderate ground conditions. To investigate pore pressure generation curves in Mabel Creek silt conditioned at various ground temperatures, the results from previous literature were combined into the results in this study, and a comparison was made for  $N=10$  as shown in Figure 4.17. Dobry (1985) provided the bound of pore pressure generation in clean sand with a  $D_r$  from 20% to 80% and a confining pressure from 25 kPa to 200 kPa. Hazirbaba (2005) conducted a series of undrained strain-controlled cyclic triaxial tests on sand with 0-20% fines, and in Figure 4.17 these results form a band for pore pressure generation of sand with fines. Significantly, the pore pressure generation in Mabel Creek silt conditioned at various temperatures is within the band of clean sand with 0-20% fines from Hazirbaba (2005), and is equal to or below the lower bound of the band of sand from Dobry (1985). This means that the Mabel Creek silt, regardless of the conditioned temperatures, has lower liquefaction potential than clean sand, but similar liquefaction potential to sand with 0-20% fines. The pore pressure generation at  $N=10$  in Mabel Creek silt conditioned at various temperatures

is bounded as shown in Figure 4.18.

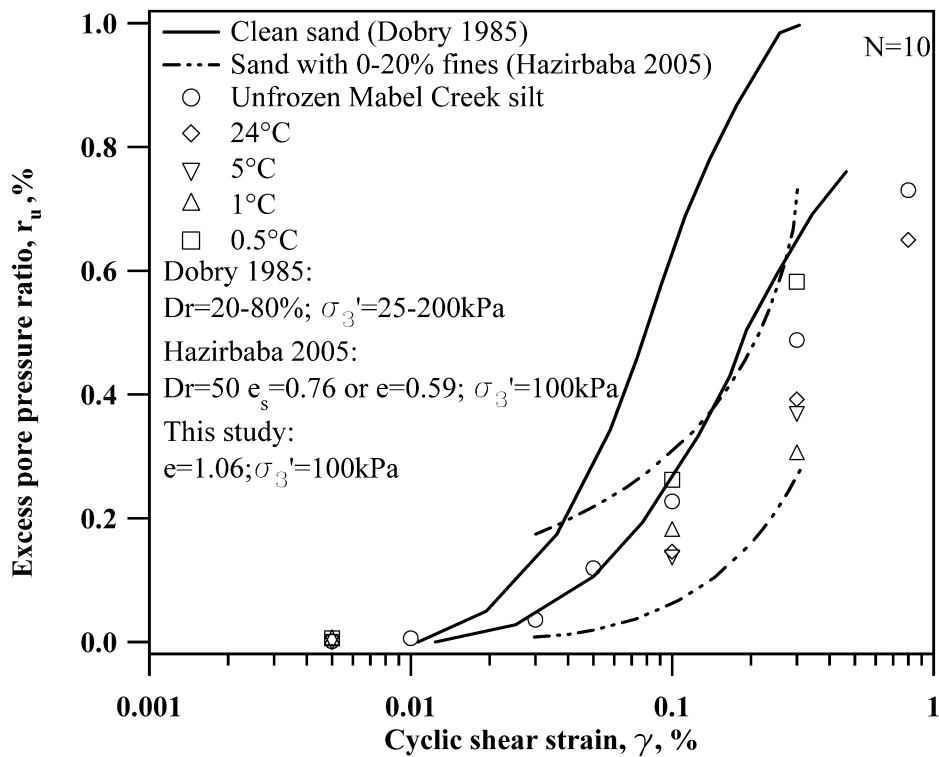


Figure 4.17 Comparison of pore pressure generation among Mabel Creek silt conditioned at various temperatures, clean sand and sand with fines

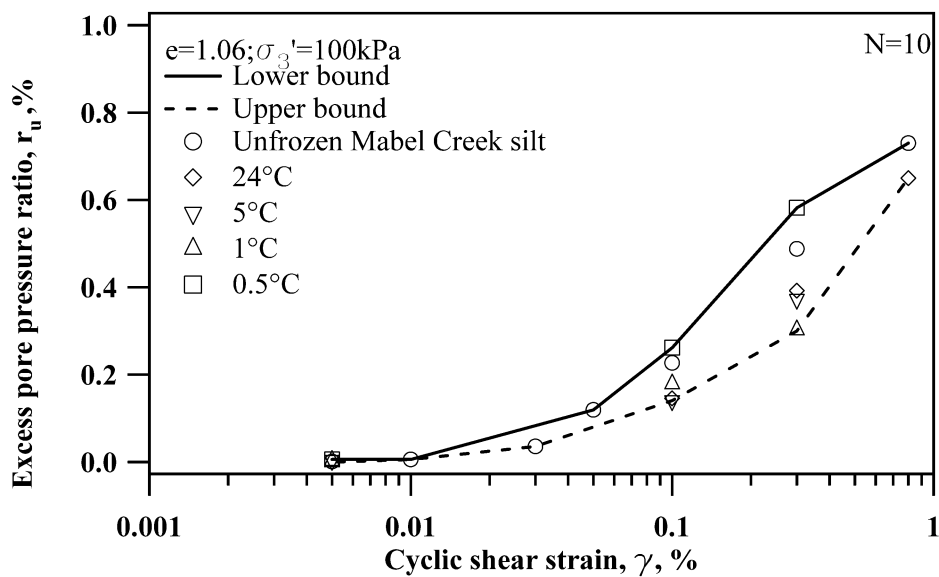
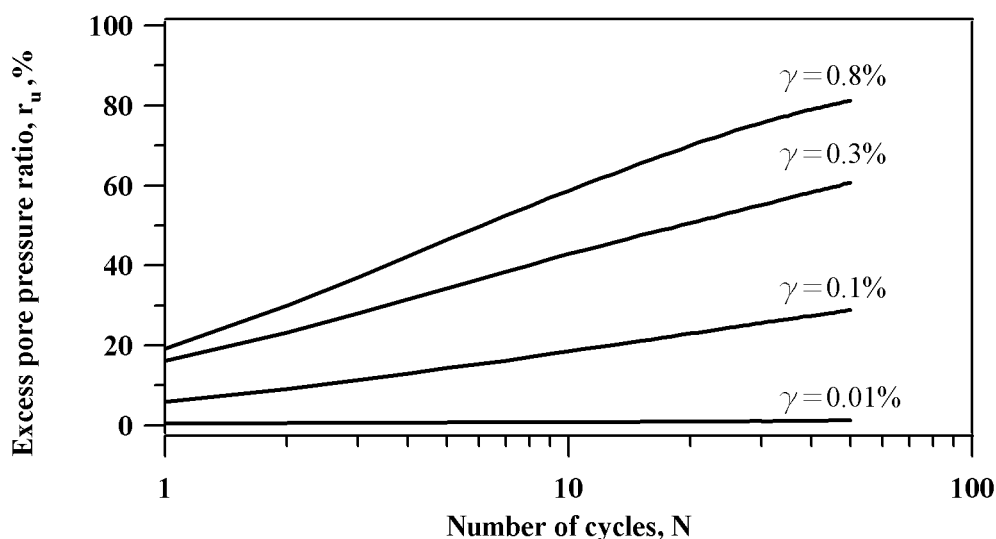


Figure 4.18 The bound of pore pressure generation in Mabel Creek silt conditioned at various temperatures

#### 4.5 Pore water pressure generation at freeze-thaw cycles

Since a specimen conditioned at 24 °C is identical to a specimen conditioned at 1 freeze-thaw cycle as mentioned in Section 3.2.3, the pore water pressure generation at 1 freeze-thaw cycle has been introduced in Section 4.2. Thus, pore pressure generation in specimens at freeze-thaw cycles is started at 2 freeze-thaw cycles. Pore pressure generation history in specimens conditioned at 2 freeze-thaw cycles is presented in Figure 4.19. For the smallest cyclic shear strain level of 0.01%, no significant  $r_u$  was measured, and  $r_u$  was always under 1.1% during 50 loading cycles. The excess pore water pressure ratio at  $\gamma=0.1\%$  is generated in a progressive manner from 6% at  $N=1$ , to 19% at  $N=10$ , to 29% at  $N=50$ . Similarly increasing,  $r_u$  at  $\gamma=0.3\%$  was found to be from 16% at  $N=1$  and 43% at  $N=10$  to 61% at  $N=50$ . For  $\gamma=0.8\%$ ,  $r_u$  was measured to be 19% at  $N=1$ , 59% at  $N=10$  and 81% at  $N=50$ .



**Figure 4.19** Excess pore pressure ratio ( $r_u$ ) versus N on Mabel Creek silt conditioned after 2 freeze-thaw cycles

Figure 4.20 presents the pore pressure generation curves in specimens conditioned at 2 freeze-thaw cycles. No significant pore generation at a shear strain of 0.01%



suggests that the threshold shear strain is greater than 0.01%. As expected, larger shear strains induce more pore water pressure ratio.

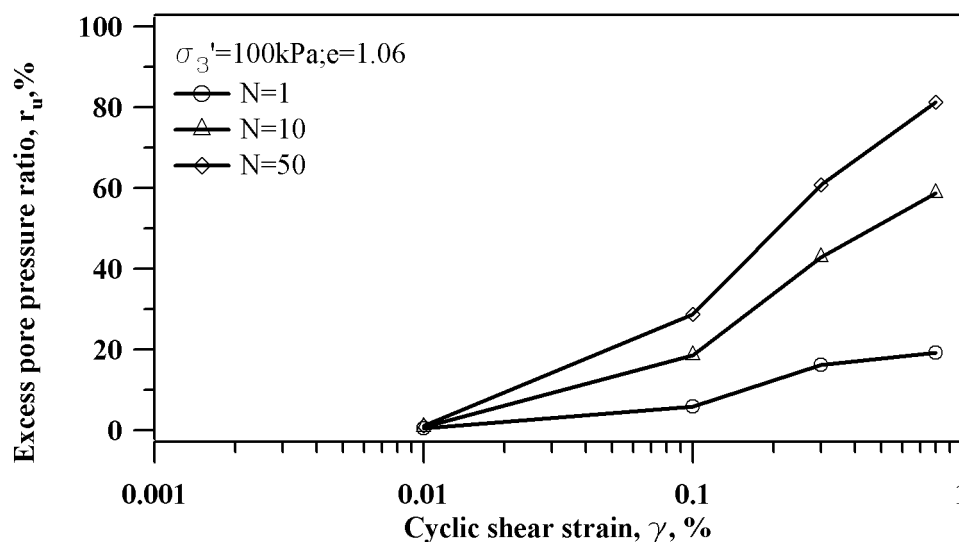


**Figure 4.20** Excess pore pressure ratio versus cyclic shear strain on Mabel Creek silt conditioned after 2 freeze-thaw cycles

Excess pore water pressure generation as the function of the number of loading cycles on specimens conditioned after 4 freeze-thaw cycles is presented in Figure 4.21. For the smallest cyclic shear strain level of 0.005%,  $r_u$  of less than 1% was generated during all cyclic loading tests. For  $\gamma=0.1\%$ ,  $r_u$  went from 6% at  $N=1$ , to 18% at  $N=10$ , and to 27% at  $N=50$ . In the same manner,  $r_u$  at  $\gamma=0.3\%$  ranged from 16% at  $N=1$ , to 40% at  $N=10$ , and to 57% at  $N=50$ . For the specimen at  $\gamma=0.8\%$ ,  $r_u$  jumped to 26% at  $N=1$  and was measured to be 58% at  $N=10$  and 78% at  $N=50$ . The generation curves of the water pressure ratio in specimens conditioned at 4 freeze-thaw cycles are presented in Figure 4.22. As a shear strain level close to and less than the threshold shear strain from these excess pore water pressure generation curves, 0.005% is suggested.

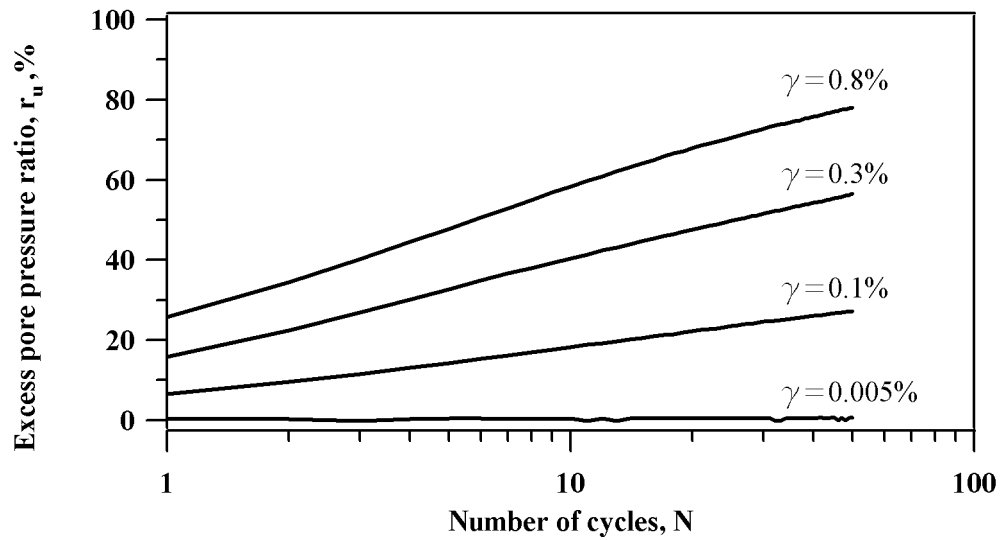


Figure 4.21 Excess pore pressure ratio ( $r_u$ ) versus N on Mabel Creek silt conditioned after 4 freeze-thaw cycles

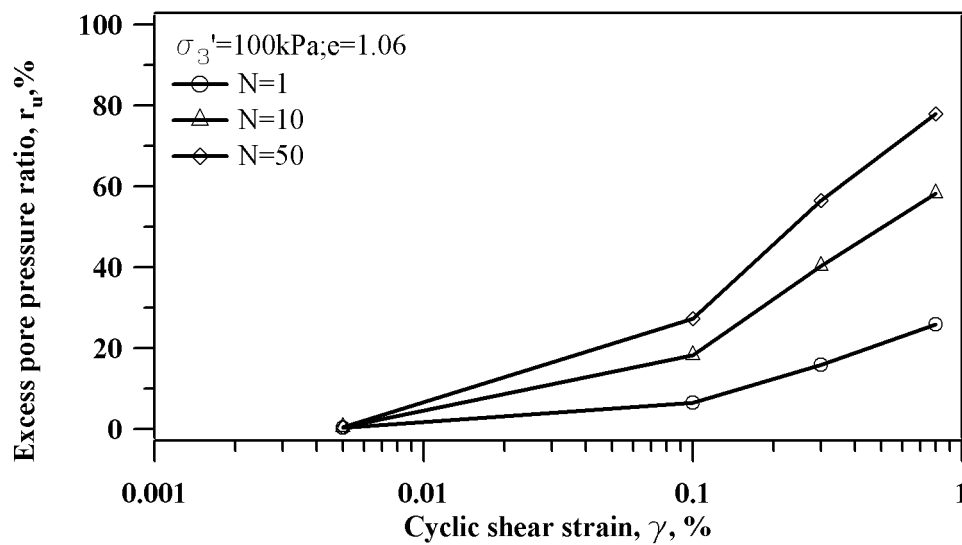


Figure 4.22 Excess pore pressure versus cyclic shear strain on Mabel Creek silt conditioned after 4 freeze-thaw cycles

#### 4.6 Impact of freeze-thaw cycles on pore water pressure generation of Mabel Creek silt

To compare the effect of freeze-thaw cycles on pore water pressure generation of

Mabel Creek silt, the excess pore pressure generation histories in specimens conditioned through 1, 2, and 4 freeze-thaw cycles and the unfrozen specimens were plotted at the shear strain of 0.1%, 0.3%, and 0.8%. The comparison of pore water pressure generations on specimens conditioned at different freeze-thaw cycles and the shear strain level of 0.1% is shown in Figure 4.23. Excess pore pressure ratio of the specimen treated after 1 freeze-thaw cycle was made up of a lower bound in comparison with other specimens at the end of the first loading cycle. No doubt, pore pressure generation in the unfrozen specimen formed an upper bound. This band width increases with increasing loading cycles. Both specimens, the one treated after 2 freeze-thaw cycles and the one treated 4 freeze-thaw cycles, behaved with almost the exact same pore water pressure generation through all 50 loading cycles. The difference of  $r_u$  among these three specimens at 1, 2, and 4 freeze-thaw cycles became smaller and smaller with increasing loading cycles, and ended at only 2% after the 50<sup>th</sup> loading cycle.

Similar, the comparison of pore water pressure generations in specimens conditioned at different freeze-thaw cycles and the shear strain level of 0.3% is shown in Figure 4.24. Excess pore pressure ratio of the specimens treated after 1, 2, and 4 freeze-thaw cycles was generated at the narrow band with increasing loading cycles. The difference of  $r_u$  among these three specimens was remained in the range of 5% through all 50 loading cycles. The unfrozen specimen began with initial excess pore water pressure ratio at 12%, which was slightly less than those of the specimens respectively treated after 2 and 4 freeze-thaw cycles. However,  $r_u$  of the unfrozen specimen was quickly beyond those of other specimens after  $N=3$  due to a very high pore water pressure generation slope. Thus the unfrozen specimen had the highest pore water pressure generation when  $\gamma=0.3\%$ .

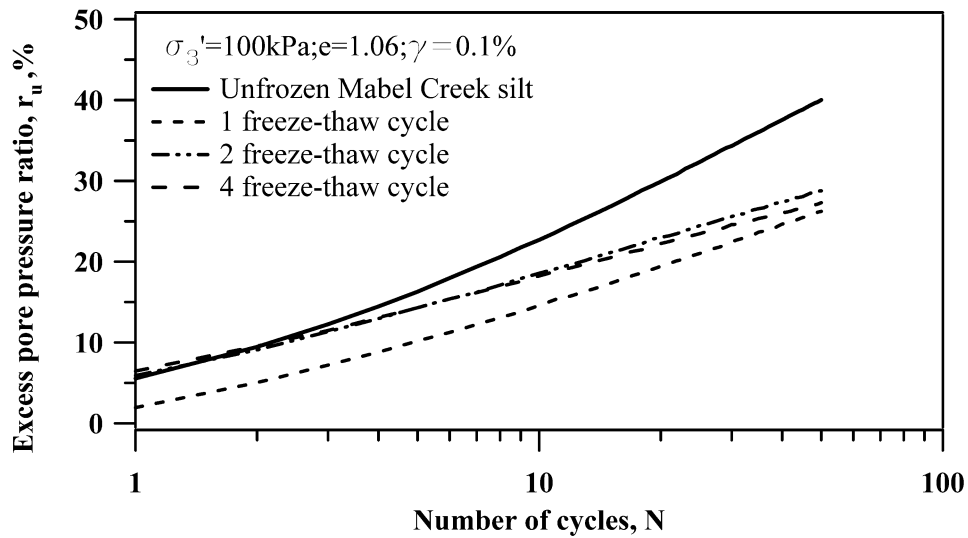


**Figure 4.23** Comparison of the pore water pressure generation in Mabel Creek silt conditioned at different freeze-thaw cycles at  $\gamma=0.1\%$

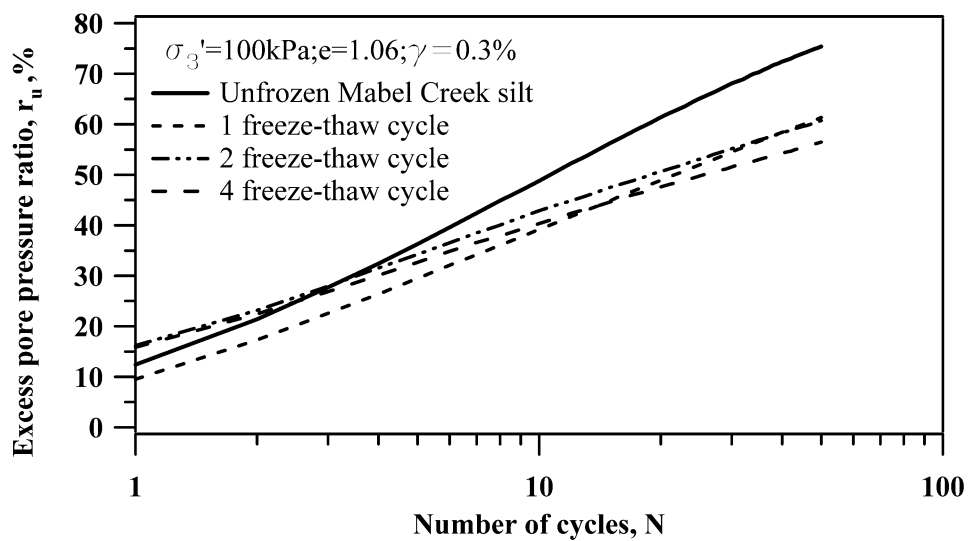


**Figure 4.24** Comparison of the pore water pressure generation in Mabel Creek silt conditioned at different freeze-thaw cycles at  $\gamma=0.3\%$

The comparison of pore water pressure generation on specimens conditioned at the different freeze-thaw cycles and the shear strain level of 0.8% is shown in Figure 4.25. The unfrozen specimen still forms the upper bound. Pore water pressure generation on the specimens treated after 2 and 4 freeze-thaw cycles showed nearly the same

behavior and forms the lower bound. The specimen treated after only 1 freeze-thaw cycle had higher excess pore water pressure generation than the specimens treated after 2 and 4 freeze-thaw cycles. The difference of  $r_u$  between the specimen treated after 1 freeze-thaw cycle and the specimens treated after 2 and 4 freeze-thaw cycles remained at 9 % through all 50 loading cycles.

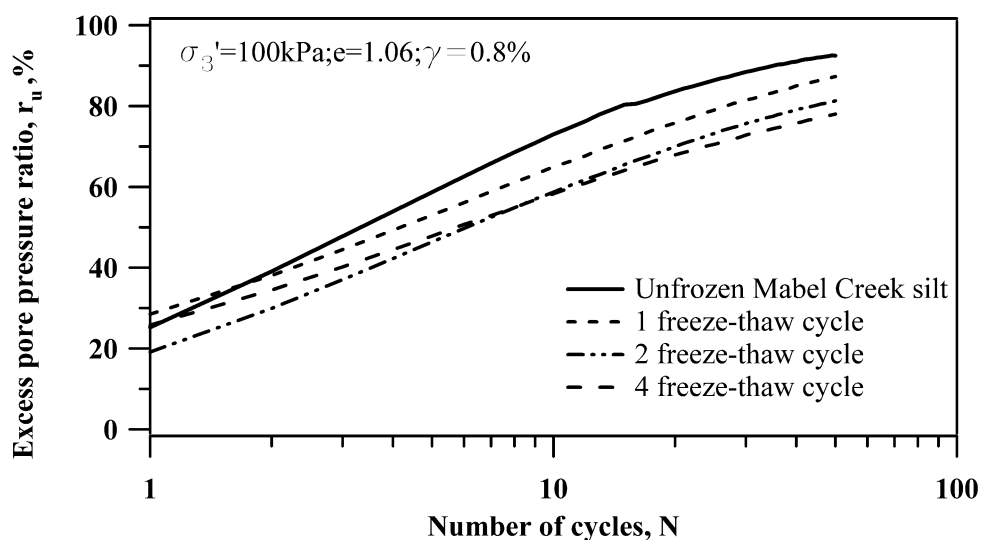


**Figure 4.25 Comparison of the pore water pressure generation on Mabel Creek silt conditioned at different freeze-thaw cycles at  $\gamma=0.8\%$**

To investigate the effect of freeze-thaw cycles on pore water pressure generation of Mabel Creek silt, the excess pore water pressure ratios are summarized in terms of number of freeze-thaw cycles, as shown in Figure 4.26~Figure 4.28 at the constant shear strain level of 0.1%, 0.3%, and 0.8%, respectively. In Figure 4.26, the excess pore water pressure ratio of a specimen at  $\gamma=0.1\%$  decreases from the unfrozen state to 1 freeze-thaw cycle, slightly increases from 1 to 2 freeze-thaw cycles, and then decreases from 2 to 4 freeze-thaw cycles. A similar trend of excess pore water pressure ratio for the specimen at  $\gamma=0.3\%$  is shown in Figure 4.27. However, for the largest shear strain of 0.8%, the excess pore water pressure ratio decreases with increasing number of freeze-thaw cycles without any fluctuation.

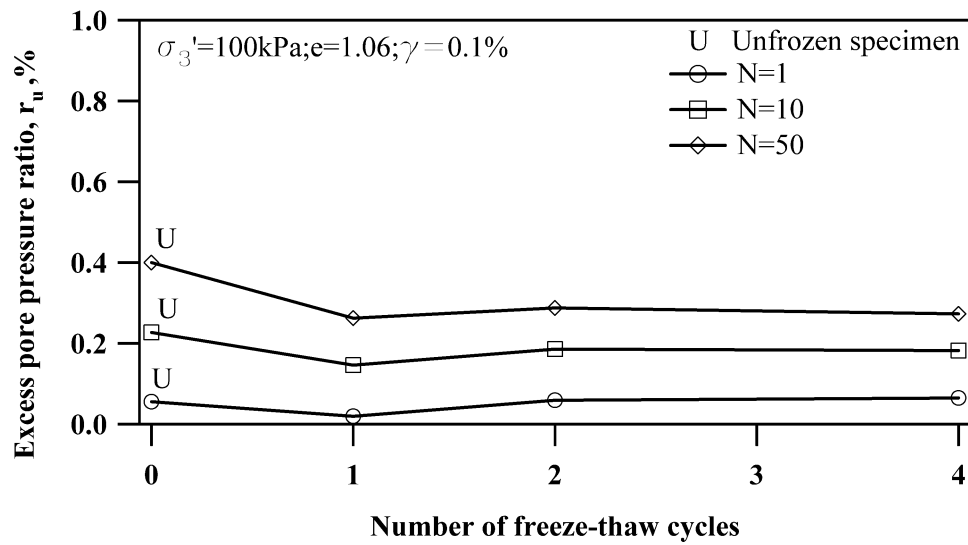


Figure 4.26 Excess pore water pressure versus the number of freeze-thaw cycles on Mabel Creek silt conditioned at  $\gamma = 0.1\%$

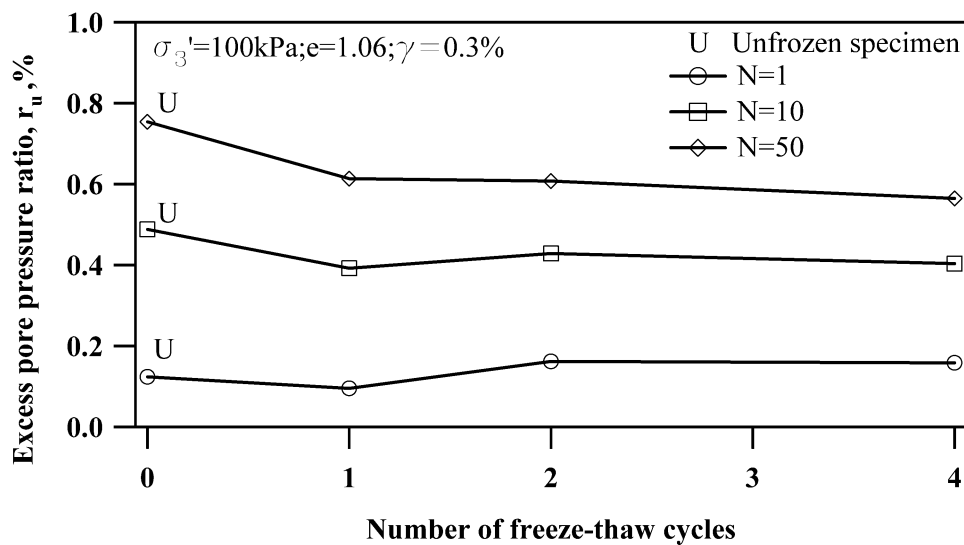
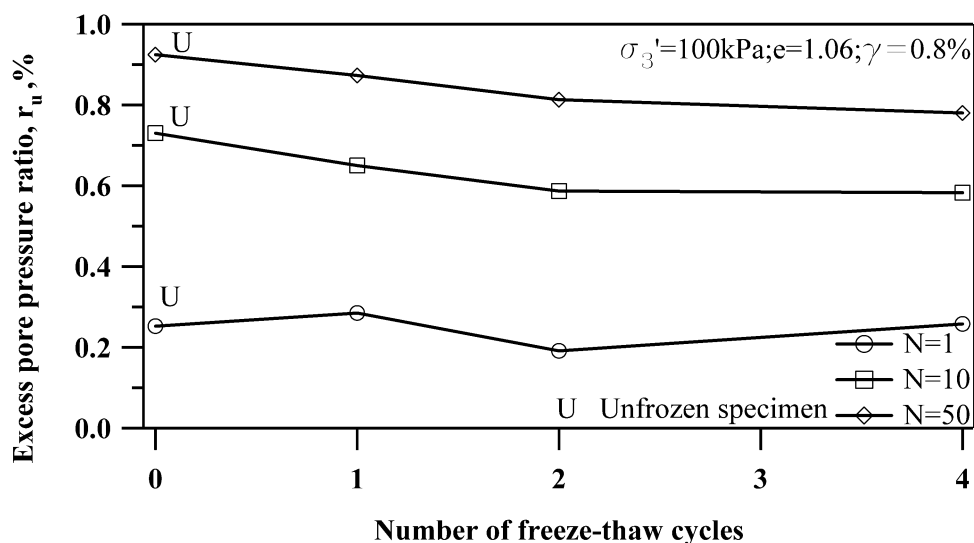
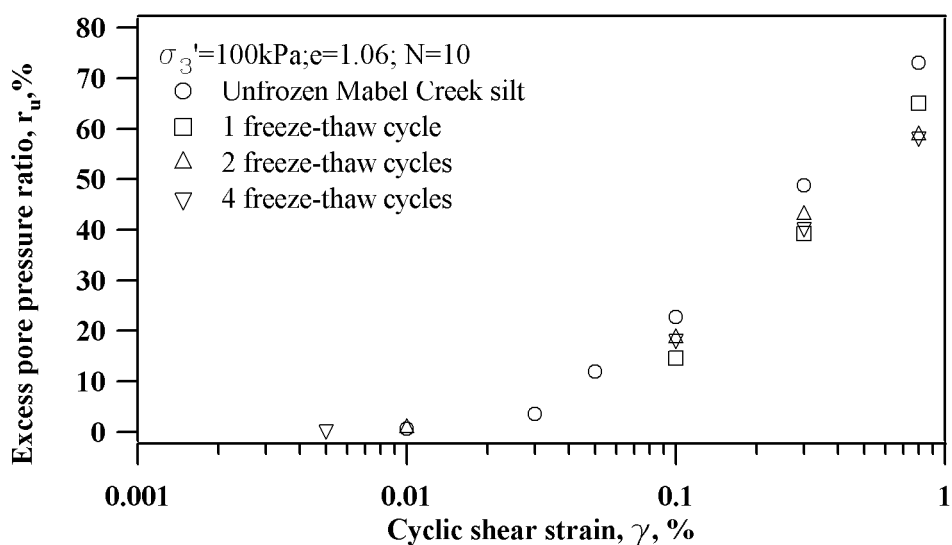


Figure 4.27 Excess pore water pressure versus the number of freeze-thaw cycles on Mabel Creek silt conditioned at  $\gamma = 0.3\%$



**Figure 4.28** Excess pore water pressure versus the number of freeze-thaw cycles on Mabel Creek silt conditioned at  $\gamma=0.8\%$

The impact of freeze-thaw cycles is compared in the pore water pressure generation curves of specimens conditioned at different numbers of freeze-thaw cycles at  $N=10$  presented in Figure 4.29. The unfrozen specimens had higher pore pressure generation than the other specimens conditioned by freeze-thaw cycles. The pore water pressure generation curves of the specimens experiencing 2 and 4 freeze-thaw cycles intersected in the narrowed band; however, the pore water pressure generation curves of the specimens that experienced 2 freeze-thaw cycles slightly passed over the curve of the specimens experiencing 4 freeze-thaw cycles with the  $r_u$  of less than 2%. Thus, it may be concluded that pore water pressure generation of specimens conditioned at 2 freeze-thaw cycles is similar to or even slightly higher than that of specimens conditioned at 4 freeze-thaw cycles. Excess pore pressure ratio of the specimen conditioned at only 1 freeze-thaw cycle was lower than that of the specimen experiencing 2 freeze-thaw cycles at  $\gamma=0.1\%$  and  $\gamma=0.3\%$ ; however, the situation was reversed at  $\gamma=0.8\%$ .



**Figure 4.29** Pore water pressure generation curves of Mabel Creek silt conditioned at different number of freeze-thaw cycles at  $N=10$

#### 4.7 Discussion of pore water pressure generation at freeze-thaw cycles

To investigate pore pressure generation curves in Mabel Creek silt conditioned at various freeze-thaw cycles, as in Section 4.4, pore water pressure generation boundaries from Dobry (1985) and Hazirbaba (2005) are introduced into the results in this study for comparison. This comparison is presented in Figure 4.30. The pore pressure generation in Mabel Creek silt conditioned at various freeze-thaw cycles is in the middle of curves for sand with 0-20% fines from Hazirbaba (2005), but under the lower bound of clean sand from Dobry (1985). Pore pressure generation at  $N=10$  in Mabel Creek silt conditioned at various temperatures is bounded as shown in Figure 4.31.



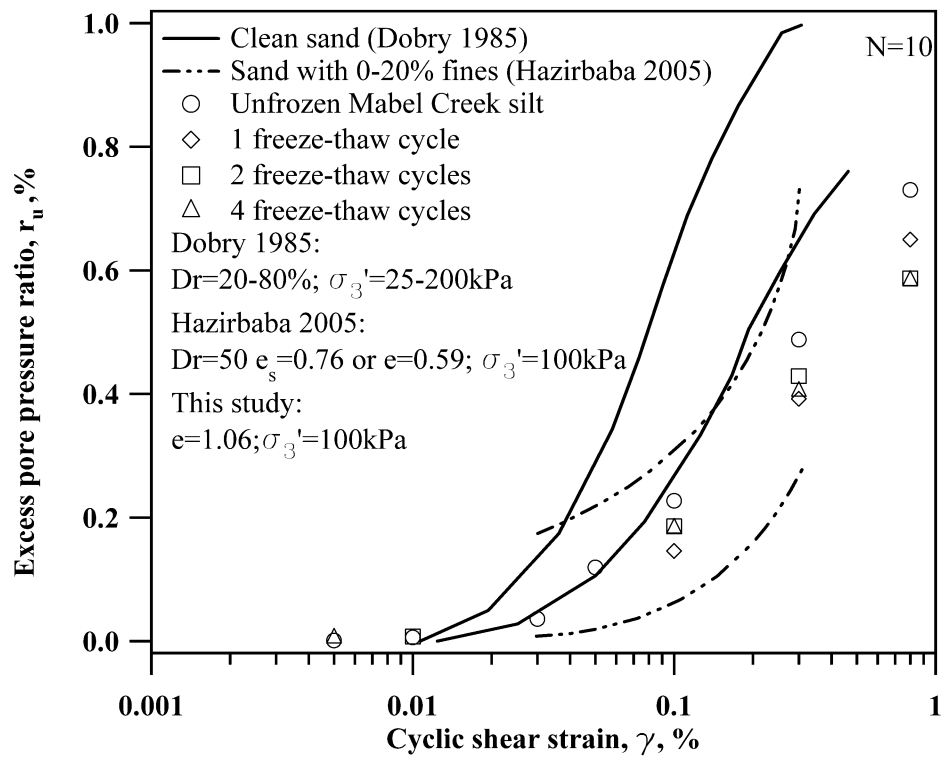


Figure 4.30 Comparison of pore pressure generation among Mabel Creek silt conditioned at various freeze-thaw cycles, clean sand and sand with fines

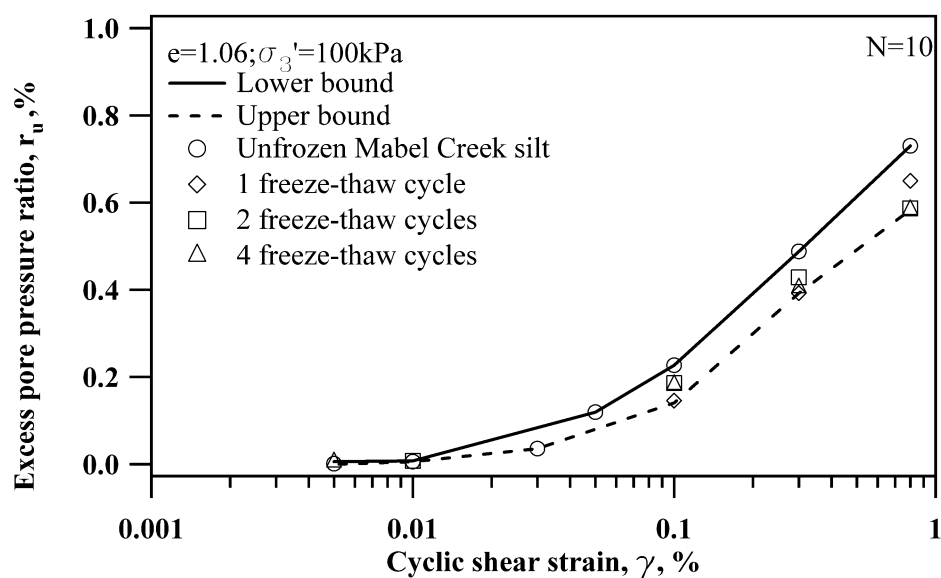


Figure 4.31 Bound of pore pressure generation in Mabel Creek silt conditioned at various freeze-thaw cycles

#### **4.8 Prediction of pore water pressure generation of Mabel Creek silt**

An understanding of how pore water pressure in soils generates during cyclic loadings provides a basis for estimating pore water pressure distribution in soils after the occurrence of seismic loadings, further variations of soil strength, and even settlement after seismic loadings. The modeling of pore water pressure generation caused by seismic loadings has been studied for many years. Basically, there are two approaches to the modeling of pore pressure generation caused by cyclic loadings. The first approach of modeling is based on a fundamental understanding of the liquefaction phenomenon. The approach takes advantage of the characteristics of rebounding and stress-strain curves in soils to express the generation of pore water pressure in soils subjected to earthquakes (Anandarajah 1994; Desai 2000; Dafalias and Manzari 2004). However, the accuracy of this kind of approach is limited by the soil stress-strain model and soil characteristic, which are attained by extra laboratory tests. The second approach makes use of results obtained from cyclic laboratory tests to build empirical or semi-empirical models of pore water pressure generation. These empirical or semi-empirical models generally required fewer soil characteristics, thus they display relatively easier application (Seed et al. 1976; Matasovic and Vucetic 1995; Talaganov 1996; Liyanathirana and Poulos 2002).

To describe the generation of pore water pressure in soils during cyclic loadings, Green et al. (2000) provided an empirical mode, the GMP model to estimate the pore water pressure developing with cyclic loadings. Unlike the models of Seed et al. (1976), Matasovic and Vucetic (1995), Talaganov (1996), and Liyanathirana and Poulos (2002), the number of loading cycles for initial liquefaction ( $N_1$ ) may be uncertain for the GMP model. This is very applicable to the generation of pore water pressure for Mabel Creek silt under the undrained cyclic strain-controlled loadings in this study. The GMP model is an energy-based model developed to be applied on non-plastic silt-sand mixtures on temperate ground. In this study, the application of

the GMP model is extended to partially frozen specimens and specimens subjected to freeze-thaw cycles. The GMP model is expressed as follows:

$$r_u = \sqrt{W_s / PEC} \leq 1 \quad (4.1)$$

Where:  $r_u$  is the excess pore water pressure ratio at the end of loading cycles;  
 PEC is “pseudoenergy capacity”, a calibration parameter; and  
 $W_s$  is the energy dissipated per unit volume of soil divided by the initial effect confining pressure.

For undrained cyclic triaxial test loadings,  $W_s$  may be expressed as follows:

$$W_s = \frac{1}{2\sigma'_o} \sum_{i=1}^{n-1} (\sigma_{d,i+1} + \sigma_{d,i}) (\varepsilon_{d,i+1} - \varepsilon_{d,i}) \quad (4.2)$$

Where:  $n$  is the number of load increments to liquefaction;  
 $\sigma_{d,i}$  is applied deviator stress at load increment  $i$ ;  
 $\varepsilon_{d,i}$  is axial strain at load increment  $i$ ; and  
 $\sigma'_o$  is initial effective stress.

In this study, the calibration parameter—PEC for specimens conditioned at different temperatures or freeze-thaw cycles may be found by method of the least squares from all tests results in the same thermal treatment condition. PEC for specimens conditioned at 24 °C, 5 °C, 1 °C, and 0.5 °C; specimens subjected to 2 and 4 freeze-thaw cycles; and unfrozen specimens is summarized in Table 4.1. The  $R^2$  values, from comparing the measured and predicted excess pore water pressure ratio according to the corresponding PEC, are also displayed in Table 4.1. It is obvious that the application of PEC in the GMP Model can attain the best fit for the test results. The  $R^2$  value for the unfrozen silt specimen with  $\gamma=0.01\%$  is found to be only 0.70, the other  $R^2$  values are always equal to or even greater than 0.95. The comparison of the predicted  $r_u$  from the GMP model and the measured  $r_u$  for specimens at each condition is presented in Figure 4.32~Figure 4.38. The maximum difference between predicted  $r_u$  and measured  $r_u$  occurred for the specimen conditioned at 0.5 °C with  $\gamma=0.1\%$ . The

maximum value reached about 0.12. Other comparisons displayed less difference or even approximate superposition between predicted  $r_u$  and measured  $r_u$ . Thus, the GMP model attained the best fit for measured  $r_u$  regardless of the thermal conditions of specimens. When the Mabel Creek silt's stress-strain behavior is determined by a constitutive model or stress-strain tests, the GMP can provide a prediction of excess pore water pressure ratio according to the above-obtained PEC.

**Table 4.1** PEC for GMP model on Mabel Creek silt and corresponding  $R^2$

Mabel Creek silt specimen No.	PEC	$R^2$					
		$\gamma=0.01\%$	$\gamma=0.03\%$	$\gamma=0.05\%$	$\gamma=0.1\%$	$\gamma=0.3\%$	$\gamma=0.8\%$
Unfrozen silt specimen	0.058	0.71	0.95	0.99	0.99	0.97	0.97
Specimen conditioning at 24 °C/experiencing 1 freeze-thaw cycle	0.100	--	--	--	0.98	0.97	0.98
Specimen conditioning at 5 °C	0.120	--	--	--	0.98	0.97	--
Specimen conditioning at 1 °C	0.176	--	--	--	0.98	0.97	--
Specimen conditioning at 0.5 °C	0.071	--	--	--	0.96	0.96	--
Specimen experiencing 2 freeze-thaw cycles	0.122	--	--	--	0.97	0.95	0.96
Specimen experiencing 4 freeze-thaw cycles	0.147	--	--	--	0.96	0.95	0.97

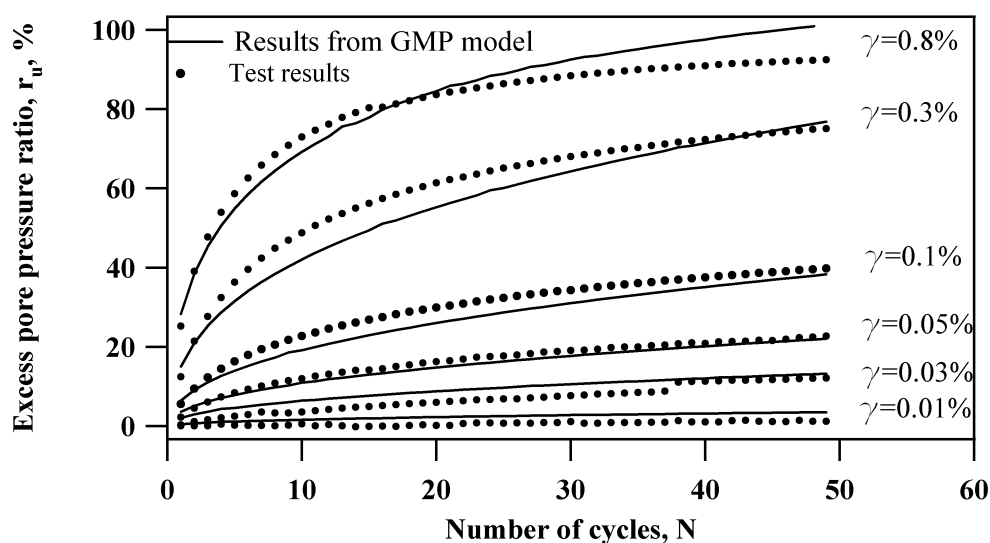


**Figure 4.32** The comparison of predicted  $r_u$  from GMP model and measured  $r_u$  on unfrozen Mabel Creek silt

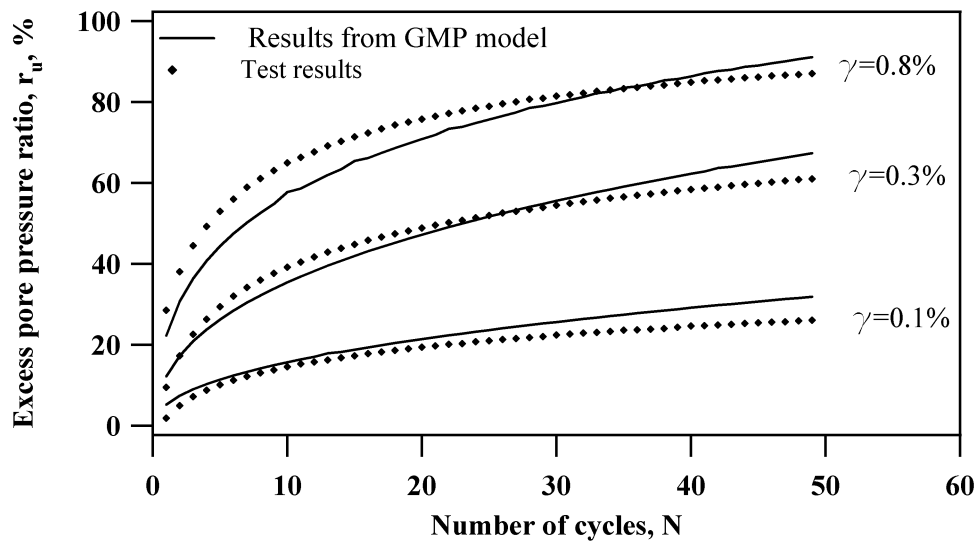


Figure 4.33 The comparison of predicted  $r_u$  from GMP model and measured  $r_u$  on Mabel Creek silt conditioned at 24 °C or experiencing 1 freeze-thaw cycle

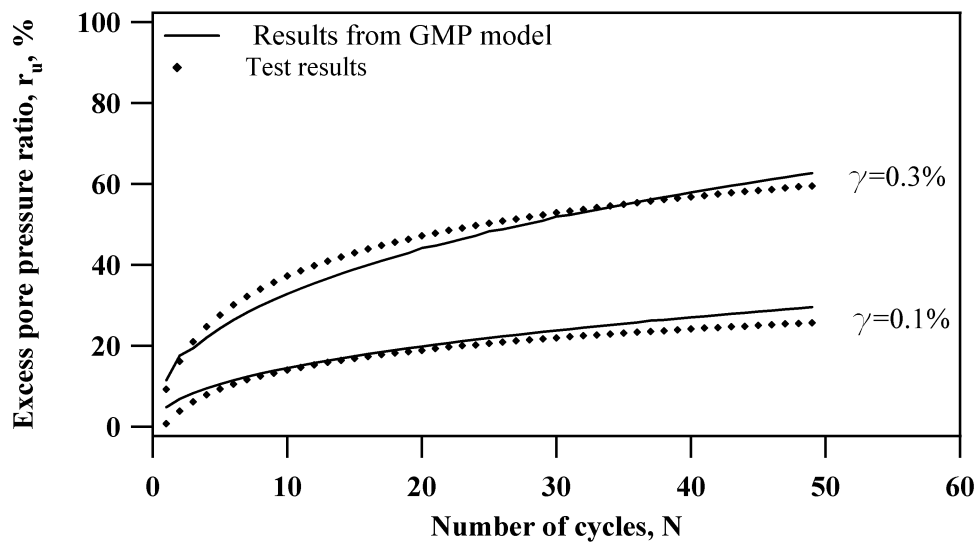


Figure 4.34 The comparison of predicted  $r_u$  from GMP model and measured  $r_u$  on Mabel Creek silt conditioned at 5 °C

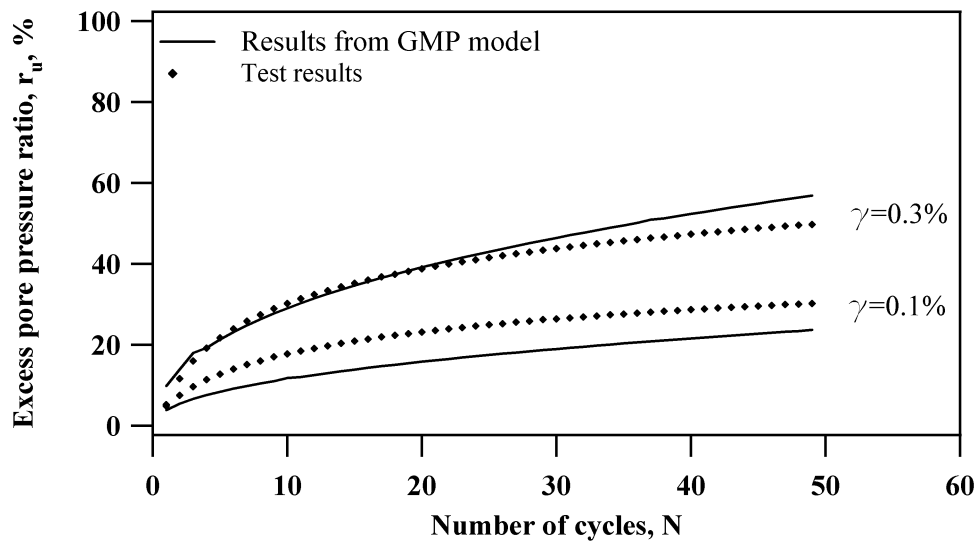


Figure 4.35 The comparison of predicted  $r_u$  from GMP model and measured  $r_u$  on Mabel Creek silt conditioned at 1 °C

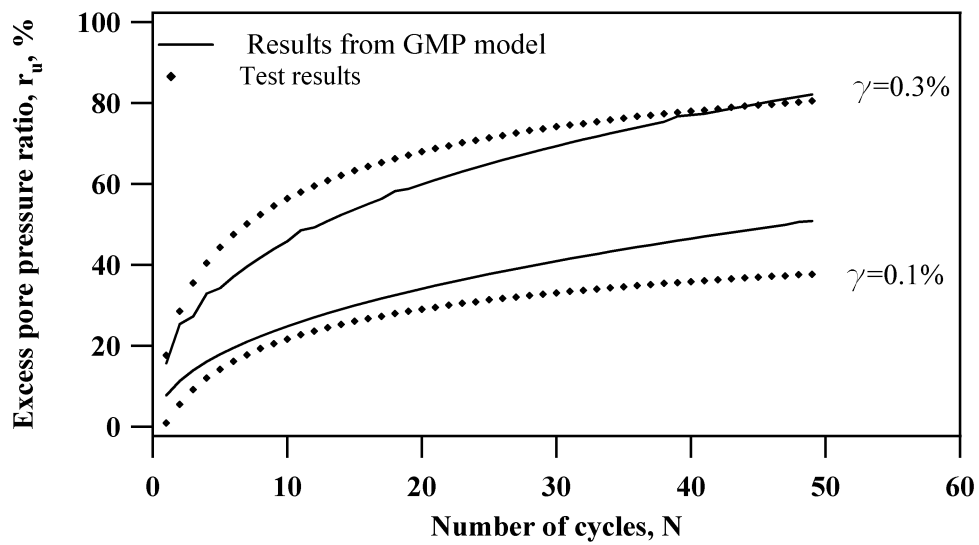
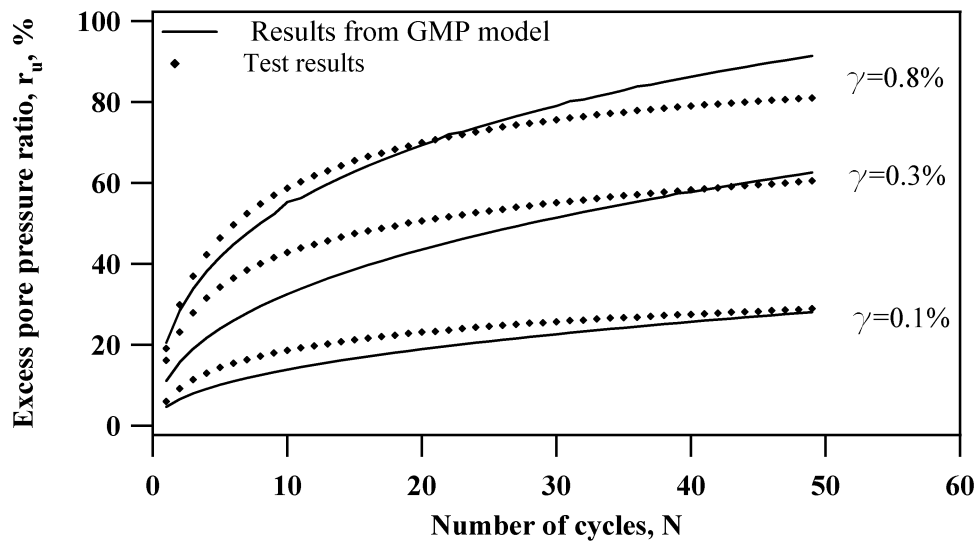
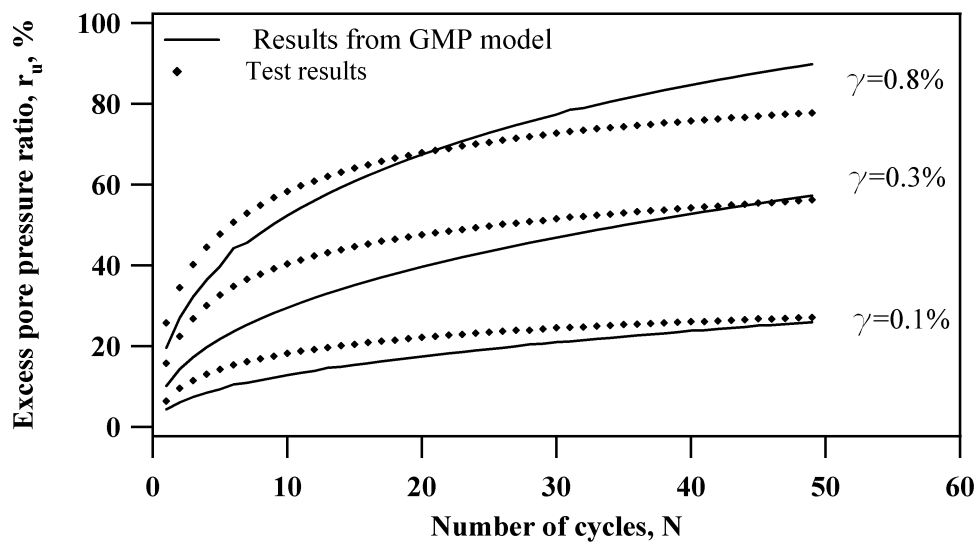


Figure 4.36 The comparison of predicted  $r_u$  from GMP model and measured  $r_u$  on Mabel Creek silt conditioned at 0.5 °C



**Figure 4.37** The comparison of predicted  $r_u$  from GMP model and measured  $r_u$  on Mabel Creek silt experiencing 2 freeze-thaw cycles



**Figure 4.38** The comparison of predicted  $r_u$  from GMP model and measured  $r_u$  on Mabel Creek silt experiencing 4 freeze-thaw cycles

The effect of temperature on partially frozen or thawed specimens was reflected on PEC as shown in Figure 4.39. The relationship between PEC and the conditioning temperature on partially frozen or thawed specimens is unclear. However, PEC was found to have a trend of increase with the number of freeze-thaw cycles on specimens as shown in Figure 4.40.

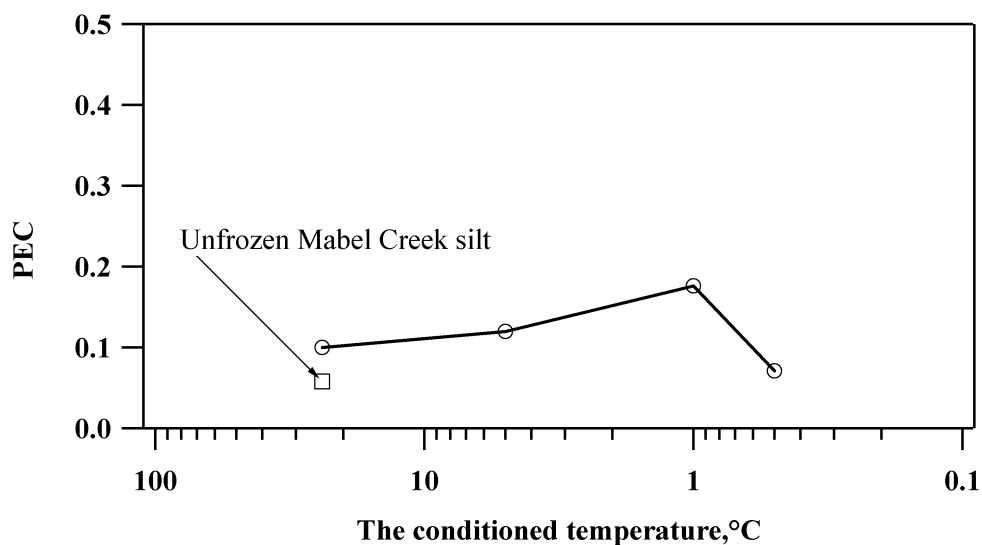


Figure 4.39 PEC versus the conditioning temperature on Mabel Creek silt

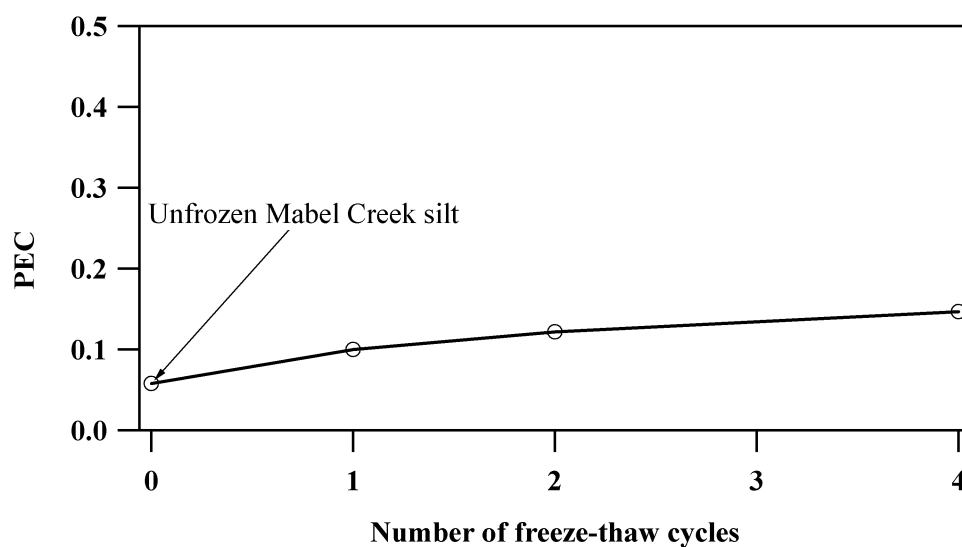


Figure 4.40 PEC versus the number of freeze-thaw cycles on Mabel Creek silt

#### 4.9 Impact of thermal condition paths on pore pressure generation of Mabel Creek silt

The same thermal conditioning target temperatures (i.e., 0.5 °C and -0.2 °C) may be reached by different paths. Different paths may cause different liquefaction potential at the specific target temperature. To confirm this assumption, pore pressure history and pore pressure generation curves are compared for specimens at the target



temperatures, but by three different conditioning paths. The near-freezing temperatures of 0.5 °C and -0.2 °C were chosen as target temperatures, because 0.5 °C and -0.2 °C are close to the freezing point and a change of thermal conditioning paths may cause different freezing and thawing.

Figure 4.41 and Figure 4.42 shows an evaluation of thermal conditioning paths on the liquefaction potential of specimens at the target temperature of 0.5 °C. A large shear strain of  $\gamma=0.3\%$  was chosen for evaluation. Thermal Conditioning Path 1 caused the largest excess pore pressure ratio at any given number of loading cycles, but longer conditioning time at 0.5 °C (Thermal Conditioning Path 2) decreased liquefaction potential. The lowest pore pressure generation occurred on thermal Conditioning Path 3. A similar order of thermal conditioning path impact is reflected in pore pressure generation curves, as shown in Figure 4.42.

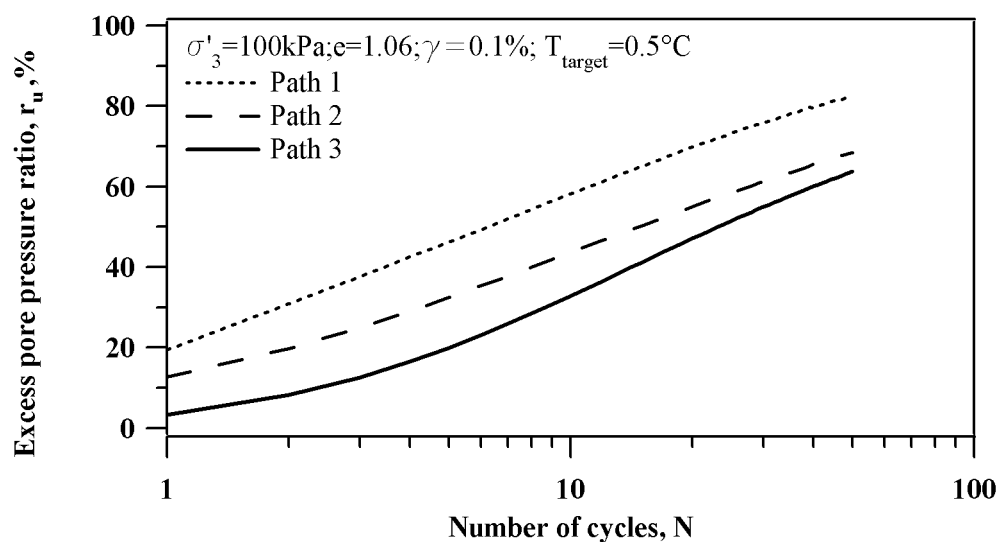


**Figure 4.41** Effect of thermal conditioning paths on pore water pressure history of Mabel Creek silt at target temperature of 0.5 °C and  $\gamma=0.3\%$

Similarly, Figure 4.43 and Figure 4.44 show the influence of thermal conditioning paths on liquefaction potential of specimens at the target temperature of -0.2 °C. For  $\gamma=0.1\%$ , Path 1 and Path 2 could not cause the excess pore pressure generation, even

more interestingly, they cause negative pore pressure ratios, probably because most of the specimens conditioned by Path 1 or Path 2 were still in a frozen state. However, Path 3 did not freeze the specimen completely, and therefore pore pressure generation was observed under cyclic loading. A similar thermal conditioning path influence is reflected in pore pressure generation curves, as shown in Figure 4.44.

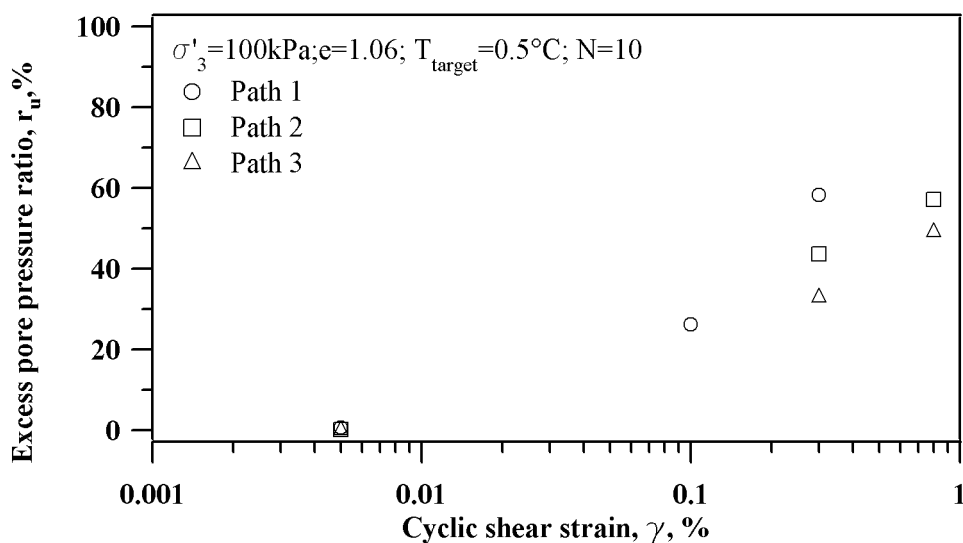


Figure 4.42 Effect of thermal conditioning paths on pore water pressure generation curve of Mabel Creek silt at target temperature of 0.5 °C

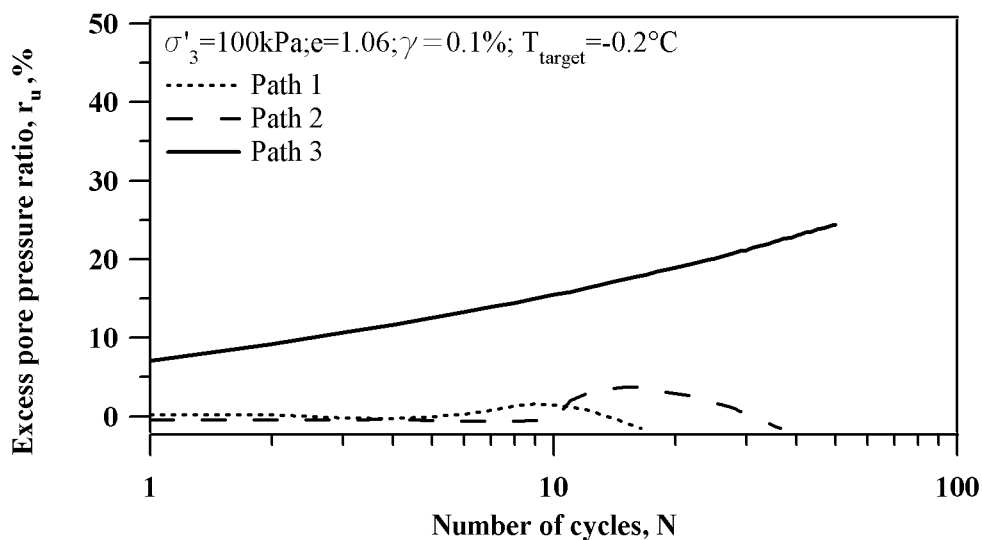
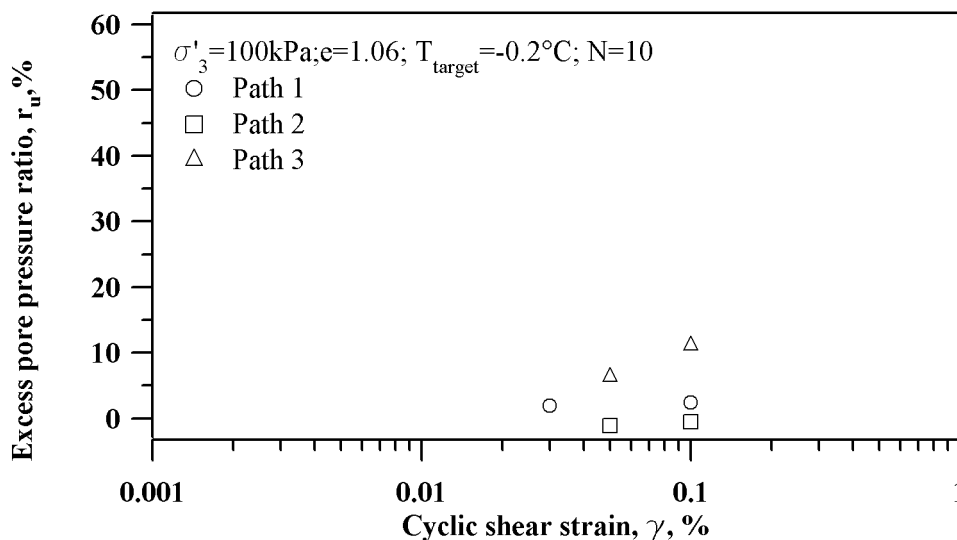


Figure 4.43 Effect of thermal conditioning paths on pore water pressure history of Mabel Creek silt at target temperature of -0.2 °C and  $\gamma = 0.1\%$



**Figure 4.44** Effect of thermal conditioning paths on pore water pressure generation curve of Mabel Creek silt at target temperature of  $-0.2\text{ }^{\circ}\text{C}$

#### 4.10 Summary

In this chapter pore water pressure generation of unfrozen specimens was displayed as a baseline to further study the effect of temperature rise and freeze-thaw cycles on pore water pressure generation. Pore water pressure generation of specimens conditioned at  $24\text{ }^{\circ}\text{C}$ ,  $5\text{ }^{\circ}\text{C}$ ,  $1\text{ }^{\circ}\text{C}$ ,  $0.5\text{ }^{\circ}\text{C}$ , and  $-0.2\text{ }^{\circ}\text{C}$  was analyzed. The pore water pressure generation of specimens experiencing 2 and 4 freeze-thaw cycles also was investigated. The influence of temperature and freeze-thaw cycles on pore water pressure generation was evaluated.

During study of the temperature effect on pore water pressure of partially frozen or frozen specimens, the specimens thawed at  $0.5\text{ }^{\circ}\text{C}$  had the largest pore water pressure generation in comparison with unfrozen specimens and specimens thawed at  $1\text{ }^{\circ}\text{C}$ ,  $5\text{ }^{\circ}\text{C}$ , and  $24\text{ }^{\circ}\text{C}$ . When the conditioning temperature was raised to  $1\text{ }^{\circ}\text{C}$ ,  $5\text{ }^{\circ}\text{C}$ , or  $24\text{ }^{\circ}\text{C}$ , substantial decrease of pore water pressure generation was observed, and pore water pressure generation decreased to less than that of the unfrozen specimens. Similar pore water pressure generation was found on the specimens conditioned at  $5\text{ }^{\circ}\text{C}$  and

24 °C. No increase or a drop in pore water pressure was observed for specimens conditioned at -0.2 °C.

During study of the freeze-thaw-cycles effect on pore water pressure of Mabel Creek silt, the freeze-thaw cycles strongly decreased pore water pressure generation for specimens. The main decrease of pore water pressure generation occurred only for 1 freeze-thaw cycle. The decrease effect of further freeze-thaw on pore water pressure generation was obviously weakened with an increased number of freeze-thaw cycles. Almost no variation in pore water pressure generation was observed with increased number of freeze-thaw cycles from 2 to 4.

By comparing pore pressure generation of Mabel Creek silt, clean sand, and sand with 0-20% fines, pore pressure generation in Mabel Creek silt, regardless of conditioning temperature and number of freeze-thaw cycles, is only equivalent to that in sand with 0-20% fines.

The GMP model was provided to predict the pore pressure generation of Mabel Creek silt subjected to various thermal conditions (i.e., temperature treatment and number of freeze-thaw cycles) under undrained strain-controlled cyclic loadings. The test results were consistent with the results predicted by the GMP model. This indicates that the GMP model can be applicable to fine-grained soil's pore pressure generation by strain-controlled cyclic loadings, even if these fine-grained soils are conditioned at different temperatures or freeze-thaw cycles. The prediction of pore pressure generation may be conducted only by attaining stress-strain history and selection of PEC, which has been gained in this study.

The thermal conditioning path was found to strongly affect the liquefaction potential of Mabel Creek silt. This investigation was conducted to compare the pore pressure generation of Mabel Creek silt at 0.5 °C and 0.2 °C through three different conditioning

paths. Comparison indicates that the conditioning paths will affect the liquefaction potential of Mabel Creek silt. For the target temperature of 0.5 °C, short term (2 days) thawed conditioning (Path 1) would maximally increase liquefaction potential. For the target temperature of -0.2 °C, short term (2 days) and long term (7 days) thawed conditioning caused no difference. The Mabel Creek silt in these two conditions still acted like a fine-grained soil in a frozen state and pore pressure could not be generated under cyclic loading. However, direct freezing at -0.2 °C for 2 days (Path 3) could not cause freezing in a large portion of the sample and pore pressure could still be generated under cyclic loading.

## **5 Dynamic Properties of Mabel Creek Silt**

### **5.1 Introduction**

Dynamic properties of soil play a major role in determining behavior and deformation characteristics under seismic loading conditions. Shear modulus ( $G$ ) and damping ratio ( $D$ ) are the two dynamic properties commonly used to examine strain dependent nonlinear behavior of soil. Shear modulus and damping ratio are affected by many factors, such as confining pressure, void ratio, geologic age, cementation, overconsolidation ratio, plasticity index, cyclic strain, strain rate, and number of loading cycles (Hardin and Drnevich 1972; Kokusho et al. 1982; Dobry and Vucetic 1987). Additionally, temperature and water content have significant impact on dynamic response of soil (Vinson 1978; Czajkowski and Vinson 1980; Fukuda and Huang 1991).

In this study, shear modulus and damping characteristics of Mabel Creek silt were investigated for temperature and freeze-thaw effects. This chapter provides the reader with values for dynamic shear modulus and damping ratio for Mabel Creek silt conditioned at various temperatures, including near-freezing temperature, and at various freeze-thaw cycles. The ground temperatures studied were 24 °C, 5 °C, 1 °C, 0.5 °C, and -0.2 °C. The seasonal variation of ground temperature was simulated by subjecting soil specimens to 1, 2, and 4 freeze-thaw cycles. The unfrozen specimens refer to the specimens without any freezing or thawing treatments. The results from the unfrozen specimen were considered as a baseline in this study. All specimens were prepared at a consolidation void ratio of 1.06 and an initial effective confining pressure of approximately 100 kPa. Undrained triaxial strain-controlled tests were conducted to acquire dynamic shear modulus and damping ratio. Moreover, shear strain and number of loading cycles were also considered in evaluating shear modulus and damping ratio.

## 5.2 Dynamic properties of unfrozen Mabel Creek silt

Figure 5.1 illustrates how dynamic shear modulus ( $G$ ) for unfrozen Mabel Creek silt varies with: a) number of load cycles; b) developed excess pore pressure; and c) induced cyclic shear strain. The trend in Figure 5.1a. suggests that for shear strains between 0.005% and 0.05%, the shear modulus remains constant irrespective of the number of loading cycles; however, at  $\gamma=0.8\%$ , the number of loading cycles appears to have a significant influence on shear modulus indicating that shear modulus decreases with increase in the number of loading cycles. This may be attributed to the decrease in effective confining pressure caused by the excess pore water pressure buildup under undrained conditions as shown in Figure 5.1b. Larger values of shear modulus were obtained when  $r_u$  is equal to or near zero, while significant degradation was observed when  $r_u$  was close to 100%. Figure 5.1c shows the variation of shear modulus with respect to the induced cyclic shear strain. The shear modulus generally decreases with increased level of cyclic shear strain, which is traditionally referred to as cyclic degradation.

Figure 5.2 shows the damping ratio ( $D$ ) for unfrozen Mabel Creek silt. Similar evaluations to those presented for shear modulus were made for damping in Figure 5.2. According to the history of damping ratio, which is shown in Figure 5.2a, there are three different trends. The damping response of the specimens tested at shear strains between 0.005% and 0.01% was found to be similar:  $D$  was approximately equal in value of 4~5% at these strain levels and remained nearly constant with increasing number of loading cycles. The specimens tested at 0.05%, 0.1%, and 0.3% shear strains showed a slight decrease in damping with increasing number of loading cycles. The damping response of the specimen tested at  $\gamma=0.8\%$  showed a slight increase in damping values with increasing number of loading cycles up to  $N=10$ ; however, an increase in damping was found to occur at a much greater rate beyond  $N=10$ . Variation of damping ratio during damping ratio history may be attributed to

generation of pore pressure induced by cyclic loading. The relationship between excess pore pressure generation and damping ratio presented in Figure 5.2b reflects this attribution. Damping ratio remained a constant value (approximately 5%) at  $\gamma=0.005\%$  and  $\gamma=0.01\%$  when the excess pore pressure was not generated at all. At  $\gamma=0.05\%$ ,  $\gamma=0.1\%$  and  $\gamma=0.3\%$ , damping ratio decreased with an increase in the corresponding  $r_u$  to 40%. As  $r_u$  increased to values between 40%~80%, the damping ratio remained nearly constant. For example, D was at 18% and 22%, respectively, for  $\gamma=0.1\%$  and for  $\gamma=0.3\%$ . When  $r_u$  was near 100% (i.e., the liquefaction state), a dramatic increase in damping ratio occurred, which was observed at  $\gamma=0.8\%$ : damping ratio even increased to 63% at the corresponding  $r_u=93\%$ . The damping ratio versus cyclic shear strain is presented in Figure 5.2c. In general, the damping ratio appears to increase with increasing cyclic shear strain.

### **5.3 Dynamic properties of Mabel Creek silt conditioned at 24 °C, 5 °C, 1 °C, 0.5 °C, and -0.2 °C**

The shear modulus for specimens conditioned at 24 °C is presented in Figure 5.3. More specifically, the influence of load cycles, excess pore pressure, and cyclic shear strain on the shear modulus is examined in Figure 5.3a to Figure 5.3c. The impact of number of loading cycles is shown in Figure 5.3a. This figure shows that the shear modulus remained unchanged at 41.5 MPa for the small shear strain of 0.005%. This shear strain is less than the threshold shear strain. Degradation of shear modulus occurred at medium to large shear strain between 0.1% and 0.8%. Shear modulus was shown to degrade with pore pressure; see Figure 5.3b. At  $\gamma=0.005\%$  the excess pore pressure was found to be approximately zero. At this value, there was no degradation in shear modulus. Shear modulus was found to degrade as pore pressure increased.

A shear modulus of approximately 41.5 MPa was found not to change when  $r_u$  was near zero. Shear modulus at  $\gamma=0.8\%$  degraded to 0.6 MPa at  $N=50$ ; this corresponded



to an  $r_u$  of 87%. A decrease in shear modulus with an increase in cyclic shear strain is shown in Figure 5.3c.

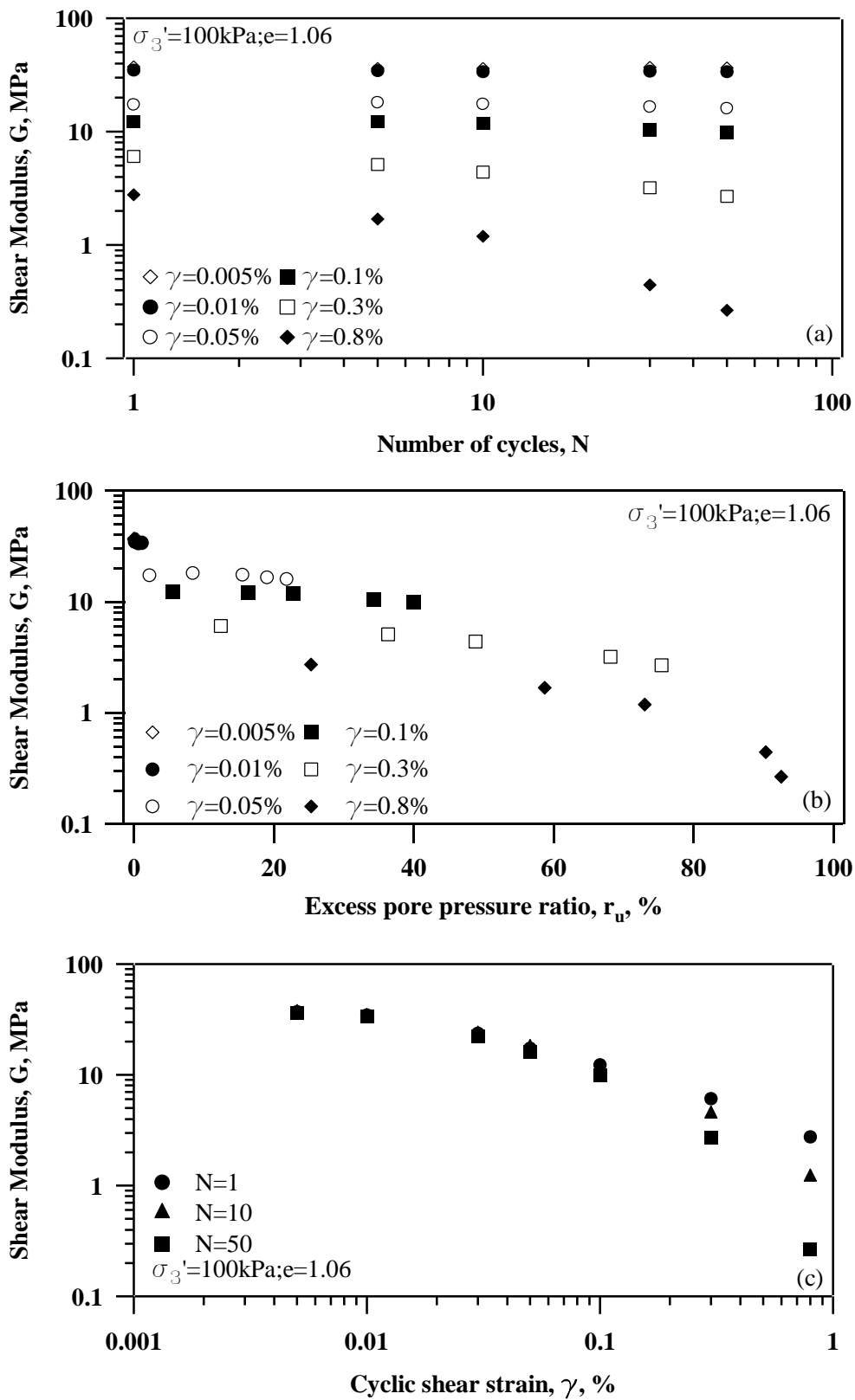


Figure 5.1 Shear modulus ( $G$ ) on unfrozen Mabel Creek silt: (a)  $G$  vs  $N$ ; (b)  $G$  vs  $r_u$ ; (c)  $G$  vs  $\gamma$

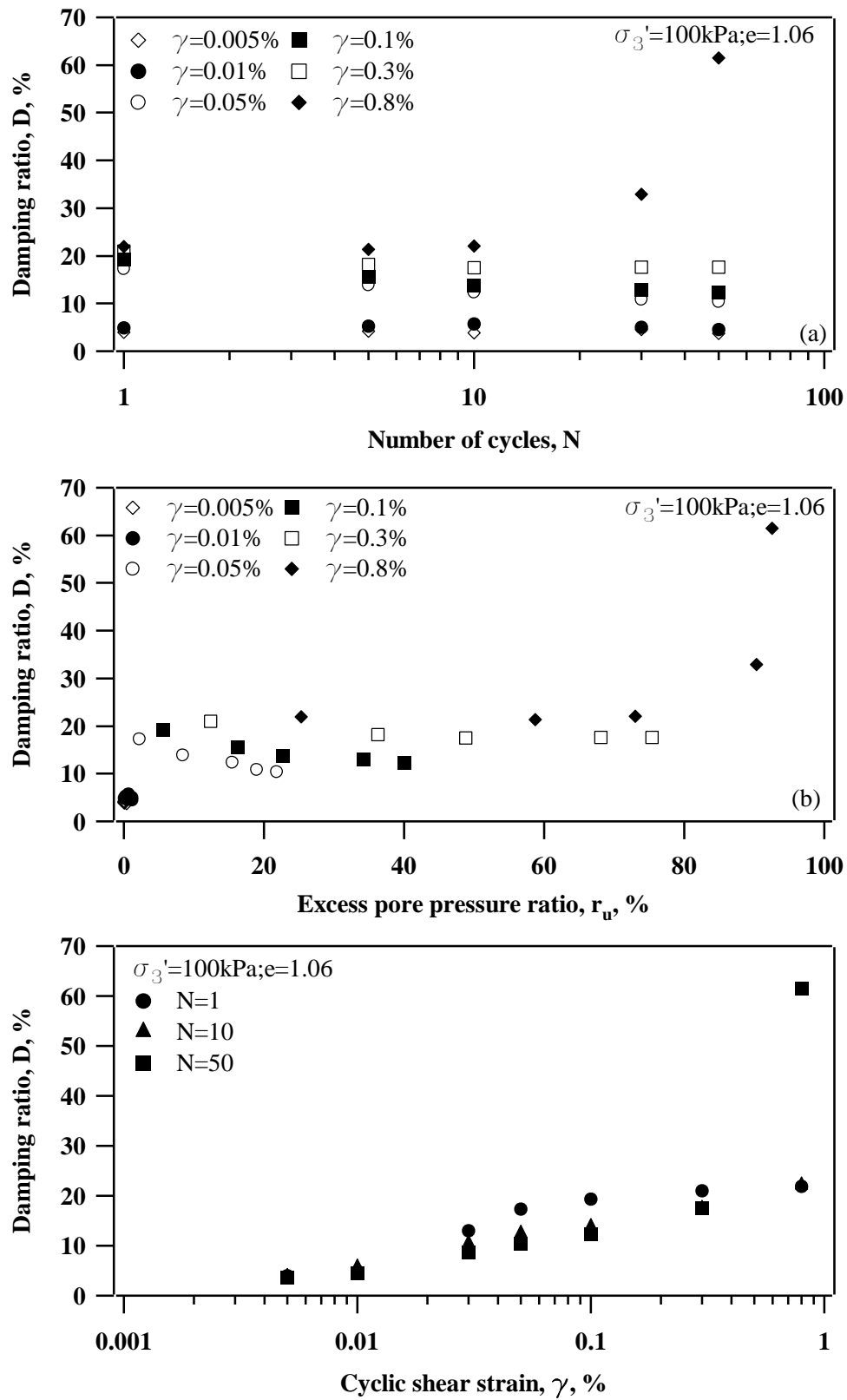


Figure 5.2 Damping ratio ( $D$ ) on unfrozen Mabel Creek silt: (a)  $D$  vs  $N$ ; (b)  $D$  vs  $r_u$ ; (c)  $D$  vs  $\gamma$

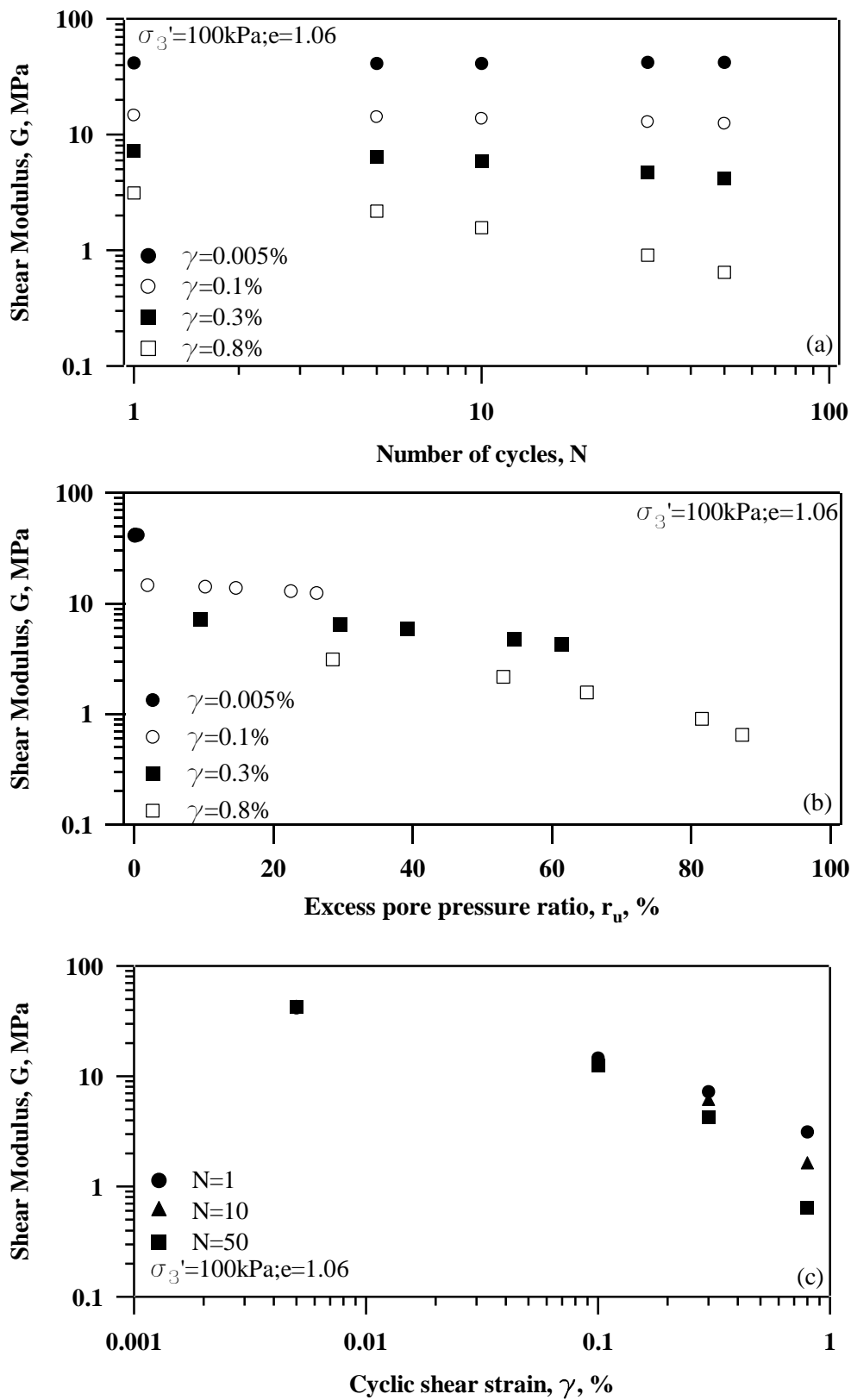


Figure 5.3 Shear modulus ( $G$ ) on Mabel Creek silt conditioned at 24 °C: (a)  $G$  vs  $N$ ; (b)  $G$  vs  $r_u$ ; (c)  $G$  vs  $\gamma$

Figure 5.4 shows damping ratio for specimens conditioned at 24 °C. Damping ratio histories for shear strains between 0.005% and 0.8% were found to follow two trends; see Figure 5.4a. At the small shear strain level of 0.005%, the damping ratio remained constant at approximately 5% during 50 loading cycles. For medium to large shear strain levels from 0.1% to 0.8%, the damping ratio was found to decrease with increasing loading cycles, although constant damping ratios after  $N=10$  were found to occur at  $\gamma=0.3\%$  and 0.8%. The influence of pore pressure generation on damping ratio is shown in Figure 5.4b. Similar to the unfrozen specimens, findings for the specimens conditioned at 24 °C show that constant and small damping ratios were observed at  $r_u$  near zero (0), while a decrease in damping ratios was observed with increase in  $r_u$  at the range of 0 to 40%. However, damping ratios remained nearly constant with increase  $r_u$  (values between 40% to 87%). For the limited data set, no dramatic increase in damping ratio occurred when  $r_u$  was close to 100%. There was an increasing trend in damping ratio with an increasing cyclic shear strain. This trend is shown in Figure 5.4c.

The shear modulus for specimens conditioned at 5 °C during testing for cyclic loading is presented in Figure 5.5. For a small shear strain level of 0.005%, pore pressure was not generated, and shear modulus remained at about 45 MPa through the cyclic loading test; the shear modulus did not degrade. Shear modulus slightly reduced from 15.2 MPa at  $N=1$  to 13.4 MPa at  $N=50$  for  $\gamma=0.1$ . Excess pore pressure ratio increased from 1% at  $N=1$  to 26% at  $N=50$ . As  $\gamma$  increased to 0.3%, shear modulus decreased from 7.7 MPa at  $N=1$  to 4.6 MPa at  $N=50$  while excess pore pressure ratio increased from 9% to 60%. Like the trend for shear modulus with respect to induced shear strain on specimens conditioned at 24 °C, shear modulus on specimens conditioned at 5 °C decreased with increasing cyclic shear strain as shown in Figure 5.5c.

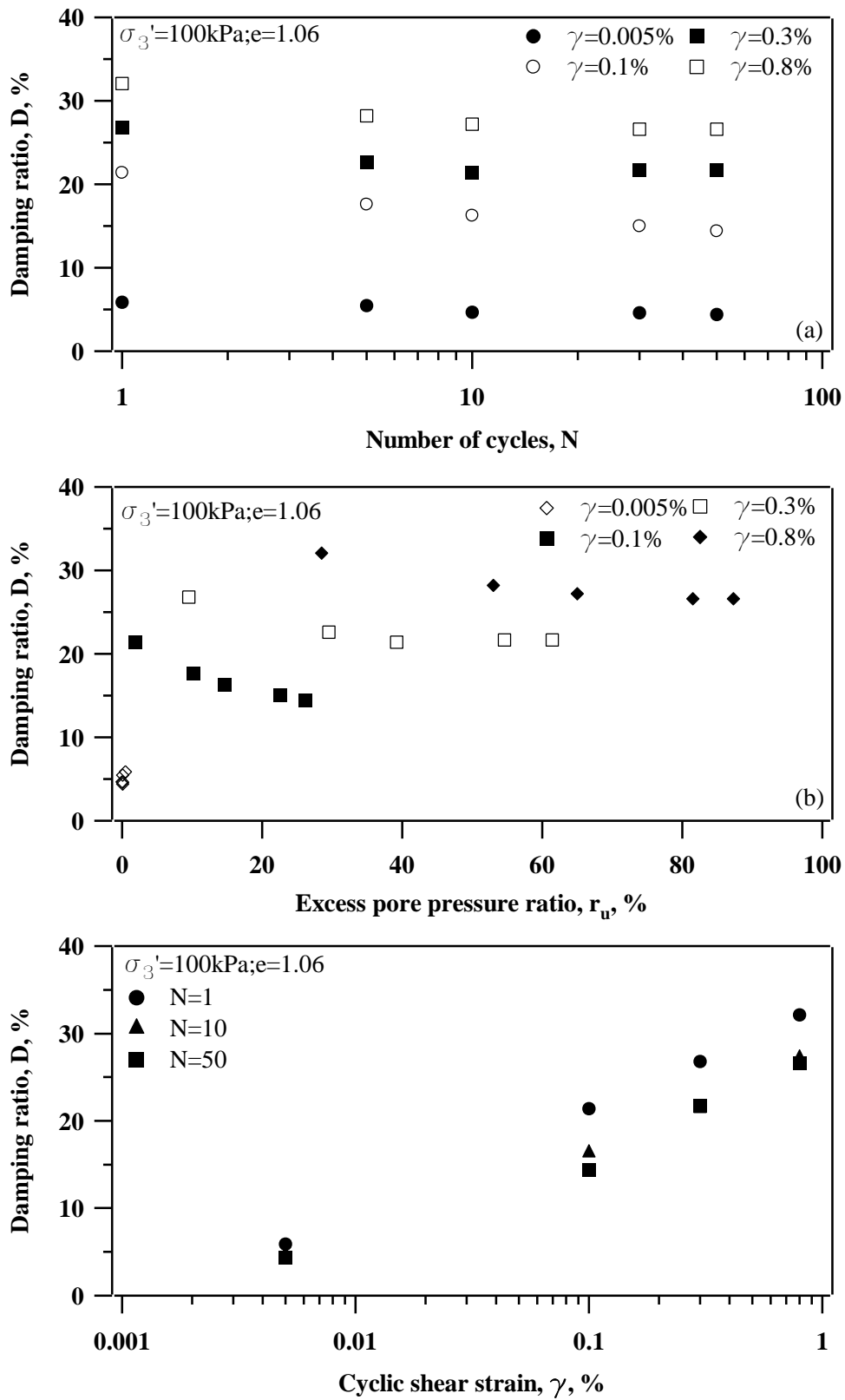


Figure 5.4 Damping ratio ( $D$ ) on Mabel Creek silt conditioned at 24 °C: (a)  $D$  vs  $N$ ; (b)  $D$  vs  $r_u$ ; (c)  $D$  vs  $\gamma$

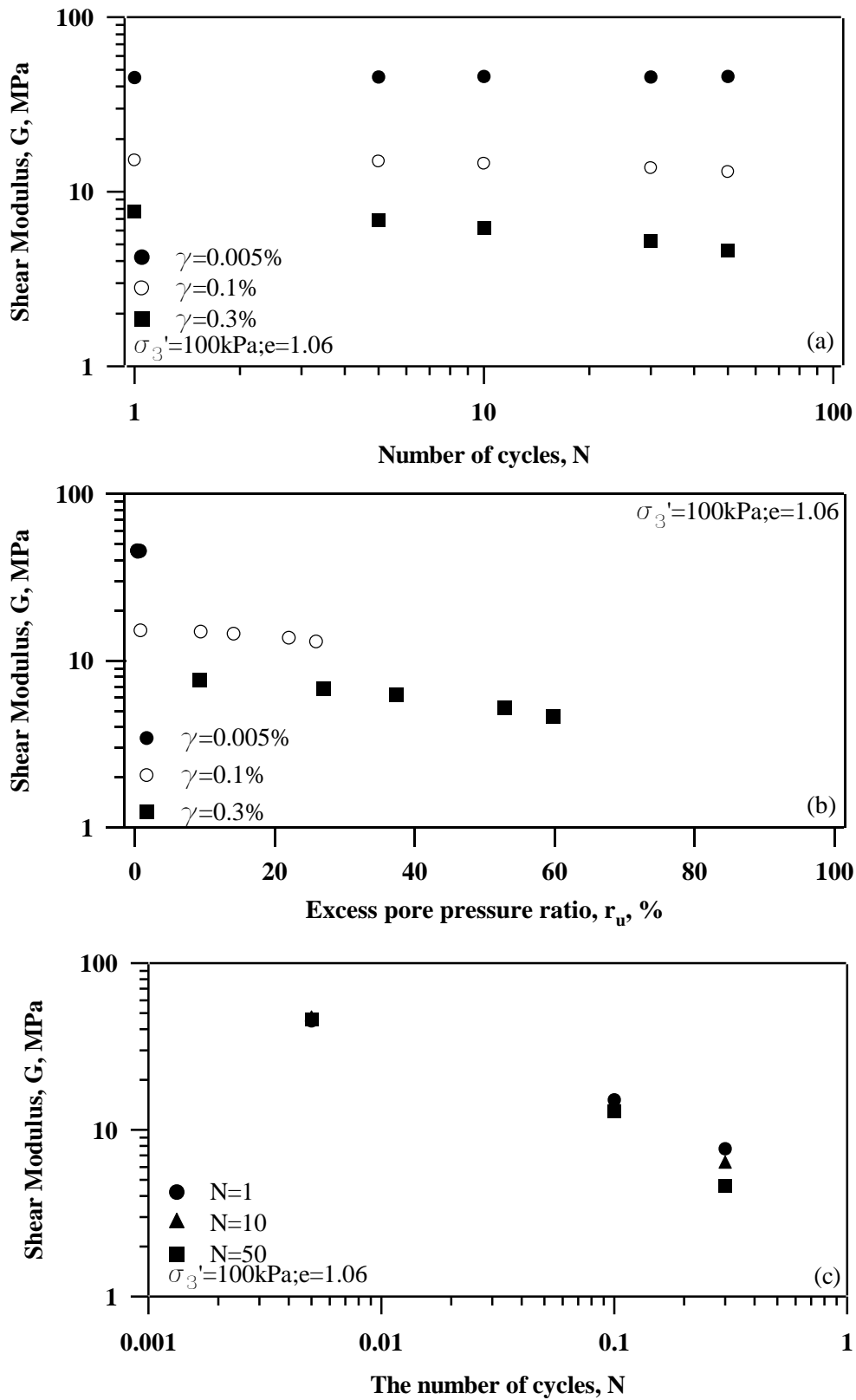


Figure 5.5 Shear modulus ( $G$ ) on Mabel Creek silt conditioned at 5 °C: (a)  $G$  vs  $N$ ; (b)  $G$  vs  $r_u$ ; (c)  $G$  vs  $N$

Damping ratio variability for specimens conditioned at 5 °C is presented in Figure 5.6. Shear strains between 0.005% and 0.3% are presented. For small shear strain levels near 0.005%, the damping ratio was nearly a constant 4%. Further, it remained at nearly a constant value of 4% during the cyclic loading test when  $r_u = 0$ . As  $\gamma$  increased to 0.1%, damping ratios decreased from 22% at  $N=1$  to 14% at  $N=50$  while the corresponding  $r_u$  increased from 1% at  $N=1$  to 26% at  $N=50$ . In the same manner for the specimen with  $\gamma=0.3\%$ , damping ratio decreased from 23% at  $N=1$  to 17% at  $N=50$ ; meanwhile  $r_u$  changed from 9% to 60%. Damping ratio was found to have an increasing trend with increasing shear strain; see Figure 5.6c.

Shear modulus for specimens conditioned at 1 °C is shown in Figure 5.7. This figure shows that shear modulus remained constant (no degradation), and no pore pressure was generated at small shear strains near 0.005%. Degradation of shear modulus was observed at large shear strains between 0.1% and 0.3%. Shear modulus at  $\gamma=0.1\%$  slightly reduced from 14.1 MPa at  $N=1$  to 12.5 MPa at  $N=50$  while  $r_u$  varied from 5% at  $N=1$  to 30% at  $N=50$ . The buildup of the excess pore pressure ratio changed from 5% at  $N=1$  to 50% at  $N=50$  for  $\gamma=0.3\%$ . The change in the excess pore pressure ratio induced a degradation in shear modulus from 8.6 MPa at  $N=1$  to 5.7 MPa at  $N=50$ . Shear modulus was found to degrade with an increase in cyclic shear strain but was independent of the loading cycle; see Figure 5.7c.

Figure 5.8 presents the damping ratio for specimens conditioned at 1 °C. At small shear strain levels of 0.005%, the damping ratio remained nearly constant at approximately 0.05 with increasing loading cycles and no pore pressure generation occurred. A decreasing trend in damping ratio was observed during cyclic loadings for specimens at  $\gamma=0.1\%$ . Further, the damping ratio decreased from 21% at  $N=1$  to 14% at  $N=50$  while the corresponding  $r_u$  generated varied from 5% at  $N=1$  to 30% at  $N=50$ . A similar decreasing damping ratio was found at a shear strain level of 0.3%. The



damping ratio for specimens at  $\gamma=0.3\%$  decreased from 24% at  $N=1$  to 18% at  $N=50$  as  $r_u$  increased from 5% at  $N=1$  to 50% at  $N=50$ . An increase in damping ratio with increase in cyclic shear strain also was observed for specimens conditioned at  $1\text{ }^\circ\text{C}$ ; see Figure 5.8c.

Shear modulus for specimens conditioned at  $0.5\text{ }^\circ\text{C}$  is shown in Figure 5.9. Shear modulus was approximately constant (about 77 MPa) at the small shear strain values of 0.005%. At these values, there was no pore pressure generation. Shear modulus values for specimens conditioned at  $0.5\text{ }^\circ\text{C}$  were much higher than for the specimens conditioned at  $1^\circ\text{C}$ ,  $5^\circ\text{C}$ , and  $24^\circ\text{C}$ . At  $\gamma=0.1\%$  the shear modulus decreased from 20.0 MPa at  $N=1$  to 17.2 MPa at  $N=50$ . This corresponded to an increase in excess pore pressure ratio from 5% at  $N=10$  to 42%. At  $\gamma=0.3\%$  the excess pore pressure ratio in the specimens rapidly increased from 20% at  $N=1$  to 83% at  $N=50$ . Subsequently, the shear modulus dramatically decreased from 7.9 MPa at  $N=1$  to 3.3 MPa at  $N=50$ . Figure 5.9c illustrates that shear modulus decreased as cyclic shear strain increased. Figure 5.10 shows damping ratio for samples conditioned at  $0.5\text{ }^\circ\text{C}$ . Similarly, at small shear strains near 0.005%, damping ratios were nearly constant with a value approximating 10%. This continued with increasing cyclic loadings as a corresponding  $r_u$  was generated. At  $\gamma=0.1\%$  the damping ratio decreased from 25% at  $N=1$  to 19% at  $N=50$ . This was accompanied by a pore pressure generation that changed from 5% at  $N=1$  to 42% at  $N=50$ . However, the damping ratio did not always experience a decreasing trend with increasing loading cycles at  $\gamma=0.3\%$ . As excess pore pressure ratio increased from 20% at  $N=1$  to 58% at  $N=10$ , the damping ratio decreased from 26% at  $N=1$  to 21% at  $N=10$ . Further, an additional increase in excess pore pressure ratio resulted in a decrease in the damping ratio from 21% at  $N=10$  to 23% at  $N=50$ . Though the damping ratio for specimens conditioned at  $0.5\text{ }^\circ\text{C}$  appeared to be different at  $\gamma=0.3\%$ , the damping ratio still increased with increasing cyclic shear strain as shown in Figure 5.10c.

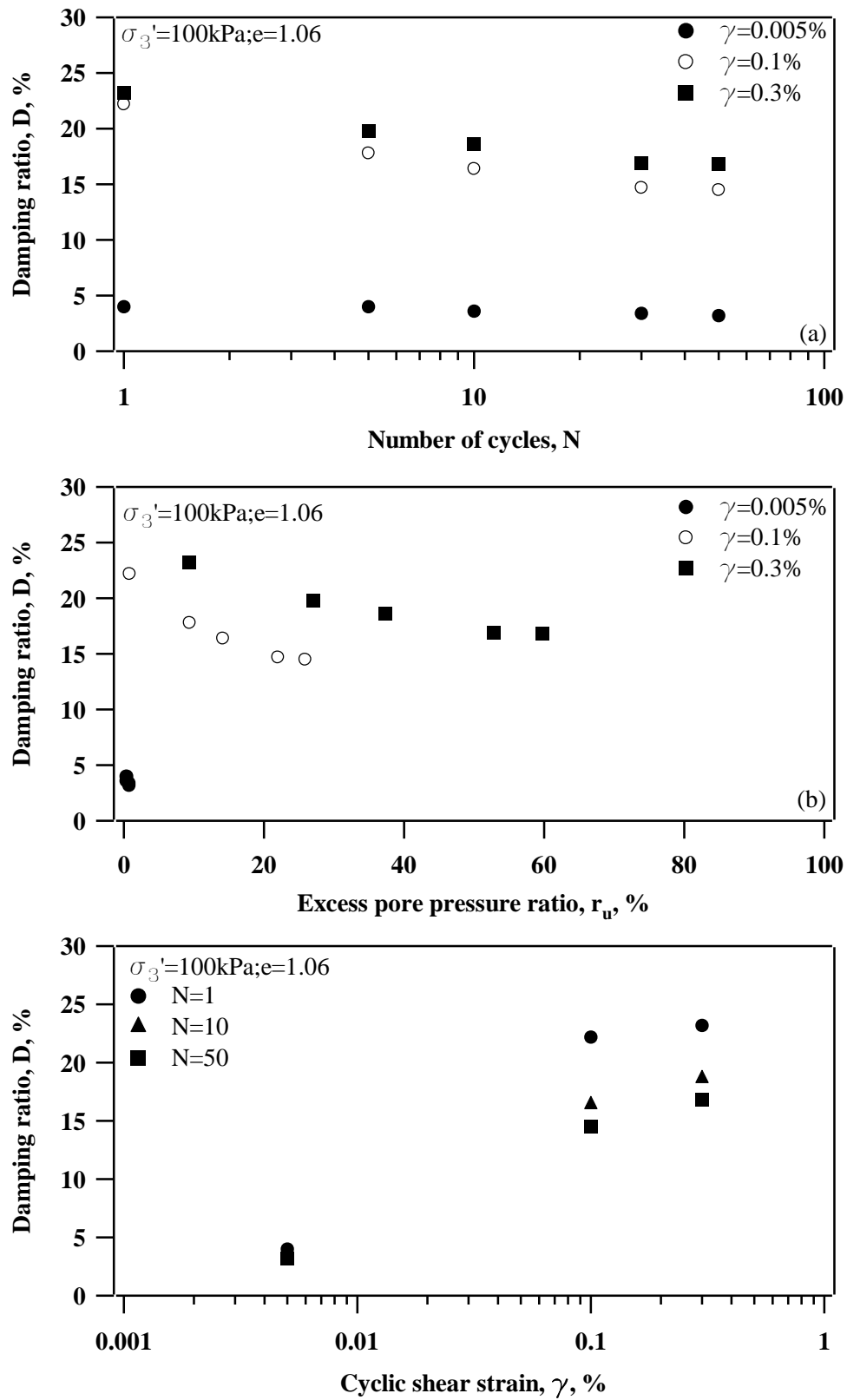


Figure 5.6 Damping ratio ( $D$ ) on Mabel Creek silt conditioned at 5 °C: (a)  $D$  vs  $N$ ; (b)  $D$  vs  $r_u$ ; (c)  $D$  vs  $\gamma$

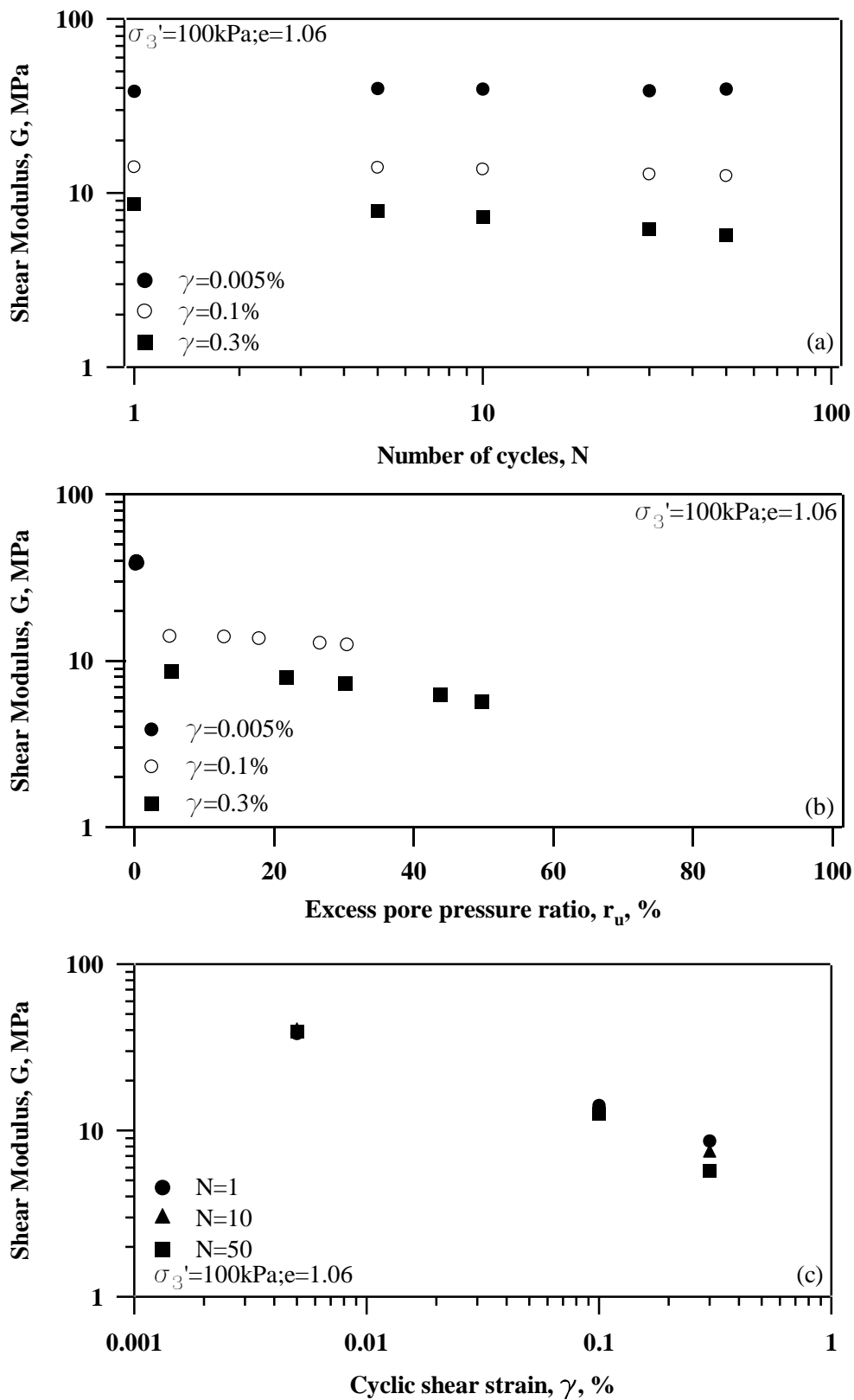


Figure 5.7 Shear modulus ( $G$ ) on Mabel Creek silt conditioned at 1 °C: (a)  $G$  vs  $N$ ; (b)  $G$  vs  $r_u$ ; (c)  $G$  vs  $\gamma$

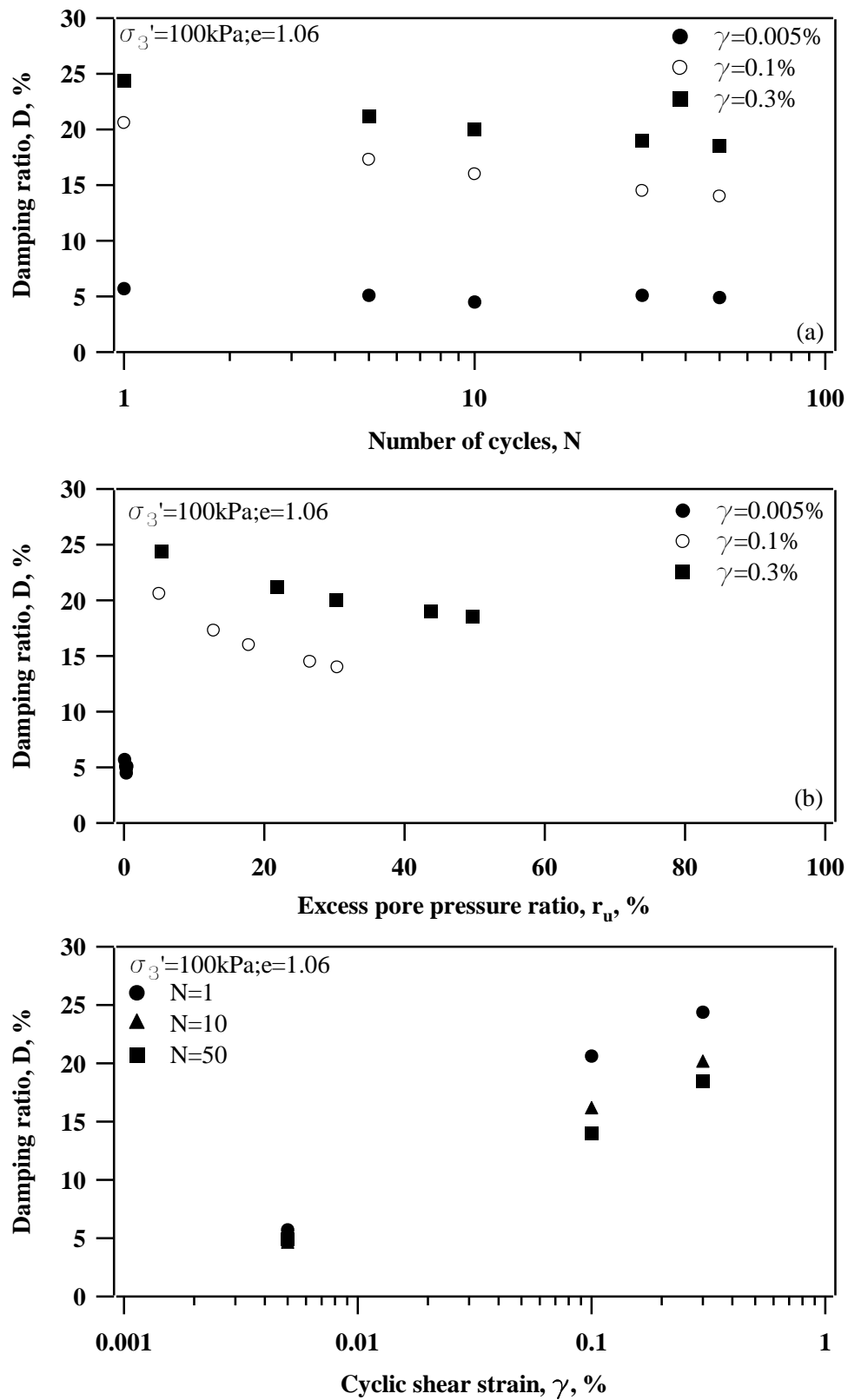


Figure 5.8 Damping ratio ( $D$ ) on Mabel Creek silt conditioned at  $1\text{ °C}$ : (a)  $D$  vs  $N$ ; (b)  $D$  vs  $r_u$ ; (c)  $D$  vs  $\gamma$

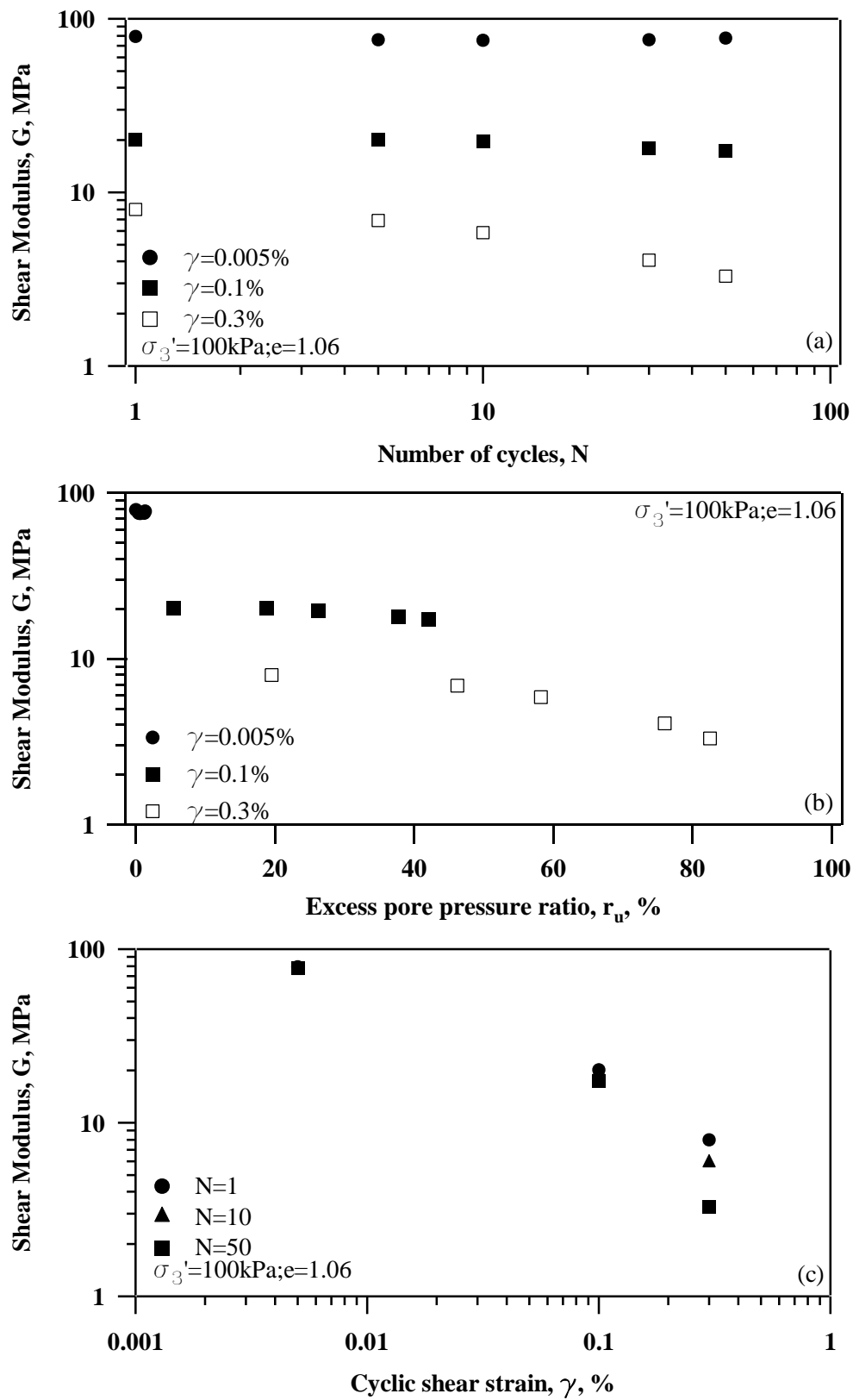


Figure 5.9 Shear modulus ( $G$ ) on Mabel Creek silt conditioned at  $0.5\text{ }^{\circ}\text{C}$ : (a)  $G$  vs  $N$ ; (b)  $G$  vs  $r_u$ ; (c)  $G$  vs  $\gamma$

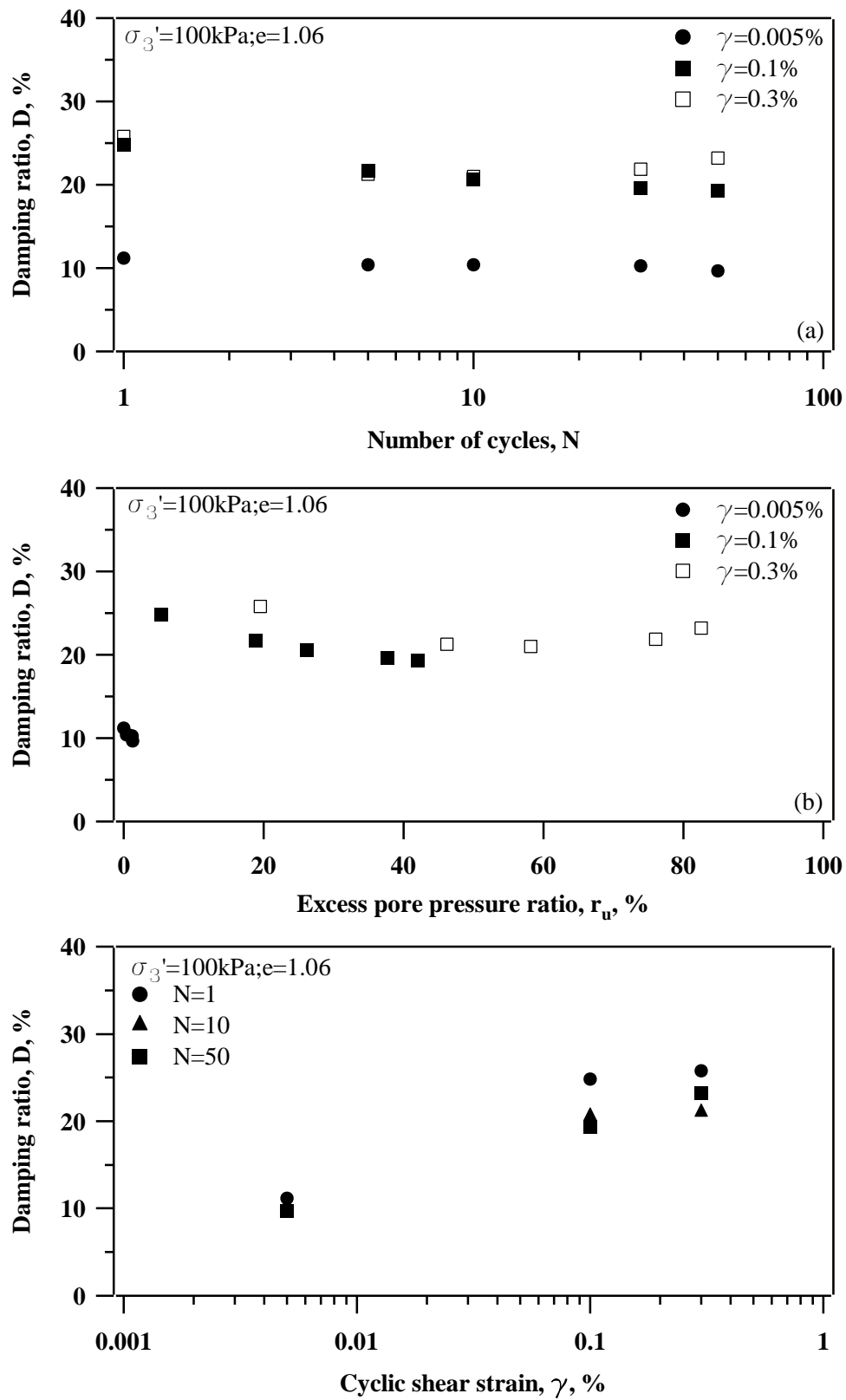


Figure 5.10 Damping ratio ( $D$ ) on Mabel Creek silt conditioned at  $0.5\text{ }^{\circ}\text{C}$ : (a)  $D$  vs  $N$ ; (b)  $D$  vs  $r_u$ ; (c)  $D$  vs  $\gamma$

The shear modulus for specimens conditioned at  $-0.2\text{ }^{\circ}\text{C}$  is shown in Figure 5.11. Degradation of the shear modulus with increasing load cycles was not observed at  $\gamma=0.005\%$ ,  $\gamma=0.03\%$ , or  $\gamma=0.1\%$ . The measured shear modulus was nearly constant and the value was approximately 330 MPa at  $\gamma=0.005\%$  as the excess pore pressure ratio developed from 1% to 9%. Similarly, a constant shear modulus of approximately 170 MPa was observed at  $\gamma=0.03\%$  with increased excess pore pressure ratio from 2% at  $N=1$  to 5% at  $N=50$ . Even when excess pore pressure ratio decreased to a negative value of  $-7\%$  at  $\gamma=0.1\%$ , the shear modulus still remained nearly constant at 80 MPa. Regardless of negative or positive pore pressure generation, the shear modulus was found to always decrease with increasing shear strain; see Figure 5.11c.

Damping ratios for specimens conditioned at  $-0.2\text{ }^{\circ}\text{C}$  are presented in Figure 5.12. Unlike the specimens that were conditioned at other temperatures, the excess pore pressure generation in specimens conditioned at  $-0.2\text{ }^{\circ}\text{C}$  was minimal to negative, and the corresponding damping ratio did not fluctuate very much. The data show that when  $\gamma=0.005\%$ , the damping ratio is approximately 4% when  $r_u$  is 9%. At  $\gamma=0.03\%$  the measured damping ratio was nearly constant at 24% while the excess pore pressure ratio generated was 5% at  $N=50$ . The results show that a negative excess pore pressure ratio of  $-7\%$  existed for  $\gamma=0.1\%$  during 50 loading cycles and that there was a decrease in damping ratio from 30% at  $N=1$  to 27% at  $N=50$ . The trend that damping ratio increases with increasing shear strain was observed for specimens conditioned at  $-0.2\text{ }^{\circ}\text{C}$ ; see Figure 5.12c.

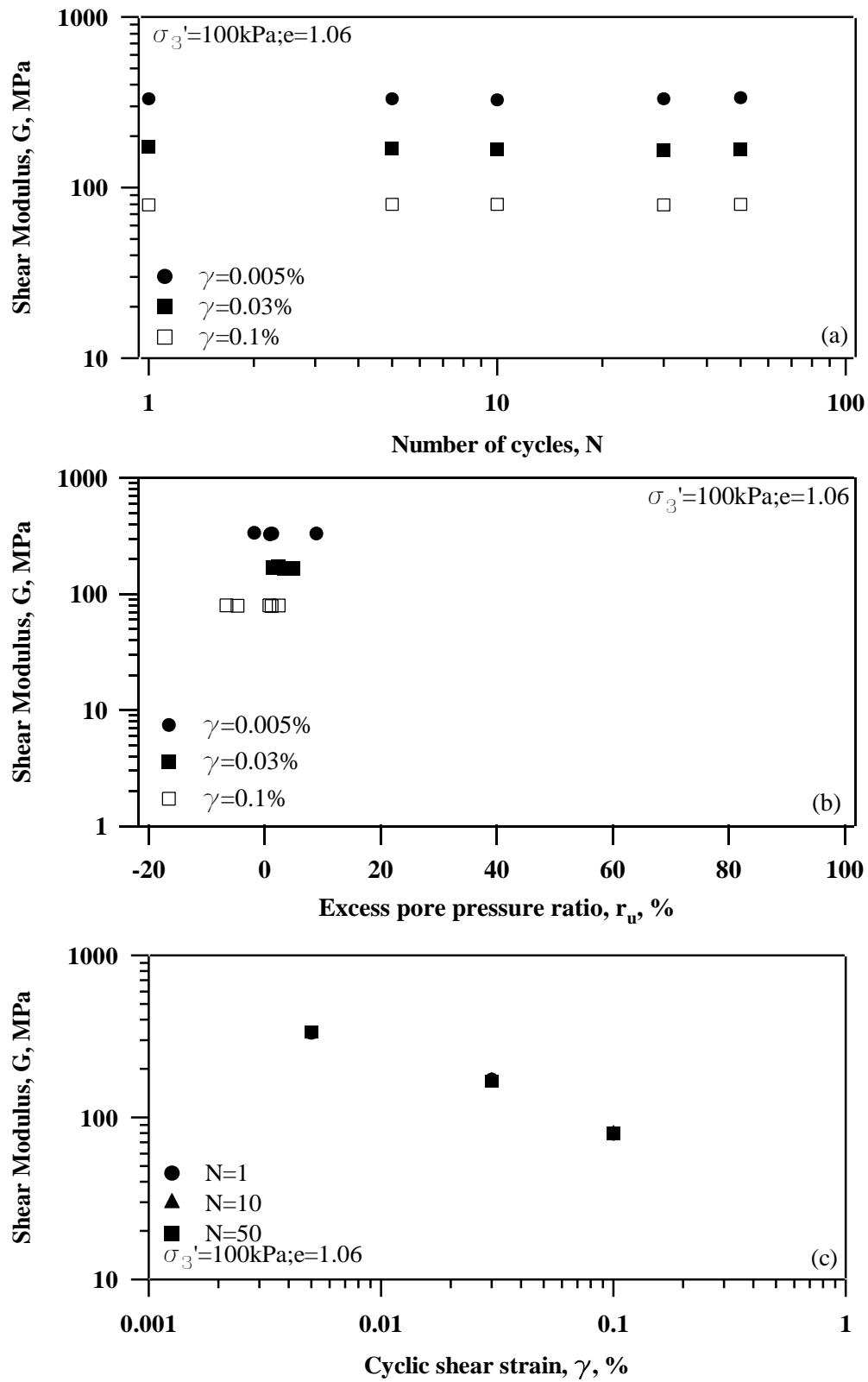


Figure 5.11 Shear modulus ( $G$ ) on Mabel Creek silt conditioned at  $-0.2\text{ }^{\circ}\text{C}$ : (a)  $G$  vs  $N$ ; (b)  $G$  vs  $r_u$ ; (c)  $G$  vs  $\gamma$



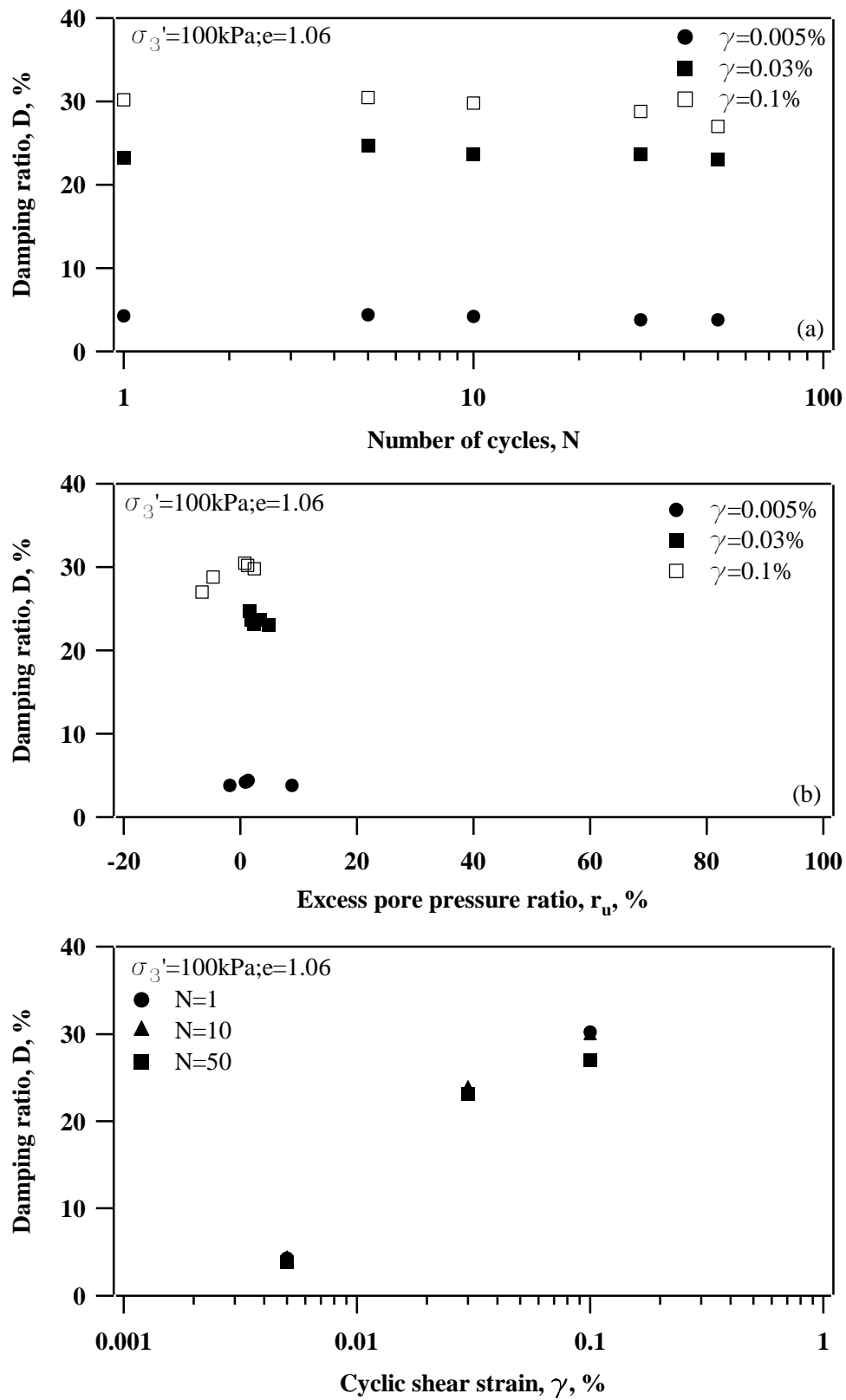


Figure 5.12 Damping ratio ( $D$ ) on Mabel Creek silt conditioned at  $-0.2\text{ °C}$ : (a)  $D$  vs  $N$ ; (b)  $D$  vs  $r_u$ ; (c)  $D$  vs  $\gamma$

## 5.4 Temperature effect on dynamic properties

### 5.4.1 Temperature effect on shear modulus

A comparison of the dynamic shear modulus for specimens of unfrozen Mabel Creek silt and specimens of the Mabel silt conditioned at 24 °C, 5 °C, 1 °C, 0.5 °C, and -0.2 °C was made in terms of number of load cycles at shear strain levels of 0.005%, 0.1% and 0.3%, respectively. Figure 5.13a shows a comparison for a shear strain level of 0.005%. Shear modulus values were dependent on conditioning temperature and constant with increasing load cycles for a shear strain level of 0.005%. The largest shear modulus occurred when specimens were conditioned at -0.2 °C, whereas the smallest shear modulus occurred for unfrozen specimens. The second largest shear modulus was observed when specimens were conditioned at 0.5 °C. Shear modulus for specimens conditioned at 24 °C was slightly larger than for specimens conditioned at 1 °C and smaller for specimens conditioned at 5 °C. This phenomenon did not seem to change with the number of load cycles. However, differences in shear modulus between unfrozen specimens and those that were conditioned at 1 °C, 5 °C, and 24 °C were small (see the log-scale for shear modulus).

Figure 5.13b shows how the Mabel Creek silt dynamic shear modulus at  $\gamma=0.1\%$  varies with specimen conditioning temperature. Maximum shear modulus occurred when specimens were at -0.2 °C and the corresponding minimum shear modulus occurred in unfrozen specimens. The second highest shear modulus was measured in specimens conditioned at 0.5 °C. Shear modulus in specimens conditioned at 1 °C, 5 °C, and 24 °C were similar, no matter the number of load cycles.

Figure 5.13c shows the dynamic shear modulus for specimens subjected to a shear strain level of 0.3% and conditioned at various temperatures. The shear modulus for all specimens was found to decrease with increasing load cycle. Unfrozen specimens were found to have the smallest shear modulus. The largest shear modulus did not

occur on the specimen conditioned at 0.5 °C but occurred on the specimen conditioned at 1 °C. Shear modulus for specimens conditioned at 5 °C was slightly larger than the shear modulus in specimens conditioned at 24 °C. Shear modulus for specimens conditioned at 0.5 °C was significantly smaller than the values for -0.2 °C. Further, the shear modulus for the specimens conditioned at 0.5 °C had a similar value to specimens conditioned at 1 °C from N=1 to N=5. However, the shear modulus was significantly smaller than values measured for specimens conditioned at 24 °C with increasing loading cycles from N=10 to N=50.

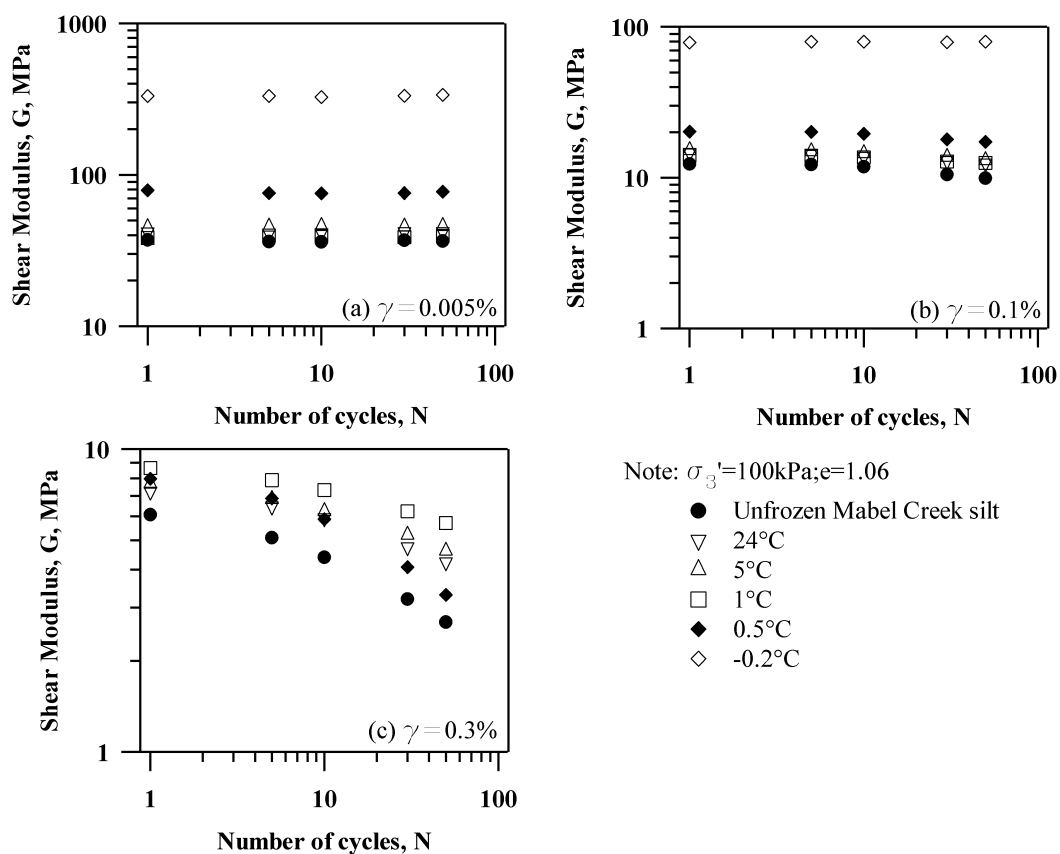
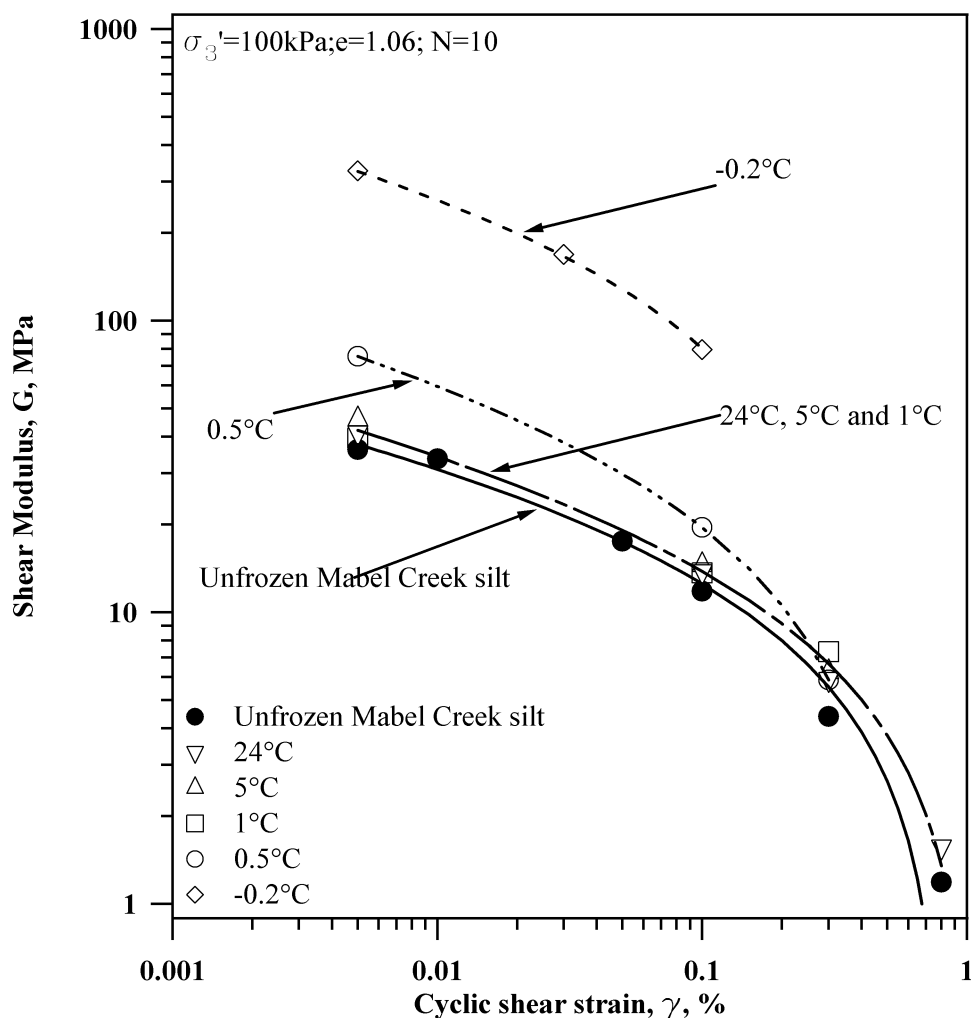


Figure 5.13 Temperature rise effect on shear modulus of Mabel Creek silt

Conditioned temperature effects on shear modulus as a function of cyclic shear strain are shown in Figure 5.14. Shear modulus values for unfrozen specimens are the lower bound whereas the highest shear modulus (upper bound) occurs for specimens that were conditioned at  $-0.2\text{ }^{\circ}\text{C}$ . The second highest shear modulus was found to occur in specimens that were at  $0.5\text{ }^{\circ}\text{C}$ , and the shear strain level was between  $0.005\%$  and  $0.1\%$ . The shear modulus for specimens conditioned at  $0.5\text{ }^{\circ}\text{C}$  and subjected to large shear strains ( $\gamma=0.3\%$ ) was less than or equal to those values where the specimens were conditioned at  $1\text{ }^{\circ}\text{C}$ ,  $5\text{ }^{\circ}\text{C}$ , and  $24\text{ }^{\circ}\text{C}$ .



**Figure 5.14** Shear modulus versus cyclic shear strain on Mabel Creek silt conditioned at the different temperatures for  $N=10$

Temperature effects on shear modulus were investigated by introducing a normalized process of  $G/G_{\max}$  to all specimens at various temperatures.  $G_{\max}$  was derived from the cyclic triaxial undrained strain-controlled tests with a small shear strain ( $\gamma < \gamma_t$ ). The normalized modulus reduction ( $G/G_{\max}$ ) in all specimens conditioned at various temperatures forms curves in a narrow band; see Figure 5.15. The modulus reduction in specimens conditioned at  $-0.2^\circ\text{C}$  and  $0.5^\circ\text{C}$  formed the lower bound. The unrecognizable and similar normalized modulus reduction observed in specimens conditioned at  $1^\circ\text{C}$ ,  $5^\circ\text{C}$ , and  $24^\circ\text{C}$  provided the upper bound.

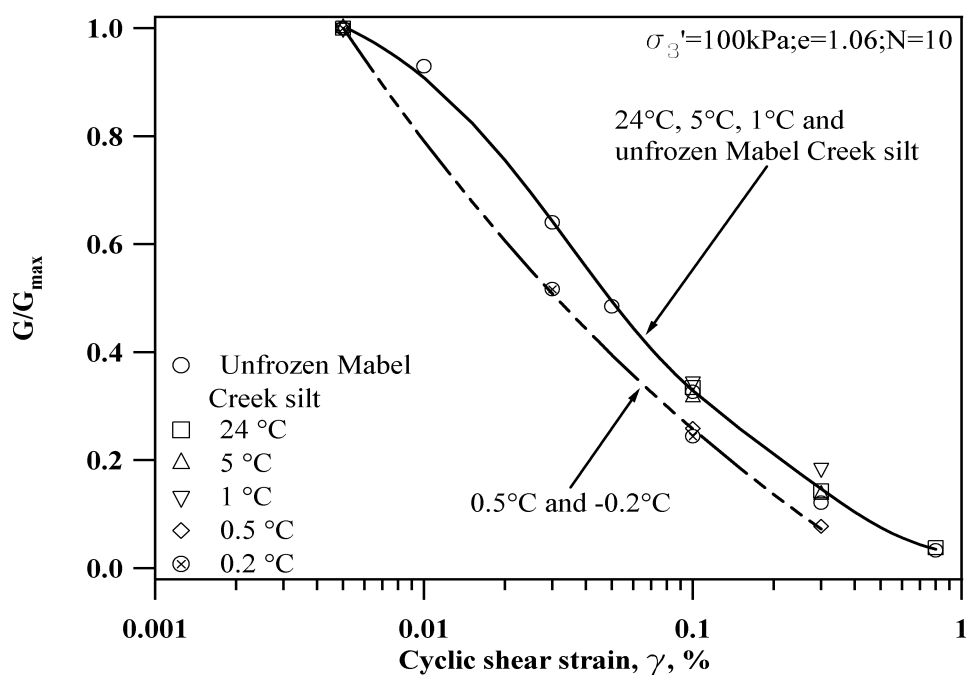


**Figure 5.15** The normalized modulus reduction ( $G/G_{\max}$ ) versus  $\gamma$  in specimens conditioned at various temperatures

Under undrained cyclic loading tests, damping ratio and shear modulus will vary with an increased number of loading cycles, as was found in Sections 5.2, 5.3, and 5.6. Damping ratio and shear modulus depend on both effective pore water pressure and cyclic shear strain. That is to say, an increase in pore water pressure induced under undrained cyclic loading decreases the effective confining pressure. Further, the cyclic shear strain was found to influence the soil's dynamic properties. Thus, investigation

and comparison of the impact of temperature and freeze-thaw cycles on dynamic properties should not overlook the influence of excess pore pressure and cyclic shear strain. They should involve the consideration of  $r_u$  and  $\gamma$ .

The variation in dynamic shear modulus as a function of excess pore water pressure ratio for samples conditioned at different temperatures and shear strain values of  $\gamma=0.005\%$ ,  $\gamma=0.1\%$ , and  $\gamma=0.3\%$  is presented in Figure 5.16. For the small shear strain of 0.005%, specimens conditioned at 0.5 °C show the highest shear modulus, while unfrozen specimens had the lowest shear modulus. At  $\gamma=0.1\%$  the largest shear modulus occurred when specimens were conditioned at 0.5 °C, and the smallest shear modulus was found when the specimens were unfrozen. The variation in shear modulus with increasing shear strain for specimens conditioned at 1 °C, 5 °C, and 24 °C behaved in a similar manner and was difficult to distinguished, as was the case at  $\gamma=0.3\%$ .

Temperature effects on shear modulus were studied by testing partially frozen, thawed and frozen specimens of the Mabel Creek silt. Also, the influence of temperature was somewhat revealed by examining the damping ratio versus the conditioned temperature at shear strain levels of 0.005%, 0.1%, and 0.3%; see Figure 5.17 to Figure 5.19. At the small shear strain of 0.005%, and conditioning temperatures between -0.2 °C and 1 °C, test results show a significant decrease in shear modulus with an increase in the conditioning temperature. However, when specimens were conditioned at temperatures between 1 °C and 24 °C, test results show that the change in shear modulus was minimal. A similar trend in shear modulus was found at the larger shear strain of 0.1%; see Figure 5.18. At this shear strain, the shear modulus was found to decrease at conditioned temperatures from -0.2 °C to 1 °C and remain nearly constant for conditioned temperatures above 1 °C; see Figure 5.18. At a shear strain of 0.3%, data from the specimen conditioned at -0.2 °C were not shown because of the limited capacity of the test instruments. Unlike the cases at  $\gamma=0.005\%$  and

$\gamma=0.1\%$ , shear modulus remained nearly the same for conditioned temperatures between 0.5 °C to 1 °C. Additionally, a conditioned temperature from 1 °C to 24 °C caused a slight decrease of the shear modulus.

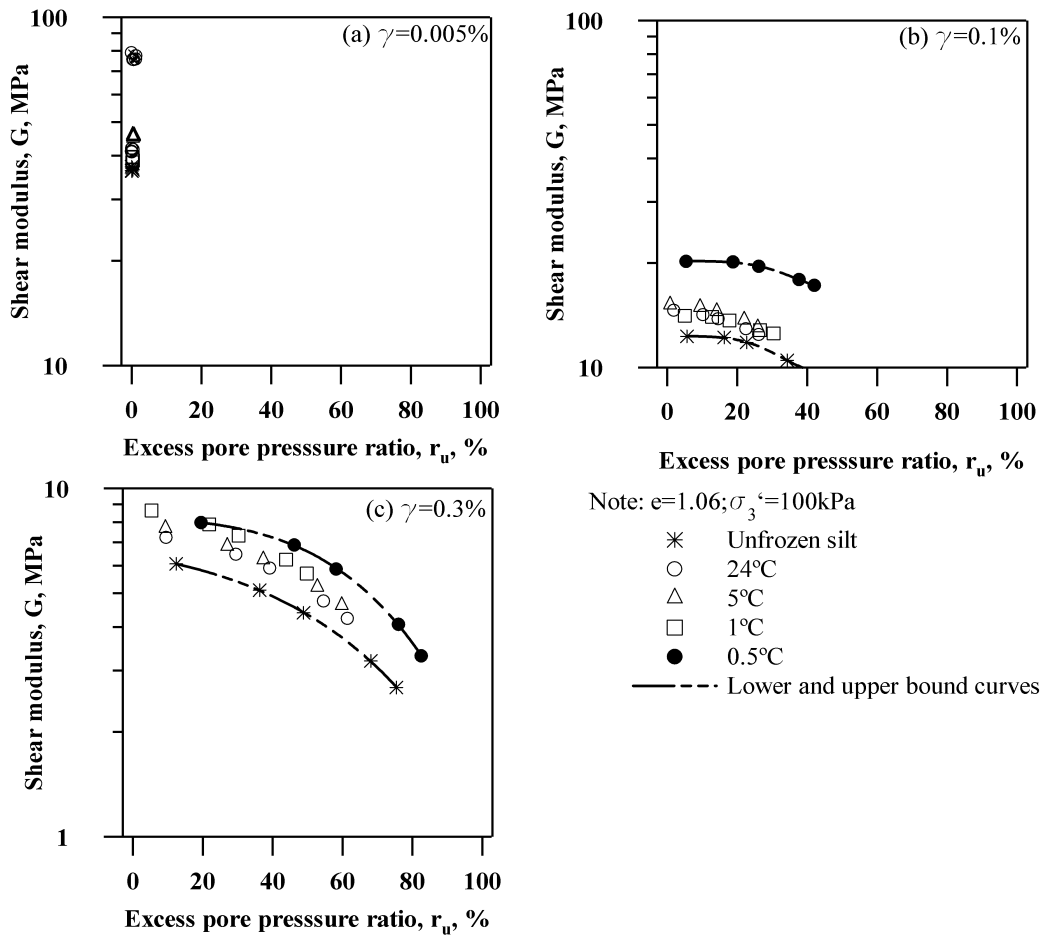


**Figure 5.16** Shear modulus ( $G$ ) versus  $r_u$  on Mabel Creek silt conditioned at the various temperatures

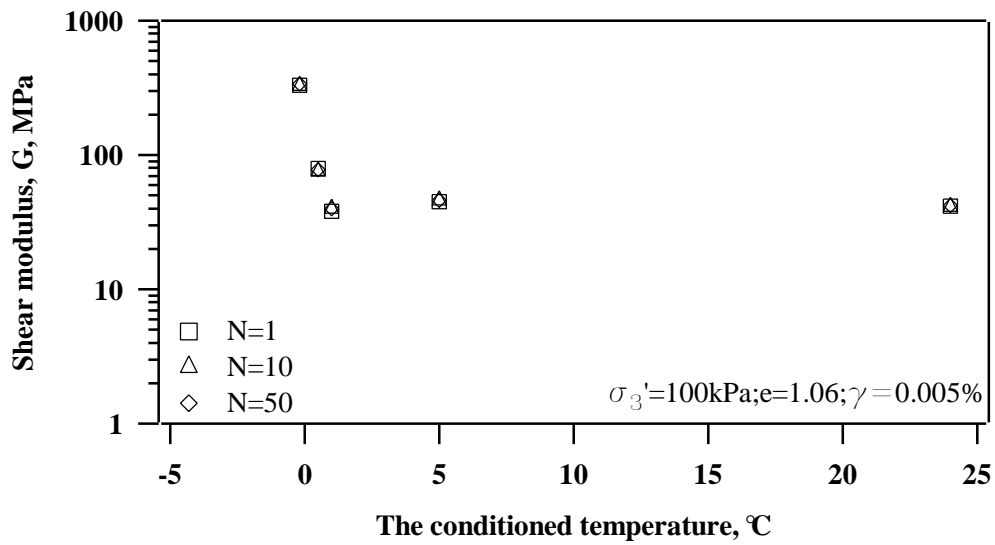


Figure 5.17 Shear modulus versus the conditioned temperature on Mabel Creek silt for  $\gamma = 0.005\%$

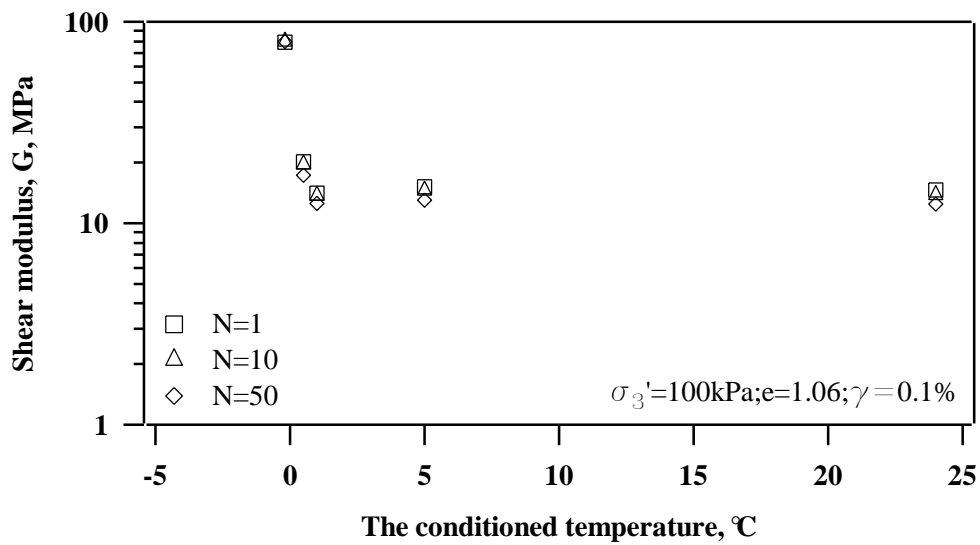
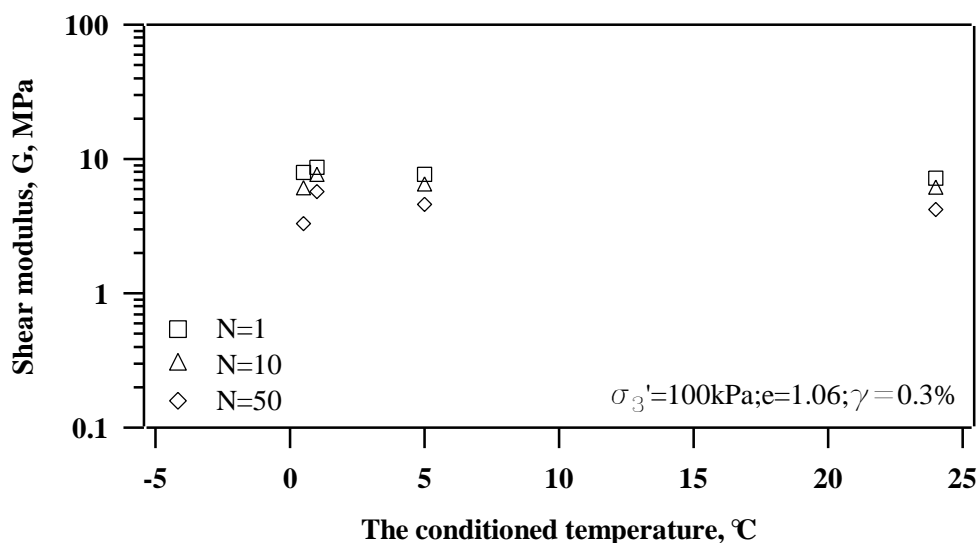


Figure 5.18 Shear modulus versus the conditioned temperature on Mabel Creek silt for  $\gamma = 0.1\%$





**Figure 5.19** Shear modulus versus the conditioned temperature on Mabel Creek silt for  $\gamma=0.3\%$

#### 5.4.2 Temperature effect on damping ratio

Damping ratios for specimens of unfrozen Mabel Creek silt and specimens conditioned at 24 °C, 5 °C, 1 °C, 0.5 °C, and -0.2 °C as a function of the number of loading cycles are summarized for the following three different shear strains: 0.005%, 0.1%, and 0.3%; see Figure 5.20. The influence of an increase in specimen temperature on damping ratio was compared for frozen or partially frozen Mabel Creek silt. Figure 5.20a shows a damping ratio comparison for specimens conditioned at different temperatures when the shear strain level was 0.005%. At this small shear strain level, the damping ratio for specimens remained nearly constant at a value in the range of 4~10% regardless of the number of load cycles or the conditioning temperature. The largest damping ratio of approximately 10% was found to occur when specimens were conditioned at 0.5 °C. A nearly constant damping ratio approximating 5% was observed on unfrozen specimens and specimens conditioned at -0.2 °C, 1 °C, 5 °C, and 24 °C, regardless of the number of load cycles. Thus, it may be concluded that specimens conditioned at -0.2 °C, 1 °C, 5 °C, 24 °C and the unfrozen specimen have similar damping ratios of approximately 5% under cyclic loading and

small shear strain.

A comparison between damping ratios for specimens conditioned at different temperatures at a shear strain level of 0.1% is shown in Figure 5.20b. This figure shows the effect of temperature rise on the damping ratio. All specimens show a trend that the damping ratio decreases with increasing loading cycles at a shear strain level of 0.1%. The unfrozen specimen had the smallest damping ratios, whereas the damping ratios of the specimen conditioned at -0.2 °C was the largest. Damping ratios for the unfrozen specimen and the specimen conditioned at -0.2 °C after 50 loading cycles were 12% and 27%, respectively. The specimen conditioned at 0.5 °C had the second largest damping ratios with values of 25% at N=1 and 19% at N=50. The specimen conditioned at 5 °C showed a slightly larger damping ratio than the specimens conditioned at 1 °C and 24 °C; however, the difference in damping ratios was approximately 2%. Thus, the damping ratios for specimens conditioned at 1 °C, 5 °C, and 24 °C may be considered to be the same or to have behaved in a similar manner.

Similarly, a damping ratio comparison between specimens conditioned at different temperatures when the shear strain level was 0.3% is shown in Figure 5.20c. This figure shows that damping ratios are the smallest when the material is unfrozen. The unfrozen damping ratio for a shear strain level of 0.3% is changed from 21% at N=1 to 18%. The damping ratio was found to decrease with an increase in the number of load cycles in all specimens except the specimen conditioned at 0.5 °C. The damping ratio of the specimen conditioned at 0.5 °C first decreased from N=1 to N=10 and then slightly increased from N=10 to N=50. The damping ratio for a specimen conditioned at 0.5 °C increased to 23% at the end of the 50<sup>th</sup> loading cycle, whereas the damping ratio for the specimen conditioned at 24 °C was 22% for the same 50<sup>th</sup> loading cycle. The difference of damping ratios for specimens conditioned at 1 °C, 5 °C, and 24 °C was observed at the shear strain level of 0.3%. The damping ratio of the specimen

conditioned at 5 °C was larger than that of the specimen conditioned at 24 °C and smaller than that of the specimen conditioned at 1 °C for any given number of loading cycles.

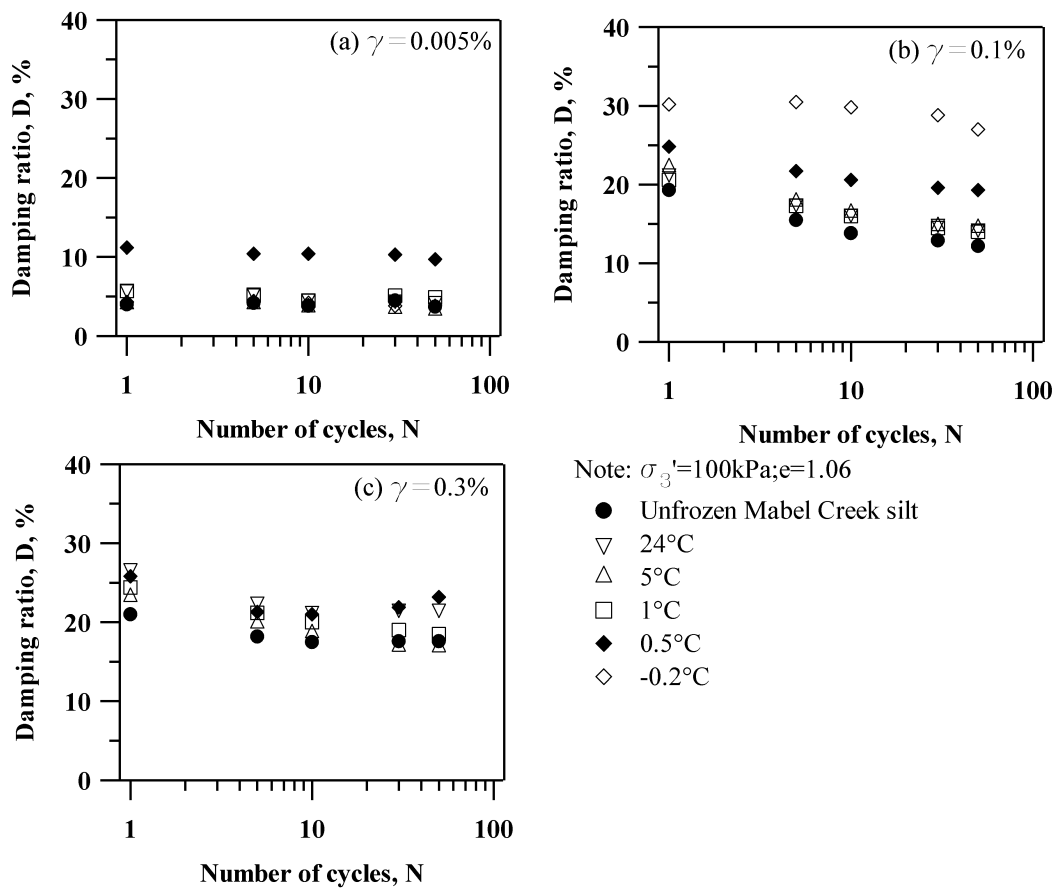


**Figure 5.20** Temperature rise effect on damping ratio of Mabel Creek silt

Damping ratios as a function of cyclic shear strain in all specimens conditioned at various temperatures are shown in Figure 5.21. Damping ratios for the unfrozen specimens give the smallest; these are the lower bound. Damping ratios in specimens conditioned at -0.2 °C formed the upper bound curve. The second largest damping ratios were found in specimens conditioned at 0.5 °C. Specimens conditioned at 1 °C, 5 °C, and 24 °C were observed to have nearly similar damping ratio curves.

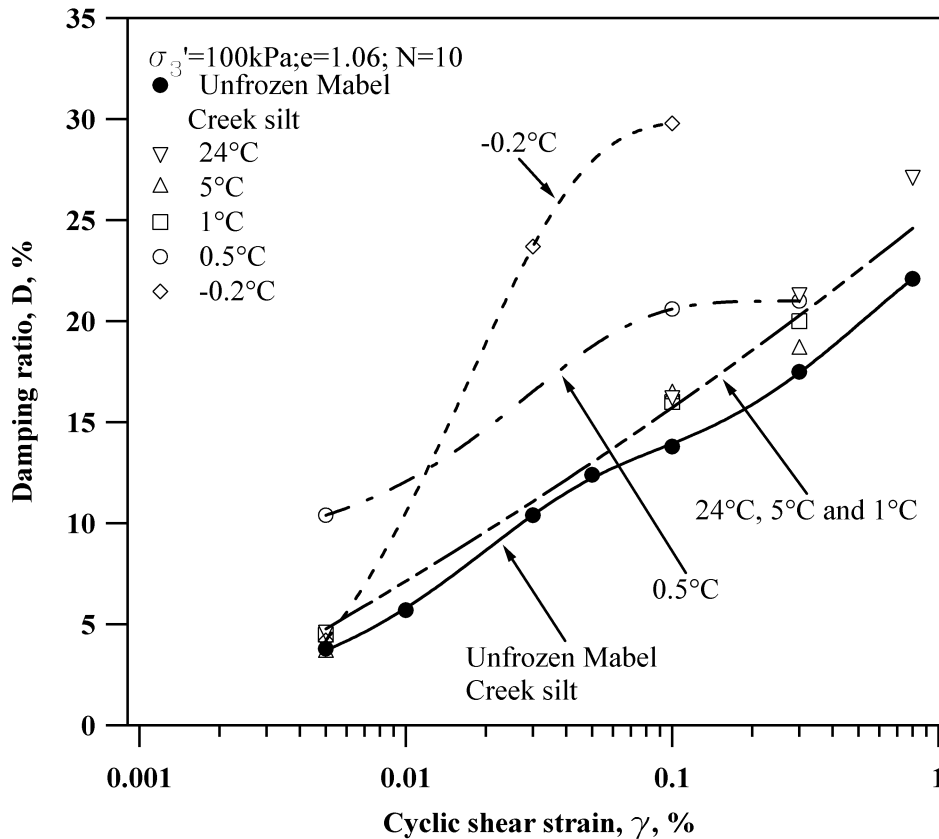


**Figure 5.21** Damping ratio versus cyclic shear strain on Mabel Creek silt conditioned at the different temperatures for  $N=10$

The temperature effect on damping ratio and on the excess pore water pressure ratio were compared at  $\gamma=0.005\%$ ,  $\gamma=0.1\%$ ,  $\gamma=0.3\%$ , and  $\gamma=0.8\%$  as shown in Figure 5.22. For  $\gamma=0.005\%$ , the specimen conditioned at  $0.5\text{ }^{\circ}\text{C}$  was found to have a large damping ratio. For  $\gamma=0.1\%$ , the unfrozen specimen and the specimens conditioned at  $1\text{ }^{\circ}\text{C}$ ,  $5\text{ }^{\circ}\text{C}$ , and  $24\text{ }^{\circ}\text{C}$  showed similar damping ratios: all were less than that of the specimen conditioned at  $0.5\text{ }^{\circ}\text{C}$ . For  $\gamma=0.3\%$ , the specimens conditioned at  $0.5\text{ }^{\circ}\text{C}$  and  $24\text{ }^{\circ}\text{C}$  provided the upper bound in damping ratios. The unfrozen specimen provided the lower bound of damping ratio.

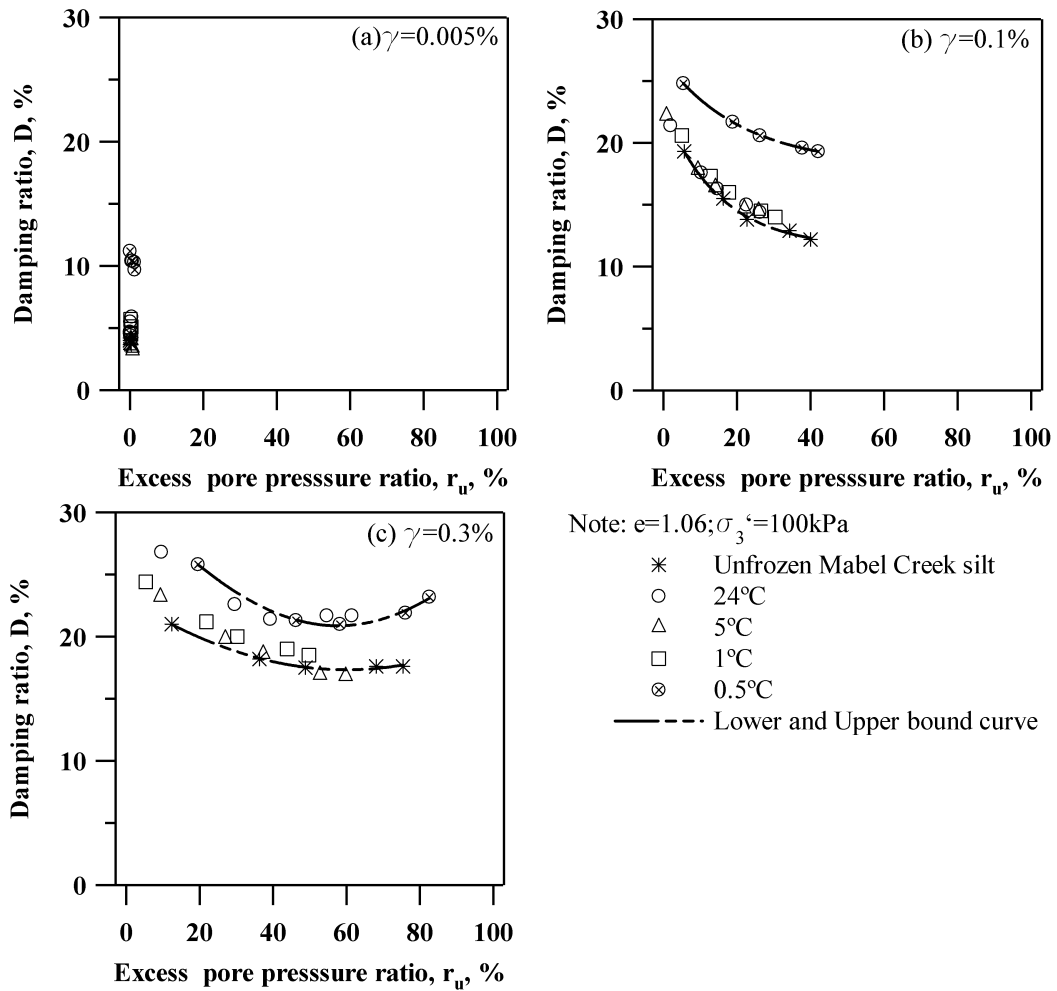


**Figure 5.22 Damp ratio (D) versus  $r_u$  on Mabel Creek silt conditioned at the different temperatures**

The effect of temperature rise on damping ratio was investigated for partially frozen and frozen specimens of the Mabel Creek silt. A summary of these results is presented in Figure 5.23~Figure 5.25. These figures show how the damping ratio varied as a function of the specimen conditioning temperature and shear strain levels of 0.005%, 0.1%, and 0.3%. For small shear strain of 0.005%, the increase from  $-0.2\text{ }^\circ\text{C}$  to  $0.5\text{ }^\circ\text{C}$  increased the damping ratio. When specimen conditioning temperature was increased from  $5\text{ }^\circ\text{C}$  to  $24\text{ }^\circ\text{C}$ , the damping ratio was found to slightly increase. For the larger shear strain of 0.1%, the damping ratio increased with temperature for the temperature range of  $0.5\text{ }^\circ\text{C}$  to  $1\text{ }^\circ\text{C}$ . Change of the damping ratio with increased temperature from

1 °C to 24 °C was minimal in comparison with the change of damping ratio induced at temperatures from 0.5 °C to 1 °C. At the largest shear strain of 0.3%, there was a slight decrease in the damping ratio, and this occurred for specimen conditioning temperatures between 0.5 °C and 5 °C. At this shear strain, there was only a slight increase in damping ratio for higher conditioning temperatures.

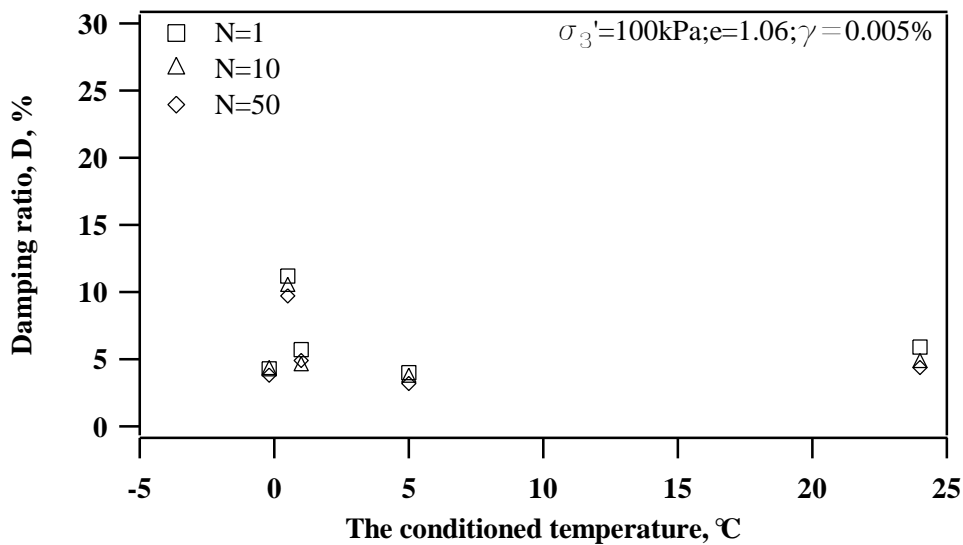


Figure 5.23 Damping ratio versus the conditioned temperature on Mabel Creek silt for  $\gamma = 0.005\%$

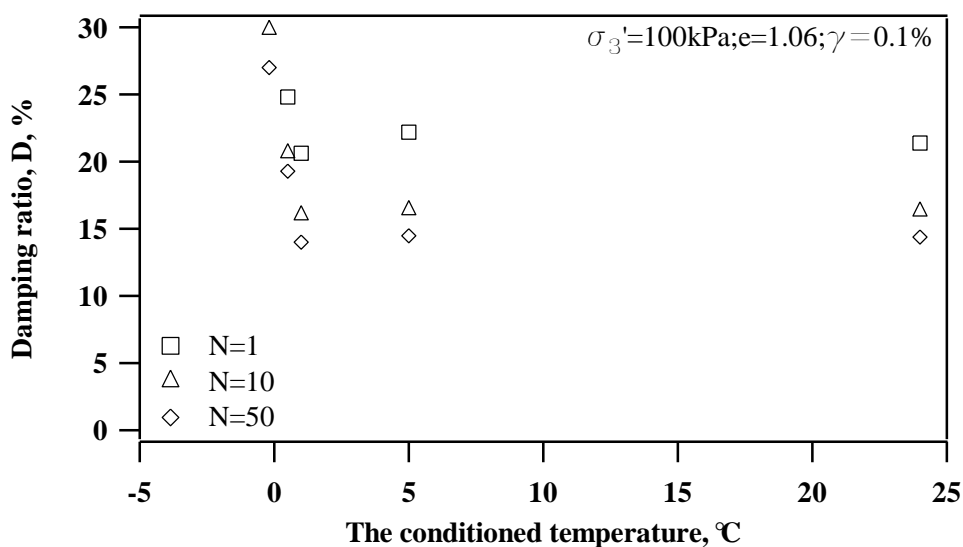
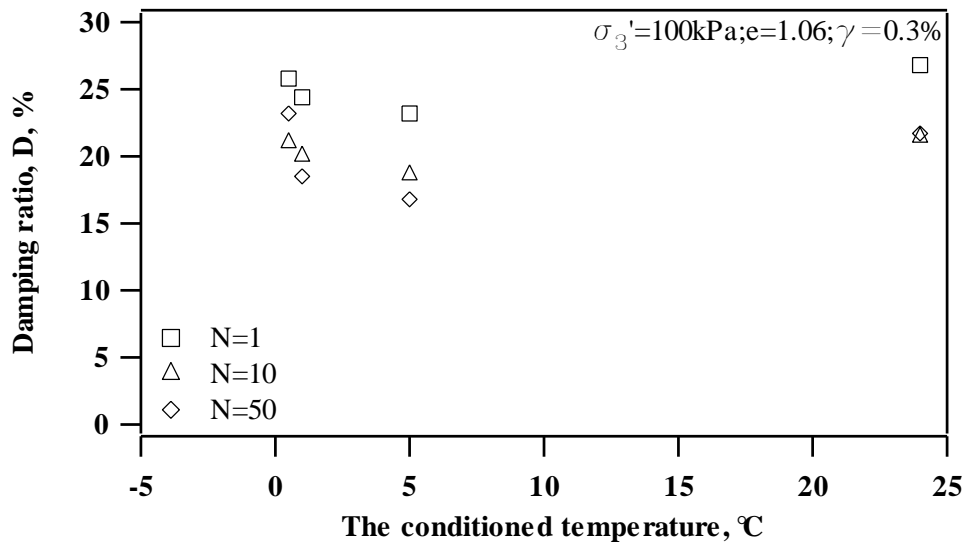


Figure 5.24 Damping ratio versus the conditioned temperature on Mabel Creek silt for  $\gamma = 0.1\%$



**Figure 5.25** Damping ratio versus the conditioned temperature on Mabel Creek silt for  $\gamma=0.3\%$

### 5.5 Discussion of dynamic properties at various temperatures

To further evaluate temperature effect on dynamic properties, dynamic shear modulus and damping ratios in this study were compared with those from previous studies in frozen and unfrozen fine-grained soil. Czajkowski and Vinson (1980) conducted triaxial strain-controlled tests on Alaska silt. Their studies were conducted for the purpose of evaluating dynamic properties of Alaska frozen silt. As part of their study, specimens of Alaska silt were prepared at water contents of 20.5% and 38.9%. Specimens were conditioned at three temperatures below freezing temperatures; these were:  $-1\text{ }^{\circ}\text{C}$ ,  $-4\text{ }^{\circ}\text{C}$ , and  $-10\text{ }^{\circ}\text{C}$ . A combination of Czajkowski and Vinson's 1980 results and the results in this study provides a foundation of knowledge regarding the influence of temperature on dynamic properties. These examined temperatures include below freezing, near freezing and above freezing temperature. A comparison between damping ratios is presented in Figure 5.26. An increase in temperature for the Alaska silt will likely reflect a trend for the damping ratio to increase. Near freezing, the damping ratio in this study was found to be an upper bound value. For temperatures above freezing, an increase in temperature was found to cause the

damping ratio to decrease. Figure 5.26 shows the variation in damping ratio with increasing temperature from below freezing to above freezing, the damping ratio was found to increase with increasing temperature below freezing. It reached a maximum at or near freezing temperature, and it decreased with additional temperature increase above freezing. Figure 5.27 shows a comparison for shear modulus. Shear modulus for specimens in the frozen state was greater than the shear modulus for specimens near the freezing state. The shear modulus for specimens near the freezing state was greater than that of the shear modulus for specimens above the freezing state. However, when temperature is above freezing temperature, the increase in the conditioned temperature cannot induce much change in shear modulus.

Dynamic properties for unfrozen fine-grained soil (Vucetic and Dobry 1991) were compared with the results from this study. Variations in the damping ratios for specimens of the Mabel Creek silt conditioned at various temperatures were evaluated and compared with results from Vucetic and Dobry (1991); see Figure 5.28. The curve of damping ratio versus induced shear strain in unfrozen Mabel Creek silt was found to be along a narrowed band formed by the curves for  $IP=0$  and  $IP=15$ . Mabel Creek silt was measured to have an  $IP$  of 5.3, which is consistent with the findings by Vucetic and Dobry (1991). An increase in the damping ratio at above freezing temperatures was observed near the damping ratio curve at  $PI=0$ . However, at near freezing temperatures, the damping ratio was higher than upper bound values for fine-grained soil from Vucetic and Dobry (1991). Normalized modulus reduction curves for the Mabel Creek silt at various temperatures were combined with the results from Vucetic and Dobry (1991); see Figure 5.29. Except for the value of  $G/G_{max}$  at the small shear strains, normalized shear modulus reduction at near freezing temperatures like  $0.5\text{ }^{\circ}\text{C}$  and  $-0.2\text{ }^{\circ}\text{C}$  almost superpose the curve at  $PI=0$ . Normalized shear modulus reduction at above freezing temperature was located between the curve at  $PI=0$  and the curve at  $PI=15$ .



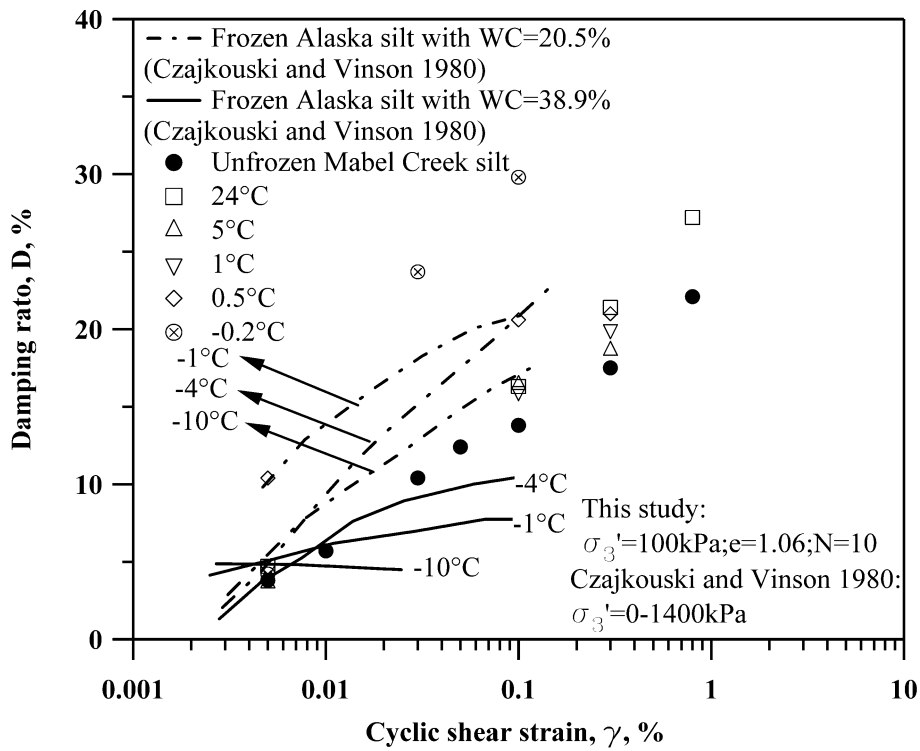


Figure 5.26 Comparison of damping ratio between Mabel Creek silt conditioned at various temperatures and frozen Alaska silt

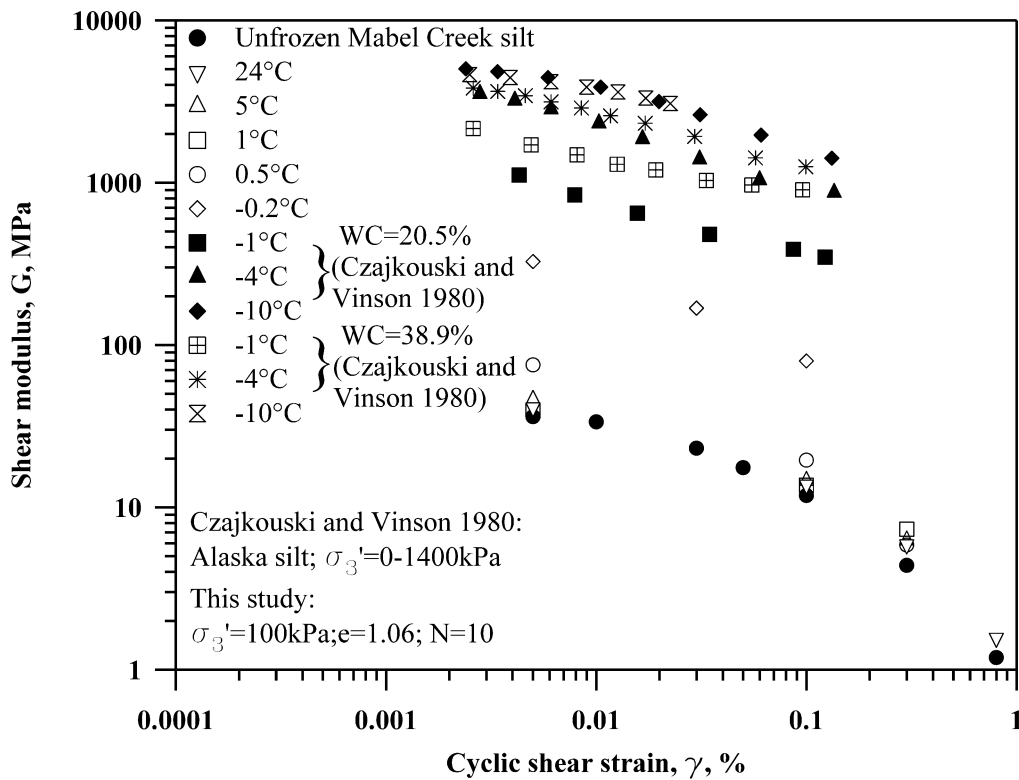


Figure 5.27 Comparison of shear modulus between Mabel Creek silt conditioned at various temperatures and frozen Alaska silt

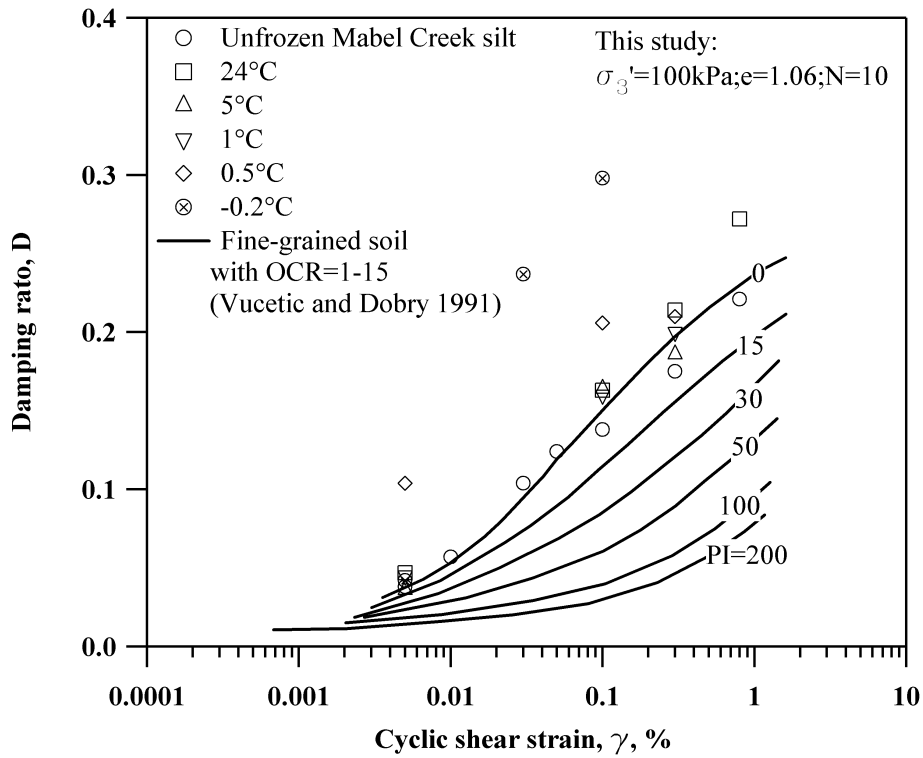


Figure 5.28 Comparison of damping ratio between Mabel Creek silt conditioned at various temperatures and fine-grained soil (from Vucetic and Dobry 1991)

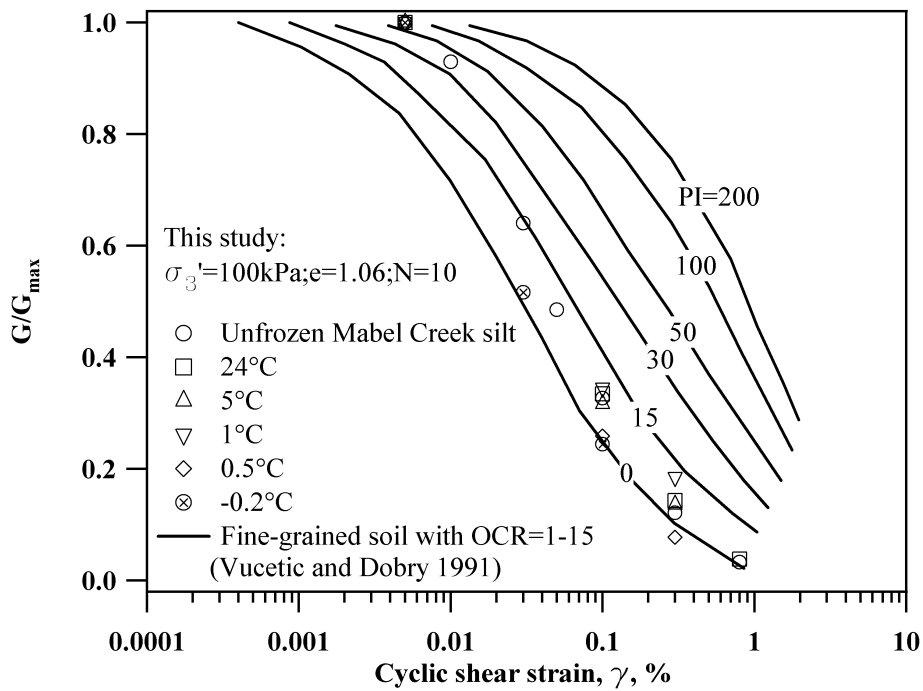


Figure 5.29 Comparison of normalized shear modulus reduction between Mabel Creek silt conditioned at various temperatures and fine-grained soil (from Vucetic and Dobry 1991)

## 5.6 Dynamic properties of Mabel Creek silt conditioned by the freeze-thaw cycles

Shear modulus for specimens conditioned after 2 freeze-thaw cycles is shown in Figure 5.30. A constant shear modulus of approximately 41.0 MPa was observed at  $\gamma=0.005\%$  with no pore pressure generation during the whole cyclic loading test. Slight degradation of shear modulus for  $\gamma=0.1\%$  was measured from 14.5 MPa at  $N=1$  to 12.5 MPa at  $N=50$ . During these tests the excess pore pressure ratio increased from 6% at  $N=1$  to 29% at  $N=50$ . There was a reduction in shear modulus at  $\gamma=0.3\%$ . The value reduced from 7.2 MPa at  $N=1$  to 4.5 MPa at  $N=50$ . During this test the excess pore pressure ratio increased from 16% at  $N=1$  to 61% at  $N=50$ . At  $\gamma=0.8\%$  there was a significant degradation of shear modulus from 3.2 MPa at  $N=1$  to 0.8 MPa at  $N=50$ , and during these tests the excess pore pressure ratio increased substantially from 19% at  $N=1$  to 81% at  $N=50$ . Figure 5.30c shows the reduction in shear modulus with increasing levels of shear strain.

Figure 5.31 shows the influence of 2 freeze-thaw cycles on damping ratio for specimens of the Mabel Creek silt. Damping ratios for shear strain levels between 0.01% and 0.8% are presented. The test results show that when specimens were conditioned at 2 freeze-thaw cycles, 2 different damping ratio histories occurred. For example, Figure 5.31a shows that the damping ratio at small shear strain (such as 0.01%) is nearly constant, but there was a continuous decrease in damping ratio with an increase in loading cycles at medium to large shear strain values of 0.1%, 0.3%, and even 0.8%. At 0.01%, a constant damping ratio of approximately 5% was observed when excess pore pressure ratio was generated from 0% at  $N=1$  to 1% at  $N=50$ . At the larger shear strain level of 0.1%, the damping ratio decreased from 23% at  $N=1$  to 15% at  $N=50$  while the excess pore pressure ratio was developed from 6% at  $N=1$  to 29%. Similarly, the damping ratio for specimens at  $\gamma=0.3\%$  were found to decrease from 28% at  $N=1$  to 20% at  $N=50$ , and this was accompanied by an increase

of excess pore pressure ratio from 16% at  $N=1$  to 61% at  $N=50$ . Even at  $\gamma=0.8\%$  the pore pressure generation of  $r_u=81\%$  resulted in a decrease in the damping ratio from 31% at  $N=1$  to 25% at  $N=50$ . For specimens conditioned after 2 freeze-thaw cycles, increasing cyclic shear strain resulted in an increase in the damping ratio for all loading cycles; see Figure 5.31c.

Figure 5.32 shows the shear modulus for specimens conditioned after 4 freeze-thaw cycles. These specimens were at shear strain levels between 0.005% and 0.8%. A constant shear modulus of about 41.0 MPa was observed at  $\gamma=0.005\%$  with a corresponding  $r_u$  of approximately 0%. A slight degradation in shear modulus occurred at  $\gamma=0.1\%$  and  $\gamma=0.3\%$ . Degradation of shear modulus for  $\gamma=0.1\%$  ranged from 15.2 MPa at  $N=1$  to 13.1 MPa at  $N=50$ . For these tests the generation of the excess pore pressure ratio increased from 7% at  $N=1$  to 27% at  $N=50$ . Similarly, shear modulus decreased from 7.1 MPa at  $N=1$  to 4.8 MPa at  $N=50$  with development of the excess pore pressure ratio from 16% at  $N=1$  to 57% at  $N=50$ . A dramatic reduction in shear modulus occurred at  $\gamma=0.8\%$ . During this test the specimen rapidly softened from a  $G$  of 3.5 MPa at  $N=1$  to a  $G$  of 0.9 MPa at  $N=50$  while the excess pore pressure ratio changed from 26% at  $N=1$  to 78% at  $N=50$ . A reduction of shear modulus with increasing cyclic shear strain is seen in Figure 5.32c.

Damping ratios for specimens conditioned after 4 freeze-thaw cycles are shown in Figure 5.33. At the small shear strain of 0.005, the damping ratio was found to be a nearly constant value of 2% while  $r_u$  was approximately 0. At  $\gamma=0.1\%$  the damping ratio was found to decrease from 24% at  $N=1$  to 16% at  $N=50$ , and the corresponding excess pore pressure ratio increased from 7% at  $N=1$  to 27% at  $N=50$ . In the same manner, the damping ratio at  $\gamma=0.3\%$  decreased from 30% at  $N=1$  to 22% at  $N=50$  while the excess pore pressure ratio changed from 16% at  $N=1$  to 57% at  $N=50$ . The damping ratio at  $\gamma=0.8\%$  behaved differently. For example, the damping ratio initially decreased from 32% at  $N=1$  to 27% at  $N=10$  with the excess pore pressure ratio

generation changing from 26% at  $N=1$  to 58% at  $N=10$ . At  $N=50$  the excess pore pressure ratio increased to 78%. Subsequently, at  $N=50$  the damping ratio slightly increased 27% at  $N=10$  to 29% at  $N=50$ . The data show that the damping ratio for a specimen conditioned for 4 freeze-thaw cycles tends to increase with an increase in cyclic shear strain; see Figure 5.33c.

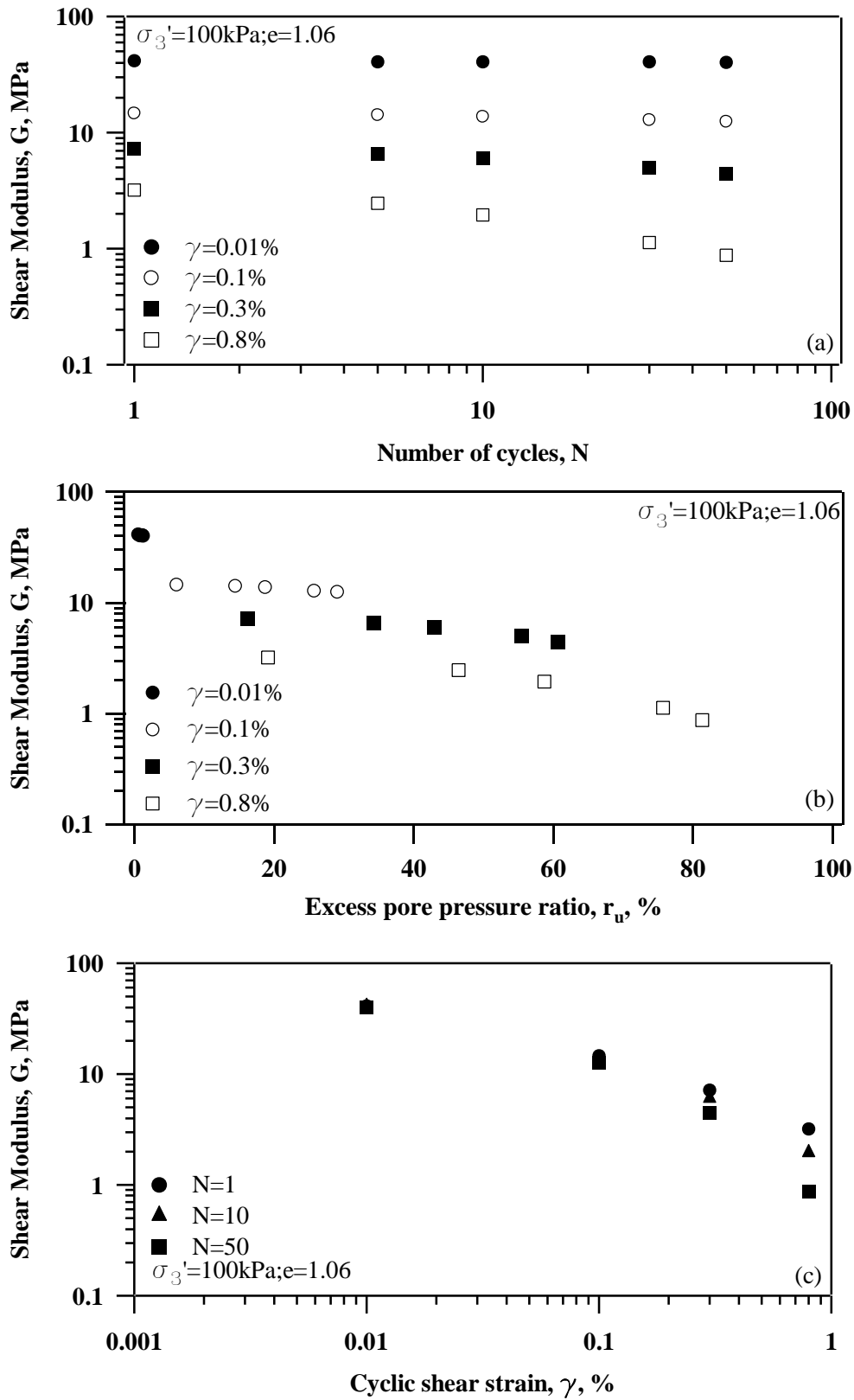


Figure 5.30 Shear modulus ( $G$ ) on Mabel Creek silt conditioned at 2 freeze-thaw cycles: (a)  $G$  vs  $N$ ; (b)  $G$  vs  $r_u$ ; (c)  $G$  vs  $\gamma$

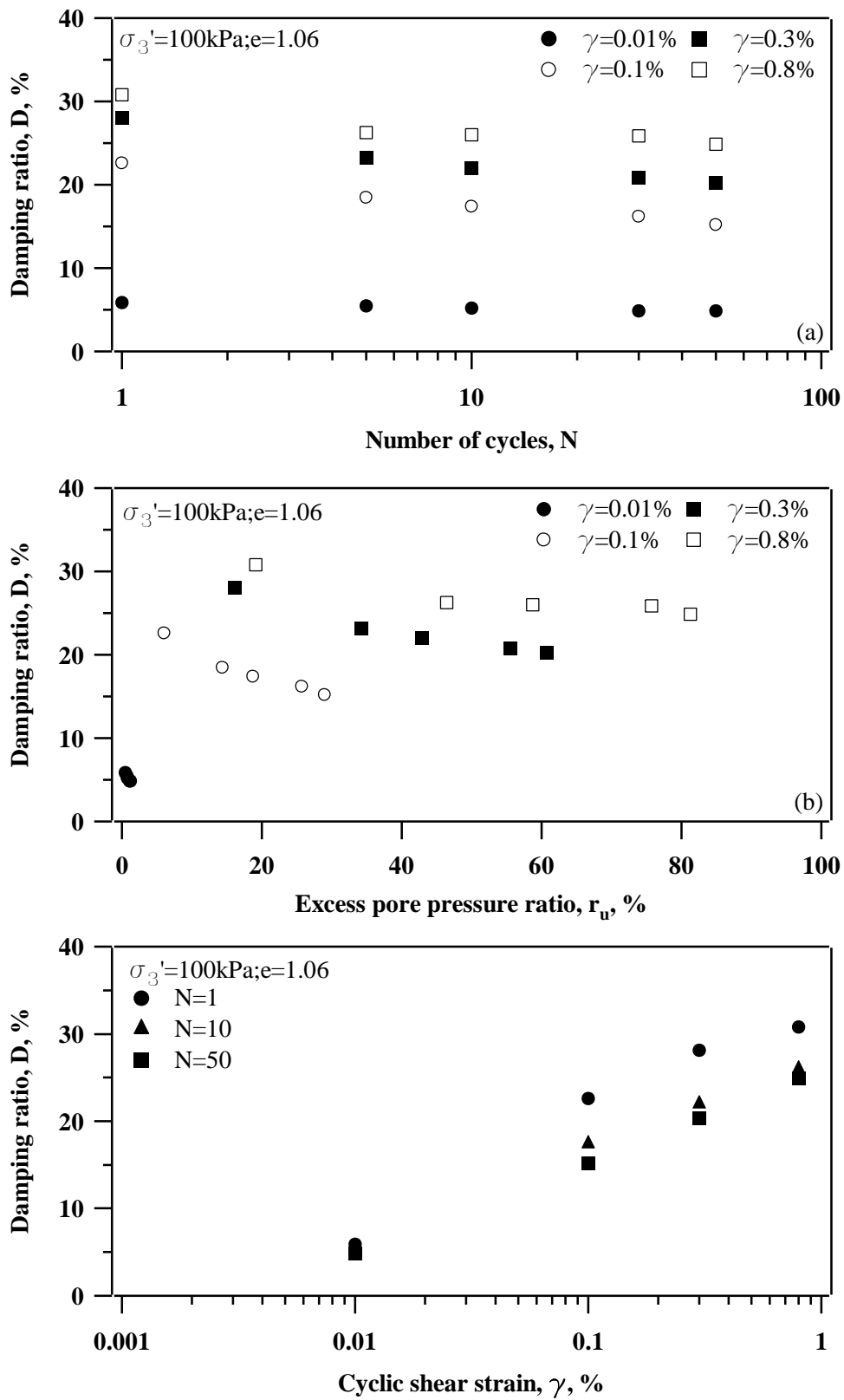


Figure 5.31 Damping ratio ( $D$ ) on Mabel Creek silt conditioned at 2 freeze-thaw cycles: (a)  $D$  vs  $N$ ; (b)  $D$  vs  $r_u$ ; (c)  $D$  vs  $\gamma$

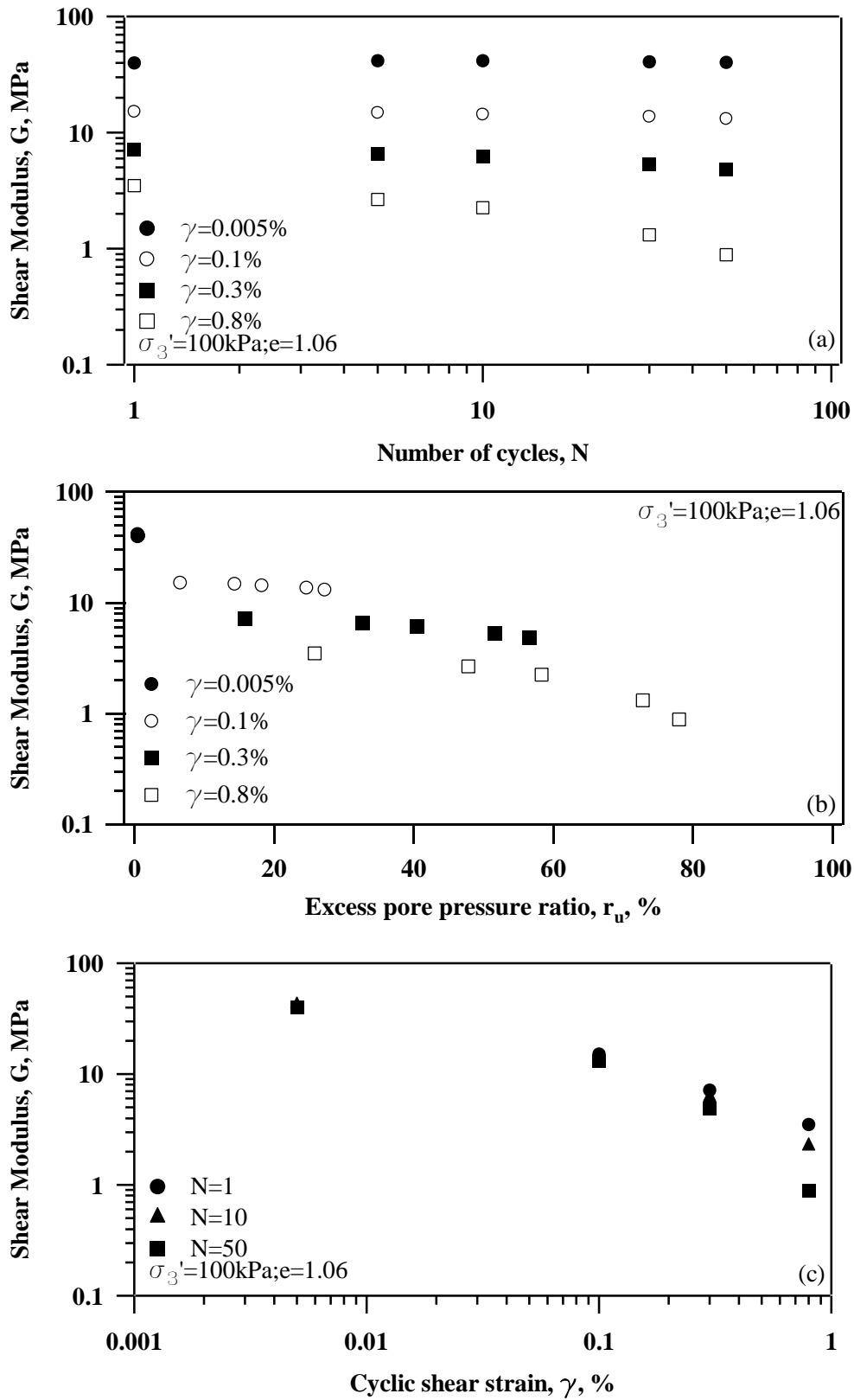


Figure 5.32 Shear modulus ( $G$ ) on Mabel Creek silt conditioned at 4 freeze-thaw cycles: (a)  $G$  vs  $N$ ; (b)  $G$  vs  $r_u$ ; (c)  $G$  vs  $\gamma$



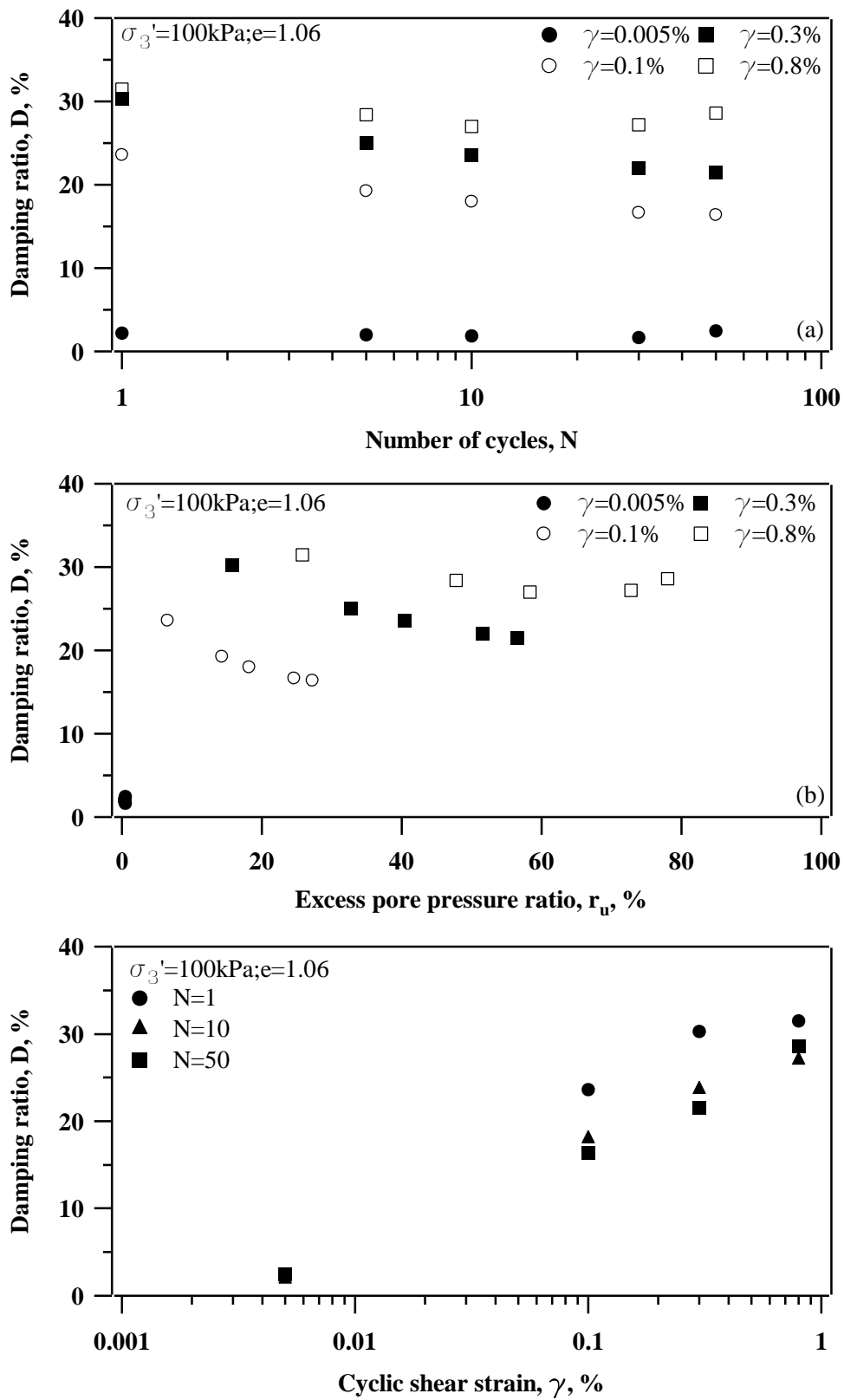


Figure 5.33 Damping ratio ( $D$ ) on Mabel Creek silt conditioned at 4 freeze-thaw cycles: (a)  $D$  vs  $N$ ; (b)  $D$  vs  $r_u$ ; (c)  $D$  vs  $\gamma$

## 5.7 The effect of freeze-thaw cycle on dynamic properties

### 5.7.1 Effect of freeze-thaw cycles on shear modulus

An effect of freeze-thaw cycles on shear modulus as a function of the number of load cycles was studied for shear strain levels of 0.005%, 0.1%, 0.3%, and 0.8%. The results of these studies are shown in Figure 5.34. Figure 5.34a shows the influence of freeze-thaw cycles on shear modulus for a small shear strain of 0.005% and any given number of loading cycles. The shear modulus remained approximately constant with the number of load cycles. The unfrozen specimen was found to have the smallest shear modulus; however, similar shear modulus was obtained for the specimens that were subjected to 1, 2, and 4 freeze-thaw cycles at  $\gamma=0.005\%$ .

Shear modulus as a function of the number of load cycles for specimens subjected to 1, 2, and 4 freeze-thaw cycles at  $\gamma=0.1\%$  is shown in Figure 5.34b. The influence of freeze-thaw cycles on the specimens at  $\gamma=0.1\%$  is similar to that of specimens in Figure 5.34a.

Shear modulus for the large strain level of 0.3% on Mabel Creek specimens subjected to 1, 2, and 4 freeze-thaw cycles is shown in Figure 5.34c. In these tests, the data showed that the shear modulus decreased as loading cycles increased. The smallest shear modulus still occurred for the unfrozen specimen, while the largest shear modulus occurred for the specimen subjected to 4 freeze-thaw cycles. The second largest shear modulus was observed for the specimen subjected to 2 freeze-thaw cycles. The difference of shear modulus between the specimens subjected to 2 and 4 freeze-thaw cycles became more and more obvious with increasing loading from  $N=5$  to  $N=50$ .

The shear modulus for specimens conditioned at 1, 2, and 4 freeze-thaw cycles was found to be affected by the freeze-thaw cycles at the large shear strain level of 0.8%.

At this shear strain, shear modulus increased with the number of load cycles; see Figure 5.34d. The smallest shear modulus still occurred with unfrozen specimens. Specimens that experienced 1 freeze-thaw cycle had the second smallest shear modulus. The largest shear modulus occurred for the specimen that experienced 4 freeze-thaw cycles.

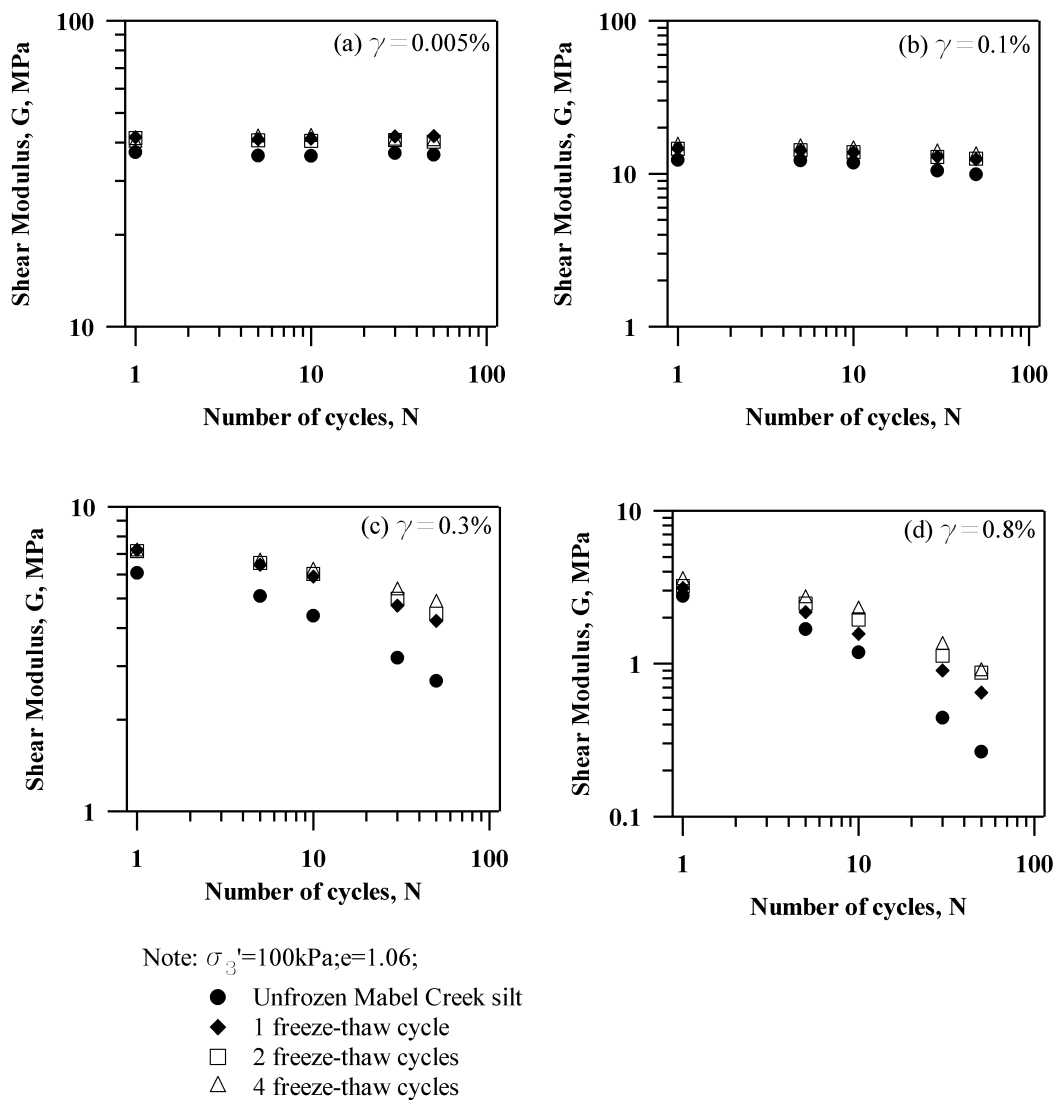
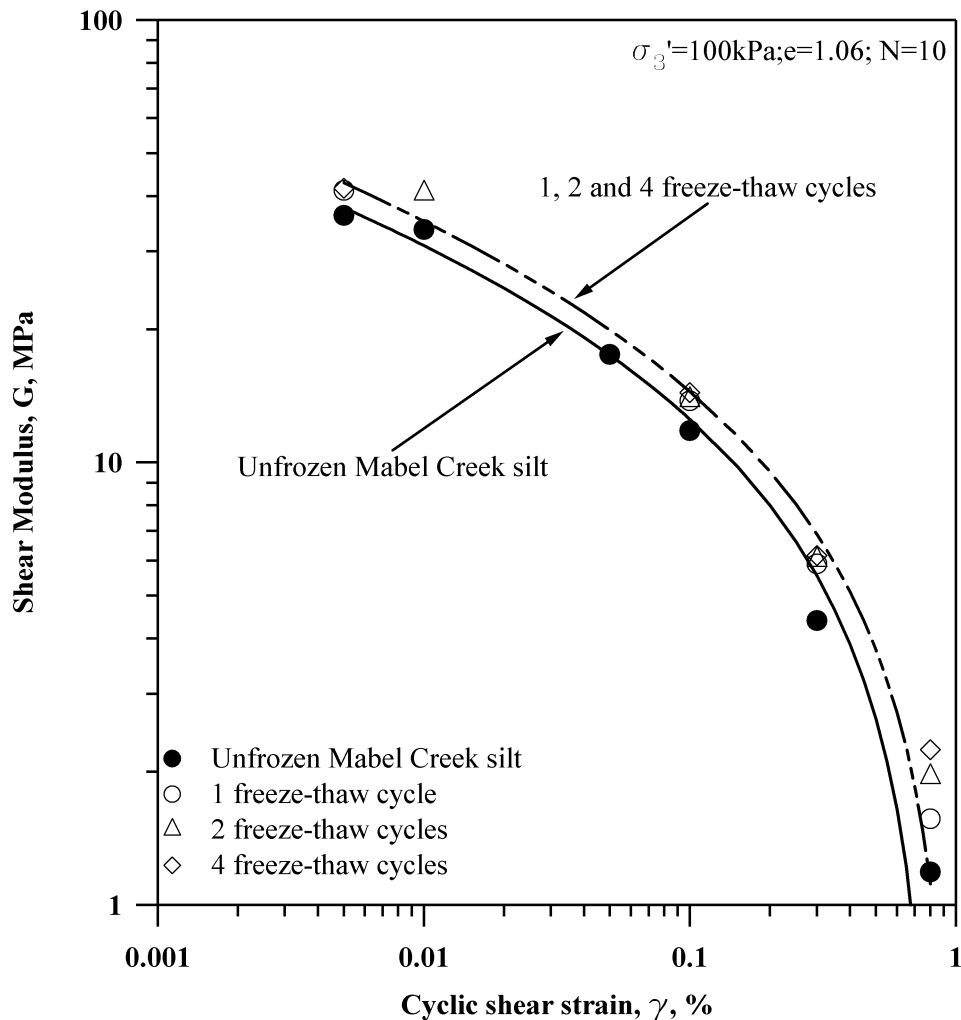
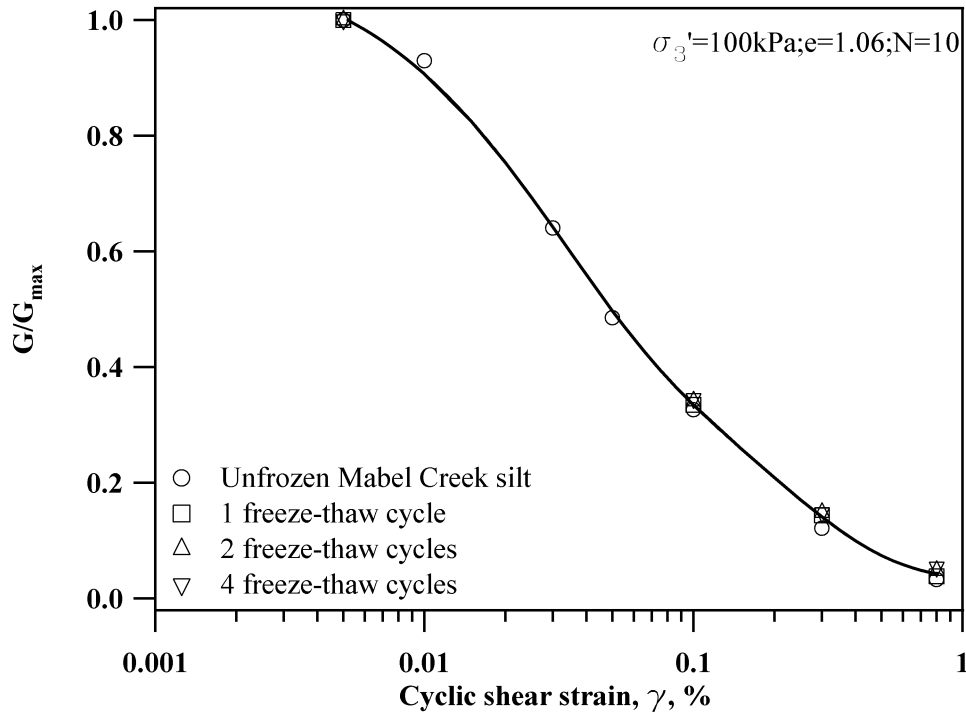


Figure 5.34 Effect of freeze-thaw cycles on shear modulus of Mabel Creek silt

The influence of cyclic shear strain on shear modulus for specimens that were subjected to 1, 2, and 4 freeze-thaw cycles is shown in Figure 5.35. The data show that shear modulus will always decrease with increasing shear strain. The lower value of shear modulus (lower bound) occurs for the unfrozen specimens. As the number of freeze-thaw cycles increased, the shear modulus increased. Normalized shear modulus was found to reduce with cyclic shear strain for all specimens; see Figure 5.36. The effect of freeze-thaw cycles on shear modulus appears to be minimal; see Figure 5.36.



**Figure 5.35** Shear modulus versus cyclic shear strain on Mabel Creek silt that experienced the different freeze-thaw cycles for  $N=10$



**Figure 5.36 The modulus reduction ( $G/G_{\max}$ ) versus  $\gamma$  in specimens conditioned at various freeze-thaw cycles**

The effect of freeze-thaw cycles on dynamic shear modulus for specimens of Mabel Creek silt as a function of excess pore water pressure ratio was compared at  $\gamma=0.1\%$ ,  $\gamma=0.3\%$ , and  $\gamma=0.8\%$ ; see Figure 5.37. For  $\gamma=0.005\%$ , an unfrozen specimen was found to have the largest shear modulus. For  $\gamma=0.1\%$ , an unfrozen specimen was found to have the smallest shear modulus, and a specimen conditioned at 1 freeze-thaw cycle gave the second smallest shear modulus. Similar trends in shear modulus were observed at  $\gamma=0.3\%$ ; however, shear modulus did not appear to be affected by the number of freeze-thaw cycles. A similar trend in shear modulus was also observed when  $\gamma=0.8\%$ ; however, the difference in shear modulus between the specimen subjected to 1 freeze-thaw cycle and the specimen subjected to 2 freeze-thaw cycles was not obvious.

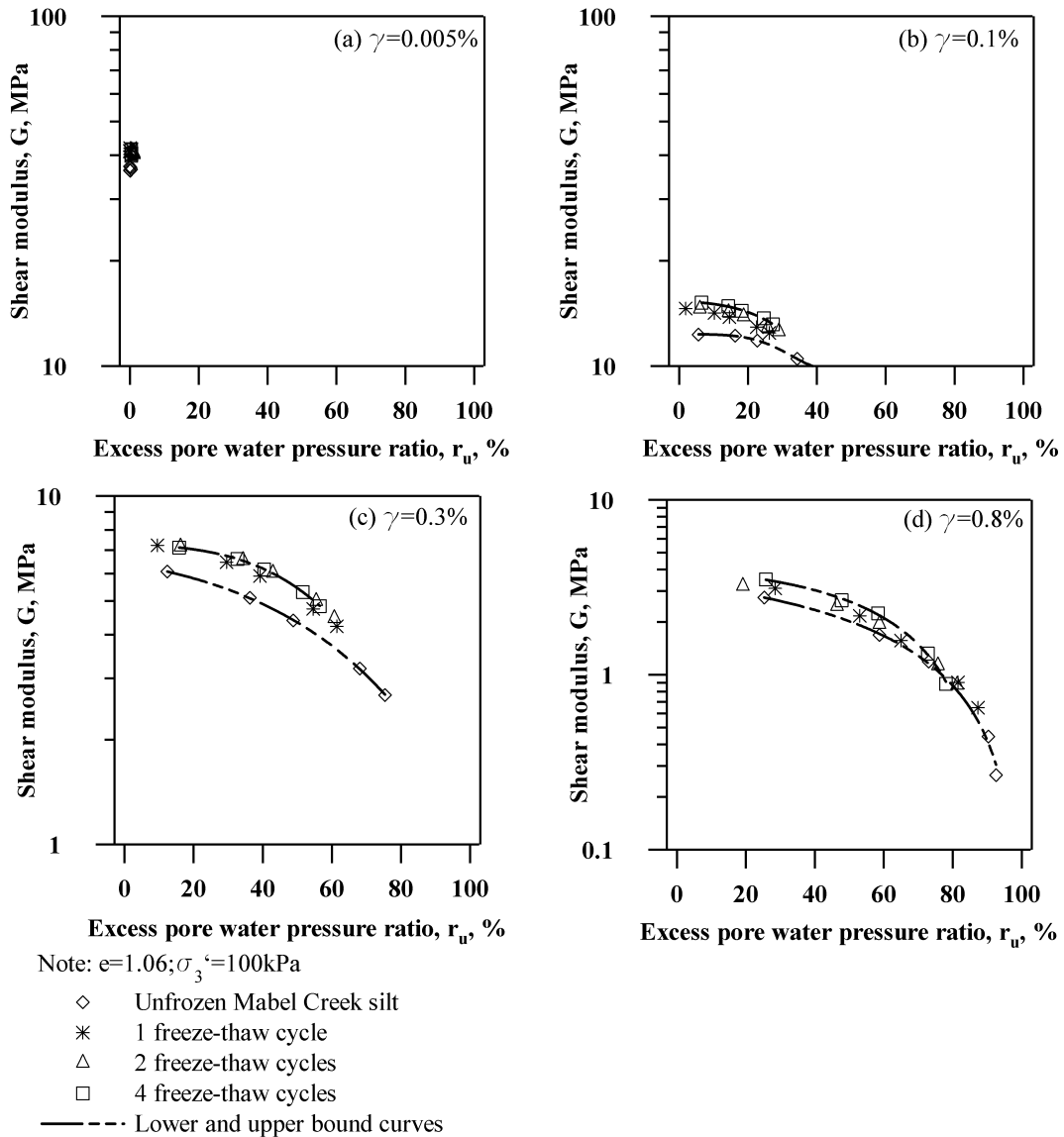


**Figure 5.37 Shear modulus ( $G$ ) versus  $r_u$  on Mabel Creek silt experiencing the different freeze-thaw cycles**

Figure 5.38 to Figure 5.41 show the effects of freeze-thaw cycles on shear modulus for specimens at shear strains of 0.005%, 0.1%, 0.3%, and 0.8%. Figure 5.38 demonstrates the variation of shear modulus with increasing freeze-thaw cycles at the small shear strain of 0.005%. One freeze-thaw cycle dramatically increased the shear modulus, but increasing freeze-thaw cycles from 2 to 4 did not affect the shear modulus. At the large shear strain levels of 0.1%, 0.3%, and 0.8%, shear modulus was

found to increase as the number of freeze-thaw cycles were increased from 1 to 4. However, this trend was not obvious at the shear strain of 0.1%. As the shear strain level was increased from 0.1% to 0.8%, this trend became more and more significant.

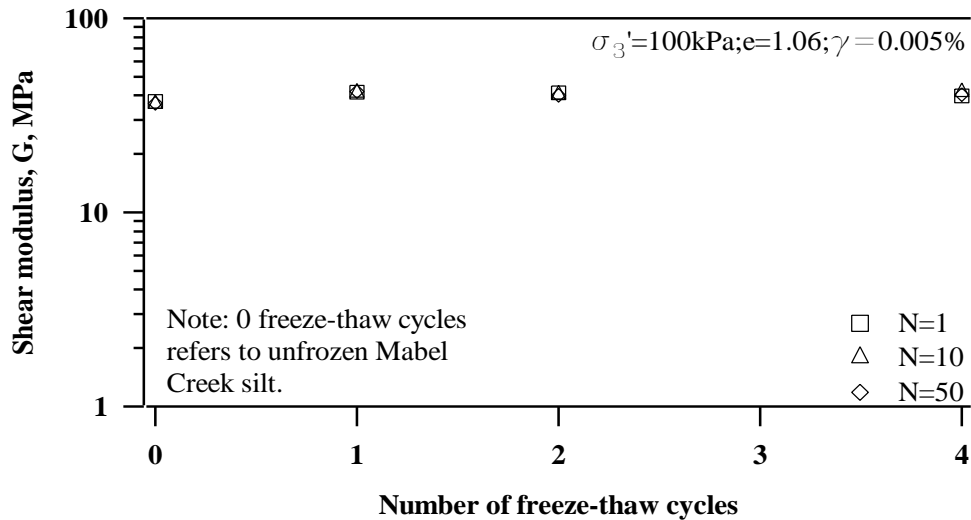


Figure 5.38 Shear modulus versus number of freeze-thaw cycles on Mabel Creek silt for  $\gamma=0.005\%$

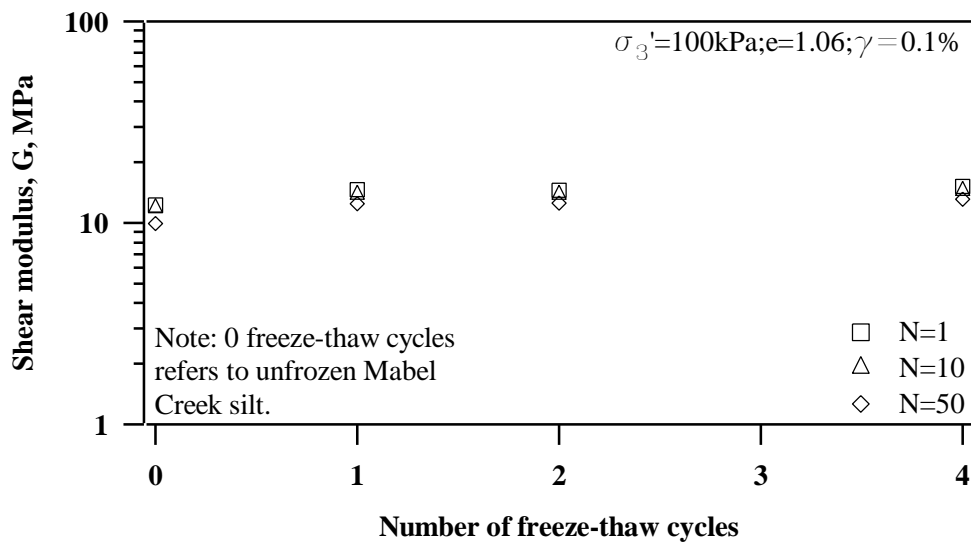


Figure 5.39 Shear modulus versus number of freeze-thaw cycles on Mabel Creek silt for  $\gamma=0.1\%$

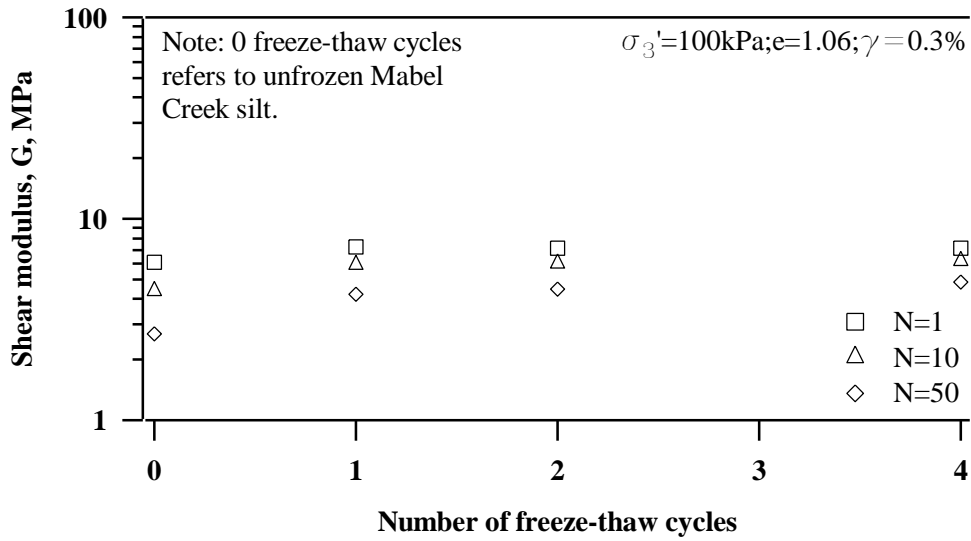


Figure 5.40 Shear modulus versus number of freeze-thaw cycles on Mabel Creek silt for  $\gamma=0.3\%$

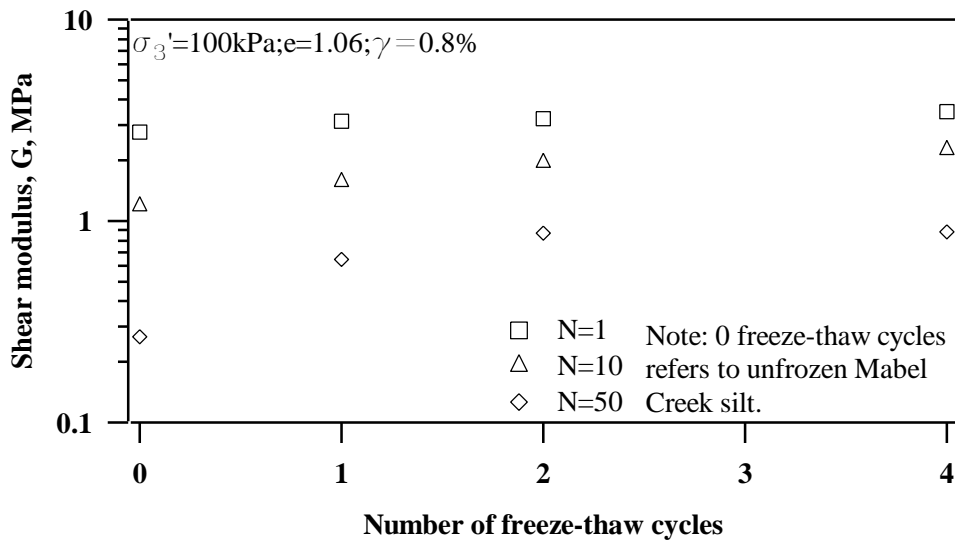


Figure 5.41 Shear modulus versus number of freeze-thaw cycles on Mabel Creek silt for  $\gamma=0.8\%$

### 5.7.2 Freeze-thaw cycle effects on damping ratio

As shown in Figure 5.42, the influence of freeze-thaw cycles on the damping ratio at various loading cycles was studied for shear strain levels of 0.005%, 0.1%, 0.3%, and 0.8%. Figure 5.42a shows the variation in damping ratio for the Mabel Creek silt conditioned at 1, 2, and 4 freeze-thaw cycles at the small shear strain of 0.005%. The



damping ratios for all specimens were nearly constant during the whole cyclic loading process. A specimen subjected to 4 freeze-thaw cycles was found to have the smallest damping ratio. The unfrozen specimen had the second smallest damping ratio. The damping ratios for specimens subjected to 1 and 2 freeze-thaw cycles were nearly the same; see Figure 5.42. The difference between damping ratios for the unfrozen specimen and the specimen subjected to 4 freeze-thaw cycles was less than 1%. The difference between damping ratios for the unfrozen specimen and the specimen experiencing 1 and 2 freeze-thaw cycles was less than 2%.

Figure 5.42b provides a comparison of damping ratios as a function of number of loading cycles on Mabel Creek silt when specimens were subjected to 1, 2, and 4 freeze-thaw cycles at the shear strain level of 0.1%. At the large shear strain of 0.1%, all specimens showed a trend that the damping ratio will decrease with an increase in the number of load cycles. The smallest damping ratios were obtained on an unfrozen specimen, and the second smallest damping ratio occurred on a specimen that had been subjected to 1 freeze-thaw cycle. Damping ratio for specimens subjected to 4 freeze-thaw cycles had a slightly larger value than that of specimens subjected to 2 freeze-thaw cycles; however, the difference between damping ratios for these two specimens was very small (i.e., less than 1%).

Figure 5.42c shows the variation in the damping ratio as a function of the number of loading cycles on the Mabel Creek silt subjected to 1, 2, and 4 freeze-thaw cycles at a shear strain level of 0.3%. For the first 10 loading cycles, the damping ratios for specimens subjected to different freeze-thaw cycles displayed the same trend illustrated in Figure 5.42b. However, a slightly increase in the damping ratio for a specimen subjected to 1 freeze-thaw cycle after 10 loading cycles changed this trend. The damping ratios for a specimen experiencing 1 freeze-thaw cycle became larger than that for a specimen experiencing 2 freeze-thaw cycles, but were still smaller than those for a specimen experiencing 4 freeze-thaw cycles.

Damping ratio as a function of the number of load cycles for specimens subjected to 1, 2, and 4 freeze-thaw cycles at a large shear strain level of 0.8% is shown in Figure 5.42d. A dramatic increase in damping ratio was found to occur for unfrozen specimens with increasing loading cycles. Before 30 load cycles, the unfrozen specimen had the smallest damping ratio, but the damping ratio became the largest after 30 loading cycles. The influence of freeze-thaw cycles on damping ratios for specimens subjected to 1, 2, and 4 freeze-thaw cycles at  $\gamma=0.8\%$  was difficult to ascertain. Damping ratios were found to be nearly the same for all load cycles.

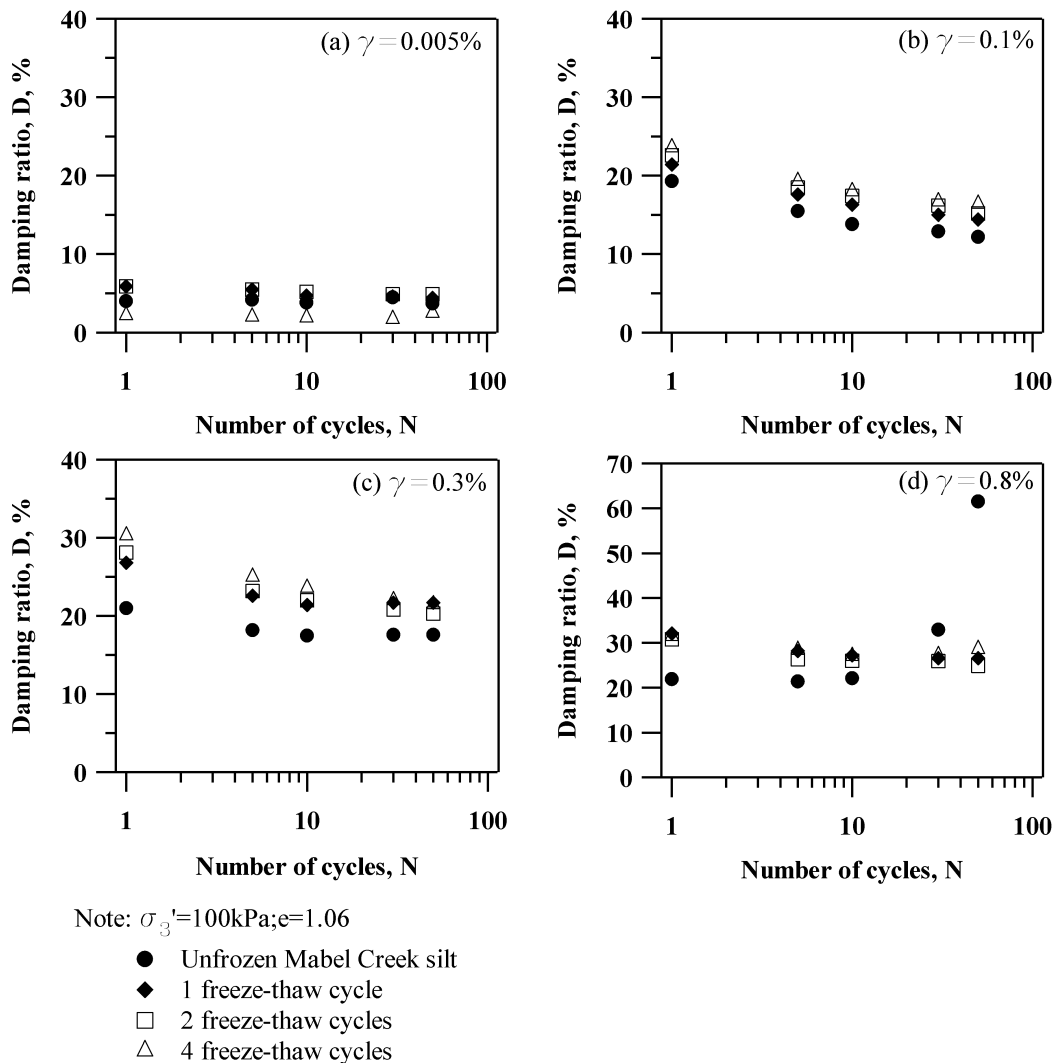
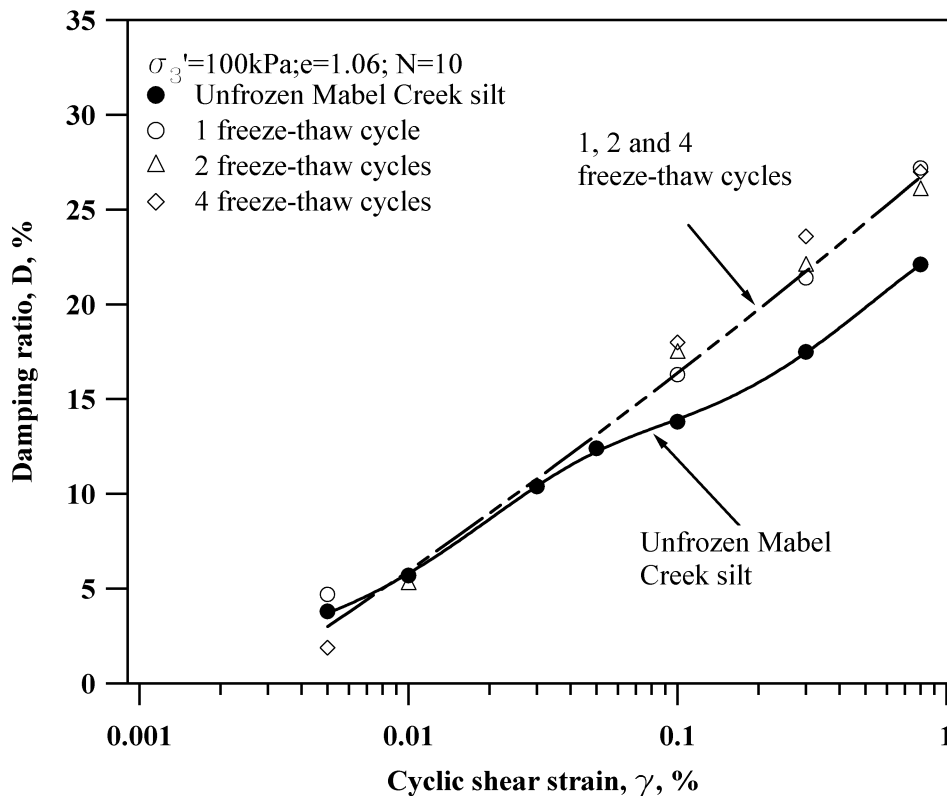


Figure 5.42 Effect of freeze-thaw cycles on damping ratio of Mabel Creek silt

Damping ratios for unfrozen specimens subjected to 1, 2, and 4 freeze-thaw cycles were evaluated in terms of the cyclic shear strain, and are shown in Figure 5.43. Damping ratios from unfrozen specimens formed the lower bound. The freeze-thaw cycles increased damping ratio; however, damping ratios in specimens experiencing 1, 2, and 4 freeze-thaw cycles were nearly the same.



**Figure 5.43** Damping ratio versus cyclic shear strain on Mabel Creek silt experiencing the different freeze-thaw cycles for  $N=10$

The effect of freeze-thaw cycles on damping ratio and on the excess pore water pressure ratio were compared at  $\gamma=0.005\%$ ,  $\gamma=0.1\%$ ,  $\gamma=0.3\%$ , and  $\gamma=0.8\%$  as shown in Figure 5.44. For  $\gamma=0.005\%$ , the specimen conditioned at 4 freeze-thaw cycles was found to have a small damping ratio. For  $\gamma=0.1\%$ , the unfrozen specimen and the specimen experiencing 1 freeze-thaw cycle showed similar damping ratios: both were less than those of the specimens that experienced 2 and 4 freeze-thaw cycles. The

largest damping ratios were found for specimens that were subjected to 2 and 4 freeze-thaw cycles. At  $\gamma=0.3\%$ , a specimen conditioned at 2 and 4 freeze-thaw cycles provided the upper bound in damping ratios. Only the unfrozen specimen provided the lower bound of damping ratio. At  $\gamma=0.8\%$ , damping ratios for specimens subjected to 1, 2, and 4 freeze-thaw cycles were indistinguishable. An unfrozen specimen had the lowest damping ratio when  $r_u < 0.8$ . An additional increase in  $r_u$  dramatically increased damping ratios for the unfrozen specimens.

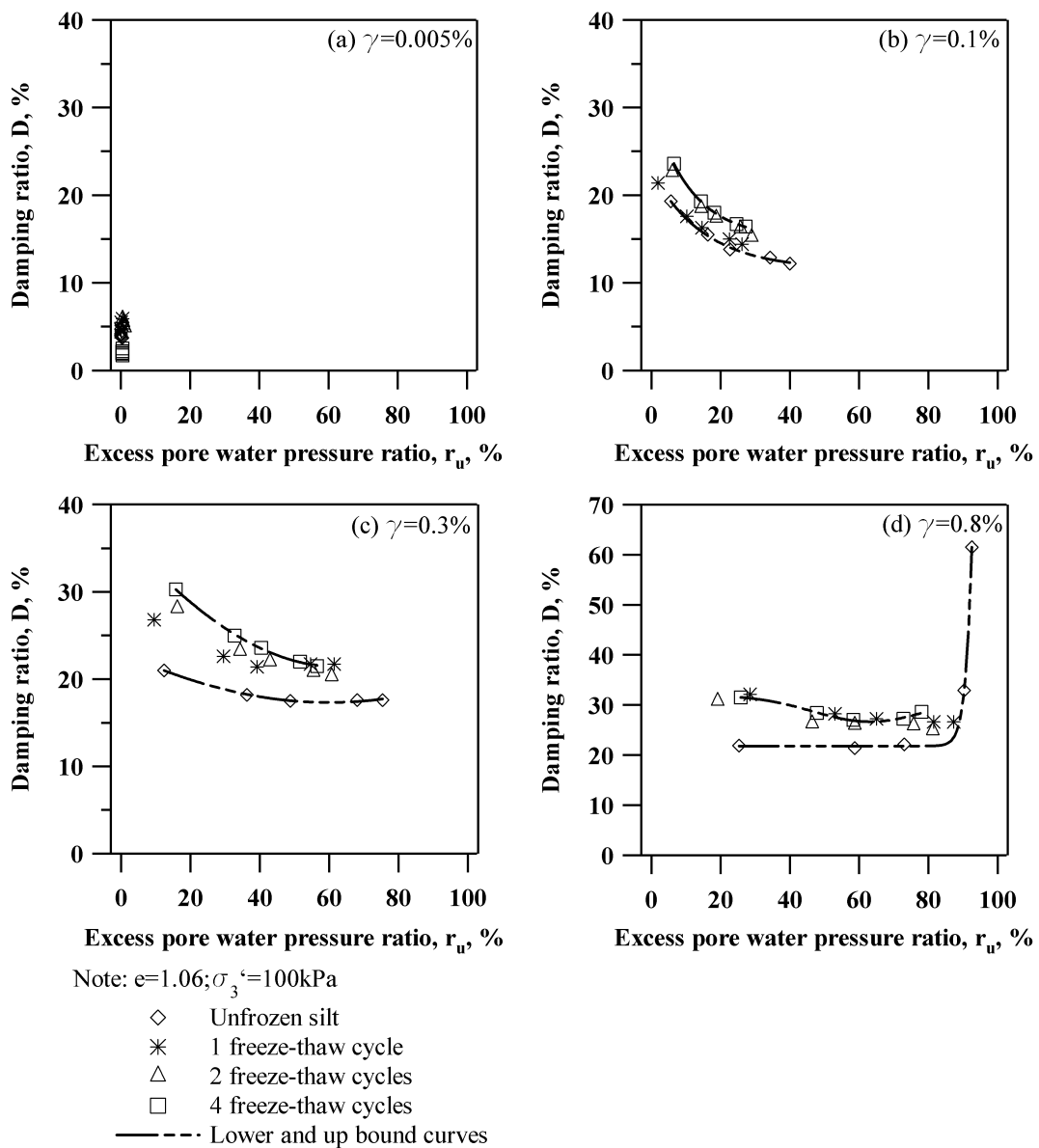


**Figure 5.44** Damping ratio ( $D$ ) versus  $r_u$  on Mabel Creek silt experiencing the different freeze-thaw cycles

The effect of up to 4 freeze-thaw cycles on damping ratios on specimens of the Mabel Creek silt was compared and evaluated for the number of freeze-thaw cycles at different shear strain levels of 0.005%, 0.1%, 0.3%, and 0.8%; see Figure 5.45 to Figure 5.48. At a small shear strain of 0.005%, 1 freeze-thaw cycle caused an increase in the damping ratio. When specimens were subjected to an additional freeze-thaw cycle (i.e., 2 freeze-thaw cycles) the damping ratio remained nearly the same. When specimens were subjected to 4 freeze-thaw cycles, the damping ratio changed from 5% to 2%. In general, the variation in damping ratio with increase in number of freeze-thaw cycles from 0 to 4 was very small and less than 3%. For a shear strain level of 0.1%, damping ratio was found to increase for freeze-thaw cycles from 0 to 4. A similar trend was found for the damping ratio when the freeze-thaw cycles were increased at the shear strain of 0.3%; see Figure 5.47. At the largest shear strain of 0.8%, a dramatic increase in damping ratio was found to occur for unfrozen specimens when the number of load cycles was increased. The effect of freeze-thaw cycles on damping ratio is obvious between the unfrozen specimen and the specimen experiencing 1 freeze-thaw cycle. However, there was little effect on the damping ratio when the number of freeze-thaw cycles was changed from 1 to 4 at  $\gamma=0.8\%$ . Therefore, all these test results show that when specimens were subjected to 1, 2, and 4 freeze-thaw cycles, the damping ratio was affected primarily in the first freeze-thaw cycle. This observation was consistent for shear strain levels of 0.005%, 0.1%, 0.3%, and 0.8%. In summary, there was some variation in damping ratio with an increase in freeze-thaw cycles from 1 to 4 at all shear strain levels, but the effect was minimal.

## **5.8 Discussion of dynamic properties at various freeze-thaw cycles**

As discussed in Section 5.5, dynamic properties for Mabel Creek silt at 1, 2, and 4 freeze-thaw cycles were correlated with the dynamic properties for fine-grained soils with different PIs from other investigators. This information may be seen in Figure 5.49 and Figure 5.50. The damping ratio for the Mabel Creek silt experiencing

freeze-thaw cycles was higher than that found for fine-grained soils by Vucetic and Dobry (1991). However, freeze-thaw cycles did not induce a significant difference in normalized shear modulus reduction or the normalized shear modulus reduction at various freeze-thaw cycles. The values from the Mabel Creek silt were grouped between high and low values of PI=0 and PI=15 by Vucetic and Dobry (1991).

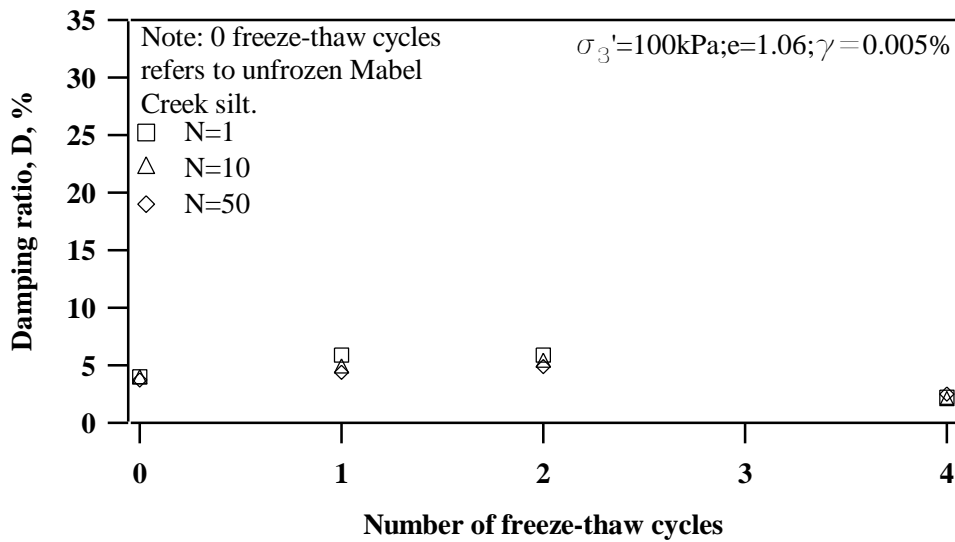


Figure 5.45 Damping ratio versus number of freeze-thaw cycles on Mabel Creek silt for  $\gamma=0.005\%$

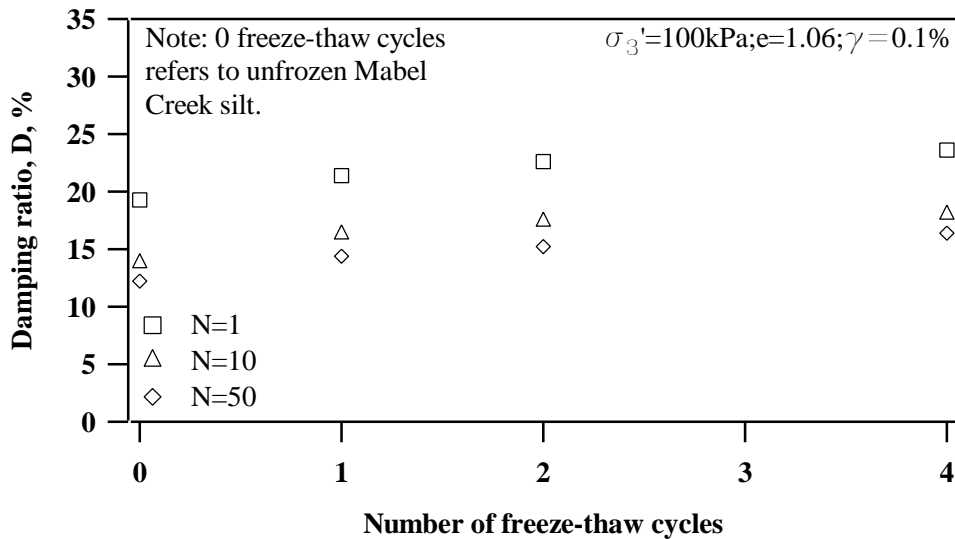


Figure 5.46 Damping ratio versus number of freeze-thaw cycles on Mabel Creek silt for  $\gamma=0.1\%$

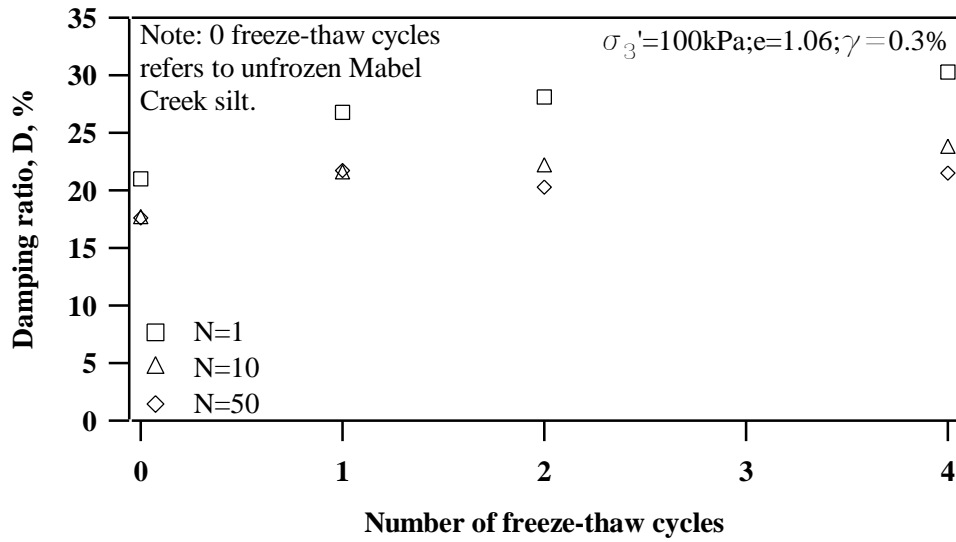


Figure 5.47 Damping ratio versus number of freeze-thaw cycles on Mabel Creek silt for  $\gamma = 0.3\%$

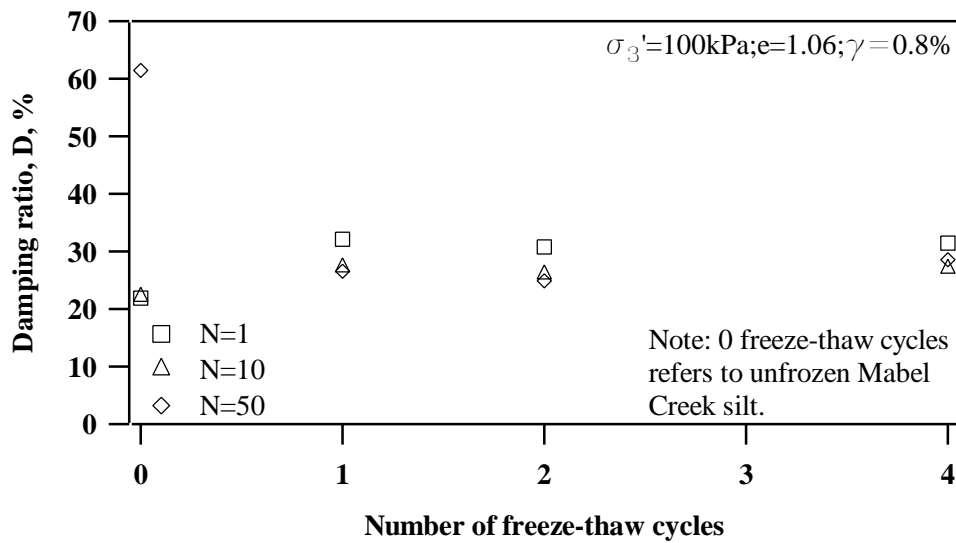
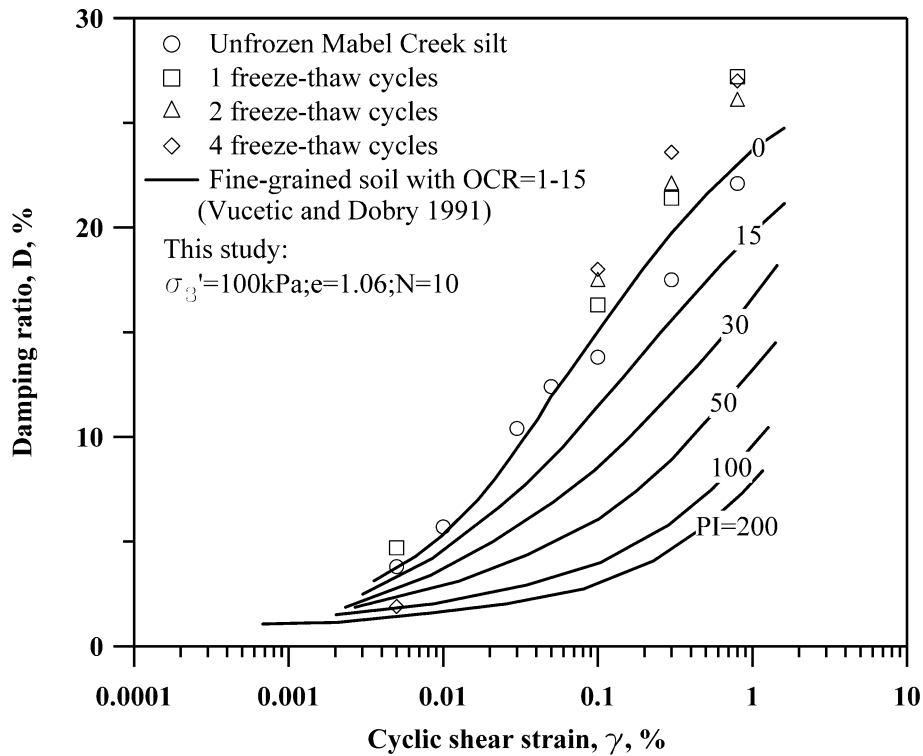
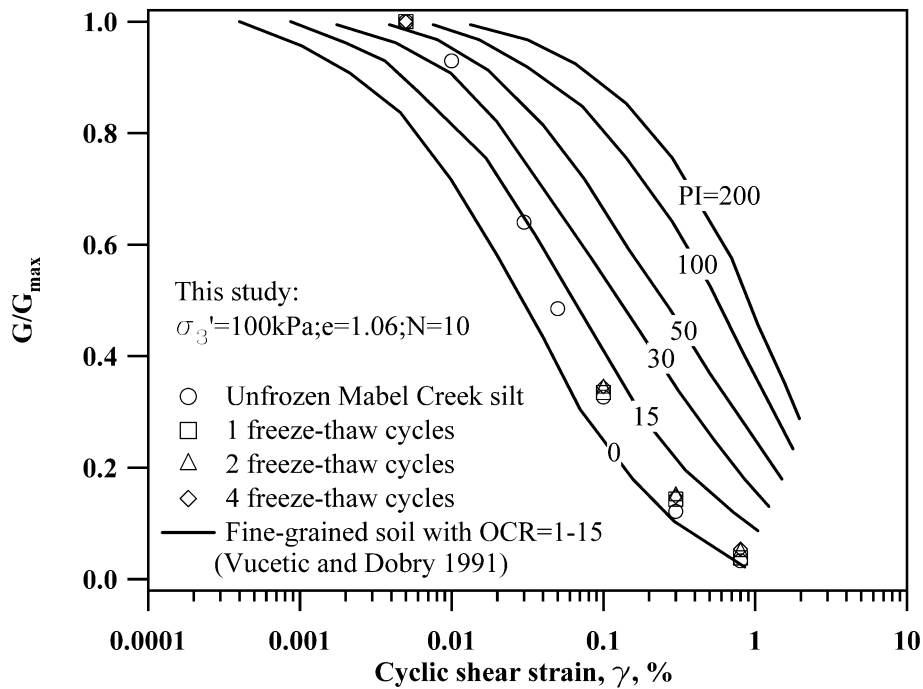


Figure 5.48 Damping ratio versus number of freeze-thaw cycles on Mabel Creek silt for  $\gamma = 0.8\%$



**Figure 5.49** Comparison of damping ratio between Mabel Creek silt conditioned at various freeze-thaw cycles and fine-grained soil (from Vucetic and Dobry 1991)



**Figure 5.50** Comparison of normalized shear modulus reduction between Mabel Creek silt conditioned at various freeze-thaw cycles and fine-grained soil (from Vucetic and Dobry 1991)



## 5.9 Thermal conditioning path effect on dynamic properties

Similarly, the effect of thermal conditioning paths on dynamic properties was investigated at the target temperatures of 0.5 °C and -0.2 °C. A comparison of dynamic properties for different thermal conditioning paths was conducted under the conditions of given number of loading cycles, given excess pore pressure ratio at large cyclic shear strain, and given cyclic shear strain. The large strain was chosen when checking the variation of dynamic properties with increasing number of loading cycles or excess pore pressure.

Figure 5.51 shows the comparison of  $G$  for different thermal conditioning paths at a target temperature of 0.5 °C. From the degradation of  $G$  with increasing  $N$  at  $\gamma=0.3\%$  as shown in Figure 5.51a, the specimen conditioned on Path 3 displays smaller shear modulus in comparison with the specimens conditioned on Path 1 and Path 2. Conditioning Path 1 caused the highest shear modulus before  $N=30$ ; however, further increasing of  $N$  made  $G$  of the specimen on Path 3 decrease to a smaller value than that of the specimen on Path 2. But when the excess pore pressure ratio is considered in terms of the degradation of  $G$  as shown in Figure 5.51b, it is clear that the conditioning on Path 1 causes the highest  $G$  in the specimen. As shown in Figure 5.51c, the curves of  $G$  versus cyclic shear strain  $\gamma$  at  $N=10$  also display the highest shear modulus in specimens conditioning on Path 1. The exception was for  $\gamma=0.8$ , where  $G$  at  $N=10$  on Path 3 was higher than  $G$  on Path 2. This is because higher pore pressure generation occurred in specimens on Path 2.

The impact of thermal conditioning paths on damping ratio  $D$  at the target temperature of 0.5 °C is shown in Figure 5.52. Figure 5.52a and Figure 5.52b display comparisons of  $D$  at  $\gamma=0.1\%$ . Clearly, the highest value of  $D$  was observed in the specimen on Path 2, and  $D$  in the specimen on Path 3 had the lowest value. The curve of  $D$  and  $\gamma$  also shows that the conditioning of Path 3 makes  $D$  of the specimen less,

as shown in Figure 5.52c. This is perhaps because less freezing had occurred in specimens on Path 3 in comparison with the other two conditioning paths.

The impact of thermal conditioning paths on  $G$  and  $D$  of Mabel Creek silt at the target temperature of  $-0.2\text{ }^{\circ}\text{C}$  is displayed in Figure 5.53 and Figure 5.54. The conditionings of Path 1 and Path 2 both caused a similar constant  $G$  with increasing  $N$  at  $\gamma=0.1\%$ , as shown in Figure 5.53a and Figure 5.53b, which is perhaps because the specimens were still in a frozen state. However, the conditioning of Path 3 caused a significantly lower value of  $G$  at  $\gamma=0.1\%$ . A similar effect of thermal conditioning paths on  $G$  was observed for the curves of  $G$  versus  $\gamma$ , as shown in Figure 5.53c. Though the similar impact of Path 1 and Path 2 was observed on  $G$  of specimens at  $\gamma=0.1\%$ , the situation changed with the consideration of  $D$  at  $\gamma=0.1\%$ . From Figure 5.54a and Figure 5.54b, the specimens on Path 1 display the largest  $D$ , the specimens on Path 2 the second largest, and the specimens on Path 3 the third largest. The curve of  $D$  versus  $\gamma$ , as shown in Figure 5.54c, also show a similar trend of the impact of thermal conditioning paths on  $D$ .

Different conditioning paths caused different dynamic properties, though the final conditioning temperatures at the cyclic loading test were the same. This can probably be attributed to the different freezing and thawing state on the different conditioning paths. For the target temperature of  $0.5\text{ }^{\circ}\text{C}$ , the longer conditioning at  $0.5\text{ }^{\circ}\text{C}$  (Path 2) caused much more thawing than Path 1. Path 3 did not go through the frozen state, and the specimen remained at nearly completely unfrozen state. For the target temperature of  $-0.2\text{ }^{\circ}\text{C}$ , Path 1 and Path 2 caused slow thawing in the specimen; the effect of this thawing was not obvious. The conditioning of Path 3 was to freeze soil specimens, thus, a larger unfrozen portion existed in specimens on Path 3 than in specimens on Path 1 and Path 2.

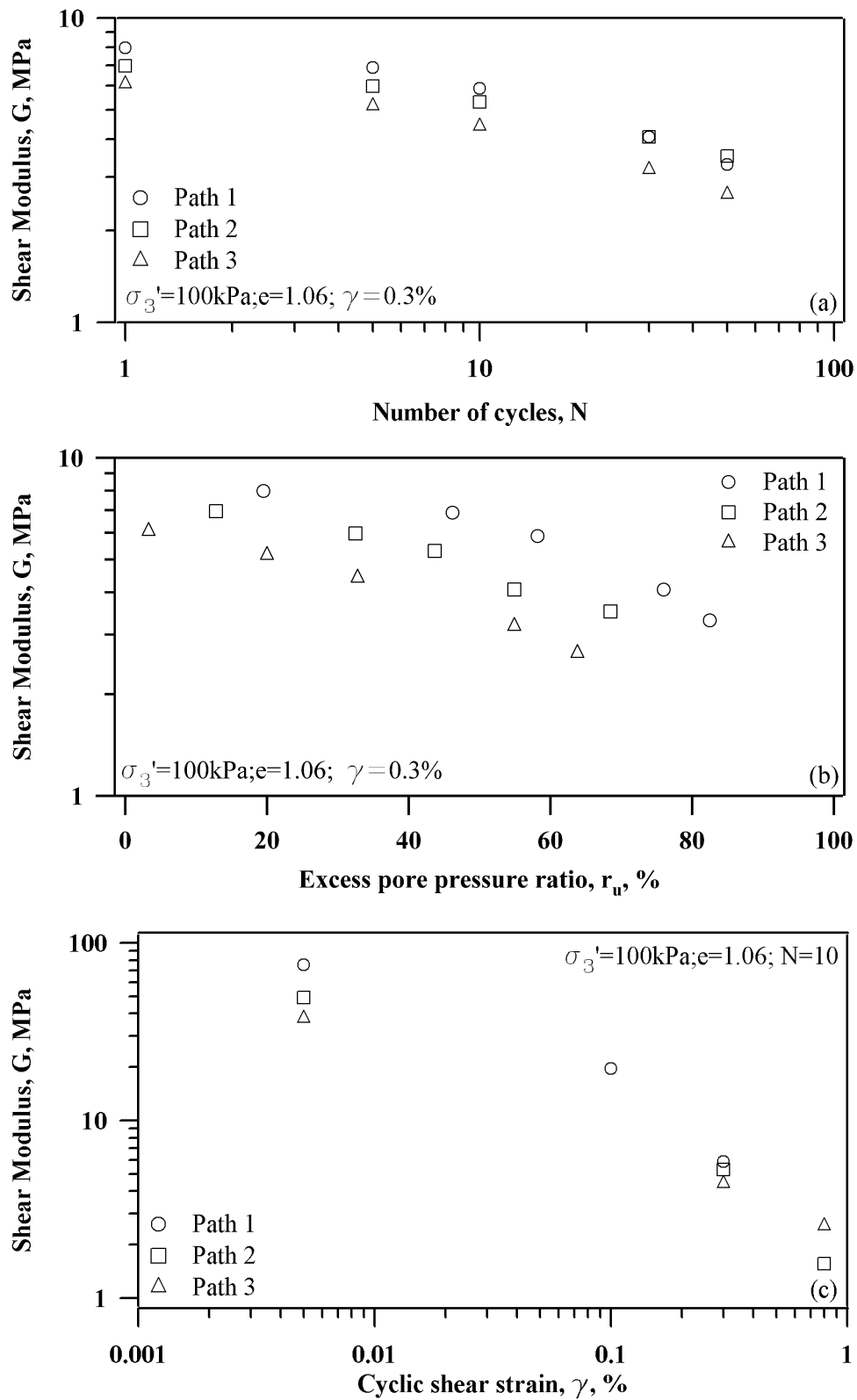


**Figure 5.51** Effect of thermal conditioning paths on  $G$  of Mabel Creek silt at the target temperature of  $0.5\text{ }^{\circ}\text{C}$

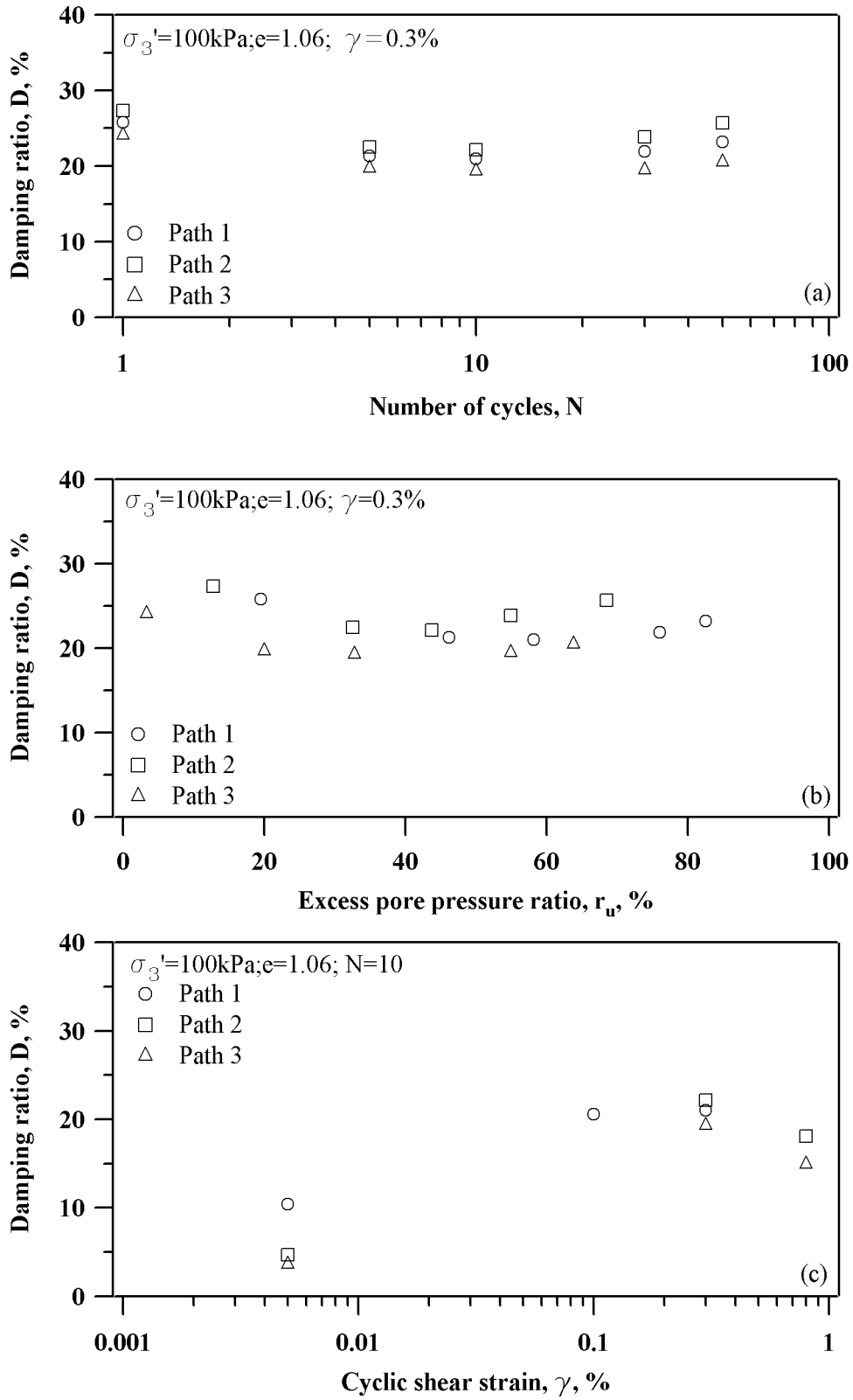
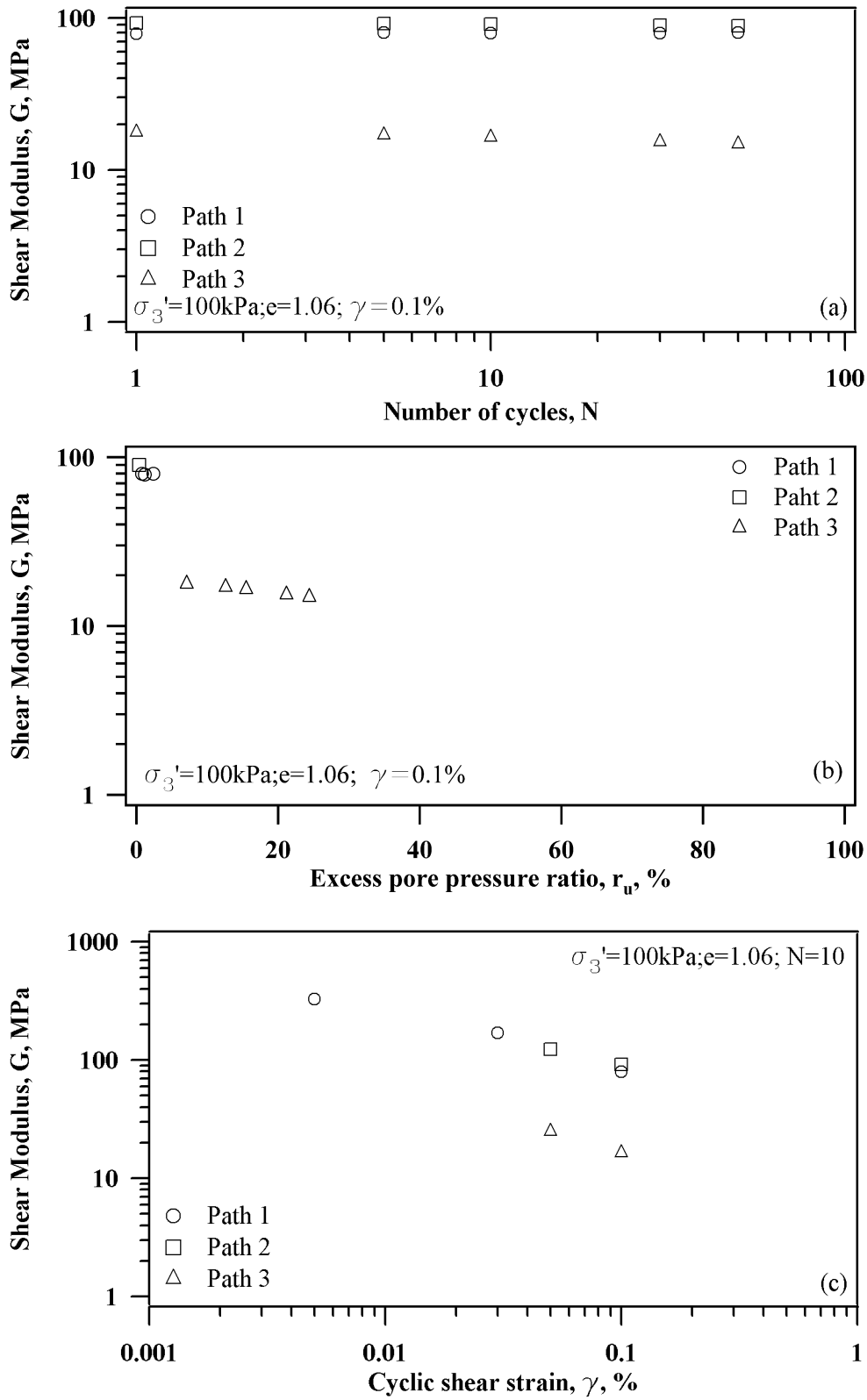
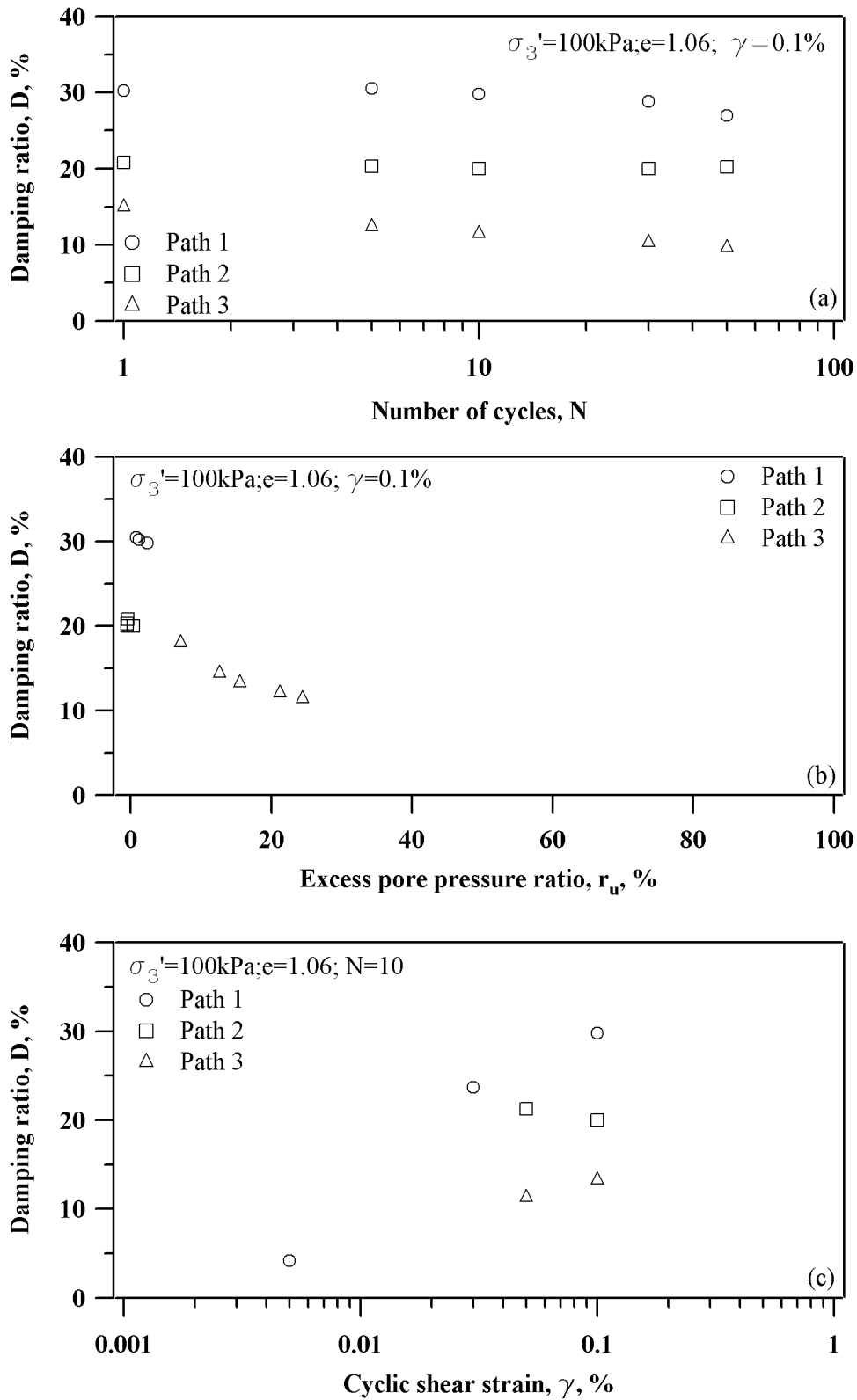


Figure 5.52 Effect of thermal conditioning paths on  $D$  of Mabel Creek silt at the target temperature of  $0.5\text{ }^{\circ}\text{C}$



**Figure 5.53** Effect of thermal conditioning paths on  $G$  of Mabel Creek silt at the target temperature of  $-0.2^\circ\text{C}$



**Figure 5.54** Effect of thermal conditioning paths on  $D$  of Mabel Creek silt at the target temperature of  $-0.2\text{ }^\circ\text{C}$

### 5.10 Degradation of dynamic shear modulus in undrained cyclic tests

When the Mabel Creek silt was cyclically loaded under undrained strain-controlled conditions, the dynamic shear modulus was observed to decrease with increasing loading cycles due to an increase in pore water pressure and a corresponding decrease in effective confining pressure. Idriss et al. (1978) found that the degradation of shear modulus with increasing loading cycles in cohesive soil would conform to the following equation:

$$G_N = N^{-t} G_1,$$

in which  $N$  is the number of loading cycles;  $t$  is the degradation parameter that is related to  $PI$ , overconsolidation ratio, and cyclic strain amplitude; and  $G_1$  is the shear modulus at the end of the first loading cycle.

In this study, this model was extensively applied to the Mabel Creek silt at various conditioned temperatures and freeze-thaw cycles. A regression was applied to this model in order to attain a degradation parameter. This was done to predict the variation in shear modulus with the number of loading cycles. The data correlated well with this model. Thus, it is assumed that the degradation parameter indicates that the model of Idriss et al. (1978) is applicable for Mabel Creek silt. A summary of the degradation parameter on Mabel Creek silt at various temperatures is presented in Table 5.1. The results show that the degradation parameter increases with increasing cyclic strain amplitude. This is consistent with findings by Idriss et al. (1978). The specimens conditioned at  $-0.2\text{ }^{\circ}\text{C}$  are not included in these regressions. This is because the shear modulus remained the same regardless of the number of load cycles.

**Table 5.1 Degradation parameter of shear modulus on Mabel Creek silt**

Specimen	t		
	$\gamma=0.1\%$	$\gamma=0.3\%$	$\gamma=0.8\%$
1	0.042	0.173	0.425
2	0.035	0.115	0.324
3	0.030	0.111	-
4	0.024	0.091	-
5	0.032	0.177	-
6	0.033	0.100	0.264
7	0.031	0.083	0.257

Note:

- 1: Unfrozen silt specimen
- 2: Specimens conditioned at 24 °C or experiencing 1 freeze-thaw cycle
- 3: Specimens conditioned at 5 °C
- 4: Specimens conditioned at 1 °C
- 5: Specimens conditioned at 0.5 °C
- 6: Specimens experienced 2 freeze-thaw cycles
- 7: Specimens experienced 4 freeze-thaw cycles

Normalized shear modulus degradation (the ratio of shear modulus at  $N=n$  to shear modulus at  $N=1$ ) is presented in Figure 5.55 to Figure 5.56. Normalized shear modulus degradation was used to evaluate temperature effect on the degradation of shear modulus for specimens at  $\gamma=0.1\%$  and  $\gamma=0.3\%$ . At  $\gamma=0.1\%$ , the degradation curves for the specimens conditioned at different temperatures were within a narrow band, but the effects that temperature had on the results were uncertain. However, temperature effect on degradation of shear modulus was observed at  $\gamma=0.3\%$ . At  $\gamma=0.3\%$ , a specimen conditioned at 0.5 °C and a unfrozen specimen were found to have similar degradation curves, which were below the degradation curves at 1 °C, 5 °C, and 24 °C. The shear modulus degradation curves for specimens conditioned at 5 °C and 24 °C behaved in a similar manner. The specimen conditioned at 1 °C had the slowest degradation of shear modulus.



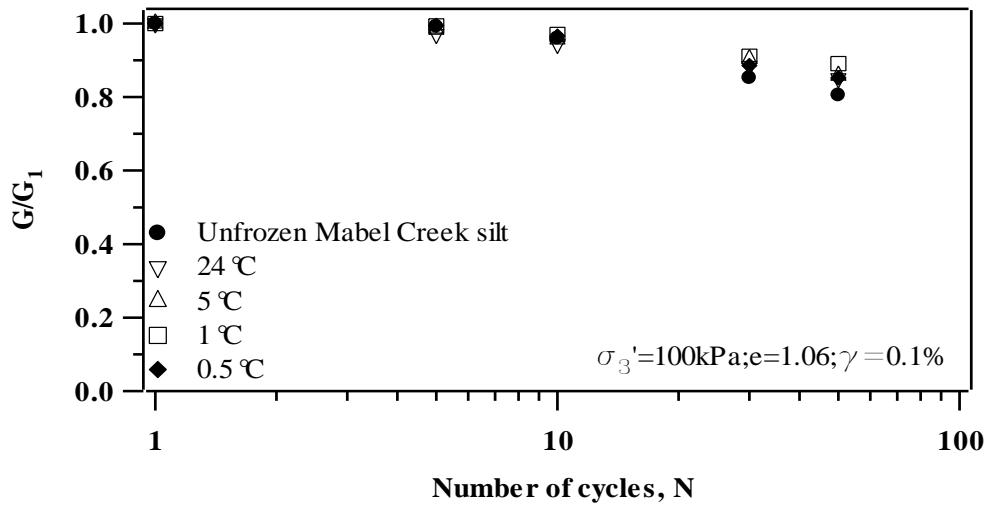


Figure 5.55 The degradation curves of unfrozen Mabel Creek silt and Mabel Creek silt conditioned at 0.5 °C, 1 °C, 5 °C, and 24°C at  $\gamma=0.1\%$

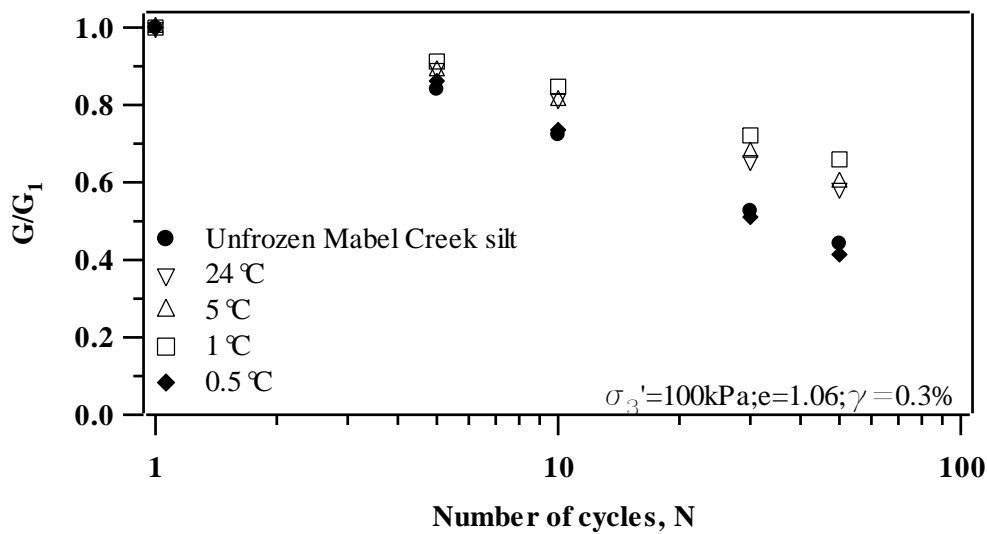
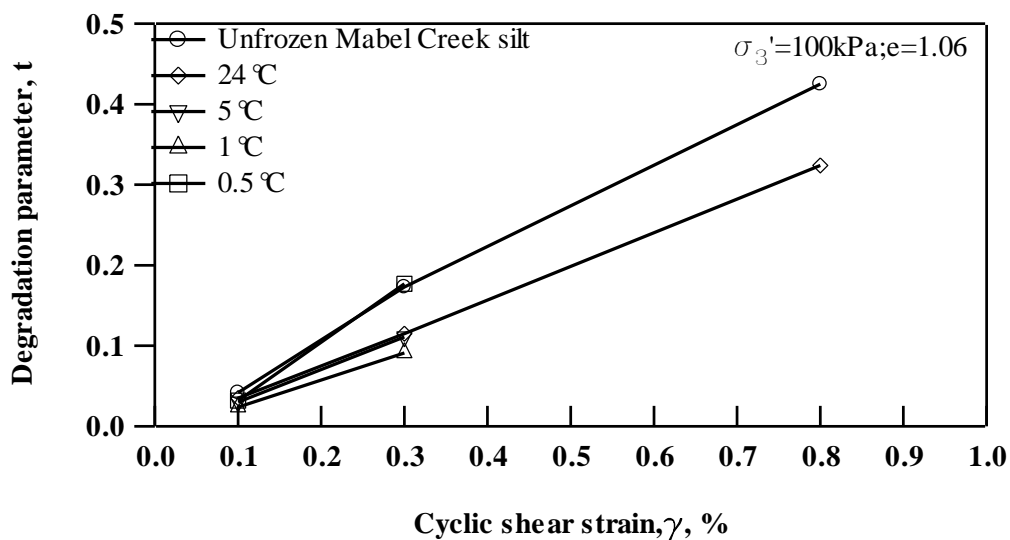


Figure 5.56 The degradation curves of unfrozen Mabel Creek silt and Mabel Creek silt conditioned at 0.5 °C, 1 °C, 5 °C, and 24°C at  $\gamma=0.3\%$

Degradation parameters for Mabel Creek silt conditioned at different temperature was evaluated as a function of cyclic strain as shown in Figure 5.57. Figure 5.57 provides a possible prediction of the degradation parameter for a given shear strain and a given temperature condition. The degradation parameter for Mabel Creek silt behaved nearly linearly. It shows an increase with increasing cyclic strain. The distinction of

these degradation parameters due to temperature effect in Mabel Creek silt was not significant when  $\gamma$  was small (0.1%); however, the distinction became more and more obvious with increasing cyclic strain. Unfrozen specimens and the specimens conditioned at 0.5 °C may be categorized together for the degradation parameter and showed a similar trend. The specimens conditioned at 1 °C, 5 °C, and 24 °C may also be categorized together for the degradation parameter. A similar trend of the degradation parameter, which was different from the trend for the unfrozen specimens and the specimens conditioned at 0.5 °C, was observed for the specimens conditioned at 1 °C, 5 °C, and 24 °C.



**Figure 5.57** Degradation parameter ( $t$ ) versus  $\gamma$  on unfrozen Mabel Creek silt and Mabel Creek silt conditioned at 0.5 °C, 1 °C, 5 °C, and 24 °C

The freeze-thaw cycle effect on the degradation of shear modulus of Mabel Creek silt was evaluated as normalized shear modulus gradation curves at  $\gamma=0.1\%$ ,  $\gamma=0.3\%$ , and  $\gamma=0.8\%$ , as shown in Figure 5.58 to Figure 5.60. Like Figure 5.55, the freeze-thaw cycle effect on the degradation of shear modulus for the Mabel Creek silt was difficult to distinguish at a small shear strain level of 0.1%. However, with increasing shear modulus, the freeze-thaw cycle effect on the degradation of shear modulus for Mabel Creek silt became significant. At  $\gamma=0.3\%$  and  $\gamma=0.8\%$ , the degradation of shear

modulus with an increasing number of loading cycles became smaller and smaller with an increasing number of freeze-thaw cycles.

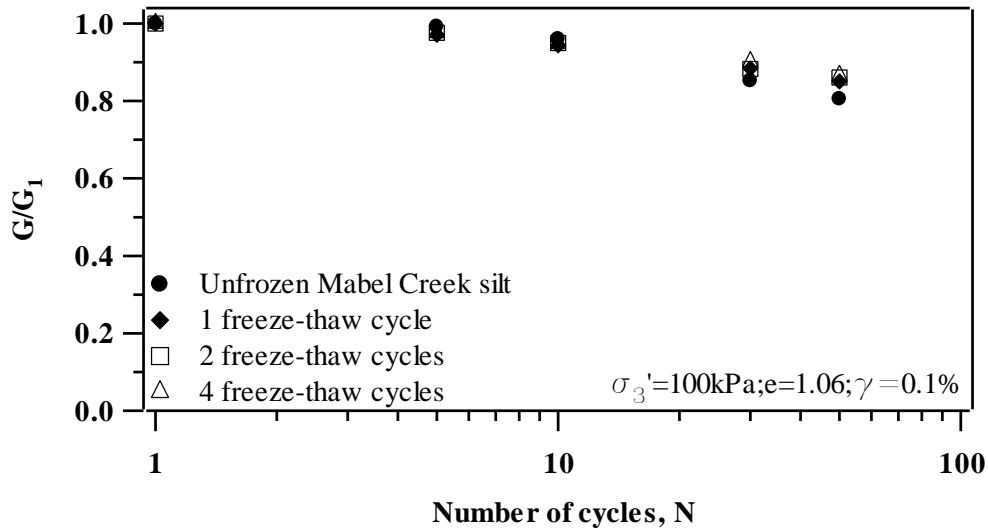


Figure 5.58 The degradation curves of Mabel Creek silt experiencing freeze-thaw cycles at  $\gamma=0.1\%$

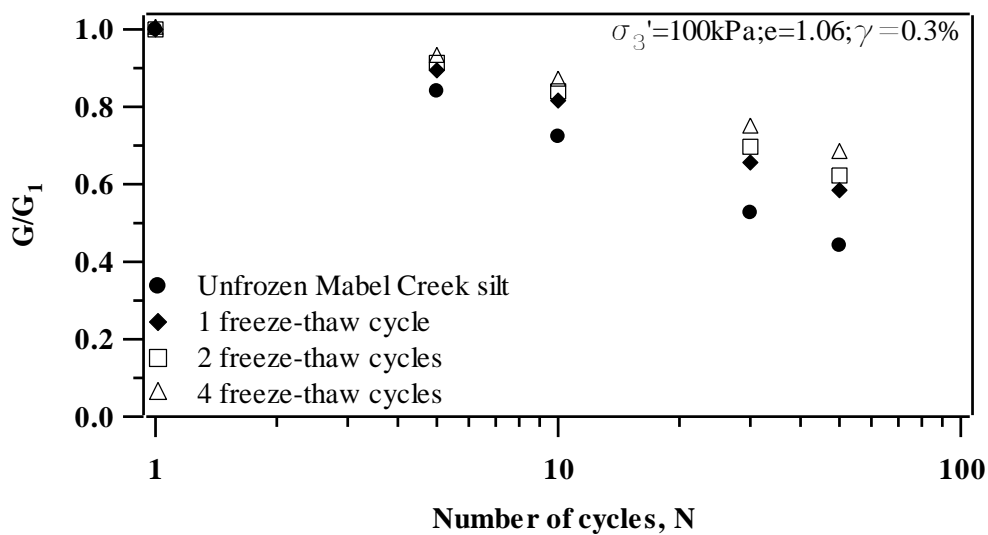
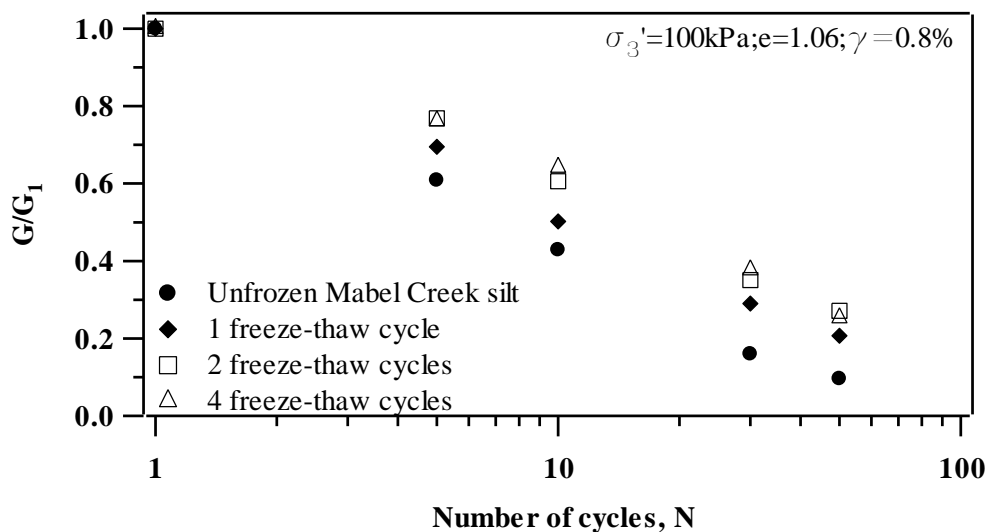


Figure 5.59 The degradation curves of Mabel Creek silt experiencing freeze-thaw cycles at  $\gamma=0.3\%$



**Figure 5.60** The degradation curves of Mabel Creek silt experiencing freeze-thaw cycles at  $\gamma=0.8\%$

The degradation parameters for Mabel Creek silt experiencing a different number of freeze-thaw cycles were evaluated as a function of cyclic strain; see Figure 5.57. This figure provides engineers with a possible prediction of the degradation parameter for a given shear strain and a given freeze-thaw cycle. For small shear strain, the effect of the freeze-thaw cycles on the degradation parameter was not obvious; however, with an increase in cyclic strain, the influence of the freeze-thaw cycles on the degradation parameter became more and more significant. In general, increasing the number of freeze-thaw cycles from 1 to 4 decreased the degradation parameter for any given cyclic shear strain. However, with an increase in the number of freeze-thaw cycles, the decrease of the degradation parameter became more and more obvious. A trend that the degradation parameter increases with increased cyclic shear strain also is observed in Figure 5.61.

### 5.11 Summary

Initially, this chapter provided an introduction to the dynamic characteristics (damping ratio and dynamic shear modulus) for reconstituted specimens of unfrozen

Mabel Creek silt, Mabel Creek silt conditioned at 24 °C, 5 °C, 1 °C, 0.5 °C, and -0.2 °C, and Mabel Creek silt conditioned at 2 and 4 freeze-thaw cycles. The effect of temperature on dynamic characteristics of Mabel Creek silt was studied by comparing test results between Mabel Creek silt conditioned at 24 °C, 5 °C, 1 °C, 0.5 °C, -0.2 °C, and unfrozen Mabel Creek silt. Moreover, the impact of freeze-thaw cycles on dynamic characteristics was examined through a comparison of damping ratio and dynamic shear modulus on the unfrozen Mabel Creek silt and Mabel Creek silt conditioned at 1, 2, and 4 freeze-thaw cycles. The impact of temperature and freeze-thaw cycling on dynamic properties was further evaluated by comparison of results in this study with previous results from the literature.

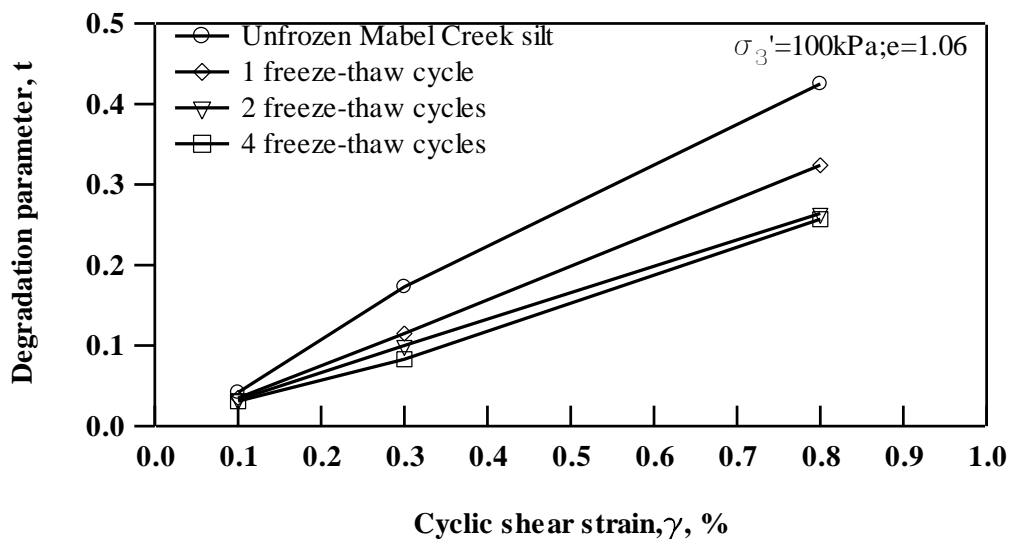


**Figure 5.61** Degradation parameter ( $t$ ) versus  $\gamma$  on Mabel Creek silt experiencing freeze-thaw cycles

The applicable results in this study show that when Mabel Creek silt is near the freezing temperature, regardless of the conditioned temperatures, there will be a decrease in the damping ratio. The trend was changed when the specimens liquefied. In general, Mabel Creek silt conditioned at a temperature from -0.2 °C to 24 °C showed a decrease in the damping ratio. Among these different thawing temperatures from -0.2 °C to 24 °C, the largest damping ratios occurred for specimens thawed at -0.2 °C, and the second largest damping ratio was for specimens thawed at 0.5 °C. Damping

ratios for specimens conditioned at 1 °C, 5 °C, and 24 °C were nearly the same (they were grouped in a very narrow band). Unfrozen specimens had the lowest damping ratio. For dynamic shear modulus, this freezing and thawing process, regardless of the thawing temperatures, increased shear modulus. In general, the largest increase of shear modulus occurred for Mabel Creek silt thawed at -0.2 °C, and the second largest increase of shear modulus occurred for Mabel Creek silt thawed at 0.5 °C. However, the largest increase in shear modulus was changed when the pore water pressure was close to the effective confining pressure (i.e., the liquefaction state).

Increasing the number of freeze-thaw cycles for shear strain larger than 0.01% increased the damping ratio and the shear modulus. The decrease in the damping ratio and the shear modulus became smaller and smaller with an increase in the number of freeze-thaw cycles. When the number of freeze-thaw cycles was increased from 2 to 4, a slight increase in damping ratio and shear modulus was observed. However, this trend still was changed when Mabel Creek silt liquefied or was close to liquefaction.

By combining dynamic properties for the Mabel Creek silt at near freezing and above freezing temperatures into dynamic properties for a frozen silt from Czajkowski and Vinson (1980), there may be a hypothesis that damping ratio increases with an increase in temperature when specimens are below freezing. Further, the dynamic properties reach a maximum at near freezing temperature, but decrease with additional increase in temperature above freezing. Also, shear modulus always decreased with increase of temperature from below freezing temperatures to above freezing temperature.

The Unfrozen Mabel Creek silt is a low plastic soil with a PI of 5.3. This soil has dynamic characteristics that are consistent with results from Vucetic and Dobry (1991). The condition of an above freezing temperature from 1 °C to 24 °C only increased damping ratio and induced a damping ratio curve equal to or above the

curve at  $PI=0$ . Near freezing temperature and a treatment of freeze-thaw cycles caused an increase of damping ratio and formed damping ratio curves far above the upper bound for fine-grained soil with  $PI=0-200$  attained from Vucetic and Dobry (1991). But the normalized shear modulus reduction is not significantly affected by freeze-thaw cycles and temperature.

The thermal conditioning path was found to strongly affect the dynamic properties of Mabel Creek silt. This investigation was conducted to compare the pore pressure generation of Mabel Creek silt at  $0.5\text{ }^{\circ}\text{C}$  and  $0.2\text{ }^{\circ}\text{C}$  but through three different conditioning paths. The comparison indicates that the conditioning paths will affect dynamic properties of Mabel Creek silt, which is because the different conditioning paths cause the different frozen portion within the soil.

The degradation of shear modulus under undrained cyclic loadings may be reflected by the Idriss et al. (1978) model. The degradation parameter ( $t$ ) for Mabel Creek silt conditioned at each thermal condition was attained from test results in this study. For each thermal condition, the degradation parameter was found to be proportional to increased cyclic shear strain. The temperature effect was investigated for the degradation parameter. Unfrozen soil and the Mabel Creek silt conditioned at  $0.5\text{ }^{\circ}\text{C}$  showed a similar also degradation parameter while the Mabel Creek silt conditioned at  $24\text{ }^{\circ}\text{C}$ ,  $5\text{ }^{\circ}\text{C}$ , and  $1\text{ }^{\circ}\text{C}$  also showed similar degradation parameters. Also, the gradation parameter decreased with increasing freeze-thaw cycles.

## 6 Post-cyclic-loading Settlement

After soil is subjected to cyclic loading, an increase in pore water pressure in a saturated soil will dissipate. This difference in pore water pressure between soil boundaries and the micro-structure is referred to as reconsolidation (Ishihara 1996). Reconsolidation displaces water out of the saturated soil while dissipating pore water pressure. Correspondingly, the gross volume for a saturated soil will decrease because the incompressible water mitigates out of the soil so as to eventually cause the soil to settle. The amount of post-cyclic-loading settlement is dependent on the discharged water volume and dissipated pore water pressure caused by cyclic loadings. Lee and Albaise (1974) concluded that reconsolidated volumetric strain,  $\epsilon_v$ , (the ratio of the discharged water volume,  $\Delta V$ , to the gross soil volume,  $V$ ) for non-liquefaction conditions was determined by the dissipated pore pressure. Reconsolidated volumetric strain increased with an increase in the dissipated pore water pressure developed during undrained cyclic loading. How pore water pressure was generated did not affect the volume strain to reconsolidate. Nagase et al. (1988) studied the reconsolidated volume strain after liquefaction. A conclusion was made that the reconsolidated post-liquefaction settlements for the liquefaction state were different, even for the same 100% excess pore water pressure ratio, i.e., the pore water pressure is close or equal to the confining pressure. Pore water pressure is not the only measurement to determine post-liquefaction settlement magnitudes. Maximum shear strain is introduced to determine volumetric strain following completed liquefaction. The abrupt increase of reconsolidated volumetric strain after liquefaction may be explained as an increase of maximum shear strain following liquefaction.

Though the excess peak pore water pressure was applied in most previous research (Lee and Albaise 1974; Derakhshandi et al. 2008) as the main factor influencing post-cyclic-loading settlement, the excess peak pore water pressure is not an actual



value to account for dissipation causing settlement. From the excess peak pore water, the elastic cyclic pore water pressure is recoverable and not included in the discharged water volume (Dobry et al. 1982). Thus, excess pore water pressure was used in this study to represent an important factor in predicting post-cyclic-loading settlement. Certainly, the excess peak water pressure also was applied in order to make a comparison with previous research.

### **6.1 Post-cyclic-loading settlement for unfrozen Mabel Creek silt**

Figure 6.1 shows reconsolidated volume strain as a function of excess pore water pressure ratio for specimens of unfrozen Mabel Creek silt. The unfrozen specimens refer to the specimens without any freezing or thawing treatments. The results from the unfrozen specimen were considered as a baseline in the analysis of post-cyclic-loading settlement. Among the data points, five data were obtained from the cyclic triaxial strain-controlled tests. The maximum shear strain level in the cyclic triaxial strain-controlled test was 0.8%. This is the only data point to cause liquefaction in all the cyclic strain-controlled tests. In this study, 4 cyclic triaxial stress-controlled tests conducted and terminated at 10% axial strain were used as part the study to predict post-liquefaction settlement on unfrozen specimens. Post-cyclic-loading settlement is dependent on both: (a) the increase in pore water pressure and (b) the maximum shear strain under cyclic loading. It is independent of how the pore water pressures are generated (Lee and Albaise 1974). Therefore, in this study the susceptibility of post-cyclic-loading settlement may be addressed from all data attained by cyclic stress-controlled tests and cyclic strain-controlled tests.

Figure 6.1 illustrates that the reconsolidated volume strain increased as the excess pore water pressure ratio increased; however, the increase in reconsolidated volumetric strain was slow and flat when  $r_u$  was small. When  $r_u$  was equal to 60%, the reconsolidated volumetric strain only reached 1%. With further increases in  $r_u$ , the

increase in reconsolidation volumetric strain speeded up. This was especially true when  $r_u$  was close to 0.90, the liquefaction state. Near liquefaction, the reconsolidated volumetric strain changed dramatically. The reconsolidated volumetric strain ( $\epsilon_v$ ) at  $r_u = 92.5\%$  was 3.1%, but the reconsolidated volumetric strain ( $\epsilon_v$ ) at  $r_u = 93\%$  and  $r_u = 96\%$  reached 4.4% and 5.0%, respectively. The results also indicated that the pore water pressure alone could not reflect the feature of reconsolidated volumetric strain on the liquefied soil. Thus, maximum shear strain was introduced in this study to describe the variation in post-liquefaction settlement.

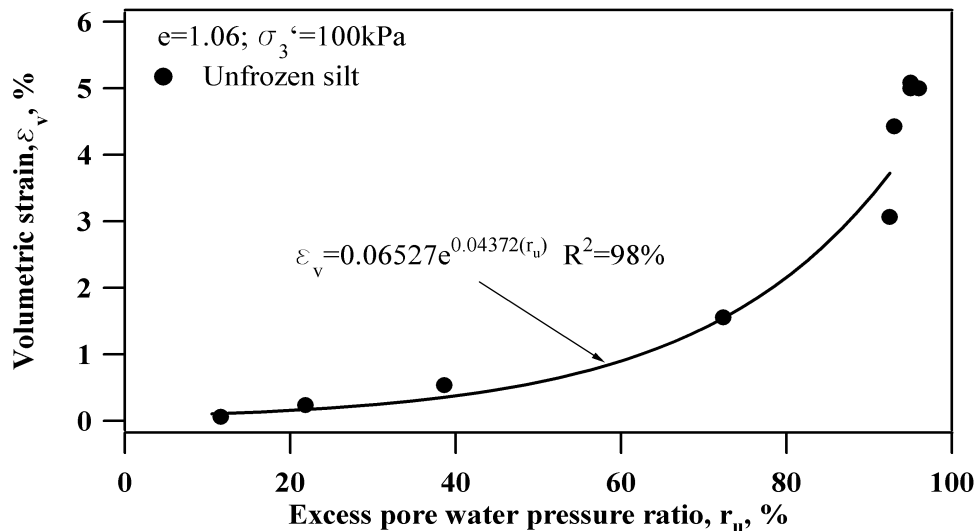


**Figure 6.1** Reconsolidated volume strain versus excess pore water pressure ratio on unfrozen Mabel Creek silt

Figure 6.2 shows the reconsolidated volumetric strain as a function of the maximum shear strain for specimens of liquefied unfrozen Mabel Creek silt. The reconsolidated volumetric strain was distinguished by the maximum shear strain, though the excess pore water pressure ratios were close and in the range of 92-96%.

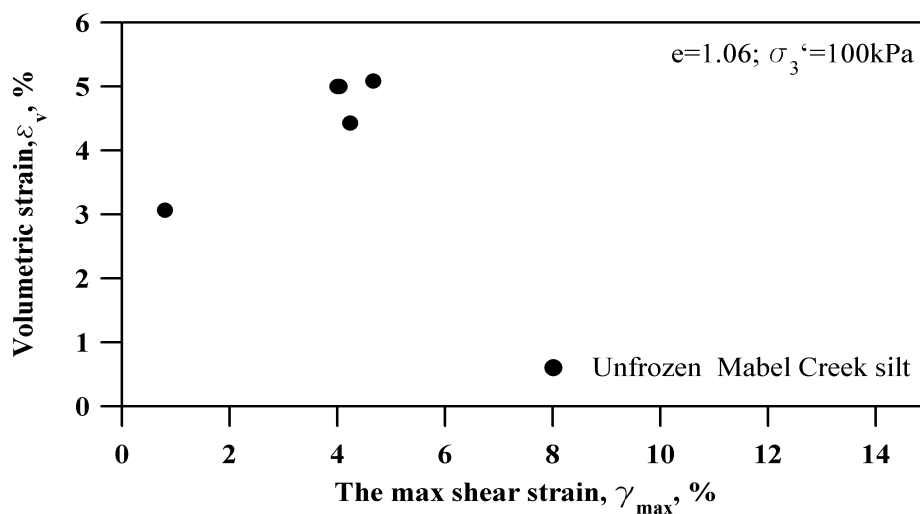


**Figure 6.2** Reconsolidated volume strain versus the max shear strain on unfrozen Mabel Creek silt

## 6.2 Post-cyclic-loading settlement of Mabel Creek silt conditioned at 0.5 °C, 1 °C, 5 °C, and 24 °C

The reconsolidated volume strain as a function of the excess pore water pressure ratio for the Mabel Creek silt conditioned at 1 °C, 5 °C, and 24 °C is presented in Figure 6.3. The consolidated volumetric strain for the specimens conditioned at these three temperatures increased with an increase in the excess pore water pressure ratio. A curve drawn through all data for the specimens conditioned at 1 °C, 5 °C, and 24 °C in Figure 6.3 indicates that post-cyclic-loading settlement is similar for the three temperature conditions. For the reconsolidated volumetric strain of 1%, excess pore water pressure ratio reached 67%. For the excess pore water pressure ratio of 90%, the reconsolidated volumetric strain reached 2.4%.

The variability in the reconsolidated volume strain as the excess pore water pressure ratio increases is shown in Figure 6.4 for specimens of Mabel Creek silt conditioned at 0.5 °C. Though the reconsolidated volumetric strain still increased with the increasing excess pore water pressure ratio, specimens conditioned at 0.5 °C had the smallest post-cyclic-loading settlement. For the reconsolidated volumetric strain of

1%, the excess pore water pressure ratio reached 85%, which was much greater than 67% for specimens conditioned at 1 °C, 5 °C, and 24 °C.

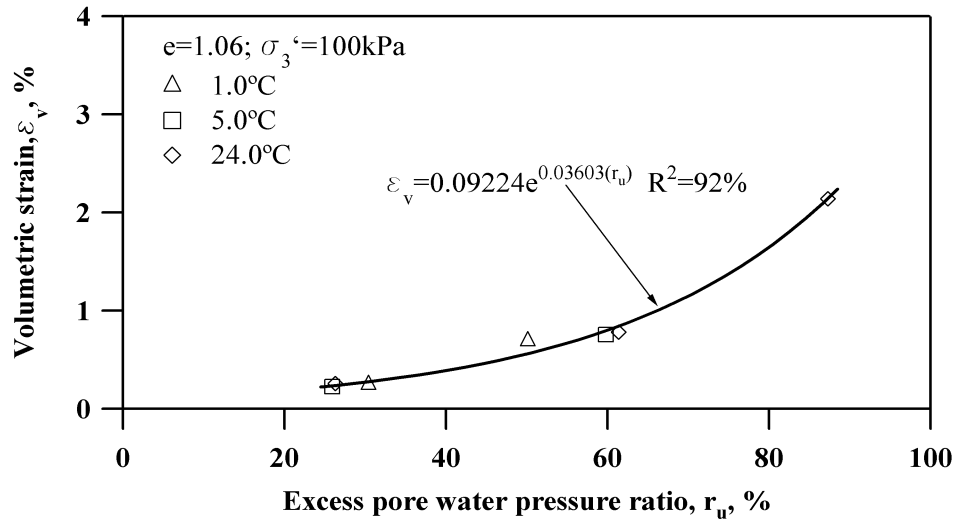


Figure 6.3 Reconsolidated volume strain versus excess pore water pressure ratio on Mabel Creek silt conditioned at 1 °C, 5 °C, and 24 °C

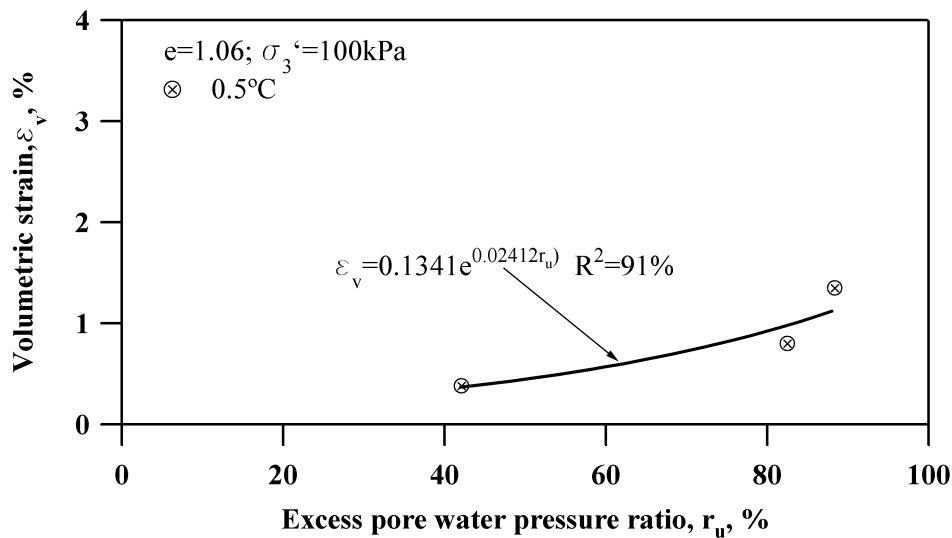
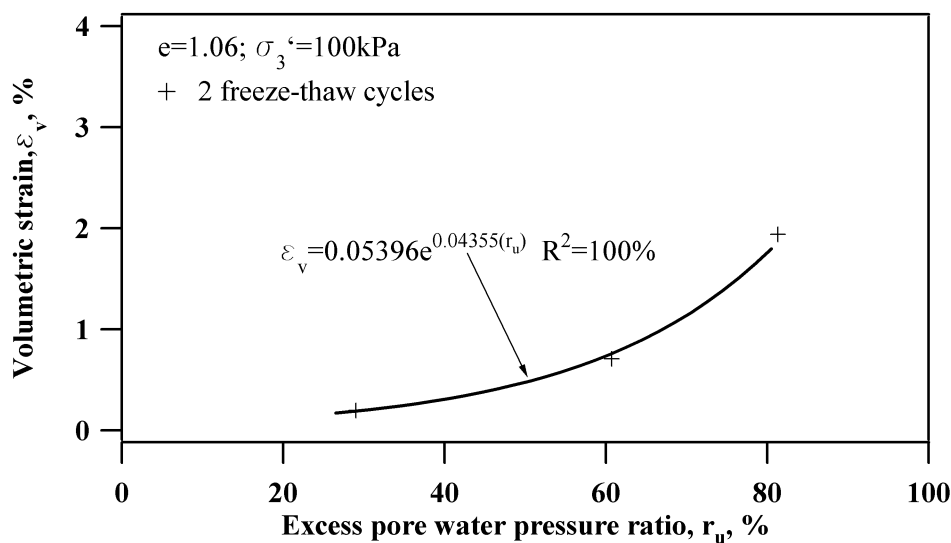


Figure 6.4 Reconsolidated volume strain versus excess pore water pressure ratio on Mabel Creek silt conditioned at 0.5 °C

### 6.3 Post-cyclic-loading settlement of Mabel Creek silt conditioned by the freeze-thaw cycles

The post-cyclic-loading settlement behavior for reconditioned specimens of Mabel Creek silt conditioned at 2 freeze-thaw cycles is shown in Figure 6.5. It is shown that for 2 freeze-thaw cycles, reconsolidated volumetric strain increased with an increase in the excess pore water pressure ratio. For volumetric strains ( $\epsilon_v$ ) less than 1%, the increasing trend of volumetric strain ( $\epsilon_v$ ) with the increasing  $r_u$  was slow. The volumetric strain ( $\epsilon_v$ ) at  $r_u = 29\%$  only reached 0.2%. Volumetric strain ( $\epsilon_v$ ) reached only 0.7% at  $r_u = 61\%$ . However, when the volumetric strain ( $\epsilon_v$ ) was greater than 1%, there was a trend for volumetric strain ( $\epsilon_v$ ) to increase quickly for an increase in  $r_u$ . For example, the volumetric strain ( $\epsilon_v$ ) at  $r_u = 81\%$  jumped to 2.0%.



**Figure 6.5** Reconsolidated volume strain versus excess pore water pressure ratio on Mabel Creek silt conditioned after 2 freeze-thaw cycles

For purposes of comparison, the post-cyclic-loading settlement behaviors of specimens of Mabel Creek silt were studied for 4 freeze-thaw cycles; see Figure 6.6. The results show that the reconsolidated volumetric strain increased with an increase in excess pore water pressure ratio. For example, the initial value of the volumetric

strain ( $\epsilon_v$ ) was 0.17% when  $r_u$  was equal to 27%. This slowly increased with the increasing  $r_u$  until the volumetric strain ( $\epsilon_v$ ) reached 1% at  $r_u = 67\%$ ; then the increase in volumetric strain was dramatic. For  $r_u=78\%$ , the volumetric strain ( $\epsilon_v$ ) jumped to 1.9%.

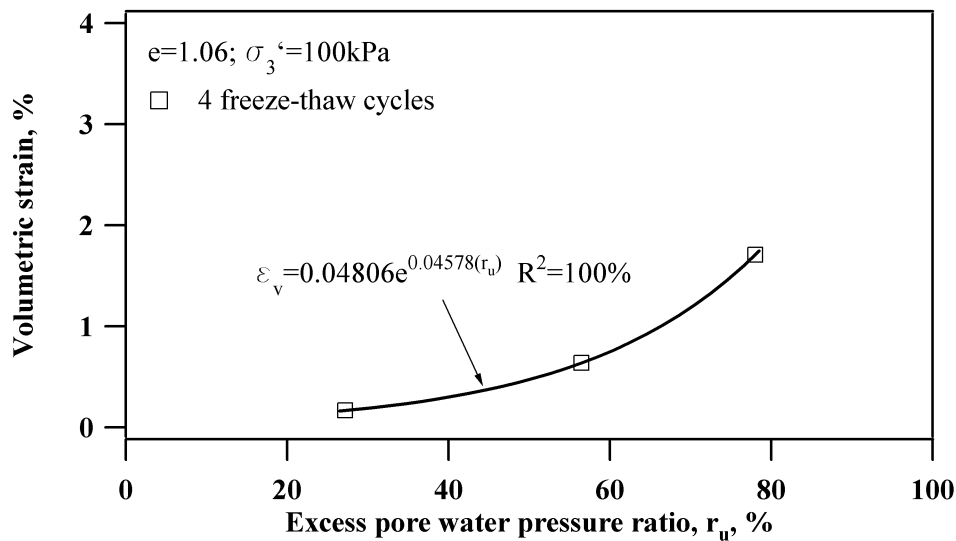


**Figure 6.6** Reconsolidated volume strain versus excess pore water pressure ratio on Mabel Creek silt conditioned after 4 freeze-thaw cycles

#### 6.4 Soil types effect on post-cyclic-loading settlement of unfrozen state

Excess pore water pressure is hypothesized to be the primary factor that influences post-cyclic-loading settlement in soils. Excess pore water pressure was extensively applied in this study to predict post-cyclic-loading settlement. Most of the previous researchers used excess peak pore water pressure in their study. In order to compare results of this study with previous studies, the excess pore water pressure was converted into excess peak pore water pressure. Post-cyclic-loading settlements for non-liquefied soil for three soil types (sand, silty sand, and unfrozen Mabel Creek silt) are compared and shown in Figure 6.7. Mabel Creek silt had the highest reconsolidated volumetric strain for any given excess peak pore water pressure. Monterey sand with loose density had approximate 1.0% reconsolidated volume strain

when  $r_u$  was close to 1.0. Silty sand with 10 to 20% fine content at the same  $r_u$  was found to cause a 2.5% reconsolidated volumetric strain. However, the resulting volumetric strain for specimens of Mabel Creek silt may be as much as 3.5% for a corresponding  $r_u$ . It may be estimated that dramatic settlement will be caused in the ground under cyclic loadings. Comparison of soil settlement caused by cyclic loadings in the liquefaction state also indicates that the silt has a higher susceptibility to post-liquefaction settlement than sand, as shown in Figure 6.8. This figure provides a comparison between Mabel Creek silt and Fuji sand for a post-liquefaction reconsolidated volumetric strain at maximum shear strain. For a given maximum shear strain of 4%, the corresponding reconsolidated volumetric strain for the loose Fuji river sand only reached about 1.4%. Reconsolidated volumetric strain in the Mabel Creek silt may reach 5.0%. Thus, silt has higher post-cyclic-loading settlement susceptibility than sand. This is the case regardless of the state of liquefaction or non-liquefaction.

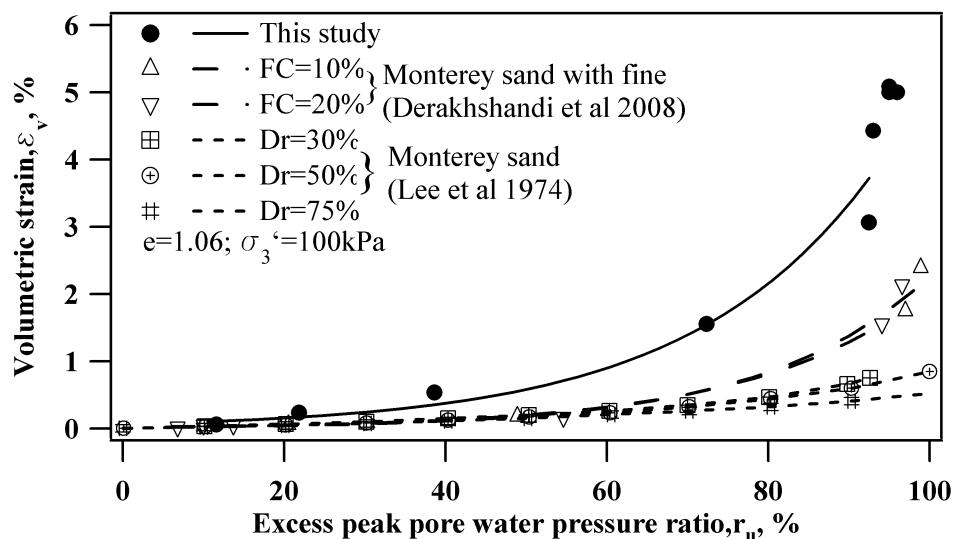
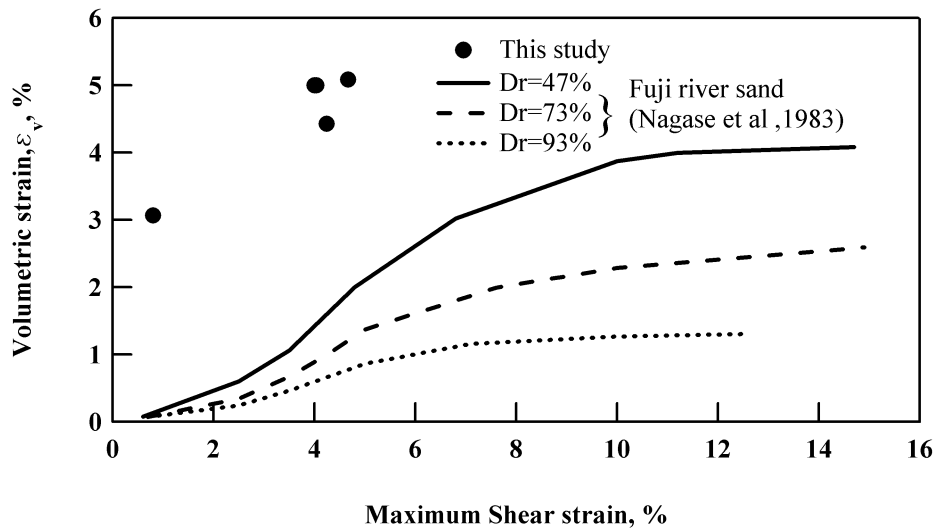


Figure 6.7 Comparison of reconsolidated volumetric strains between sand, silty sand, and Mabel Creek silt



**Figure 6.8 Comparison of the characteristics of post-liquefaction volumetric strains between sand and Mabel Creek silt**

### **6.5 Temperature rise effect on post-cyclic-loading settlement for frozen or partially frozen Mabel Creek silt**

The influence of raising the temperature of frozen or partially frozen specimens of the Mabel Creek silt was studied. The post-cyclic-loading settlements for these conditions were examined and are presented in Figure 6.9. This figure shows reconsolidated volumetric strain and excess pore water pressure ratio response for specimens conditioned at 0.5 °C, 1 °C, 5 °C, and 24 °C. Specimens conditioned at 1 °C, 5 °C, and 24 °C were found to have similar behavior (reconsolidated volumetric strain for any given water pressure). It also may be seen that for any given water pressure caused by cyclic loadings, unfrozen Mabel Creek silt had the highest reconsolidated volumetric strain; the specimen of Mabel Creek silt conditioned at 1 °C, 5 °C, and 24 °C had the second highest reconsolidated volumetric strain; and the specimen of Mabel Creek silt conditioned at 0.5 °C had the lowest reconsolidated volumetric strain. For example,  $r_u = 60\%$  for unfrozen specimens could reach a reconsolidated volumetric strain ( $\epsilon_v$ ) of 1%; and  $r_u = 67\%$  for specimens conditioned at 1 °C, 5 °C, and 24 °C was needed to reach reconsolidated volumetric strain ( $\epsilon_v$ ) of 1%. However, for specimens



conditioned at 0.5 °C, an  $r_u$  of 85% was needed to cause a volumetric strain of 1% during subsequent reconsolidation. Though post-cyclic-settlement specimen susceptibilities conditioned at different temperatures are diverse, similar reconsolidated volumetric strains for the specimens conditioned at all above-mentioned temperatures occurred for excess pore water pressure ratios less than about 40%; see Figure 6.9. With further increase of the excess pore water pressure ratio, the diversity of the post-cyclic-loading settlement susceptibility on Mabel Creek silt conditioned at different temperatures was manifested.

#### **6.6 Freeze-thaw-cycles effect on post-cyclic-loading settlement of frozen or partially frozen Mabel Creek silt**

The effect of freeze-thaw cycles on post-cyclic-loading settlement for specimens of Mabel Creek silt was studied by comparing relationships between reconsolidated volumetric strain and the excess pore water pressure ratio on specimens: (a) that were prepared for freeze-thaw conditions of 1, 2, and 4 freeze-thaw cycles and (b) that were unfrozen. A specimen conditioned at 24 °C actually experienced the process of 1 freeze-thaw cycle at the same time, thus this thermal condition at 24 °C is referred to as 1 freeze-thaw cycle in this section. All data are presented in Figure 6.10. The treatment of the freeze-thaw cycles obviously decreases the post-cyclic-loading settlement susceptibility. However, the reconsolidated volumetric strains for specimens conditioned at 1, 2 and 4 freeze-thaw cycles did not display any difference for any given excess pore water pressure. It may indicate that subsequent freeze-thaw cycles (more than 4) will not cause any change to the post-cyclic-loading settlement susceptibility of Mabel Creek silt. Thus, it is concluded that the first freeze-thaw cycle strongly decreases the post-cyclic-loading settlement susceptibility; however, further freeze-thaw cycles were found to have minimal influence on the variation of post-cyclic-loading settlement susceptibility of the Mabel Creek silt.

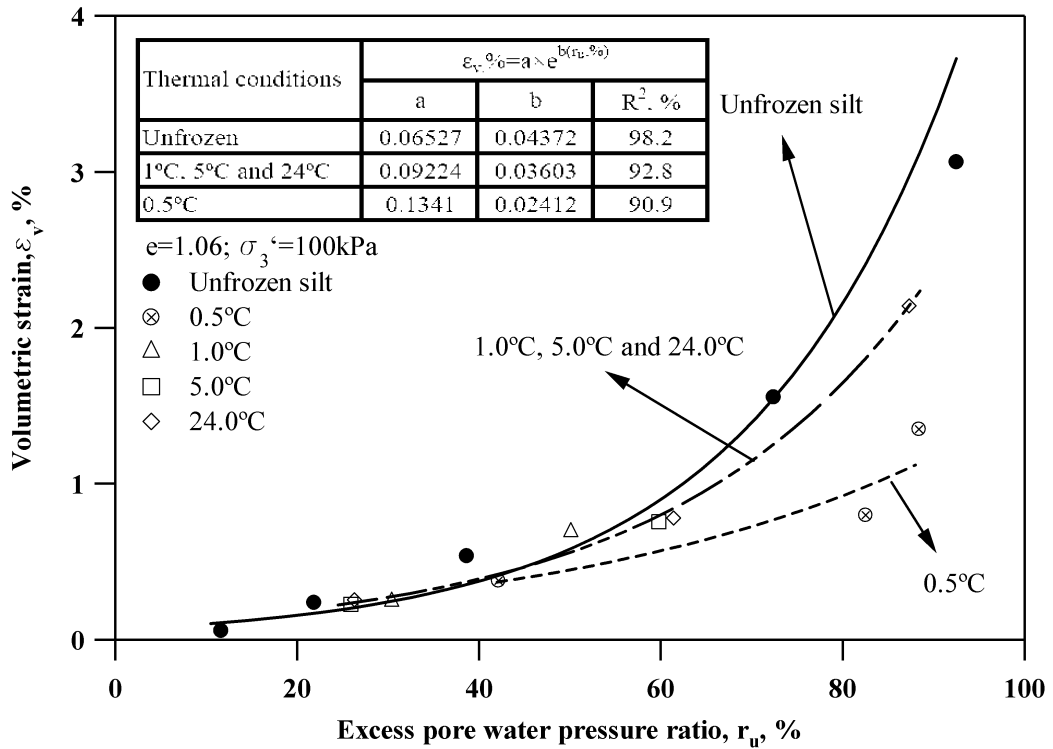


Figure 6.9 Temperature rise effect on reconsolidated volumetric strain of Mabel Creek silt due to dissipation of pore water pressure

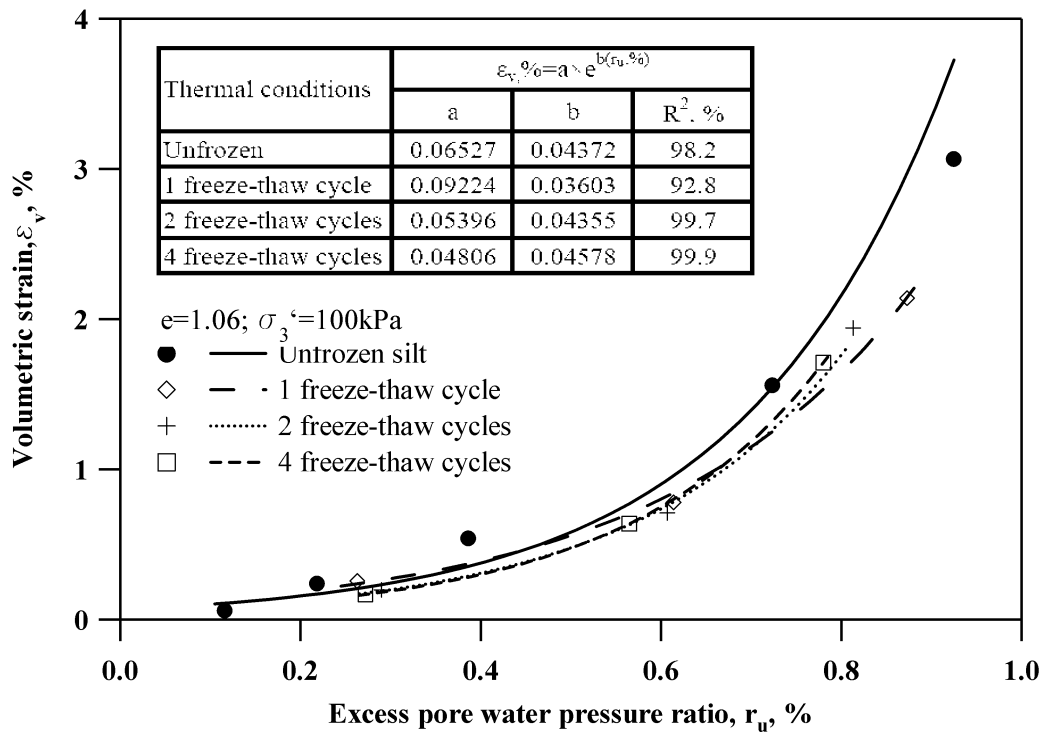


Figure 6.10 The freeze-thaw cycles effect on reconsolidated volumetric strain of Mabel Creek silt due to dissipation of pore water pressure

## **6.7 Determination of post-cyclic-loading volumetric strain as a function of cyclic shear strain on Mabel Creek silt**

The prediction of post-cyclic-loading soil settlement is dependent on equivalent cyclic shear strain, and the number of loading cycles. The number of load cycles is determined by examining earthquake characteristics or other appropriate cyclic loadings. The number of load cycles is needed in order to estimate the expected pore water pressure that will be caused by the estimated cyclic loading.

Then, the estimated pore water pressure is used to predict the expected settlement that is likely to be caused by the dissipation of the pore water pressure. It will be possible to avoid the determination of the excess pore water pressure and to directly estimate the amount of post-cyclic-loading volumetric strain. For this purpose, the cyclic shear strain,  $\gamma$ , and the volumetric strain,  $\epsilon_v$  are combined by giving the excess pore water pressure. Combinations of shear strain ( $\gamma$ ) and volumetric strain ( $\epsilon_v$ ) thus were developed and plotted to establish a family of curves for the Mabel Creek silt. These curves were developed to accommodate all thermal conditions (thawed, partially frozen, and frozen); see Figure 6.11 to Figure 6.17. The results of this study show that the post-cyclic-loading volumetric strain will always increase with an increase in cyclic shear strain for any given number of loading cycles. The post-cyclic-loading volumetric strain was also found to increase with the number of loading cycles for any given cyclic shear strain.

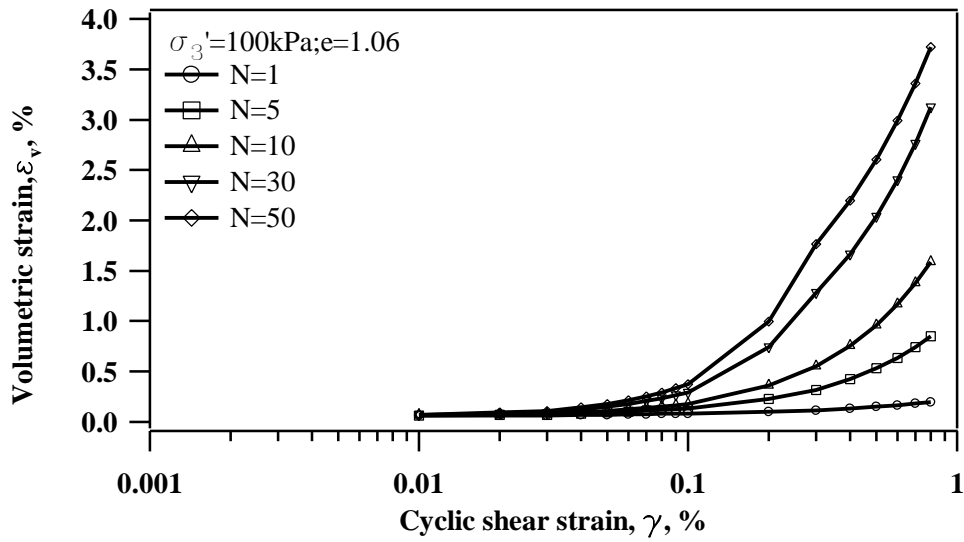


Figure 6.11 Chart for determination of the post-cyclic-loading volumetric strain as a function of cyclic shear strain on unfrozen Mabel Creek silt

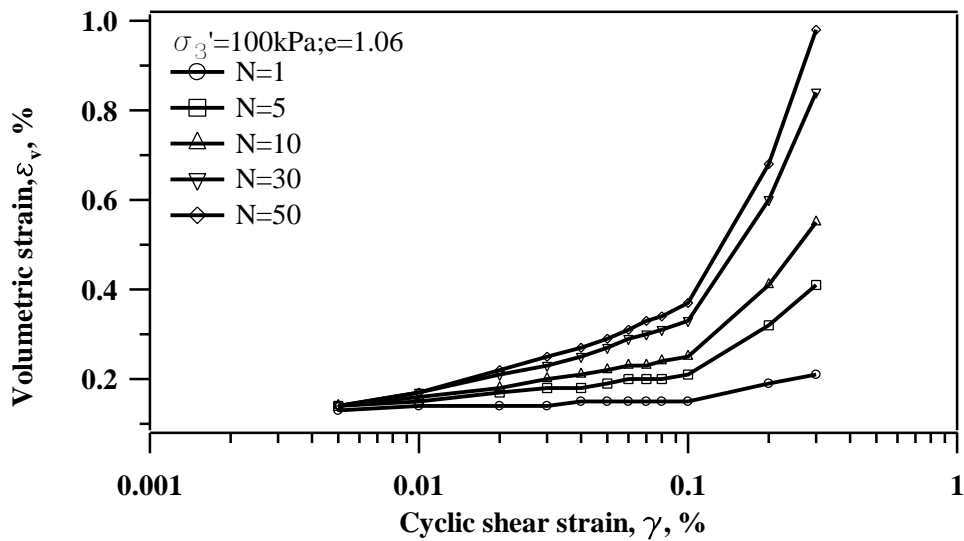


Figure 6.12 Chart for determination of the post-cyclic-loading volumetric strain as a function of cyclic shear strain on unfrozen Mabel Creek silt conditioned at 0.5 °C

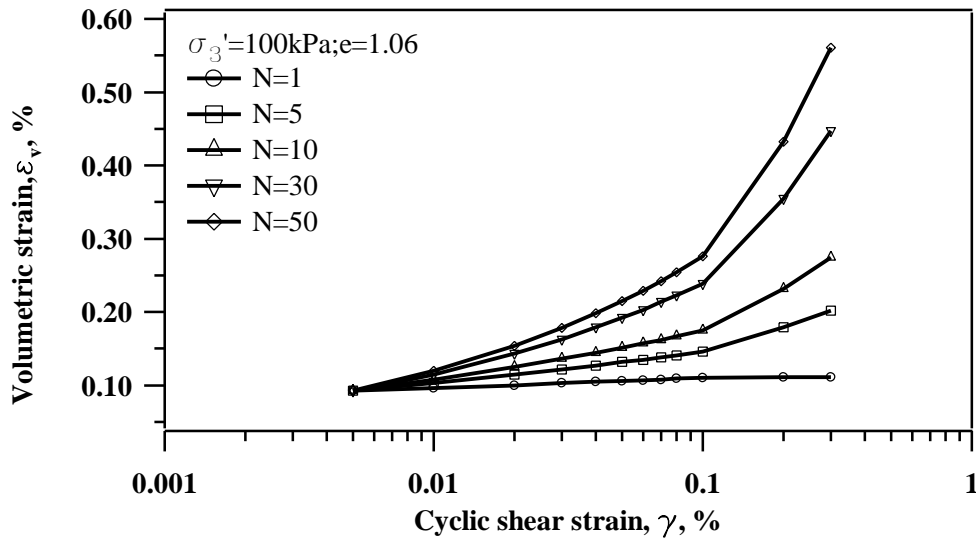


Figure 6.13 Chart for determination of the post-cyclic-loading volumetric strain as a function of cyclic shear strain on unfrozen Mabel Creek silt conditioned at 1 °C

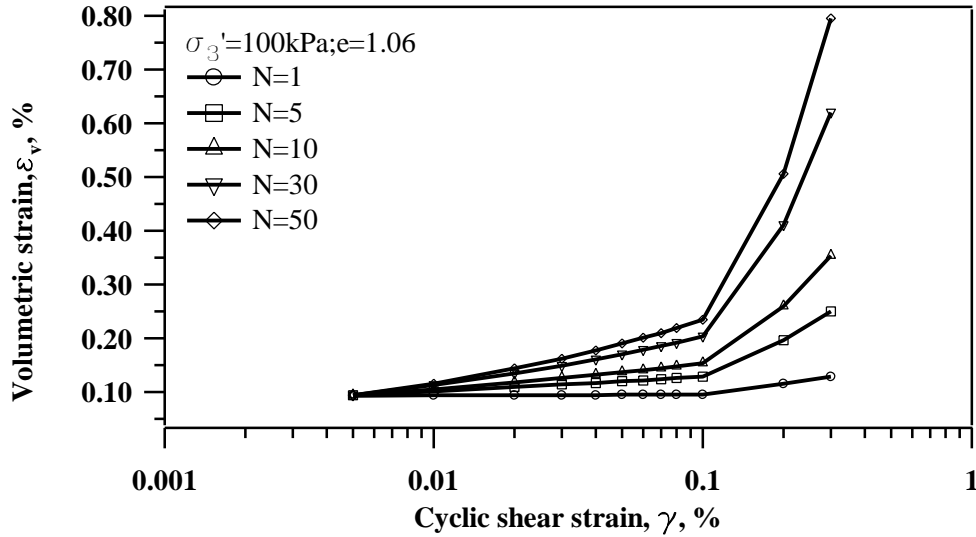


Figure 6.14 Chart for determination of the post-cyclic-loading volumetric strain as a function of cyclic shear strain on unfrozen Mabel Creek silt conditioned at 5 °C

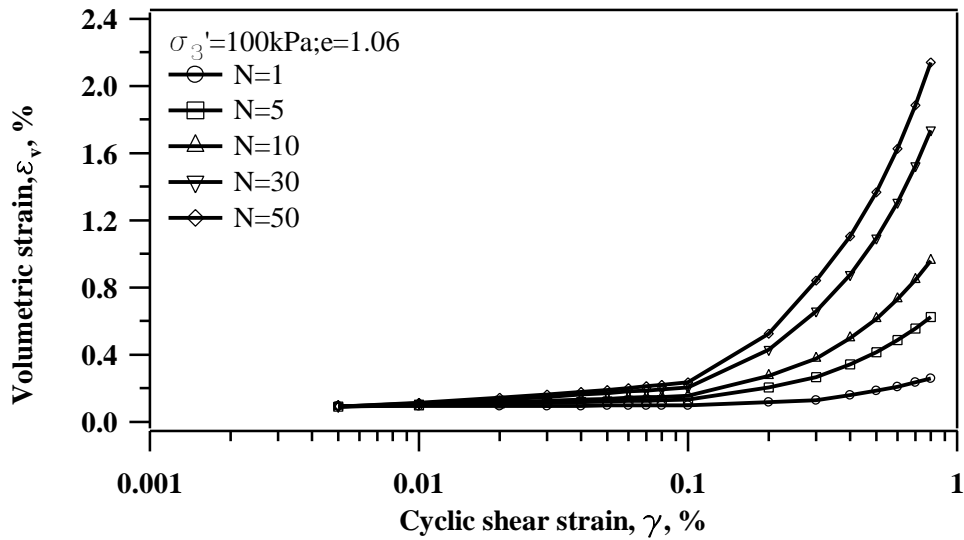


Figure 6.15 Chart for determination of the post-cyclic-loading volumetric strain as a function of cyclic shear strain on unfrozen Mabel Creek silt after 1 freeze-thaw cycle

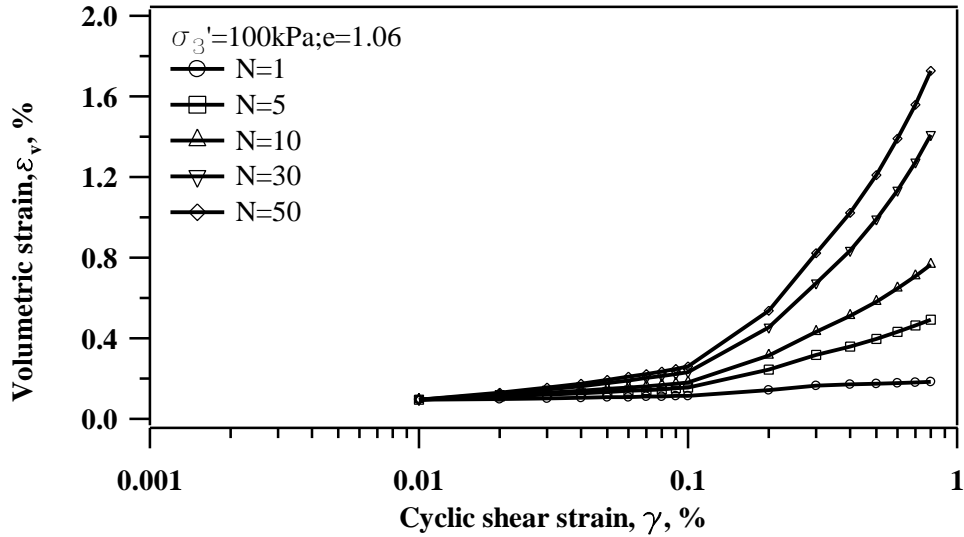
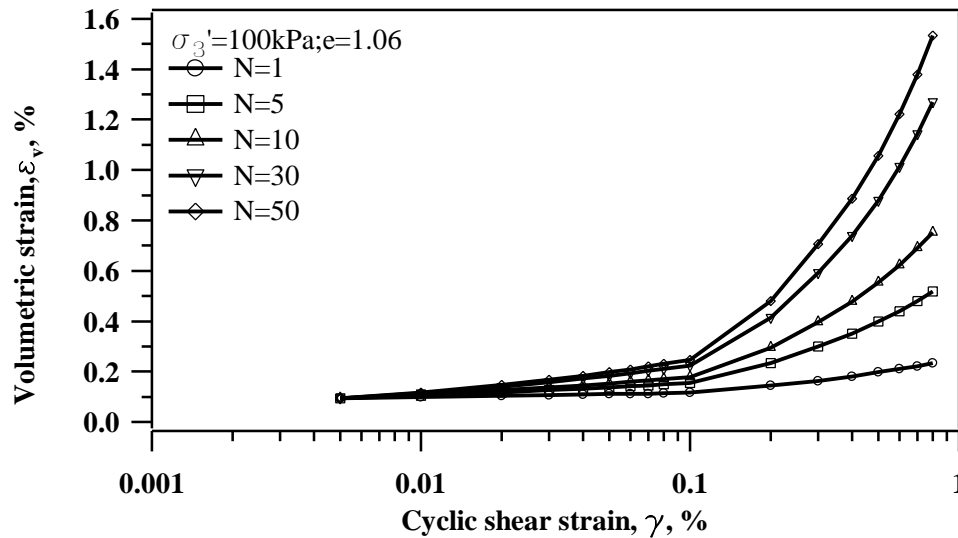


Figure 6.16 Chart for determination of the post-cyclic-loading volumetric strain as a function of cyclic shear strain on unfrozen Mabel Creek silt after 2 freeze-thaw cycles



**Figure 6.17** Chart for determination of the post-cyclic-loading volumetric strain as a function of cyclic shear strain on unfrozen Mabel Creek silt after 1 freeze-thaw cycles

## 6.8 Summary

In this chapter, cyclic-loading-induced settlement was examined for: (a) unfrozen Mabel Creek silt; (b) Mabel Creek silt conditioned at 0.5 °C, 1 °C, 5 °C, and 24 °C; and (c) Mabel Creek silt conditioned at 1, 2, and 4 freeze-thaw cycles. The influence of temperature and freeze-thaw cycles was evaluated on cyclic-loading-induced settlement. The cyclic-loading-induced settlement for the Mabel Creek silt was compared with the research results by others for sands and silty sand. Through this comparison, the soil type on cyclic-loading-induced settlement was evaluated. A series of simple charts was produced to predict cyclic-loading settlement for the Mabel Creek silt. These charts use cyclic shear strain and the number of loading cycles.

The influence of near freezing temperatures on cyclic-loading-induced settlement for the Mabel Creek silt was evaluated. Mabel Creek silt conditioned at 1 °C, 5 °C, and 24 °C had a similar response for reconsolidated volumetric strains, which was lower

than that of an unfrozen specimen. When  $r_u$  was smaller than 0.4, the reconsolidated volumetric strains for specimens conditioned at 1 °C, 5 °C, and 24 °C had a negligible response with an unfrozen specimen. When  $r_u$  was more than 0.4, the difference in volumetric strain between specimens conditioned at 1 °C, 5 °C, and 24 °C and unfrozen specimens became significant. However, the lowest volumetric strains occurred on specimens at a thawing temperature of 0.5 °C for dissipating any given pore water pressure.

Freeze-thaw cycles simulating seasonal climate change decrease the settlement susceptibility after undrained cyclic loading. One freeze-thaw cycle caused a decrease to cyclic-loading-induced volumetric strain, but the subsequent freeze-thaw cycles after 1 freeze-thaw cycle did not further decrease the effect on cyclic-loading-induced volumetric strain.

The influence of soil type on cyclic loading settlement was studied, and it may be concluded that silt has a much higher susceptibility to settlement after cyclic loading than sand or silty sand. A series of charts for cyclic reconsolidated volumetric strain versus cyclic shear strain and number of loading cycles provides the engineer with a practical means for predicting cyclic loading type settlements for the Mabel Creek silt.



## **7 Discussion**

### **7.1 Temperature effect on liquefaction potential, dynamic properties, and cyclic-loading-induced settlement**

The Mabel Creek silt conditioned at 0.5 °C had the largest pore water pressure generation in comparison with the unfrozen Mabel Creek silt and the Mabel Creek silt thawed at 1 °C, 5 °C, and 24 °C. It has been found for soil undergoing cyclic loading that a decrease in the soil's relative density will decrease liquefaction resistance and increase pore water pressure generation of soil (Peacock and Seed 1968; DeAlba et al. 1976; Dobry et al. 1982). In this study, thawing at 0.5 °C was found not to change the soil particle distribution and the effective confining pressure; however, it did increase the pore water pressure. Liquefaction potential for the silt specimen at 0.5 °C was influenced by soil density and soil fabric. It was found that as relative density decreased, the shear modulus also decreased. This is inconsistent with results from test specimens at other temperature conditions in this study. Thus the only explanation for an increase of both pore water pressure generation and shear modulus when the specimen was thawed at 0.5 °C is a change of soil density. The ice in Mabel Creek silt still was likely not completely melted at 0.5 °C; however, with enough unfrozen water induced, a partially frozen structure eventually developed. Soil particles in this structure were easily redistributed by the cyclic loading, thus rapid pore water pressure generation was observed for the soil specimen conditioned at 0.5 °C under cyclic loading. Incompletely melted ice caused high shear modulus, large damping ratio, and low post-cyclic-loading settlement. Measurement of the variation of unfrozen water content along with the temperature change in partially frozen specimens with  $e=1.06$  was conducted to prove that enough unfrozen water was thawed at 0.5 °C. A Vitel Hydra Probe was used to measure unfrozen water content. This was done by measuring the dielectric constant, which is most indicative of water

content. Figure 7.1 shows the relationship between unfrozen water content and temperature on partially frozen and frozen Mabel Creek silt. The largest variation in unfrozen water content occurred between  $-1\text{ }^{\circ}\text{C}$  and  $1\text{ }^{\circ}\text{C}$ ; 30% of the unfrozen water content melted in this temperature band. Test results show that there is dramatic variation in unfrozen water content when the temperature is increased to  $0\text{ }^{\circ}\text{C}$ . Hence the variation in unfrozen water content is very sensitive to variation in temperature when the temperature is near  $0\text{ }^{\circ}\text{C}$ . Figure 7.1 proved that enough unfrozen water was thawed at  $0.5\text{ }^{\circ}\text{C}$ . Beside, this figure showed only 4% of the unfrozen water content was produced when temperatures were between  $-10\text{ }^{\circ}\text{C}$  and  $-1\text{ }^{\circ}\text{C}$ . When temperature increased to above  $1\text{ }^{\circ}\text{C}$ , the amount of unfrozen water content stayed stable.

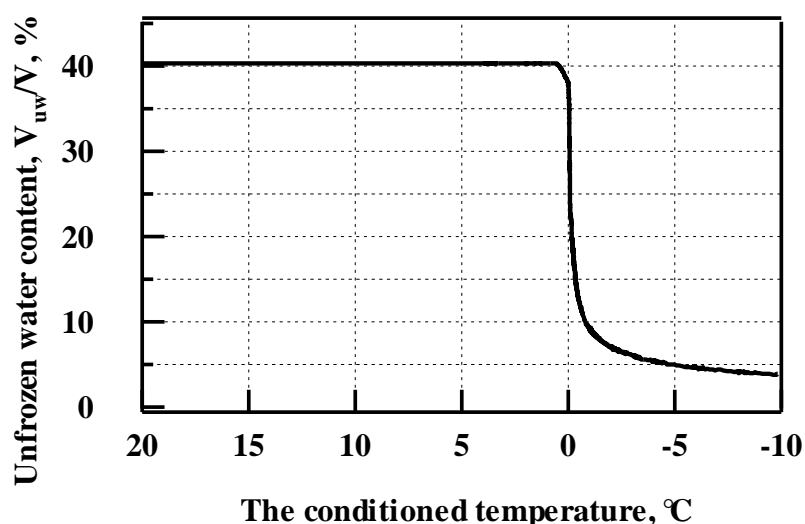


**Figure 7.1** Unfrozen water content versus conditioned temperature in Mabel Creek silt

Similar pore water pressure generation between specimens conditioned at  $5\text{ }^{\circ}\text{C}$  and  $24\text{ }^{\circ}\text{C}$  was observed, but less than that for the unfrozen Mabel Creek silt. The similarity indicated that the frozen Mabel Creek silt was completely thawed at  $5\text{ }^{\circ}\text{C}$ , thus the same soil fabric for the specimens conditioned at  $5\text{ }^{\circ}\text{C}$  and  $24\text{ }^{\circ}\text{C}$  caused the same pore water pressure generation. Figure 7.2 shows a decrease of void ratio during the freezing and thawing process with the thawing temperatures of  $5\text{ }^{\circ}\text{C}$  and  $24\text{ }^{\circ}\text{C}$ ,

which indicates that the soil was densified by the freezing and thawing process. It was proven that the specimen conditioned at 5 °C or 24 °C has smaller pore water pressure generation, larger damping ratio and larger shear modulus than the unfrozen specimen. In Figure 7.2, the positive value indicates the soil density increased and the negative value means the decrease of soil density. Thus, the post-cyclic-loading settlement on Mabel Creek silt conditioned at 5 °C or 24 °C still was smaller than that of Mabel Creek silt, though, still larger than that of Mabel Creek silt conditioned at 0.5 °C.

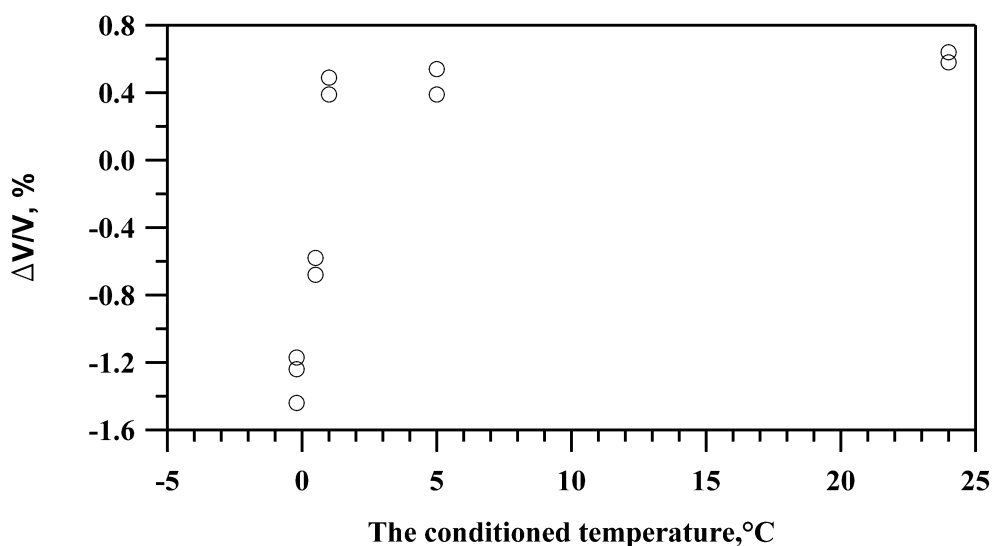


**Figure 7.2** Volumetric strain change during freezing and thawing process versus temperature

## **7.2 Effect of freeze-thaw cycles on liquefaction potential, dynamic properties, and cyclic-loading-induced settlement**

The obvious densification of freeze-thaw cycles is shown in Figure 7.3. The largest densification occurred at 1 freeze-thaw cycle. With increasing freeze-thaw cycles, the densification effect became weaker and weaker. The treatment of freeze-thaw cycles on Mabel Creek silt decreased pore water pressure generation, increased damping ratio, increased shear modulus and decreased post-cyclic-loading settlement; however, the variation of these properties became progressively smaller with increasing

freeze-thaw cycles. For treatment of freeze-thaw cycles from 2 to 4, little change in pore water pressure generation, damping ratio, shear modulus, and post-cyclic-loading settlement was observed.

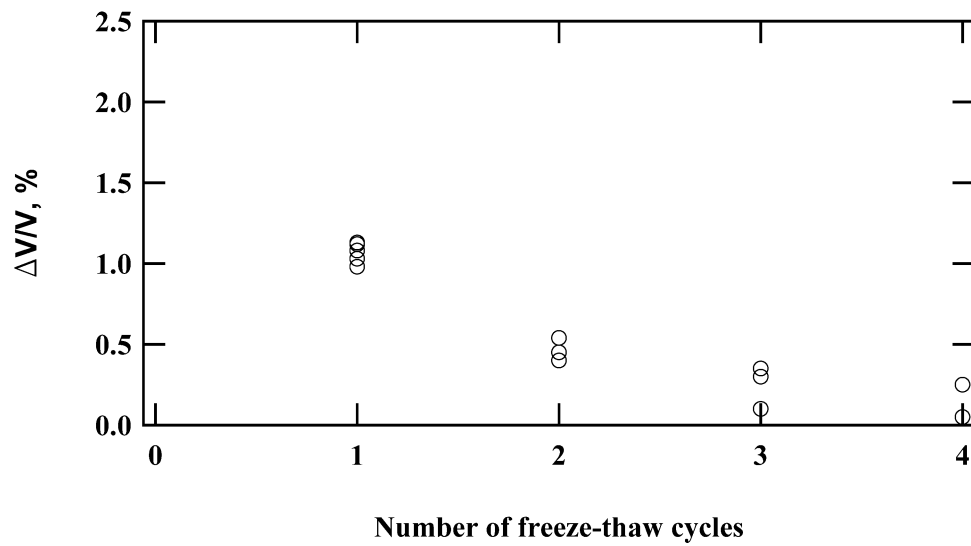


**Figure 7.3** Volumetric strain change versus the number of freeze-thaw cycles on Mabel Creek silt

## 8 Conclusion

The observations and conclusions gained from this study are:

- The UAF modified cyclic triaxial cell is applicable to the cyclic loading tests on partially frozen or thawed soil.
- Pore water pressure generation increased with increasing loading cycles and increasing cyclic shear strain regardless of the thawing temperature or the number of freeze-thaw cycles. Shear modulus ( $G$ ) of fine-grained soil decreases, and damping ratio ( $D$ ) increases with increasing cyclic shear strain.
- Frozen Mabel Creek silt thawed at near freezing temperature ( $0.5\text{ }^{\circ}\text{C}$ ) had a partially frozen structure, which caused higher pore water pressure generation, smaller damping ratio, and higher dynamic shear modulus compared with the unfrozen Mabel Creek silt or Mabel Creek silt thawed at  $1\text{ }^{\circ}\text{C}$ ,  $5\text{ }^{\circ}\text{C}$ , and  $24\text{ }^{\circ}\text{C}$ . Pore water pressure generation and damping ratio were smaller and dynamic shear modulus was larger for specimens completely thawed at  $5\text{ }^{\circ}\text{C}$  and  $24\text{ }^{\circ}\text{C}$  as compared to the unfrozen Mabel Creek silt.
- The drained freezing and thawing process under multi-axial direction densified the soil specimen. It increased the dynamic shear modulus, and decreased the damping ratio and liquefaction potential. Change of liquefaction potential and dynamic properties for Mabel Creek silt caused by freeze-thaw cycles became smaller with additional freeze-thaw cycles. Liquefaction potential and dynamic properties for the laboratory specimens of Mabel Creek silt that were subjected to 2 to 4 freeze-thaw cycles remained nearly the same.
- Pore pressure generation of Mabel Creek silt conditioned at different temperatures or number of freeze-thaw cycles can be predicted by the GMP model. As the most important parameter in the GMP model, “Pseudoenergy Capacity” (PEC), reflects an increasing trend with increased number of

freeze-thaw cycles. The effect of near freezing temperature on the PEC of partially frozen or thawed Mabel Creek silt is unclear.

- Under undrained strain-controlled cyclic loading, the trend of  $G$  for fine-grained soil with increasing loading cycles may be divided into two categories: (1)  $G$  does not change with variation of loading cycles when  $\gamma$  is less than or near to  $\gamma_t$ ; and (2)  $G$  will degrade with increasing loading cycles for large  $\gamma$ . The degradation of  $G$  is attributed to increasing pore pressure generation caused by cyclic loading. This degradation of  $G$  may be predicted by Idriss et al. (1978) model. The degradation parameter ( $t$ ) reflects the degradation degree of  $G$ . Unfrozen soil and the specimens conditioned at 0.5 °C have a similar  $t$  while the specimens conditioned at 24 °C, 5 °C, and 1 °C has a similar  $t$ . Also,  $t$  decreases with increasing freeze-thaw cycles.
- Under undrained strain-controlled cyclic loading, the trend of  $D$  for fine-grained soil with increasing loading cycles can be divided into three categories: (1)  $D$  stays constant with increasing loading cycles for a small  $\gamma$ ; (2)  $D$  decreases with increasing loading cycles for a medium  $\gamma$  (0.1%); and (3)  $D$  decreases first and then increases with increased loading cycles for a large  $\gamma$ . Variation of  $D$  with increasing loading cycles may be attributed to the generation of pore pressure. An increase of pore pressure will cause decrease of  $D$  when  $r_u$  is less than 40%; and an  $r_u$  increase to 1 will cause increase of  $D$ .
- Increase of temperature from the near-freezing state to the above-freezing state will cause a decrease in shear modulus ( $G$ ). This variation in  $G$  as it relates to temperature is more sensitive when the temperature is near zero. Damping ratio ( $D$ ) increased with increasing temperature when temperature is under the freezing point; however,  $D$  will become maximum when the specimen temperature is near the freezing point. Increase of temperature above the freezing point will decrease  $D$ .
- Reconsolidated volumetric strains for the Mabel Creek silt conditioned at thawing

temperatures of 1 °C, 5 °C, and 24 °C had similar responses for a given excess pore water pressure ratio, and all of them had lower reconsolidated volumetric strain response than that of the unfrozen specimen. In particular, when  $r_u$  was smaller than 0.4, the reconsolidated volumetric strain response was similar between conditioned specimens and the unfrozen specimen. This is due to dissipation of the pore water pressure. However, when  $r_u$  is more than 0.4, the difference becomes significant.

- Volumetric strains of specimens conditioned at a 0.5 °C thawing temperature had a lower value than specimens conditioned at all other temperatures. The first freeze-thaw cycle strongly decreased the post-cyclic-settlement; however, subsequent freeze-thaw cycles showed no further decrease in cyclic-loading-induced settlement.
- The Mabel Creek silt had a much higher post-cyclic-settlement than the sand or the silty sand.

## References

- Alkire, B. D. (1981). "Effect of variable-drainage freeze-thaw tests on post-thaw shear strength." *Transportation Research Record*,(809), 13-18.
- Alkire, B. D., and Morrison, J. A. (1983). "Comparative response of soils to freeze-thaw and repeated loading." *Special Report - United States Army, Cold Regions Research and Engineering Laboratory (Hanover, New Hampshire)*, US Army Cold Regions Research & Engineering Lab, Hanover, NH, USA, Hanover, NH, USA, 89-95.
- Anandarajah, A. (1994). "Procedures for elastoplastic liquefaction modeling of sands." *Journal of Engineering Mechanics*, 120(7), 1563-1587.
- Andersland, O., and Anderson, D. (1978). "Geotechnical engineering for cold regions." McGraw-Hill Companies, Incorporated.
- ASTM D854 (2000). "Standard test methods for specific gravity of soil solids by water pycnometer."
- ASTM D4254 (2000). "Standard test methods for minimum index density and unit weight of and calculation of relative density."
- ASTM D422 (2002). "Standard test method for particle-size analysis of soils."
- ASTM D1557 (2002). "Standard test methods for laboratory compaction characteristics of soil using modified effort (56,000 ft-lbf/ft<sup>3</sup> (2,700 kn-m/m<sup>3</sup>))."
- ASTM D4253 (2006). "Standard test methods for maximum index density and unit weight of soils using a vibratory table."
- ASTM D5311 (2004). "Standard test method for load controlled cyclic triaxial strength of soil."



- Benson, C. H., Abichou, T. H., Olson, M. A., and Bosscher, P. J. (1995). "Winter effects on hydraulic conductivity of compacted clay." *Journal of Geotechnical Engineering*, 121(1), 69-79.
- Boulanger, R. W., and Idriss, I. M. (2006). "Liquefaction susceptibility criteria for silts and clays." *Journal of Geotechnical and Geoenvironmental Engineering*, 132(11), 1413-1426.
- Bray, J. D., and Sancio, R. B. (2006). "Assessment of the liquefaction susceptibility of fine-grained soils." *Journal of Geotechnical and Geoenvironmental Engineering*, 132(9), 1165-1177.
- Castro, G. (1975). "Liquefaction and cyclic mobility of saturated sands." *American Society of Civil Engineers, Journal of the Geotechnical Engineering Division*, 101(6), 551-569.
- Chamberlain, E. J., and Gow, A. J. (1978). "Effect of freezing and thawing on the permeability and structure of soils." *Engineering Geology*, 13(1-4), 73-92.
- Chien, L. K., Oh, Y. N., and Chang, C. H. (2002). "Effects of fines content on liquefaction strength and dynamic settlement of reclaimed soil." *Canadian Geotechnical Journal*, 39(1), 254-265.
- Czajkowski, R. L., and Vinson, T. S. (1980). "Dynamic properties of frozen silt under cyclic loading." *American Society of Civil Engineers, Journal of the Geotechnical Engineering Division*, 106(9), 963-980.
- Dafalias, Y. F., and Manzari, M. T. (2004). "Simple plasticity sand model accounting for fabric change effects." *Journal of Engineering Mechanics*, 130(6), 622-634.
- DeAlba, P., Seed, H. B., and Chan, C. K. (1976). "Sand liquefaction in large-scale simple shear tests." *American Society of Civil Engineers, Journal of the Geotechnical Engineering Division*, 102(9), 909-927.

- Derakhshandi, M., Rathje, E. M., Hazirbaba, K., and Mirhosseini, S. M. (2008). "The effect of plastic fines on the pore pressure generation characteristics of saturated sands." *Soil Dynamics and Earthquake Engineering*, 28(5), 376-386.
- Desai, C. S. (2000). "Evaluation of liquefaction using disturbed state and energy approaches." *Journal of Geotechnical and Geoenvironmental Engineering*, 126(7), 618-631.
- Dobry, R. (1985). "Liquefaction of soils during earthquakes." *Rep. No. Report No. CET5-EE-001*, National Research Council (NRC), Committee on Earthquake Engineering, Washington DC.
- Dobry, R., Ladd, R. S., Yokel, F. Y., Chung, R. M., and Powell, D. (1982). "Prediction of pore water pressure buildup and liquefaction of sands during earthquakes by the cyclic strain method." *National Bureau of Standards, Building Science Series*, 168.
- Dobry, R., and Vucetic, M. (1987). "Dynamic properties and seismic response of soft clay deposits." Mexico City, 51-87.
- Eigenbrod, K. D., Knutsson, S., and Sheng, D. (1996). "Pore-water pressures in freezing and thawing fine-grained soils." *Journal of Cold Regions Engineering*, 10(2), 77-92.
- Finn, W. D. L., Pickering, D. J., and Bransby, P. L. (1971). "Sand liquefaction in triaxial and simple shear tests." *Journal of the Soil Mechanics and Foundations Division*, 97(SM4), 639-659.
- Finn, W. D. L., and Yong, R. N. (1978). "Seismic response of frozen ground." *Journal of the Geotechnical Engineering Division*, 104(10), 1225-1241.
- Finn, W. D. L., Yong, R. N., and Lee, K. W. (1978). "Liquefaction of thawed layers in frozen soil." *Journal of the Geotechnical Engineering Division*, 104(10), 1243-1255.

- Fukuda, M., and Huang, S. L. (1991). "Effects of total water content on dynamic properties of frozen soils." Publ by Soc of Petroleum Engineers of AIME, Richardson, TX, USA, Anchorage, AK, USA, 621-629.
- Goto, S. (1993). "Influence of a freeze and thaw cycle on liquefaction resistance of sandy soils." *Soils and Foundations*, 33(4), 148-158.
- Green, R. A., Mitchell, J. K., and Polito, C. P. (2000). "An energy-based pore pressure generation model for cohesionless soils." *Proc., John Booker Memorial Symp.—Developments in Theoretical Geomechanics*, D. W. Smith and J. P. Carter, eds., Balkema, Rotterdam, The Netherlands, 383–390.
- Hardin, B. O., and Drnevich, V. P. (1972). "Shear modulus and damping in soils: measurement and parameter effects." *American Society of Civil Engineers, Journal of the Soil Mechanics and Foundations Division*, 98(SM6), 603-624.
- Hazirbaba, K. (2005). "Pore pressure generation characteristics of sands and silty sands: A strain approach." Ph.D., Department of Civil Engineering. The University of Texas at Austin.
- Hsu, C. C., and Vucetic, M. (2006). "Threshold shear strain for cyclic pore-water pressure in cohesive soils." *Journal of Geotechnical and Geoenvironmental Engineering*, 132(10), 1325-1335.
- Idriss, I. M., Dobry, R., and Singh, R. D. (1978). "Nonlinear behavior of soft clays during cyclic loading." 104(12), 1427-1447.
- Ishihara, K. (1996). "Soil behaviour in earthquake geotechnics." Clarendon Press, Oxford.
- Ishihara, K., Troncoso, J., Kawase, Y., and Takahashi, Y. (2009). "Cyclic strength characteristics of tailings materials." *Soils and Foundations*, 20(4), 127-142.
- Kokusho, T., Yoshida, Y., and Esashi, Y. (1982). "Dynamic properties of soft clay for wide strain range." *Soils and Foundations*, 22(4), 1-18.

- Konrad, J. M. (1989). "Effect of freeze-thaw cycles on the freezing characteristics of a clayey silt at various overconsolidation ratios." *Canadian Geotechnical Journal*, 26(2), 217-226.
- Ladd, R. S. (1978). "Preparing test specimens using undercompaction." *ASTM Geotechnical Testing Journal*, 1(1), 16-23.
- Lambe, T. W., and Whitman, R. V. (1969). "Soil mechanics." Wiley, New York, NY.
- Lee, K. L., and Seed, H. B. (1967). "Cyclic stress conditions causing liquefaction of sand." *Journal of the Soil Mechanics and Foundations Division*, 93(SM1), 47-70.
- Lee, K. L., and Albaisa, A. (1974). "Earthquake induced settlements in saturated sands." *American Society of Civil Engineers, Journal of the Geotechnical Engineering Division*, 100(GT4), 387-406.
- Liyanathirana, D. S., and Poulos, H. G. (2002). "Numerical simulation of soil liquefaction due to earthquake loading." *Soil Dynamics and Earthquake Engineering*, 22(7), 511-523.
- MACTEC Engineering and Consulting (2004). "Tok Cutoff Earthquake Repairs Project No. ACIM-007(7)/62306, Mabel Creek Bridge No. 656." *Rep. No. Structural Foundation Engineering Report*.
- Matasovic, N., and Vucetic, M. (1995). "Generalized cyclic-degradation-pore-pressure generation model for clays." *Journal of Geotechnical Engineering*, 121(1), 33-42.
- Nagase, H., and Ishihara, K. (1988). "Liquefaction-induced compaction and settlement of sand during earthquakes." *Soils and Foundations*, 28(1), 65-76.
- Neresova, Z. A., and Tsytovich, V. A. (1963). "Unfrozen water in frozen soils." *NAS-NRC Publ.*, 230-234.
- Ohara, S., and Matsuda, H. (1988). "Study on the settlement of saturated clay layer induced by cyclic shear." *Soils and Foundations*, 28(3), 103-113.

- Othman, M. A., and Benson, C. H. (1993). "Effect of freeze-thaw on the hydraulic conductivity and morphology of compacted clay." *Canadian Geotechnical Journal*, 30(2), 236-246.
- Peacock, W. H., and Seed, H. B. (1968). "Sand liquefaction under cyclic loading simple shear conditions." *J. Soil Mech. Found. Engng Div.*, 94(No. 3), 689-708.
- Qi, J., Ma, W., and Song, C. (2008). "Influence of freeze-thaw on engineering properties of a silty soil." *Cold Regions Science and Technology*, 53(3), 397-404.
- Seed, H. B. (1968). "Landslides during earthquakes due to liquefaction." *Journal of the Soil Mechanics and Foundations Division*, 94(SM5), 1053-1122.
- Seed, H. B., and Idriss, I. M. (1971). "Simplified procedure for evaluating soil liquefaction potential." *Journal of the Soil Mechanics and Foundations Division*, 97(SM9), 1249-1273.
- Seed, H. B., Martin, P. P., and Lysmer, J. (1976). "Pore-water pressure changes during soil liquefaction." *American Society of Civil Engineers, Journal of the Geotechnical Engineering Division*, 102(4), 323-346.
- Stevens, H. W. (1975). "The response of frozen soils to vibratory loads." Cold Regions Research and Engineering Laboratory.
- Talaganov, K. V. (1996). "Stress-strain transformations and liquefaction of sands." *Soil Dynamics and Earthquake Engineering*, 15(7), 411-418.
- Tokimatsu, K., and Seed, B. H. (1987). "Evaluation of settlement in sands due to earthquake shaking." *Journal of Geotechnical Engineering*, 113(8), 861-878.
- Tsukamoto, Y., Ishihara, K., and Sawada, S. (2004). "Settlement of silty sand deposits following liquefaction during earthquakes." *Soils and Foundations*, 44(5), 135-148.

- Viklander, P. (1998). "Permeability and volume changes in till due to cyclic freeze/thaw." *Canadian Geotechnical Journal*, 35(3), 471-477.
- Vinson, T. S. (1978). "Parameter effects on dynamic properties of frozen soils." *Journal Geotechnical Engineering Division*, 104(10), 1289-1306.
- Vinson, T. S., Wilson, C. R., and Bolander, P. (1983). "Dynamic properties of naturally frozen silt." Natl Acad Press, Washington, DC, USA, Fairbanks, AK, USA, 1315-1320.
- Vucetic, M., and Dobry, R. (1991). "Effect of soil plasticity on cyclic response." *Journal of Geotechnical Engineering*, 117(1), 89-107.
- Yashinsky, M., and Eiding, J. (2003). "Performance of lifelines during the November 3, 2002 Denali, Alaska Earthquake." *Rep. No. Reconnaissance Survey Report of Technical Council on Earthquake Engineering*, American Society of Civil Engineers.
- Yoshimi, Y., Tokimatsu, K., and Ohara, J. (1994). "In situ liquefaction resistance of clean sands over a wide density range." *Geotechnique*, 44(3), 479-494.
- Yoshimi, Y., and Goto, S. (1996). "Liquefaction resistance of silty sand based on in situ frozen samples." *Geotechnique*, 46(1), 153-156.
- Youd, T. L., and Idriss, I. M. (2001). "Liquefaction resistance of soils: Summary report from the 1996 NCEER and 1998 NCEER/NSF workshops on evaluation of liquefaction resistance of soils." *Journal of Geotechnical and Geoenvironmental Engineering*, 127(4), 297-313.
- Zimmie, T. F., and La Plante, C. (1990). "Effect of freeze/thaw cycles on the permeability of a fine-grained soil." *Hazardous and Industrial Wastes - Proceedings of the Mid-Atlantic Industrial Waste Conference*, Publ by Technomic Publ Co Inc, Lancaster, PA, USA, Philadelphia, PA, USA, 580-593.

## **Appendix A. Determination of Void Ratio in Saturated Soil**

The saturated soil's void ratio may be calculated by water content and specific gravity using the following equation:

$$e = G_s (WC)$$

Where  $e$  = void ratio;

$G_s$  = Specific gravity;

WC = Water content, %.

For WC=38.3% and  $G_s=2.78$  for saturated Mabel Creek silt sampled in a site near Mabel Creek Bridge,

$$e = 2.78 \times 38.3\% = 1.06$$

## Appendix B. Case Analysis

The following example shows how to predict liquefaction potential and corresponding cyclic-loading-induced settlement. Because of limited laboratory results, the amount of settlement that can occur after liquefaction is not part of this study. This study does, however, provide a guide and methodology for determining the amount of post-cyclic-loading settlement under non-liquefaction conditions. An earthquake with a Magnitude of 7.5 is applied in this case to address cyclic-loading-induced settlement under non-liquefaction conditions.

Consider a site near Mabel Creek Bridge at Mile 76.2 on the Tok Cutoff. The highway is subjected to an earthquake that produces a peak ground acceleration of 0.20g at Magnitude 7.5. The results from a field exploration are shown in Figure B.1. Let's estimate the possible pore water pressure and the post-earthquake settlement for a Mabel Creek silt layer on a day such as November 3, which is the same day that the Denali Earthquake (2002) occurred.

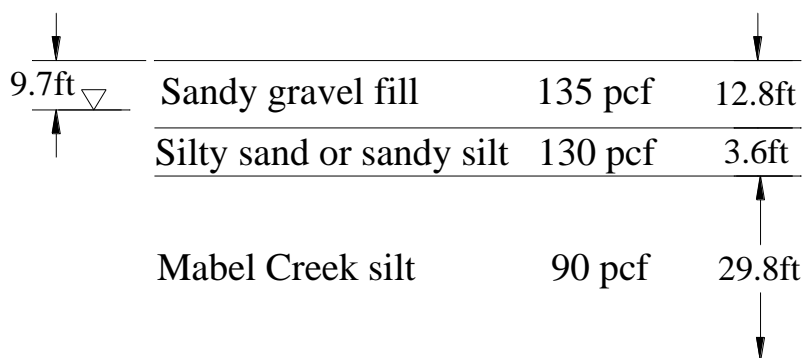


**Figure B.1** Soil profile



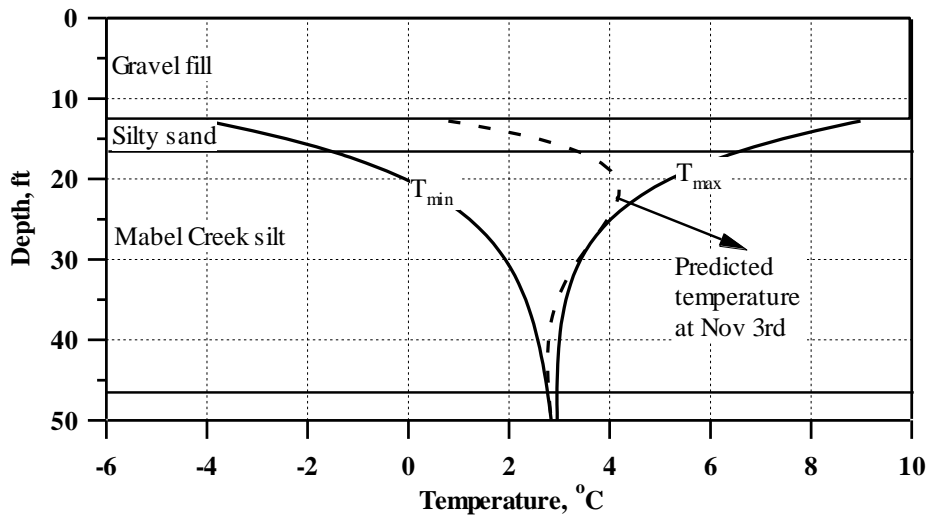


**Figure B.2 Temperature profile**

Step 1: Build up the temperature profile at the selected site.

Thirty years of climate records from Tok, Alaska were obtained from the Western Regional Climate Center. Using this data, the expected freezing isotherms or whiplash curves were developed and studied to evaluate the expected ground temperature profile in Mabel Creek. The temperature profile at this site on November 3 is shown in Figure B.2. The Mabel Creek silt layer in this study site is unfrozen on this particular day. However, the top 3.6 feet in the Mabel Creek silt layer experience seasonal freeze-thaw cycles. This is because the depth, where the value  $T_{min}$  is 0 °C. Approximately 26.2 feet in Mabel Creek silt below the depth for  $T_{min}=0$  °C can be expected to remain unfrozen.

Step 2: Determine the equivalent uniform cyclic strain at a selected depth, which was caused by wave propagation of seismic events.

Seismic shear waves are attenuated within the soil. Moreover, a seismic wave is irregular waveform, thus an equivalent uniform waveform may be used to approximate the irregular seismic waves by wave transformation. Dobry et al. (1982)

proposed a simplified method for estimating the amplitude of a uniform cyclic strain; this estimate is given by:

$$\gamma_{cyc} = 0.65 a_{max} \sigma_v r_d / (g G(\gamma_{cyc})) \tag{B.1}$$

where  $a_{max}$  is the peak ground surface acceleration;

$g$  is the acceleration of gravity;

$\sigma_v$  is the total vertical stress;

$r_d$  is the stress reduction factor, and attained from Figure 3; and

$G(\gamma_{cyc})$  is the shear modulus of the soil at  $\gamma_{cyc} = \gamma$ .

The top 3.6 feet of thickness for the Mabel Creek silt will experience freeze-thaw cycles. Subsequently, the stress reduction factor at this location is given by

$$\begin{aligned} \sigma_v(z=18.2ft) &= (135lb/ft^3)(12.8ft) + (130lb/ft^3)(3.6ft) + (90lb/ft^3)(1.8ft) \\ &= 2358lb/ft^2 \\ r_d &= 0.95 \end{aligned}$$

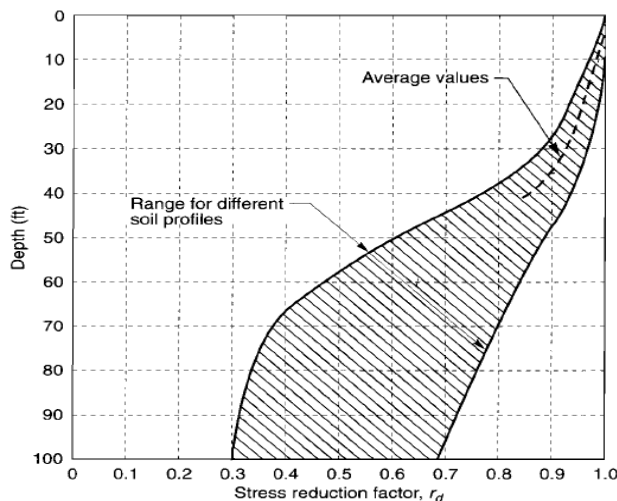


**Figure B.3 Reduction factor with depth below level or gently sloping ground surfaces. (After Seed and Idriss 1971)**

At 26.2 feet in the unfrozen Mabel Creek silt layer below the depth for for  $T_{min} = 0\text{ }^{\circ}\text{C}$ ,

the stress reduction factor is

$$\begin{aligned}\sigma_v(z=33.1\text{ft}) &= (135\text{lb/ft}^3)(12.8\text{ft}) + (130\text{lb/ft}^3)(3.6\text{ft}) + (90\text{lb/ft}^3)(16.7\text{ft}) \\ &= 3699\text{lb/f} \\ r_d &= 0.90.\end{aligned}$$

The shear modulus ( $G(\gamma_{\text{cyc}})$ ) is determined by  $\gamma_{\text{cyc}}$ , the value of  $\gamma_{\text{cyc}}$  is iteratively calculated by the following equation:

$$G(\gamma) = (G_{\text{max}})(G/G_{\text{max}}) \quad (\text{B.2})$$

where  $G_{\text{max}}$  is the maximum shear modulus;

$G/G_{\text{max}}$  is the modulus reduction as shown in Figure B.4.

$G_{\text{max}}$  is also attained by Hardin and Drnevich's (1978) method:

$$G_{\text{max}} = 625(\text{OCR})^k p_a^{0.5} (\sigma'_m)^{0.5} / (0.3 + 0.7e^2) \quad (\text{B.3})$$

where OCR is the overconsolidation ratio and 1 in this study;

$k$  is the overconsolidation ratio parameter;

$p_a$  is atmospheric pressure in same units as  $\sigma'_m$ ; and

$\sigma'_m$  is the mean principal effective stress and 100 kpa(14.5psi).

Hence  $G_{\text{max}} = 8337.5$  psi.

Since Mabel Creek silt has a PI of 5.3, the modulus reduction curve at PI = 5.3 is applied during iteration. Thus

$$\begin{aligned}\gamma_{\text{cyc}}(z=18.2\text{ft}) &= 0.065\% \\ \gamma_{\text{cyc}}(z=33.1\text{ft}) &= 0.125\%.\end{aligned}$$

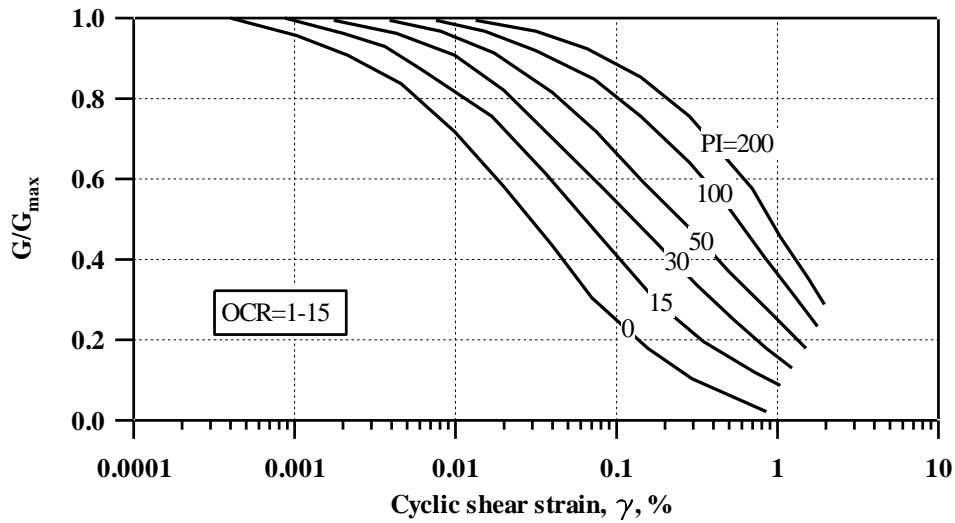


**Figure B.4 Modulus reduction curves for fine-grained soils of different plasticity. (After Vucetic and Dobry 1991)**

Step 3: Determine  $r_u$ .

From Table B.1, the equivalent number of loading cycles may be found for Magnitude 7.5, and 20 cycles is obtained. Using the equivalent number of loading cycles and Equation B.3, the corresponding excess pore water pressure ratio ( $r_u$ ) as attained from Figure B.5 and Figure B.6 from this report is:

$$r_u(z=18.2\text{ft}) = 0.155$$

$$r_u(z=33.1\text{ft}) = 0.35.$$

Generally, soils with  $r_u$  less than 0.8 will not liquefy. Thus, soils at this site do not liquefy.

**Table B.1 Earthquake magnitude, equivalent cycles, and duration (Seed et al. 1976)**

Earthquake magnitude	Equivalent cycles	Duration of strong shaking, sec
5.5~6	5	8
6.5	8	14
7	12	20
7.5	20	40
8	30	60

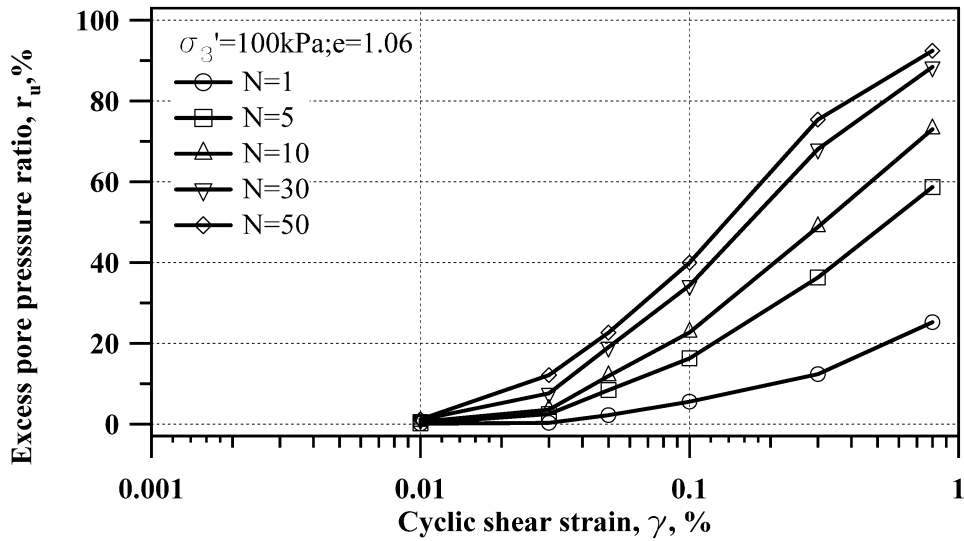


Figure B.5 Excess pore pressure ratios versus cyclic shear strain on unfrozen Mabel Creek silt (in this study)

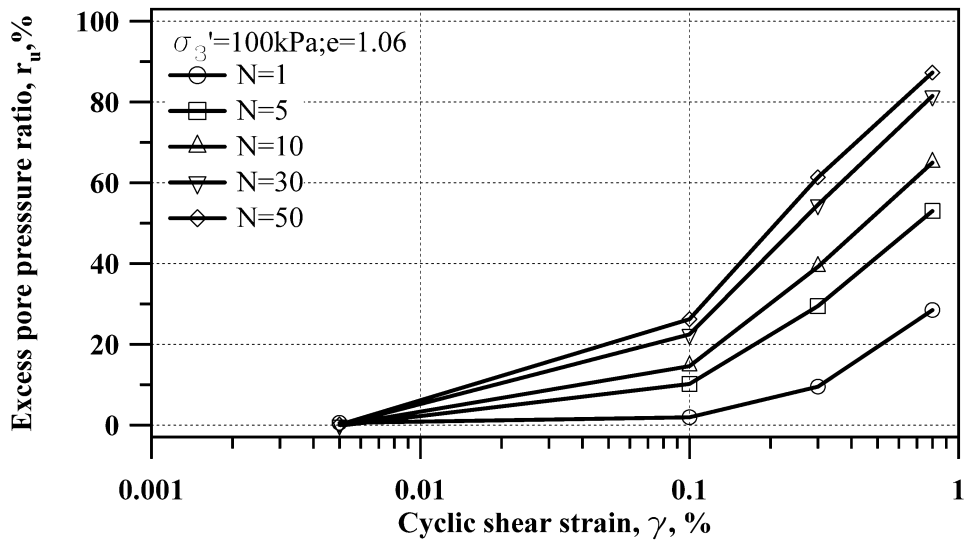


Figure B.6 Excess pore pressure ratios versus cyclic shear strain on Mabel Creek silt experiencing 1 freeze-thaw cycle (in this study)

Step 4: Determine the possible settlement due to dissipation of pore water pressure.

The corresponding reconsolidated volumetric strain due to dissipation of pore water pressure may be found from Figure B.7 and Figure B.8 in this report. These are:

$$\epsilon_v(z=18.2\text{ft}) = 0.16\% ; \text{ and}$$

$$\varepsilon_v(z=33.1\text{ft}) = 0.35\%$$

The total settlement after the earthquake in the Mabel Creek silt layer is expected to be:

$$\text{the total displacement} = (0.16\%)(3.6\text{ft}) + (0.35\% * 26.2\text{ft}) = 0.0975\text{ft} = 1.17\text{in.}$$

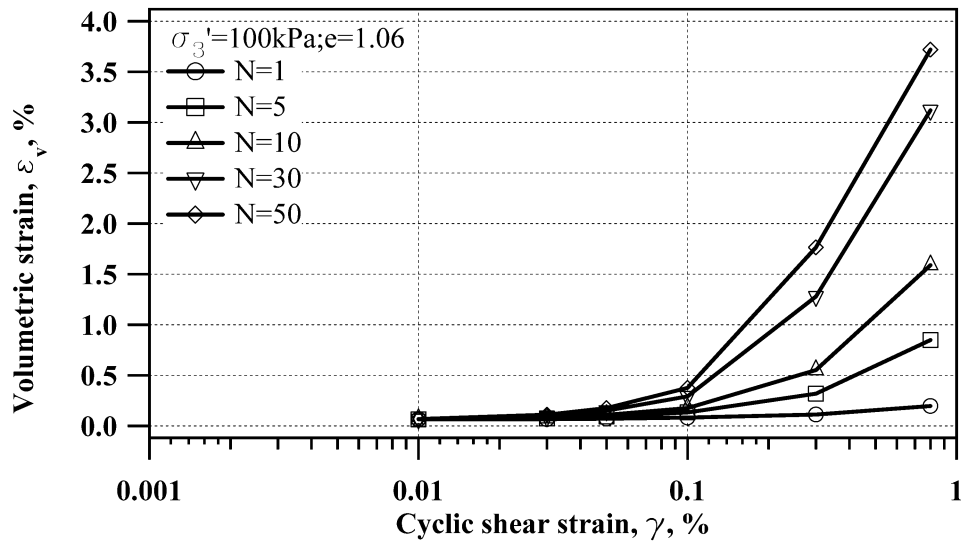


Figure B.7 Chart for determination of the post-cyclic-loading volumetric strain as a function of cyclic shear strain on unfrozen Mabel Creek silt (in this study)

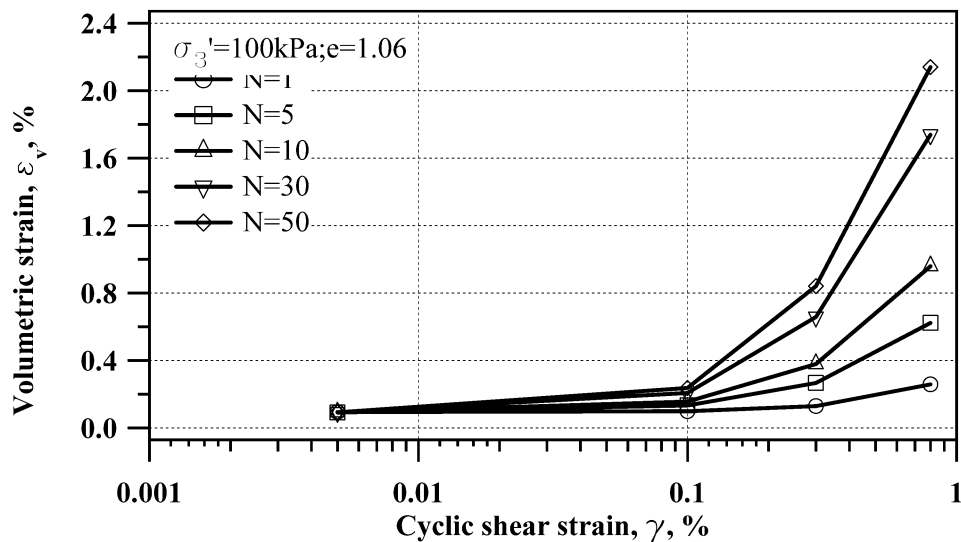


Figure B.8 Chart for determination of the post-cyclic-loading volumetric strain as a function of cyclic shear strain on unfrozen Mabel Creek silt after 1 freeze-thaw cycle (in this study)

